University Medical Center Hamburg-Eppendorf

Institute of Clinical Chemistry and Laboratory Medicine

Characterisation of XPR1 functions regulating CD4+ T-cell responses

Dissertation

Submitted to the Department of Chemistry

Faculty of Mathematics, Informatics and Natural Sciences

University of Hamburg

In fulfilment of the requirements for the degree of

Doctor of Natural Sciences (Dr. rer. nat.)

By

Marion Mengel

December 2025, Hamburg

First reviewer: Prof. Dr. Hartmut Schlüter

Second reviewer: PD Dr. Reiner Mailer

Chair of the Defence Committee: Prof. Dr. Hartmut Schlüter

Deputy Chair of the Defence Committee: Prof. Dr. Sebastian G. Wicha

Member of the Defence Committee: PD Dr. Reiner Mailer

Member of the Defence Committee: Prof. Dr. Louisa Temme

Member of the Defence Committee: Prof. Dr. Eva Tolosa

Date of oral defence: 10.04.2026

Date of publication: 15.04.2026

This study was conducted between October 2022 and December 2025 at the Institute of Clinical Chemistry and Laboratory Medicine of the University Medical Center Hamburg-Eppendorf under the supervision of Prof. Dr. Hartmut Schlüter and Dr. Reiner Mailer.

List of publications and presentations

Kröger, B.; Spohn, M.; **Mengel, M.**; Sperhake, J. P.; Ondruschka, B.; Mailer, R. K.: Expression of full-length FOXP3 exceeds other isoforms in thymus and stimulated CD4+ T cells. J. Clin. Immunol. 2024 Apr 27;44(5):114. doi: 10.1007/s10875-024-01715-8. PMID: 38676826; PMCID: PMC11055749.

Mengel, M. *et al.*: XPR1 orchestrates T-cell stimulation pathways to avert excessive cytokine production. *In preparation*.

Part of this work was presented at the following conferences:

Date	Conference	Type of presentation
June 2023	25th Meeting on T Cells, Marburg	Oral presentation
September 2024	7th European Congress of Immunology, Dublin	Oral presentation
August 2025	19th International Congress of Immunology, Vienna	Poster presentation

Inhalt

1. Abstract

Xenotropic and polytropic retrovirus receptor 1 (XPR1) is the only known phosphate exporter in mammalian cells, whose abrogation leads to embryonic lethality in mice. Recent findings suggest that XPR1 has a role in signal transduction, complex formation, and protein trafficking extending its function beyond phosphate homeostasis and indicating a potential function of XPR1 in immunoregulation. This work therefore investigates XPR1 in CD4+ T cells to unveil novel therapeutic approaches to modulate immune responses.

We found that conditional *Xpr1* knockout in T cells led to altered development and selection in the thymus. Mature XPR1 deficient CD4+ T cells showed hyperactivation and increased expression of *Il2*, as well as increased effector functions in response to antibody-mediated stimulation. In particular, XPR1 deficiency increased proliferation, cytokine expression, and induced a moderate shift towards a glycolytic metabolic phenotype in CD4+ T cells without changes in phosphate homeostasis. *In vitro* differentiation assays revealed increased expression of the proinflammatory cytokines TNF-α and IFN-γ, and IL-22, under Th1- and Th17-skewing conditions in XPR1 deficient T cells, respectively. Likewise, human Jurkat cells showed increased expression of *TNFA*, *IFNG*, and *IL22* upon siRNA-mediated *XPR1* knockdown in qPCR analyses. Moreover, antigen-specific stimulation of *Marilyn* CD4+ T cells by intravenous injection of the cognate H-Y antigen resulted in hyperactivation, increased expression of the immune checkpoint molecules CTLA-4 and PD-1, and increased expression of the proinflammatory cytokines IL-17a and IL-22 in XPR1 deficient T cells *in vivo*. T-cell receptor (TCR) downstream signalling was altered in XPR1 deficient CD4+ T cells, demonstrated by impaired Ca^{2+} influx, ERK1/2 phosphorylation, and nuclear NFAT translocation, as well as increased AKT and S6 phosphorylation, indicating a hyperactivation of PI3K-AKT-mTOR signalling. Homeostatic expansion experiments revealed a proliferation disadvantage of XPR1 deficient CD4+ T cells, while α-CD28 stimulation elicited a proliferative response in XPR1 deficient, but not control CD4+ T cells, even in the absence of α-CD3 *in vitro*. This portrays XPR1 as a negative regulator of CD4+ T-cell responses that restricts CD28-dependent co-stimulation during T-cell hyperactivation. Mechanistically, we report the interaction of XPR1 with the scaffolding protein Kidins220, which has been previously associated with TCR downstream signalling and immune synapse formation. To disrupt the interaction of XPR1 with Kidins220, we devised the cell-penetrating peptide Tat-X featuring the last 25 amino acids of XPR1's C-terminal loop, which promoted T-cell proliferation, thereby phenocopying hyperactivated XPR1 deficient CD4+ T cells. Thus, XPR1 targeting may provide a potential tool for immunotherapy to invigorate insufficient T-cell responses.

2. Zusammenfassung

Xenotropic and polytropic retrovirus receptor 1 (XPR1) ist der bisher einzig bekannte Phosphat-Exporter in Säugetieren, dessen *Knockout* im Embryo-Stadium von Mäusen lethal ist. Obwohl die XPR1-vermittelte Regulation von Phosphat-Homöostase ein zentraler Aspekt der XPR1 Forschung ist, legt die Interaktion von XPR1 mit verschiedenen Proteinen, die an Immun-Zell-Signalwegen, Komplexbildung und *Trafficking* beteiligt sind, eine Relevanz von XPR1 für die Immunmodulation nahe. Daher befasst sich diese Arbeit mit der Rolle von XPR1 in T-Zellen, um neuartige Ansätze für Immun-Modulations-Therapeutika zu eröffnen.

Ein konditioneller Knockout von XPR1 in CD4+ T-Zellen führte zu Veränderungen in Entwicklung und Selektionsprozessen im Thymus. XPR1-defiziente T-Zellen aus der Milz zeigten eine Hyperaktivierung und erhöhte *Il2*-Expression sowie gesteigerte Effektor-Funktionen in Antwort auf Antikörper-vermittelte T-Zell-Rezeptor (TZR)-Stimulation. Insbesondere erhöhte die Abwesenheit von XPR1 in CD4+ T-Zellen deren Proliferation und Zytokin-Expression und bewirkte eine Verschiebung in Richtung eines glykolytischen metabolischen Phänotyps, ohne die Phosphathomöostase zu verändern. *In vitro*-Differenzierungs-Assays zeigten eine erhöhte Expression der proinflammatorischen Zytokine TNF-α und IFN-γ sowie IL-22, unter Th1- beziehungsweise Th17-induzierenden Bedingungen in XPR1 defizienten T-Zellen. Ebenso zeigten humane Jurkat-Zellen nach siRNA-vermitteltem XPR1-Knockdown in qPCR-Analysen eine erhöhte Expression von TNF-α, IFN-γ und IL-22. Des Weiteren resultierte eine antigen-spezifische Aktivierung von *Marilyn*-CD4+ T-Zellen mittels intravenöser Injektion von H-Y-Peptid in erhöhter Aktivierung und erhöhter Expression der Immun-*Checkpoint*-Moleküle CLTA-4 und PD-1 sowieso der proinflammatorischen Zytokine IL-17a und IL-22 in XPR1-defizienten T-Zellen. TZR-vermittelte Signalwege zeigten Veränderungen in XPR1-defizienten T-Zellen, was durch verringerten Ca^{2+}-Influx, ERK1/2-Phosphorylierung und nukleäre NFAT-Translokation, sowie erhöhte AKT- und S6-Phosphorylierung deutlich gemacht wurde. Dies deutet auf eine Hyperaktivierung des PI3K-AKT-mTOR-Signalwegs hin. Homöostatische Expansions-Experimente ergaben, dass XPR1-defiziente T-Zellen einen Nachteil gegenüber Kontrollzellen bezüglich der Proliferation *in vivo* aufweisen, während eine Stimulation allein mit α-CD28 ohne α-CD3 *in vitro* ausreichte, um eine Proliferation in XPR1-defizienten, nicht aber in Kontroll-CD4+ T-Zellen hervorzurufen. Dies zeigt, dass XPR1 als negativer Regulator von CD4+ T-Zell-Antworten fungiert und die CD28-abhängige Kostimulation einschränkt, um eine T-Zell-Hyperaktivierung zu verhindern. Auf mechanistischer Ebene konnten wir die Interaktion von XPR1 und Kidins220 zeigen, einem Adaptor-Protein, das bereits zuvor mit TZR-Signalwegen und der Bildung der Immun-Synapse in Verbindung gebracht wurde. Um die Interaktion von XPR1 mit Kidins220 zu blockieren, wurde das neuartige, zellpenetrierende Peptid Tat-X aus den letzten 25

Aminosäuren der C-terminalen Schleife von XPR1 entwickelt. Tat-X-Behandlung inhibierte die Interaktion von XPR1 und Kidins220, und förderte darüber hinaus die T-Zell-Proliferation, analog zur Hyperaktivierung XPR1-defizienter CD4+ T-Zellen. Zusammenfassend stellt XPR1 daher ein potentielles Ziel für die Immuntherapie dar, um unzureichende T-Zell-Antworten zu verstärken.

3. Introduction

3.1. Immune system

The immune system is the defence of our body against harmful pathogens and against malignant tumour cells that threaten to damage our own body. The main challenge for the immune system is regulating immune homeostasis and tolerance – if the immune system is tolerant towards malignant tumour cells or pathogens, cancer progression or severe infections are imminent, whereas an immune system too responsive might attack body-own tissue and cause inflammation or autoimmune diseases (1). The immune system's regulation and the underlying mechanisms to control the plethora of its functions are complex and still not fully understood. Thorough understanding of immune system homeostasis is indispensable for modern medicine and the development of novel therapeutics.

3.1.1. Innate and adaptive immune system

The human body's immune system can be differentiated into the innate immune system, which is ready at birth and acts immediately upon pathogen contact, and the adaptive immune system, which can adjust its responses by genetic recombination to generate antibodies and cells that are specialised for combating distinct pathogens by recognising antigens in a highly specific manner. Innate and adaptive immune system show a complex interplay of regulation and communication, which is indispensable for an effective immune response (2).

The first line of defence of the innate immune system is presented by physical, chemical, and microbial barriers to the outer world. Physical barriers are skin or mucosa that prevent pathogens from crossing surfaces to enter the body or invade tissues. Chemical barriers refer to secretions from skin or mucosa, *e.g.* tears or saliva that contain lysozyme to destroy invading bacteria. Microbial barriers are presented by commensal microorganisms that inhabit surfaces of the body, *e.g.* the skin or the intestines (2).

If pathogens manage to pass these primary barriers, they are confronted with cellular and humoral components of the innate immune system. The innate immune system is specialised

on more unspecific responses mediated by pattern recognition. Pattern-recognition molecules (PRMs) like Toll-like receptors (TLRs) or NOD-like receptors (NLRs) are expressed on innate immune cells like monocytes, dendritic cells, or granulocytes. PRMs recognise pathogen-associated molecular patterns (PAMPs) or damage-associated molecular patterns (DAMPs) (2, 3). PAMPs are highly conversed, distinctively non-human structures like lipopolysaccharide (LPS), components of bacterial or fungal cell walls, flagellin, viral RNA, or others (3). DAMPs are molecules that are accessible to their respective receptors only when they are released from damaged cells. Examples for these are heat shock proteins, nucleic acids, and extracellular matrix (ECM) components (3). PAMP or DAMP recognition by PRMs leads to clearance of pathogens, *e.g.* by secretion of antimicrobial peptides (AMPs), phagocytosis or induction of apoptosis, and activation of the immune system, *e.g.* by opsonisation or antigen presentation to activate the complement system or the adaptive immune system, respectively (2–4).

The adaptive immune system is characterised by slower, but highly specific immune responses. B and T lymphocytes are the key players of the adaptive immune system. Both B cells and T cells recognise antigen via their B and T cell receptor (BCR and TCR), respectively. Through genetic rearrangement of their respective receptors during their development, mature B and T cells can develop a wide variety of receptor specificities, enabling them to recognise a plethora of antigens (5–7).

At first, naïve B and T cells scour the lymph system until they encounter antigen, leading to activation, proliferation, differentiation, and eventually migration into the inflamed tissue. Both types of lymphocytes can act using a wide range of effector mechanisms that depend on differentiation into specialised lymphocyte subsets. Lastly, lymphocytes that were activated by recognition of their cognate antigen remain as memory cells in the system, leading to a quicker response of the adaptive immune system upon re-encounter with the antigen (5–7).

B cells can differentiate into plasma cells, which specialise on antibody production. Secretion of antibodies facilitates clearing of bound pathogens or complement activation. Moreover, B cells can act as antigen-presenting cells (APC), or differentiate into memory cells to induce a quicker immune response upon reencountering the antigen they recognise (5, 6).

T cells carry out a large spectrum of effector functions. Depending on the composition of their TCR chains, one can differentiate between α/β T cells and γ/δ T cells. The latter are unconventional T cells which carry out innate-like functions (8). α/β T cells can be classified by expression of their TCR-co-receptors cluster of differentiation (CD)4 or CD8 into T-helper cells (CD4+ T cells) or cytotoxic T cells (CD8+ T cells). CD8+ T cells are mainly responsible for eliminating tumour cells or cells that are infected by viruses through recognition of cytosolic

antigens. CD4+ T cells are specialised on orchestrating the immune response by regulating other immune cells or tissue cells via cytokine secretion in immune responses against endo-lysosomal antigens (7). In the following, we focused on CD4+ T cells.

3.1.2. Development of CD4+ T lymphocytes

T cells are derived from lymphopoietic stem cells. T-cell progenitors are produced in the bone marrow and mature in the thymus. During this maturation process, they undergo different selection processes which serve as checkpoints that prevent dysfunctional cells from maturing and emerging into the periphery (9, 10).

After commitment of common lymphoid progenitor cells to the T-cell lineage, early T-cell progenitors (ETPs) that are double negative (DN) for the expression of CD4 and CD8 migrate to the distal cortex of the thymus. DN thymocytes can be differentiated into four stages of development, depending on their expression of CD44 and CD25: DN1/ETPs (CD44+CD25-), DN2 (CD44+CD25+), DN3 (CD44-CD25+), and DN4 (CD44-CD25-) (9, 10). α/β T cells are characterised by expression of a TCR that is comprised of a TCR-α and a TCR-β chain. Both chains feature a variable region which is responsible for antigen recognition, and a constant region, which features interaction sites with other proteins that are important for signal transduction of TCR downstream signalling (11). During the DN2 and DN3 stages, T-cell progenitors rearrange the genes encoding for TCR chains by undergoing recombination, which is facilitated by recombination activating gene (RAG) 1 and RAG2. This process involves rearrangement of the variable (V), diverse (D), and joining (J) region of the receptor chain genes, known as V(D)J recombination. On top of the recombination, random nucleotides are added or deleted at the junction sites. Through these mechanisms, a wide variety of specificities is achieved (9, 10, 12).

Cells that successfully recombined *Tcrd* and *Tcrg* chains commit to the γ/δ T-cell lineage, whereas cells that successfully recombined a *Tcrb* chain commit to the α/β lineage. After recombination in the DN3 stage, DN α/β thymocytes undergo a process called β-selection: they assemble a pre-TCR complex comprised of the rearranged TCR-β chain, a pre-Tα chain, and CD3. If a pre-TCR signals sufficiently, cells receive survival and proliferation signals and progress to the double positive (DP) stage, which is characterised by expression of both CD4 and CD8 (13–20, 9, 10).

DP thymocytes undergo another round of V(D)J recombination for the rearrangement of the *Tcra* gene. Thymocytes with a functional TCR comprised of rearranged TCR-β and TCR-α chains undergo positive and negative selection in the cortex. For this, self-antigen is presented

by cortical thymic epithelial cells (cTECs) in the context of major histocompability complexes (MHCs). During this process, the avidity of the TCR as a measurement for self-reactivity is crucial for selection processes (9, 10, 21, 22).

CD5 is a crucial player for functional tuning during selection processes, and correlates with the degree of TCR self-reactivity (Figure 1A). Recognition of peptide-MHC (pMHC) complexes is required to convey survival signals and thereby allow cells to pass positive selection. However, cells that bind pMHC with a level of self-reactivity too high get negatively selected, whereas cells that do not bind the pMHC die by neglect (Figure 1B). Functional tuning is mediated by CD5-mediated negative regulation of TCR signalling (Figure 1C): cells with a higher self-reactivity express higher levels of CD5, which dampens their TCR response and prevents negative selection. On the other hand, cell with a lower self-reactivity express lower levels of CD5, which enhances their TCR response and prevents death by neglect. Depending on their affinity for MHC class II or I during selection in the cortex, DP thymocytes commit to differentiation into CD4+ or CD8+ T cells, respectively (9, 10, 21, 22).

Cells single positive for expression of CD4 (SP4) or CD8 (SP8) undergo another round of selection in the medulla where they encounter a wide variety of tissue-restricted antigens presented by medullary TECs (mTECs) (Figure 1D). Cells recognising self-antigen either undergo negative selection, or – if the cell is CD4+ – have the potential to develop as a thymic-derived regulatory T cell (tTreg). This choice is dependent on the cell's ability to access niches with antigen-bearing APCs, on the cytokine environment, and on the strength of their self-reactivity, which is again affected by functional tuning (9, 10).

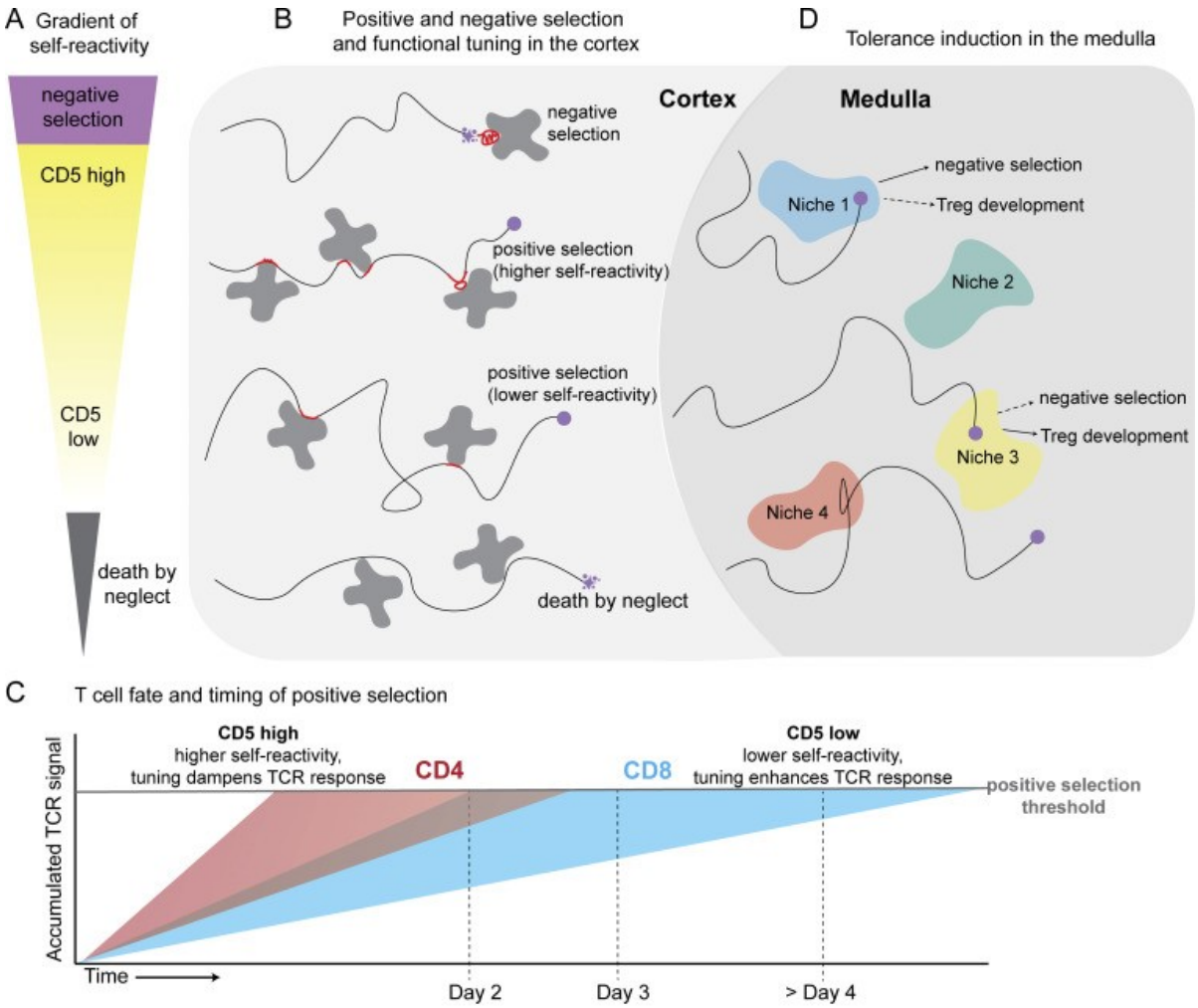

Figure 1: TCR self-reactivity is functionally tuned by CD5 during selection processes in T-cell development. **A**: Schematic view of gradient of self-reactivity that correlates with CD5 expression on DP thymocytes during selection in the cortex. Strong self-reactivity leads to negative selection (purple), whereas weak self-reactivity leads to death by neglect (grey). Cells with an intermediate self-reactivity (yellow) pass positive selection. Expression of CD5 functionally tunes TCR signalling strength and therefore, the degree of self-reactivity. High CD5 expression in thymocytes with high self-reactivity dampens the TCR signalling strength, whereas low CD5 expression in thymocytes with low self-reactivity increases the TCR signalling strength. **B**: Selection processes in the cortex depend on interaction of thymocytes (purple) with cortical thymic epithelial cells (cTECs, grey). The degree of TCR avidity to self-antigen determines the strength of TCR signalling upon contact (depicted in red). **C**: T-cell fate depends on accumulated TCR signal strength during positive selection. Schematic plot of accumulated TCR signal over time. CD5-mediated functional tuning is indicated at the top. **D**: Tolerance screening in the medulla is mediated by interaction of TCR with tissue restricted antigen (TRA) presented by medullary thymic epithelial cells (mTECs). Depending on the reactivity towards TRA, on the ability to reach limiting niches, and on the cytokine environment, self-reactive CD4+ T cells undergo negative selection or develop into thymic regulatory T cell (tTreg). Figure from (10).

3.1.3. CD4+ T-cell activation

Naïve CD4+ T cells that passed all selection stages in the thymus and matured successfully patrol the blood and lymph nodes until they encounter antigen that is presented by an APC via MHC-II. A typical example for antigen-dependent stimulation is the interaction of a CD4+ T cell with a dendritic cell in the lymph node, as shown in Figure 2 (11).

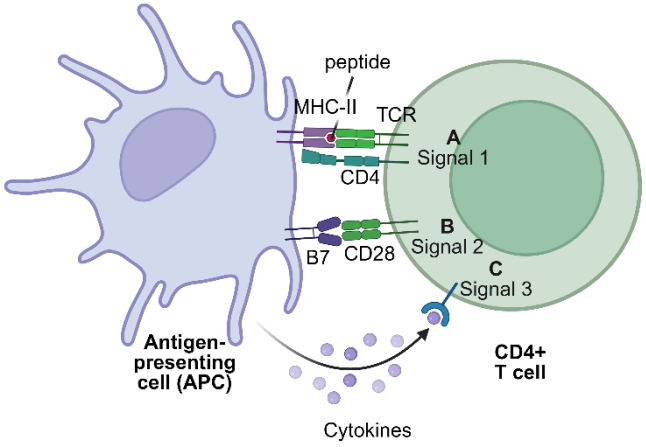

Figure 2: T-cell activation by APCs requires three signals. A: Interaction of the T-cell receptor (TCR) with a major histocompability complex class II (MHC-II) presenting an antigen peptide corresponds to signal 1. **B**: Interaction of the co-stimulatory molecule CD28 with B7 molecules presents signal 2. **C**: The third signal contributing to CD4+ T-cell activation is the cytokine environment. Figure created with BioRender.com.

A classic model of T-cell activation states that T-cell activation is dependent on three signals (23, 24). Signal 1 is presented by interactions of the TCR with pMHCs on the surface of an APC. Depending on the TCR co-receptor expressed by the T cell (CD8 or CD4), the TCR recognises MHC-I or -II.

Signal 2 is provided by interactions of the co-stimulatory molecule CD28 with B7 ligands (also known as CD80/86) expressed by the APC (23). Engagement of the TCR without synergistic co-stimulation results in anergy, therefore co-stimulation is required for successful T-cell activation. Apart from CD28, other co-stimulatory molecules like CD226, tumour necrosis factor receptor superfamily member 4 (OX40), inducible T-cell co-stimulator (ICOS), or 4-1BB, or co-inhibitory molecules like cytotoxic T-lymphocyte associated protein 4 (CTLA-4), programmed cell death protein 1 (PD-1), or T-cell immunoreceptor with Ig and ITIM domains (TIGIT) can regulate downstream T-cell signalling and enhance or dampen the relayed signals (23, 25, 26). CTLA-4 binds B7 with a higher affinity and avidity than CD28, leading to a strong inhibitory effect which is not only based on inhibitory downstream signalling, but also competition with CD28 for their shared ligand (27–29). PD-1 has been shown to suppress T-cell functions primarily by targeting CD28-mediated co-stimulatory downstream signalling

(30, 31). Both CTLA-4 and PD-1 are common targets for immune checkpoint therapy (ICT) which aims to enhance T-cell mediated anti-tumour immune responses (31).

Signal 3 is presented by the cytokine environment. Via various cytokine receptors, T cells receive signals impacting their differentiation (23, 24).

3.1.4. CD4+ T-cell effector mechanisms and T-helper subsets

Sufficient activation of CD4+ T cells by engagement of the TCR complex as well as co-stimulation lead to proliferation and differentiation of effector CD4+ T cells. Depending on the cytokine environment, distinct CD4+ T-cell subsets arise, which carry out different effector functions. Secretion of cytokines is the main mode of action by which CD4+ T cells communicate with immune and non-immune cells to regulate the immune response and inflammation. If the complex network of CD4+ T-cell effector functions is dysregulated, consequences can be chronic inflammation, autoimmunity, immune deficiency, or tumour progression (7, 32).

The cytokine environment plays the key role in facilitating differentiation into different CD4+ T-cell subsets. Some of them are T-helper (Th) 1, Th2, Th17, Th22, and regulatory T cells (Tregs) (7, 33). Subsets are characterised by expression of a set of signature cytokines and key transcription factors.

Th1-cell differentiation is mainly mediated by interleukin (IL-)12 and IFN-γ. Expression of the key transcription factor T-bet induces the expression of interferon (IFN)-γ, which leads to an IFN-γ-mediated positive feedback loop of Th1-cell differentiation. Further, expression of the proinflammatory cytokine tumour necrosis factor α (TNF-α) is characteristic for the Th1 subpopulation. TNF-α promotes inflammation by activating nuclear factor κ-light chain enhancer of activated B cells (NF-κB) and RAS-mitogen-activated protein kinase (MAPK) signalling pathways, which induce gene expression of proinflammatory chemokines and cytokines (34). Th1 cells are essential for mediating defence against intracellular pathogens like bacteria or viruses. Moreover, Th1 cells are important for anti-tumour responses (7, 35, 36). However, due to their expression of proinflammatory cytokines, Th1 cells can contribute to inflammation and autoimmunity. This has for example been shown in inflammatory bowel disease (IBD), graft-versus-host disease, type-1 diabetes, and rheumatoid arthritis (RA) (7, 36–42).

Th2 cells are characterised by expression of the cytokines IL-4, IL-5, and IL-13, and the key transcription factor GATA-3. Th2-skewing conditions include IL-2 and IL-4. Th2 cells play a

role in host defence against extracellular pathogens like helminths and nematodes, tissue repair, asthma, allergies, and regulating B-cell mediated antibody production (7, 36, 43).

Th17 cells are characterised by the expression of the cytokines IL-17, IL-21, IL-22, and IL-23, and the key transcription factor Ror-γt. Ror-γt controls the expression of IL-17, the main cytokine expressed by Th17 cells (7, 36, 44–46). Differentiation into Th17 cells is driven by transforming growth factor β (TGF-β), IL-6, IL-1β, and IL-23. Th17 cells show a plasticity depending on present cytokines during differentiation: The “classical” Th17 cells are induced by IL-6 and TGF-β, whereas “alternative” Th17 cells are induced by IL-6, IL-1β, and IL-23 (47–49). The “alternative” Th17 cells show a more pathogenic phenotype, characterised by increased expression of IFN-γ, granulocyte-macrophage colony-stimulating factor (GM-CSF), and IL-22 (7, 48–51). Th17 cells are involved in immunity at mucosal surfaces and epithelial barriers. Further, they have been implicated in chronic inflammation, anti-tumour responses, and autoimmune diseases, *e.g.*, multiple sclerosis (MS), RA, psoriasis, and IBD (7, 35, 36, 45, 52, 53).

Th22 cells are a T-helper cell subpopulation that was named accordingly due to their high expression of IL-22. IL-22 has been found to contribute to proinflammatory as well as antiinflammatory mechanisms (54–57). Apart from IL-22, Th22 cells also express IL-26, IL-13, TNF-α, and granzyme B. Th22 differentiation is driven by IL-6, TNF-α, IL-23, and IL-1β (33, 58). Expression of the transcription factors Ror-γt and aryl hydrocarbon receptor (AhR) indicates similarities to Th17 cells, however Th22 cells do not express IL-17, and TGF-β impairs differentiation into Th22 cells (33, 58, 59). Th22 cells are involved in mucosal homeostasis, host defence, barrier repair and homeostasis of the intestine, but have also been found to be involved in cancer and autoimmune diseases like RA, systemic lupus erythematosus (SLE), IBD or atopic dermatitis (59–61, 55, 56).

In striking difference to Th1, Th2, Th17, and Th22 subsets who express proinflammatory cytokines, Tregs play an important antiinflammatory role by downregulating immune responses to control immune homeostasis and tolerance. They either arise from the thymus as tTregs as described in section 3.1.2, or differentiate in the periphery (pTregs). Tregs are characterised by expression of IL-2 receptor (IL-2R)-α/CD25, and Foxp3. Foxp3 is the key transcription factor of Tregs, and crucial for development, maintenance, and the suppressive functions of Tregs, since mutations or deletion of Foxp3 result in severe dysregulation of immune responses (7, 32, 62–67). Treg-mediated immunosuppression is further achieved by expression of the immunosuppressive cytokine IL-10, by cytolysis, by metabolic disruption via IL-2Rα/CD25, cAMP, or CD39, or by CTLA-4-mediated modulation of dendritic cells (DCs)

(68). Peripheral differentiation into pTregs is driven predominantly by IL-2 and TGF-β, with TGF-β being the driver of *Foxp3* transcription (7, 32, 62–64).

The cytokine IL-2 is crucial for CD4+ T-cell functions and differentiation, and it affects all T-helper cell subsets. Activation of CD4+ T cells leads to expression of IL-2, which renders IL-2 expression suited as an early CD4+ T-cell activation marker. IL-2 is required for the initial proliferation of conventional CD4+ and CD8+ T cells (69). The response to IL-2 is controlled by the expression of IL-2R chains. IL-2 binds with low to moderate affinity to the dimeric IL-2R comprised of IL-2Rβ and IL-2Rγ, whereas it binds with high affinity to the trimeric IL-2R comprised of IL-2Rα/CD25, IL-2Rβ, and IL-2Rγ (69–73). Conventional T cells express the dimeric IL-2R, which is why a high concentration of IL-2 is required for a proliferative response of CD4+ T cells after activation (69–73). After activation, conventional T cells upregulate CD25, which facilitates differentiation into T-helper subsets. IL-2 induces signal transducer and activator of transcription (STAT)-5 signalling, which promotes differentiation into Th1- and Th2 cells while it suppresses differentiation into Th17 cells (69, 73, 74). Tregs do not express IL-2 themselves, but require IL-2 for survival. This leads to a decrease of Treg numbers in the absence of IL-2 on the one hand, while on the other hand expression of CD25 by Tregs results in preferred consumption of IL-2 by Tregs when conventional T cells do not express CD25 (68). Both these mechanisms contribute to balancing immune homeostasis.

Taken together, CD4+ T-cell differentiation into subsets finetunes responses of the immune system. Dysregulation of differentiation and the interplay of proinflammatory and antiinflammatory mechanisms can lead to a detrimental outcome of cancer, severe infections, autoimmunity, tissue damage, or chronic inflammation (7, 33).

3.1.5. TCR downstream signalling

TCR engagement activates downstream signalling cascades which eventually result in expression of target genes that define T-cell responses. Signalling cascades of co-stimulatory and co-inhibitory molecules are intertwined with TCR downstream signalling, forming a complex network of cumulating signals eventually promoting T-cell survival, metabolism, proliferation, and differentiation (75).

In general, signalling cascades rely on phosphorylation of target molecules by phosphate kinases, which leads to activation of another kinase which further transduces the signal downstream, and so forth. Adaptor proteins play an important role in this network, as they ensure co-localisation of kinases and their targets, and stabilise interaction networks.

Therefore, the formation of signalling complexes is a common mechanism for TCR downstream signalling (7, 76).

The TCR complex is subject to constant endocytosis and re-expression at the cell surface in resting T-cells (77). Activation of CD4+ T cells by APCs, as described in section 3.1.3, leads to the formation of an immunological synapse (IS), which is characterised by membrane rearrangements leading to focused localisation of signalling complexes and adhesion molecules at three distinctive supramolecular activation cluster (SMAC) (78–80). The central SMAC is predominantly comprised of the TCR complex and its ligands (78, 81). The peripheral SMAC is localised in a ring-like structure around the central SMAC, and features expression of adhesion molecules like lymphocyte function-associated antigen-1 (78, 81), which interacts with its ligand intercellular adhesion molecule-1 (ICAM-1) on APCs. The IS further features a distal SMAC, that is comprised of F-actin-rich structures that stabilise the IS (78, 81). Engagement of the TCR by pMHC leads to TCR-pMHC complexes forming microclusters in the distal SMAC, which are transported through the peripheral to the central SMAC (81, 82). The IS represents a focal point of adhesion between T cells and APCs which has been proposed to control signalling by boosting TCR triggering or facilitating TCR downregulation to adjust to the presented pMHC concentration (82–84). TCR-pMHC complexes are internalised by the T cell after activation, which is proposed to either arrest TCR signalling, or to facilitate endosomal TCR signalling (77, 81, 83, 85–87). However, the role of TCR internalisation for TCR signalling is not fully understood yet.

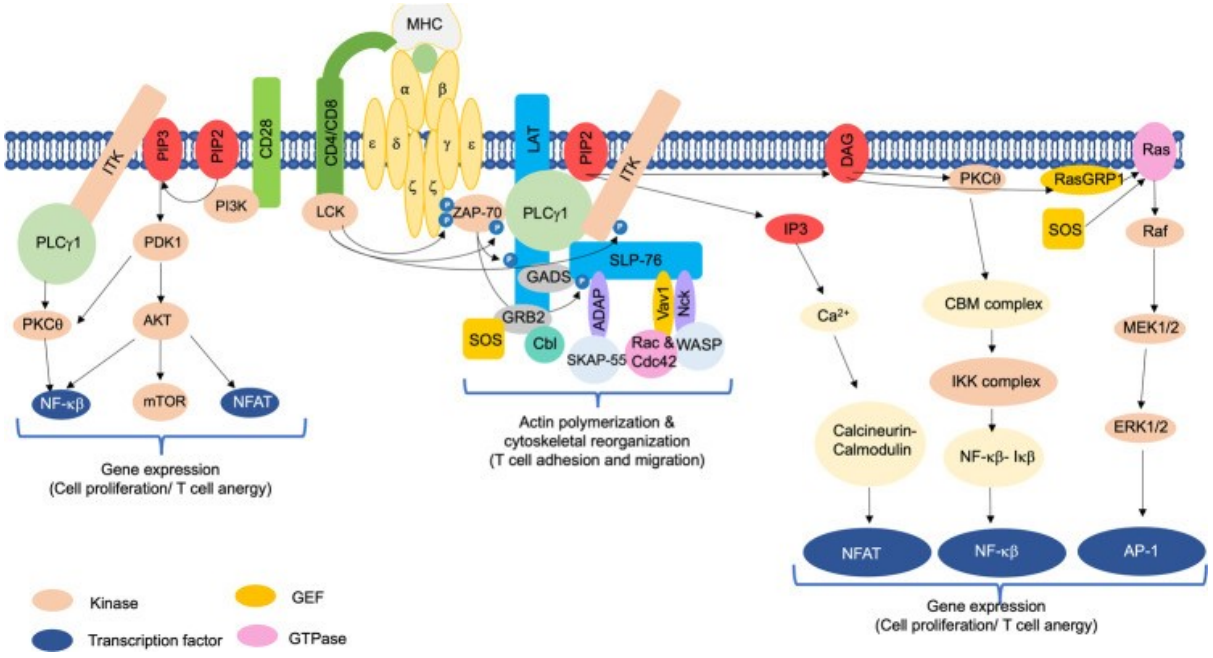

Figure 3: Overview of TCR downstream signalling and CD28-mediated co-stimulatory signalling. Engagement of the TCR-CD3-complex leads to downstream signalling, resulting in AKT/mTOR activation, the assembly of a multiprotein complexes containing LAT, and Ca^{2+}-dependent NFAT translocalisation. Arrows

correspond to activation, and transcription factors are depicted in dark blue. MHC: major histocompability complex, LCK: Lymphocyte-specific cytoplasmic kinase, ZAP-70: Zeta-chain-associated protein kinase 70, LAT: Linker for activation of T cells, PLCγ1: Phospholipase C-γ1, GRB2: Growth factor receptor-bound protein 2, SOS: Son of Sevenless, GADS: GRB2-related adaptor downstream of Shc, SLP-76: SH2 domain-containing leukocyte protein of 76 kDa, ADAP: Adhesion and degranulation promoting adaptor protein, SKAP-55: SRC kinase-associated phosphoprotein of 55 kDa, VAV1: Vav guanine nucleotide exchange factor 1, Cdc42: Cell division cycle 42, WASP: Wiskott-Aldrich syndrome protein, ITK: IL-2 inducible T-cell kinase, PIP2: Phosphatidylinositol 4,5-bisphosphate, IP3: Inositol-3-phosphate, DAG: Diacylglycerol, NFAT: Nuclear factor of activated T cells, PKCθ: Protein kinase Cθ, CBM: CARMA1-BCL10-MALT1, IKK: IκB kinases, RasGRP1: RAS guanyl releasing protein 1, MEK1/2: Mitogen-activated protein kinase kinase, ERK1/2: Extracellular signal-regulated kinase, AP-1: activator protein-1, PI3K: Phosphatidylinositol 3-kinase, PIP3: Phosphatidylinositol (3,4,5)-triphosphate, PDK1: Phosphoinositide-dependent kinase-1, AKT: Protein kinase B, mTOR: Mechanistic target of rapamycin, GEF: Guanine nucleotide exchange factor. Figure from (75).

A simplified overview of the most important signalling pathways downstream of the TCR is shown in Figure 3. The TCR exists in a complex with the δ, γ, ε and ζ chains of CD3. The CD3 invariant chains are indispensable for localisation of the TCR on the cell surface, as well as downstream signalling (75). Further, the co-receptors CD4 or CD8 are associated with the TCR complex and facilitate binding to MHC-II or -I. They also bind to the tyrosine kinase lymphocyte-specific cytoplasmic kinase (LCK) intracellularly (75). Upon engagement of the TCR complex with pMHC, the TCR complex undergoes conformal changes, which is proposed to result in release of CD3 from the inner membrane (75, 88, 89). LCK phosphorylates immunoreceptor tyrosine-based activation motifs (ITAMs) on the CD3 chains. Zeta-chain-associated protein kinase 70 (ZAP-70) is recruited to phosphorylated ITAM motifs, resulting in ZAP-70 phosphorylation by LCK (75, 90). ZAP-70 activates the adaptor proteins linker for activation of T cells (LAT) and SH2 domain-containing leukocyte protein of 76 kDa (SLP-76) (75, 91–94).

The importance of adaptor proteins for signalling is demonstrated by LAT and SLP-76. Both LAT and SLP-76 recruit several other proteins to proximal TCR signalling complexes, which lead to signal transduction via various pathways. For example, growth factor receptor-bound protein 2 (GRB2) and the guanine exchange factor son of sevenless (SOS) associate with LAT (94). The GRB2-SOS complex then phosphorylates Ras upon TCR stimulation (75, 95–97). GRB2 is also associated with the E3 ubiquitin ligase CBL which negatively regulates TCR signalling (75, 98). Further, the GRB2-related adaptor downstream of Shc (GADS) binds phosphorylated LAT and supports the association between LAT and SLP-76 (75, 99, 100).

SLP-76 is crucial for the formation and stability of the LAT-GADS-SLP-76- phospholipase C-γ1 (PLCγ1) complex, thereby playing an important role as an adaptor protein (75, 76). Moreover, it associates with various signalling complexes involved in actin polymerisation and cytoskeletal reorganisation – processes required for T-cell adhesion and migration –, such as

adhesion and degranulation promoting adaptor protein-SRC kinase-associated phosphoprotein of 55 kDa and Vav guanine nucleotide exchange factor 1 (VAV1)-Nck-Rac-Cell division cycle 42-Wiskott-Aldrich syndrome protein (75, 101–106).

Further, SLP-76 associates with IL-2 inducible T cell kinase (ITK) (75). ITK is crucial for downstream signalling pathways leading to gene expression affecting cell proliferation. ITK gets activated by LCK or SLP-76, associates with PLCγ1, and activates it by phosphorylation at multiple residues (107–110). This results in PLCγ1-mediated hydrolysis of membrane-bound phosphatidylinositol 4,5-bisphosphate (PIP2) into diacylglycerol (DAG) and inositol-3-phosphate (IP3) (111, 112). IP3 induces the Ca^{2+}-calcineurin-Nuclear factor of activated T-cells (NFAT) signalling pathway, while DAG fuels the PKCθ-IKK-NF-κB-pathway and the RASGRP1-RAS-ERK1/2-pathway (75).

IP3 engages IP3 receptors (IP3Rs) on the surface of the endoplasmic reticulum (ER), which leads to Ca^{2+} release into the cytosol from ER stores (112, 113). Calcineurin gets activated by cytosolic Ca^{2+}, which in turn leads to dephosphorylation of NFAT, which translocates into the nucleus to act as a transcription factor, most prominently for the expression of *Il2* (114).

DAG regulates protein kinase Cθ (PKCθ) activation (115, 116). Active PKCθ triggers the formation of the so-called CBM-complex, comprised of caspase recruitment domain-containing membrane-associated guanylate kinase protein-1 (CARMA1), B cell lymphoma/leukemia 10 (BCL10), and mucosa-associated lymphoid tissue translocation protein-1 (MALT1). Once assembled, the CBM-complex recruits tumour necrosis factor receptor-associated factor 6 (TRAF6). TRAF6 acts on IKKγ or NF-κB essential modifier (NEMO). This leads to activation of the IκB kinases (IKK) complex, resulting in phosphorylation, ubiquitinylation, and degradation of IκB. IκB is an inhibitor of NF-κB, therefore degradation of IκB enables NF-κB translocation to the nucleus, where it can act as a transcription factor. The PKCθ-IKK-NF-κB signalling pathway impacts T-cell survival and differentiation (117–120).

DAG can further activate RAS guanyl nucleotide-releasing protein (RasGRP1), which in turn activates RAS (121–123). RAS activation can also be facilitated by GRB2-SOS, as mentioned earlier. RAS activation initiates the RAS (MAPK) cascade by activation of RAF1, which in turn activates mitogen-activated protein kinase kinase-1/2 (MEK1/2). MEK1/2 then activates extracellular signal-regulated kinase-1/2 (ERK1/2). ERK1/2 phosphorylates Elk1, which leads to expression of c-Fos (75, 124, 125). c-Fos forms the activator protein-1 (AP-1) complex with c-Jun. c-Jun in turn stems from the VAV1-Rac1 pathway or from the JNK/p38 pathway (126–129). AP-1 acts as a transcription factor in the nucleus and associates with NFAT (126, 129,

130). The NFAT-AP-1 complex is central in controlling T-cell proliferation, survival, and proliferation (75, 114, 122, 131–135).

T-cell activation mediated only by TCR-dependent downstream signals results in anergy (75). Co-stimulatory signals are essential for sufficient stimulation of T cells. Engagement of CD28 leads to the recruitment and activation of phosphatidylinositol 3-kinase (PI3K) (75, 136, 137). PI3K catalyses the reaction of PIP2 to phosphatidylinositol (3,4,5)-triphosphate (PIP3) (75, 136, 137). This leads to the activation of phosphoinositide-dependent kinase-1 (PDK1), which acts on several downstream targets (75). On the one hand, PDK1 binds PKCθ and CARMA, thereby enhancing NF-κB signalling (138, 139). One the other hand, Protein kinase B (AKT) gets recruited to PIP3 together with PDK1 (140, 141). PDK1 phosphorylates AKT at Thr308, whereas AKT phosphorylation at Ser473 is mediated by mechanistic target of rapamycin (mTOR) complex (mTORC) 2 (142–147). Activated AKT inactivates GSK-3, which leads to prolonged NFAT translocation to the nucleus, and therefore, prolonged *Il2* expression (75, 148–150).

Further, AKT activation is tightly intertwined with mTOR signalling, since AKT is involved in mTORC1 activation, and is in turn activated by mTORC2 (140–146, 75). mTOR signalling can also be affected by other signalling pathways. For example, mTORC1 can be activated by the Ras-MAPK signalling pathway, facilitated by ERK1/2 or RSK (151, 152). mTORC1 and mTORC2 also show a complex interplay of activation and/or inhibiting each other via upstream or downstream effectors. (153–155). mTORC1 and mTORC2 control several cellular processes, among which are cell proliferation, metabolism, autophagy, cell survival, or cytoskeletal organisation (153–155). mTOR also presents an important link of the environment and metabolism, since mTOR signalling integrates environmental inputs by nutrient sensing or sensing of growth factors, and translating this into regulation of metabolism downstream of mTOR. Moreover, mTORC1 promotes differentiation into Th1 and Th17 cells, and inhibits differentiation into Th2 and Treg cells, whereas mTORC2 promotes differentiation into Th1 cells and Th2 cells, and inhibits differentiation into Treg cells (153, 154).

PI3K-AKT-mTOR signalling affects production of cytokines upon T-cell activation, *e.g.* IL-2, IFN-γ, TNF-α, IL-4, IL-5, IL-17, and IL-10 (156–159). AKT mediates PI3K-dependent effects on cytokine production, *e.g.* expression of IL-17, IFN-γ, and IL-5 (156). mTOR has shown to control translation of IL-2, TNF-α, and IFN-γ via AU-rich elements in cytokine 3'-UTRs (159). Taken together, PI3K-AKT-mTOR signalling can be affected by several regulators, and is contributing to several cellular functions of CD4+ T cells upon activation, prominently proliferation, survival, cytokine production, and differentiation.

Metabolism in T cells is tightly intertwined with their effector functions. Quiescent T cells, which are naïve T cells or memory T cells, use the TCA cycle and oxidative phosphorylation (OXPHOS) for a more catabolic leaning metabolic profile, whereas activated effector T cells have an increased energetic demand to fuel the cell for an increase of biomass and proliferation (160). This is facilitated by an increase of glycolysis, the pentose phosphate pathway, glutaminolysis, or lipid synthesis (160). A prominent observation regarding metabolism of activated effector T cells is presented by the Warburg effect (160). Under normal conditions, glycolysis is performed predominantly under anaerobic conditions. However, the Warburg effect describes increased fermentation of glucose under aerobic conditions, which results in the production of lactate (161). Metabolic profiles are not only distinct between quiescent and effector T cells, but also between different T-helper subsets (160). Tregs rely predominantly on OXPHOS and fatty acid oxidisation, whereas Th1, Th2, and Th17 cells predominantly perform aerobic glycolysis to meet their metabolic demands (160). In summary, metabolic profiles of T cells are coupled to their activation and differentiation status.

TCR downstream signalling as well as co-stimulatory and co-inhibitory signalling pathways form a complex network, which can be affect by a plethora of adaptor proteins, phosphate kinases, and other mediators. Understanding the signalling processes that orchestrate T-cell functions and unravelling the role of insufficiently characterised players enables identification of potential targets for treatment of immune deficiencies, cancer, autoimmunity, or chronic inflammation.

3.2. Xenotropic and polytropic retrovirus receptor 1 (XPR1)

Xenotropic and polytropic retrovirus receptor 1 (XPR1) is the only known inorganic phosphate exporter in metazoans. The protein sequence of XPR1 consists of 696 and 695 amino acids long, in human and mouse, respectively. The structure of human XPR1 is depicted in Figure 4. XPR1 is comprised of a N-terminal SYG/PHO/XPR1 (SPX) domain, a transmembrane core domain featuring ten transmembrane domains, an ERD1/XPR1/SYG1 (EXS) domain, and a C-terminal loop (Figure 4A). Several cryo-electron microscopy (EM) studies in the last two years revealed that XPR1 forms homodimers (Figure 4B), and different models for XPR1-mediated phosphate export have been proposed and discussed (162–166). Independently of the proposed mechanism, binding of an inositol pyrophosphate entity (*e.g.* IP6, IP7, or IP8) to the SPX domain has been found to regulate phosphate export (Figure 4B) (162–166).

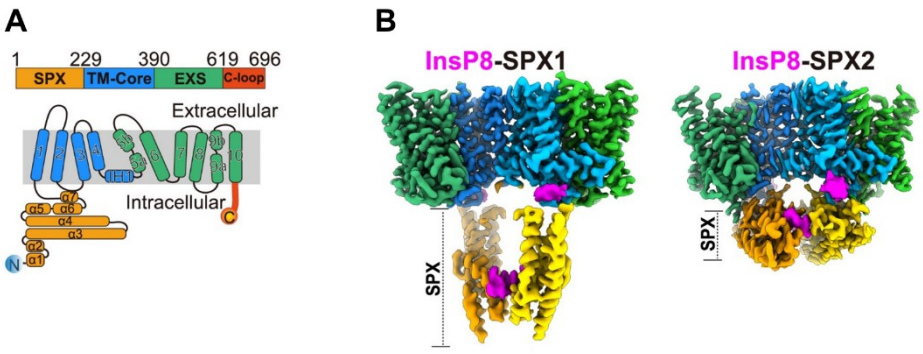

Figure 4: Structure of human XPR1. A: Schematic representation of XPR1 domain structure. SPX: SYG/PHO/XPR1 domain, TM-core: transmembrane core domain, EXS: ERD1/XPR1/SYG1 domain, C-loop: C-terminal loop. **B**: Structure of XPR1 homodimer in interaction with 1,5-InsP8 (IP8), showed from side view in two different conformations. Figure modified from (165).

In humans, XPR1 dysfunction is associated with different pathologies. Autosomal-dominant missense mutations in the SPX domain of XPR1 have been identified as a driver for primary familiar brain calcification (PFBC) (167–171). PFBC is a neurodegenerative disease characterised by calcium phosphate deposits in the basal ganglia, subcortical white matter, thalamus, and cerebellum of the brain, leading to neuropsychiatric and motor symptoms (167, 169, 171–173). XPR1 mutants identified in PFBC are found to cause accumulation of intracellular phosphate, which leads to development of the calcium phosphate deposits (169, 171, 172, 174).

Elevated expression of XPR1 has been found in ovarian and uterine cancer, and has been identified as a therapeutic vulnerability for cancer progression (175, 176). XPR1 is suspected to suppress autophagy in cancer cells via affecting the PI3K-AKT-mTOR-pathway, thereby controlling the presentation of MHC-I on the surface of tumour cells (175). Inhibition of XPR1, phosphate efflux, or autophagy has been shown to reduce tumour cell viability (175, 176).

A global homozygous knockout of *Xpr1* in mice is lethal. Studies of heterozygous *Xpr1* knockout in mice showed developmental defects as well as calcifications in the placenta and in brain vasculature (177, 178). The is accompanied by microgliosis which is not restricted to the sites of calcification, indicating a role of XPR1 for inflammation (178).

Conditional knockout of *Xpr1* in renal tubule of mice resulted in dysregulated phosphate homeostasis by proximal tubular dysfunction (179). Further, pharmacological inhibition or deficiency of XPR1 in platelets has been shown to dysregulate phosphate homeostasis due to impaired phosphate export, leading to polyphosphate (polyP) accumulation. PolyP is an inorganic molecule made up of tens to hundreds of phosphate molecules, which are linked by energy-rich phosphoanhydride bonds. Activated platelets release and expose membrane-bound polyP to activate coagulation factor XII in blood plasma, which results in contact

activation and thrombosis (180–182). Therefore, impaired phosphate export and elevated polyP levels by platelet-specific XPR1 deficiency increase thrombus formation *in vitro* and *in vivo* (180). Recently, our working group found that CD4+ T cells accumulate polyP upon activation, and that modulation of intracellular polyP affects CD4+ T-cell functions (Kröger *et al.*, manuscript in preparation).

While current studies on XPR1 mainly address XPR1 as a regulator of phosphate homeostasis via its phosphate export function, there is also evidence of XPR1 regulating trafficking of other proteins. This has been shown for the phosphate importer phosphate transporter 1 (PiT1) in human cell lines. XPR1 and PiT1 interact and co-localise in a vesicular compartment positive for the lysosomal marker lysosomal-associated membrane protein (LAMP)1 (183, 184). During XPR1 deficiency or pharmacological inhibition of the XPR1-mediated phosphate export, PiT1 is degraded (184), indicating a role of XPR1 for regulating function of other proteins by controlling their localisation, trafficking, and/or degradation. Notably, although XPR1 is the only known mammalian phosphate exporter so far, genetic deletion of *XPR1* in these studies decreased, but did not completely abrogate phosphate efflux in cell culture experiments, indicating functional redundancy and possible compensation for XPR1 loss regarding phosphate export.

Another example for XPR1 being potentially involved with trafficking is XPR1's interaction with the cargo transporting protein sorting nexin 27 (SNX27) (185, 186). Interestingly, the C-terminal end of XPR1 appears to regulate phosphate channelling as well as XPR1 localisation to intracellular organelles (184), which led to the assumption that XPR1 may act via dynamic non-export mechanisms that depend on biological context (187).

Interaction networks of XPR1 that contribute to its function in specific cell types are not fully understood yet. However, a recently identified protein interaction partner of XPR1 is kinase D interacting substrate 220 (Kidins220), also known as ankyrin repeat-rich membrane spanning (ARMS). Kidins220 is a multi-transmembrane protein that has 93 % protein sequence homology consisting of 1771 and 1793 amino acids in humans (NP_065789.1) and mice (NP_001074847.1), respectively. By its multiple interaction sites, such as 11 ankyrin repeats, a proline-rich binding site for the CrkL adaptor protein at the C-terminal region, a kinesin light chain interacting motif, and a PDZ binding motif, Kidins220 has been shown to interact with various other proteins, *e.g.* Rho guanine nucleotide exchange factor (RhoGEF), SNX27, kinesin light chain 1/2, protein kinase D, α-syntrophin, CD3-ζ, and B-Raf. Moreover, Kidins220 emerged as an adaptor protein that is involved in protein trafficking of interaction partners, thereby contributing to various cellular functions, *e.g.*, neuronal differentiation and development, neuroprotection, cancer pathogenesis, and regulation of immune responses

(188–197, 185). Importantly, Kidins220 deficiency in T cells leads to impairment of sustained ERK signalling and consequently, decreased expression of IL-2 and CD69 as well as decreased Ca^{2+} responses (197).

XPR1 and Kidins220 expression in different tissues appears to be correlated (165, 176). In 2025, two different groups published cryo EM analysis of XPR1's phosphate export mechanism, and validated that Kidins220 interacts with XPR1 (165, 166). Dysregulated phosphate homeostasis mediated by the XPR1-Kidins220 complex has been shown to be a therapeutic vulnerability in ovarian cancer (176). Thus, it has been proposed that interaction of Kidins220 and XPR1 plays an important role in regulating XPR1-mediated phosphate export, however the impact of a disrupted Kidins220-XPR1 interaction on signalling, trafficking, and its consequences *in vivo* remain elusive (165, 166).

Particularly, interactions of both Kidins220 and XPR1 with other proteins in the context of immune cell signalling and complex formation, like the IS, the TCR or BCR, the SNX27-retromer, endosomes, or lysosomal complexes (185, 186, 195, 197–206) suggest a role of XPR1 in immunoregulation. Investigating XPR1 in T cells may therefore help to reveal novel therapeutic approaches to modulate immune responses.

3.3. Aim of the study

This work aims to define the role of XPR1 for CD4+ T-cell functions. We used a mouse model with a conditional knockout of *Xpr1* in CD4+ T cells to characterise T-cell development in the thymus, and to analyse activation status, proliferation, differentiation, and cytokine production of CD4+ T cells *ex vivo*. Moreover, we investigated TCR downstream signalling pathways to unravel altered CD4+ T-cell functions due to XPR1 deficiency. Further, we crossed the conditional *Xpr1* knockout mice with *Marilyn* mice featuring a transgenic TCR, enabling us to elicit antigen-specific responses by stimulation with the cognate H-Y antigen. With this, we could validate our results in a model of physiological antigen-specific CD4+ T-cell activation and clonal expansion. Moreover, we performed siRNA-mediated knockdown of *XPR1* in human Jurkat cells to confirm XPR1-dependent immune functions in a translational approach. To unravel the molecular mechanism by which XPR1 regulates CD4+ T-cell functions, we analysed interaction of XPR1 with putative interaction partners, and addressed previous strategies to modulate XPR1 functions with viral ligands or small molecule inhibitor UNC7467. As a novel approach, we devised a membrane-permeable peptide (Tat-X) featuring the last 25 amino acids of XPR1's C-terminal loop to interfere with XPR1-mediated complex formation in a competitive manner, especially to test the hypothesis that targeting the interaction of XPR1 and Kidins220 is a potential tool to modulate CD4+ T-cell responses.

Taken together, this work aims to identify XPR1-dependent mechanisms that regulate signalling and molecular interactions in CD4+ T cells with implications for immune responses *in vivo*, and to reveal XPR1 as therapeutical target for immunomodulation in the future.

4. Results

4.1. Characterisation of mice with T-cell specific XPR1 deficiency

4.1.1. XPR1 is conditionally deleted in CD4+ T cells of cKO mice

XPR1 is a transmembrane protein and phosphate exporter that has been shown to affect protein trafficking and complex formation of adapter proteins that influences T-cell stimulation (185, 176, 197). Further, XPR1 impacts on intracellular concentrations of polyP which mediates immune activation (Kröger *et al.*, manuscript in preparation). Hence, XPR1 may represent a suitable target for modulation T-cell responses.

In order to address XPR1's role for CD4+ T-cell functions, we generated *Xpr1* knockout mice with conditional deletion in T cells (Figure 5A): mice with a floxed *Xpr1* sequence were cross-bred with mice expressing the Cre recombinase under the control of the *Cd4* promoter. Control *Cd4-Cre*$^{-}$*Xpr1*$^{fl/fl}$ mice ("CTL"), heterozygous *Cd4-Cre*$^{+}$*Xpr1*$^{+/fl}$ mice ("cHET"), and conditional *Xpr1* knockout *Cd4-Cre*$^{+}$*Xpr1*$^{fl/fl}$ mice ("cKO") were analysed. In early experiments, we also analysed *Cd4-Cre*$^{+}$ *Xpr1*$^{+/+}$ ("CTL*") instead of *Cd4-Cre*$^{-}$*Xpr1*$^{fl/fl}$ mice as the CTL genotype, as indicated in the figure legends. We found no differences between CTL and CTL* mice. While *Xpr1* deficiency causes embryonic lethality (179), mortality rate and health burden was unaffected in cKO mice compared to the *Cd4-Cre*+ reporter line, cHET, and cKO groups.

To confirm genetic ablation of *Xpr1*, CD4+ T cells were analysed by qPCR (Figure 5B) and immunoblots (Figure 5C). *Xpr1* expression was significantly decreased in cHET and cKO CD4+ T cells compared to CTL CD4+ T cells with a fold change of 0.47 ± 0.04 and 0.18 ± 0.07, respectively (Figure 5B). Similarly, when using rabbit-derived polyclonal α-XPR1 antibodies (14174-1-AP, Proteintech), the intensity of the XPR1 double band at around 82 kDa in immunoblot analyses was markedly decreased in the cKO sample compared to CTL and cHET samples (Figure 5C). In additional immunoblots utilising mouse-derived monoclonal α-XPR1 antibodies (2G8, Sigma-Aldrich), unspecific bands at several molecular weights were detected, however the putative specific double band at the expected molecular weight of XPR1 (82 kDa) displayed a decreased intensity in the cKO sample as well.

Taken together, a CD4+ T-cell specific *Xpr1* knockout mouse was successfully generated, allowing for the analysis of XPR1 functions in CD4+ T-cell responses.

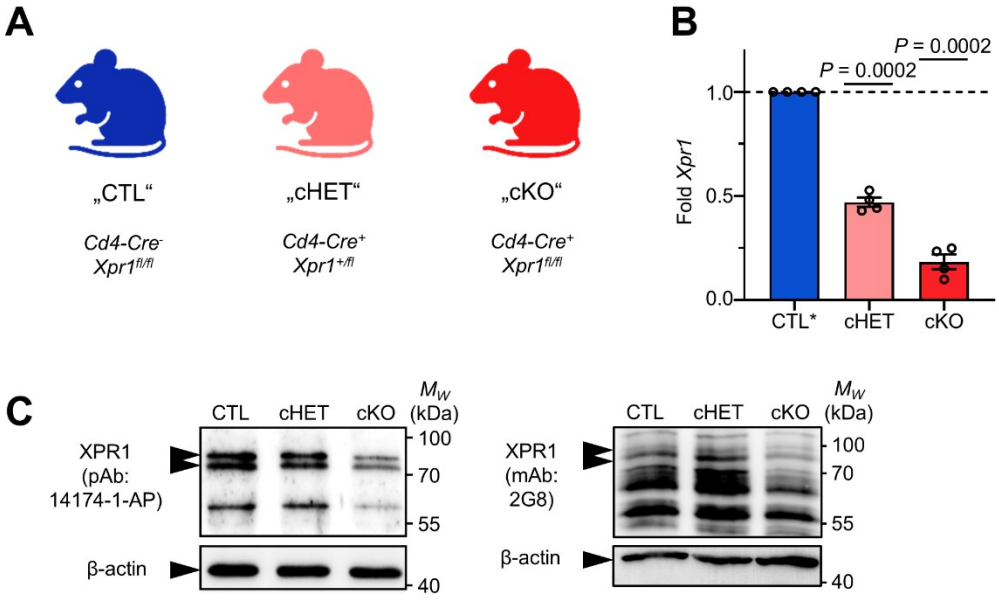

Figure 5: Conditional knockout of Xpr1 in CD4+ T cells. A: Schematic overview of the analysed genotypes, depicted as “CTL” (*Cd4-Cre⁻ Xpr1$^{fl/fl}$*), “cHET” (*Cd4-Cre⁺ Xpr1$^{+/fl}$*), and “cKO” (*Cd4-Cre⁺ Xpr1$^{fl/fl}$*). **B**, **C**: CD4+ T cells isolated by positive selection from mice with indicated genotype were analysed by qPCR (**B**) and immunoblotting (**C**) to validate reduced *Xpr1* transcription and XPR1 protein expression, respectively. CTL* corresponds to *Cd4-Cre⁺ Xpr1$^{+/+}$*. Detection of XPR1 was performed with two different primary antibodies as indicated in (**C**). Data is presented as mean ± SEM. Statistical analysis: One sample *t* test (**B**), *n* = 4.

4.1.2. XPR1 deficiency impairs the development of thymocytes

To investigate the potential role of XPR1 for CD4+ T cells, lymphoid organs of XPR1 deficient mice were phenotypically characterised. First, T-cell development was addressed by flow cytometry analysis of thymocytes. Different developmental stages of T-cell progenitors in the thymus can be assessed by expression of the surface molecules CD4 and CD8. CD4 and CD8 surface levels were analysed by flow cytometry, and used to distinguish thymocytes at CD4-CD8- (double negative, “DN”), CD4+CD8+ (double positive, “DP”), CD4+CD8- (single positive CD4, “SP4”) and CD4-CD8+ (single positive CD8, “SP8”) stages, as shown in representative dot plots (Figure 6A, left). Quantification of SP4, SP8 and DP frequencies are shown in Figure 6A, right.

The frequency of SP4 cells was significantly lower in cKO thymus samples than in CTL and cHET samples. Similarly, cKO samples showed a significantly lower frequency of SP8 cells compared to CTL samples. Between CTL and cHET thymocytes, there was a tendency for a lower SP8 frequency in cKO cells. In contrast to this, the frequency of DP cells was significantly

increased in cKO thymocytes compared to CTL thymocytes, while the frequency of DP cells showed a slight increase in cHET thymocytes compared to CTL cells.

To ensure that the decrease of SP4 and SP8 proportions in cKO thymi also translates to absolute cells numbers, CTL and cKO SP4 and SP8 cells were counted (Figure 6B). Indeed, cKO samples showed reduced absolute numbers of SP4 and SP8 cells compared to CTL samples.

Since differential frequencies of DP as well as SP4/SP8 populations were observed between cKO and CTL thymi, we next analysed DN and DP progressive stages.

DN populations were assessed for their expression of CD44 and CD25 in order to analyse the frequencies of the developmental stages DN1-DN4 (Figure 6C). The frequency of CD44-CD25+ (DN3) cells was significantly increased in cKO DN thymocytes compared to CTL DN thymocytes. Compared to cHET DN thymocytes, cKO DN thymocytes showed a tendency for an increased DN3 proportion. Increased levels of DN3 cells indicate a developmental blockade at the DN3 stage and therefore, hint at an altered thymic development in the absence of XPR1 (207).

Further, DP populations were analysed in regard to their expression of CD69, TCR-β and CD5. CD69+TCR-β+ cells, which represent cells recently gone through positive selection (208, 209), were present at a significantly lower frequency in the DP population of cKO thymocytes compared to the CTL and cHET DP thymocyte populations (Figure 6D).

Additionally, the frequency of CD5+ cells was significantly decreased in cKO DP thymocytes compared to CTL or cHET DP thymocytes (Figure 6E). CD5 is a negative regulator of TCR signalling in the context of thymic development, and has a key role for functional tuning in selection processes (9, 22, 210). Low CD5 expression in DP thymocytes has been shown to be associated with enhanced positive and negative selection (22, 210, 211). Therefore, the observed decreased CD5 expression in cKO thymocytes compared to the control indicates altered selection processes.

In summary, thymic development and selection processes in cKO mice were altered compared to the control, resulting in decreased SP4 and SP8 frequencies, as well as differences of key markers in the DN and DP populations between CTL and cKO thymocytes.

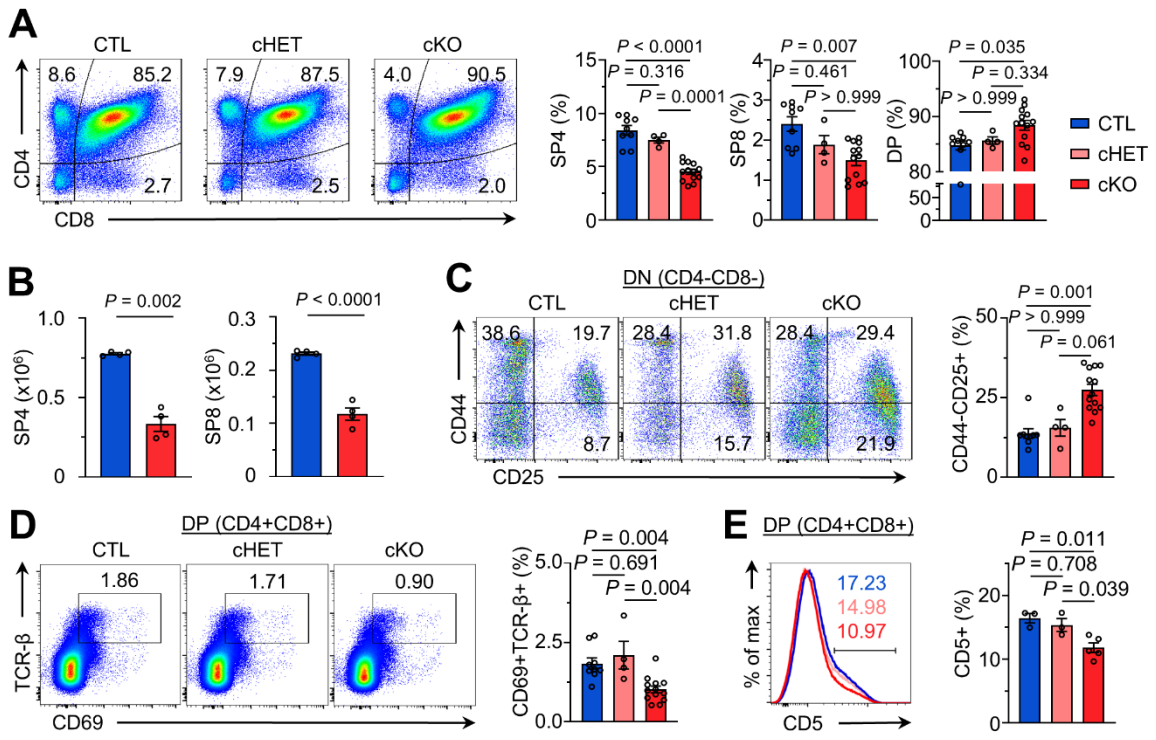

Figure 6: XPR1 deficiency alters the development of thymocytes. Thymi of CTL, cHET and cKO mice were dissected and analysed by flow cytometry. **A**: Representative dot plots and quantification of living single cell thymocytes, gated on single positive CD4 (SP4): CD4+CD8-, single positive CD8 (SP8): CD4-CD8+ and double positive (DP): CD4+CD8+ populations. **B**: Absolute counts of SP4 and SP8 thymocytes. **C**: Representative dot plots with indicated gating, and quantification of DN3 (CD44-CD25+) cells of the DN (CD4-CD8-) population. **D, E**: Representative dot plots with indicated gating, and quantification of CD69+TCR-β+ cells (**D**) and CD5+ cells (**E**) of the DP population. Data is presented as mean ± SEM. Statistical analysis: Ordinary one-way ANOVA followed by Tukey's multiple comparisons test (**A** for SP4, **D**, **E**); Kruskal-Wallis test followed by Dunn's multiple comparisons test (**A** for SP8 and DP, **C**); Welch's *t* test (**B** for SP4); Unpaired *t* test (**B** for SP8). *n* = 9, 4, 13 (CTL, cHET, cKO) for **A**, **C**, and **D**; *n* = 4 for **B**; *n* = 3, 3, 5 (CTL, cHET, cKO) for **E**.

4.1.3. CD4+ T-cell proportions in the periphery of cKO mice are decreased

To test if reduced levels of thymic SP4 and SP8 cell numbers in cKO mice translate to mature T-cell proportions in the periphery, T-cell populations in spleen and mesenteric lymph nodes (mLNs) from CTL*, cHET, and cKO mice were analysed (Figure 7).

In line with decreased SP4 proportions in the thymus, the frequency of CD4+ T cells was significantly decreased in spleens and mLNs from cKO mice compared to CTL* and cHET littermates: only about half of the size of CD4+ T-cell populations in spleens and mLNs ofcontrols was present in the respective lymphoid organs of cKO mice (spleen: 15.96 ± 0.50 % (CTL*), 14.91 ± 0.49 % (cHET), 9.38 ± 0.43 % (cKO). mLNs: 29.07 ± 2.05 % (CTL*), 27.49 ± 1.51 % (cHET), 18.57 ± 1.53 %). CD8+ T-cell proportions were similarly decreased (data not shown), and subsequent analyses focused on CD4+ T-cell phenotype and function.

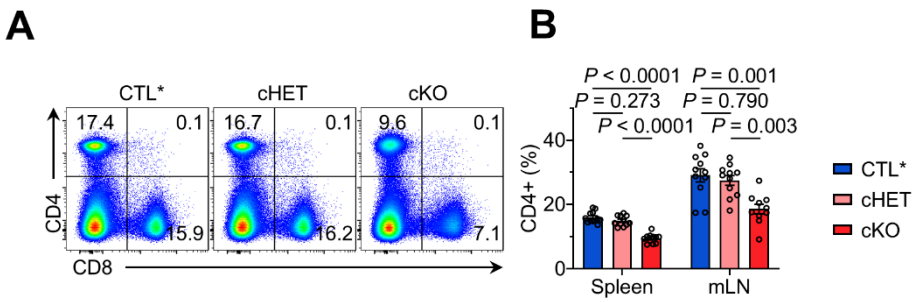

Figure 7: Proportions of CD4+ and CD8+ T cells in the periphery. Spleens and mesenteric lymph nodes (mLNs) of CTL, cHET and cKO mice were dissected and analysed by flow cytometry. **A**: Representative flow cytometry plots. **B**: Quantification of CD4+ T-cell proportions of indicated organs are shown. CTL* corresponds to *Cd4-Cre*$^{+}$ *Xpr1*$^{+/+}$ in this figure. Data is presented as mean ± SEM. Statistical analysis: Ordinary one-way ANOVA followed by Tukey's multiple comparisons test. *n* = 12, 11, 11 (CTL*, cHET, cKO) for spleen; *n* = 11, 11, 10 (CTL*, cHET, cKO) for mLNs.

4.1.4. PolyP levels are not altered in XPR1 deficient CD4+ T cells

XPR1 has been shown to facilitate phosphate export, which restricts polyP generation and pro-thrombotic activity in platelets (180). To address a potential role of XPR1 for the regulation of phosphate/polyP homeostasis in T cells, we analysed polyP levels of CD4+ T cells from CTL, cHET and cKO mice (Figure 8).

PolyP was isolated from unstimulated CD4+ T cells *ex vivo* using phenol-chloroform extraction to compare polyP levels and chain length distribution by urea PAGE and negative DAPI staining. To ensure comparable cell numbers were processed, equivalent aliquots of each sample were taken for lysis, and subsequent detection of β-actin via immunoblots prior to polyP isolation by phenol-chloroform extraction. In PAGE, polyP molecules are separated according to their chain length. To visualise polyP, negative DAPI staining was performed: while repeated UV light exposure does not disintegrate DAPI in proximity to DNA or RNA, polyP bound to DAPI facilitates its disintegration and polyP can be observed as black signal. DNA or RNA contaminations result in bright white signals.

In Figure 8A, isolated polyP from lysed CD4+ T cells was analysed by urea PAGE. Three samples per genotype and one control sample from a CTL* mouse were analysed. A synthetic polyP molecule "383-mer" was used as a polymer length reference. DNA/RNA contaminations were visible at the top of the gel, apparent by the white signal. In all lanes, polyP was detected by a black smear across the upper half of the gel. The intensity of the black smear did not differ between the three genotypes, as also indicated by densitometric quantification of the urea gel (Figure 8B). The immunoblot loading controls detecting β-actin showed comparable

intensities for each sample, with a slight decrease in intensity in the first CTL sample (Figure 8A).

For a more reliable quantification of polyP levels, Malachite Green Assays of unstimulated CD4+ T cells were performed after polyP extraction (Figure 8C). Between CTL, cHET and cKO CD4+ T cells, no significant differences in polyP levels were observed.

Taken together, these findings show that XPR1 deficiency does not alter polyP content or length distribution in CD4+ T cells, suggesting XPR1 is dispensable for polyP homeostasis in CD4+ T cells.

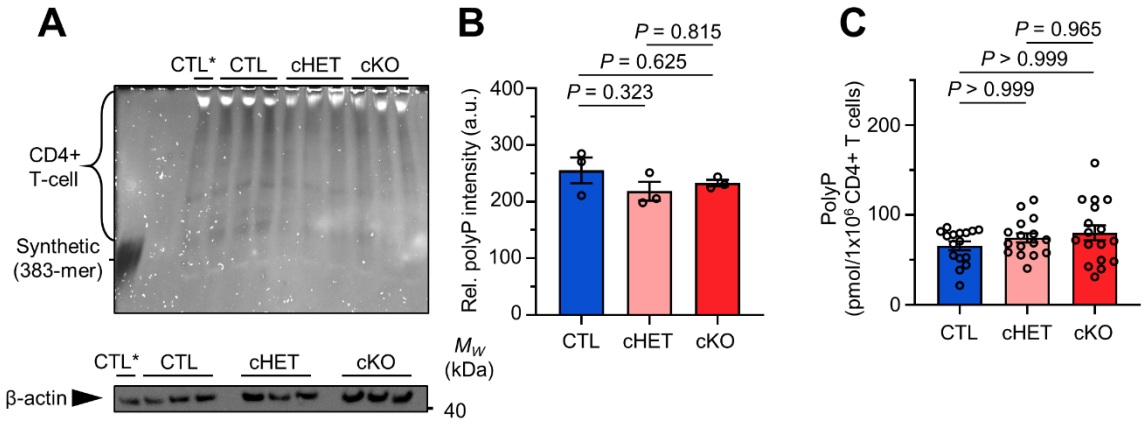

Figure 8: PolyP levels in XPR1 deficient CD4+ T cells are unchanged. PolyP was extracted from CD4+ T cells *ex vivo*. **A**: Top: Urea PAGE of polyP from 1x10^6 CD4+ T cells per lane. Bottom: As a loading control aliquots of lysates were analysed by β-actin immunoblotting before polyP extraction; CTL* corresponds to *Cd4-Cre*$^+$ *Xpr1*$^{+/+}$. **B**: Densitometric analysis of the urea PAGE gel shown in (**A**). **C**: PolyP content per 1x10^6 CD4+ T cells determined by Malchite Green Assays. Data is presented as mean ± SEM. Statistical analysis: Ordinary one-way ANOVA followed by Tukey's multiple comparisons test (**B**); Kruskal-Wallis test followed by Dunn's multiple comparisons test (**C**). *n* = 3 for **B**; *n* = 16, 16, 17 (CTL, cHET, cKO) for **C**.

4.1.5. XPR1 deficient CD4+ T cells display a hyperactivated phenotype upon stimulation

Since cKO mice possess a decreased frequency of circulating CD4+ T cells, we next investigated a potentially altered immune stimulation of these cells. For this, flow cytometry analysis of *ex vivo* isolated or *in vitro* stimulated CD4+ T cells was performed. PD-1, CD44, CD62L, CD25, and CD69 were included in the staining panel. PD-1 is an immune checkpoint molecule responsible for co-inhibitory signalling, and further an exhaustion marker (212). CD69 and CD25 are widely accepted to be early and late markers of T-cell activation, respectively, with an increased expression corresponding to higher activation (213). While CD44^{low}CD62L^{high} T cells have been identified as naïve, CD44^{high}CD62L^{low} T cells are

recognised as effector memory cells (214–217). Therefore, high CD44 expression and low CD62L expression correspond to an activated phenotype. Representative histograms with indicated gating as well as quantifications are shown in Figure 9. We found significantly increased proportions of CD69 on the surface of unstimulated cKO T cells *ex vivo* compared to the control (Figure 9A). For CD44, CD25, and PD-1, a tendency towards increased expression in unstimulated cKO T cells in comparison to CTL CD4+ T cells was apparent. For CD62L expression, no significant difference between CTL and cKO cells was observed. After 72 h of α-CD3/α-CD28 stimulation (Figure 9B), cKO CD4+ T cells showed significantly increased proportions of both CD44 and CD69 compared to CTL CD4+ T cells. For the other markers, no significant differences or trends were observed.

In summary, XPR1 deficient CD4+ T cells showed a tendency or a significant upregulation of CD44 and CD25 surface levels in naïve and stimulated CD4+ T cells. CD69 and PD-1 showed a tendency or a significant upregulation on unstimulated cKO cells, while there were no differences observed between stimulated CTL and cKO cells. This indicates that XPR1 deficiency results in an exhausted CD4+ T-cell phenotype. Further, a higher activation status without or with antibody-mediated stimulation was observed in XPR1 deficient CD4+ T cells.

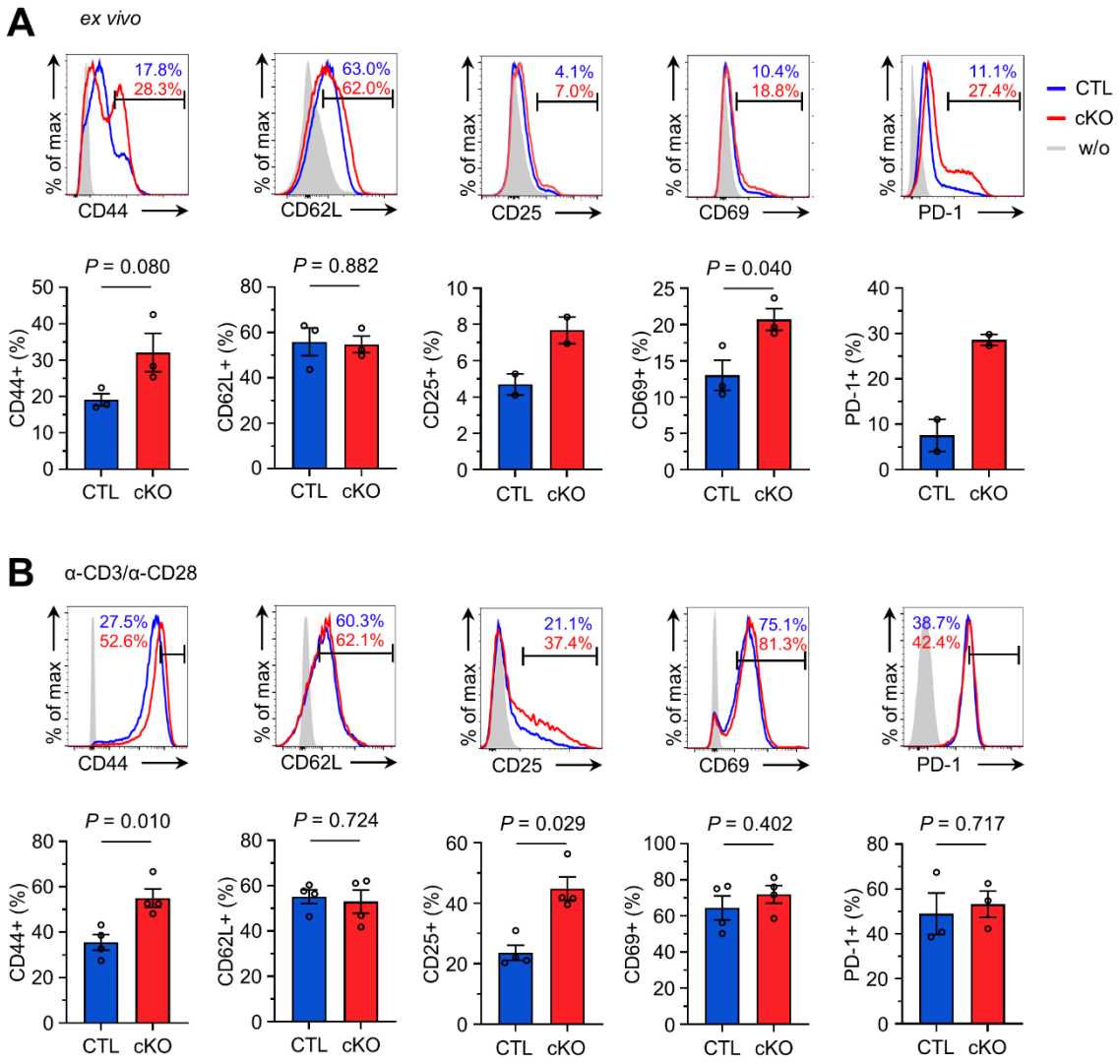

Figure 9: Activation marker panel of CD4+ T cells *ex vivo* or stimulated with α-CD3/α-CD28. Representative flow cytometry histograms and quantification of surface expression of CD44, CD62L, CD25, CD69, and PD-1. Unstained samples are labelled as "w/o". **A**: Analysis of CD4+ T cells *ex vivo*. **B**: Naïve CD4+ T cells were stimulated for 72 h with 5 µg/mL α-CD3 and 1 µg/mL α-CD28 before analysis. Data is presented as mean ± SEM. Statistical analysis: Unpaired *t* test (**A**, **B** for CD44, CD62L, CD69, and PD-1); Mann-Whitney test (**B** for CD25). *n* = 4 for **B** (CD44, CD62L, CD25, CD69), *n* = 3 for **A** (CD44, CD62L, CD69) and **B** (PD-1), *n* = 2 for **A** (CD25, PD-1).

Since overall these results of naïve and α-CD3/α-CD28 stimulated CD4+ T cells indicate a hyperactivated phenotype of cKO samples compared to the control, gene expression was analysed next. We performed an RNA microarray of naïve CD4+ T cells that were stimulated with α-CD3/α-CD28 for 6 h in collaboration with Dr. Timur Alexander Yorgan (Institute for Osteology and Biomechanics, University Medical Centre Hamburg-Eppendorf).

Results were filtered by removing hits for non-coding regions and hits that correspond to pseudogenes. Significant hits ($P < 0.05$) of differentially expressed genes with a fold change >|2| between CTL and cKO are presented in a volcano plot (Figure 10A) and listed in the appendix (Table 23). Overall, 60 genes showed significant up- or downregulation by >|2| fold.

Nine hits corresponded to TCR chains, with the fold change depicted in Figure 10B. Five of these hits corresponded to genes encoding for TCR-α J or V chains (*Traj57*, *Traj46*, *Traj59*, *Trav19*, *Trav2*), two genes encoded TCR-γ constant chains (*Tcrg-C4; Trgj4* and *Tcrg-C3*), and two genes encoded TCR-δ J or V chains (*Trdj1; Trdj2; Trdc* and *Trdv1*). This differential gene expression of TCR chains demonstrates an altered TCR repertoire under conditional knockout of *Xpr1*, further highlighting developmental differences as already shown in thymus analyses in section 4.1.2.

Figure 10C shows a heat map of the fold change for the remaining 51 differentially expressed genes, with 31 being upregulated and 20 being downregulated in stimulated cKO CD4+ T cells. The most prominent hit was *Il2* with a 23.2-fold higher expression in XPR1 deficient CD4+ T cells compared to the control. *Il2* encodes for the cytokine IL-2 which is a central player for CD4+ T-cell activation (73, 218, 219). Similarly, transcription of CD44 (*Cd44*), which is frequently used as a marker for CD4+ T-cell activation, was upregulated as well (215, 217). Further, the gene *Inpp4b*, which encodes for inositol polyphosphate-4-phosphatase, type II, 105kDa (INPP4B), a negative regulator of T-cell activation (220), was downregulated in this experiment. These hits indicate a hyperactivation of CD4+ T cells.

BHLHE40, also known as Dec1, is a transcription factor that is upregulated in a CD28 co-stimulation-dependent mechanism upon TCR stimulation (221–223). *Bhlhe40* was upregulated in stimulated cKO CD4+ T cells by 10.99-fold, indicating an important role of CD28 co-stimulation in the activation of cKO CD4+ T cells.

Interestingly, the gene *Tigit* was upregulated by 2.73-fold in cKO CD4+ T cells compared to the control. TIGIT is an inhibitory receptor, downregulating T-cell functions upon engagement by its ligand CD155 (26, 224).

Moreover, signalling via ERK or the Ca^{2+}/NFAT pathway was affected, apparent by upregulation of *Map3k8* and *Jun* and *Fos* (225–232, 126–129). Further, signalling via the PI3K/AKT/mTOR pathway appeared to be differentially regulated in cKO CD4+ T cells compared to the control as well, pointed out by upregulation of *Lif*, *Tspan31,* and *Tpi1,* as well as downregulation of *Itga6* and *Pdk1* (233–245, 138, 145). Most of these hits also have been shown to affect T-cell effector mechanisms, metabolism, or differentiation. Metabolism and differentiation of CD4+ T cells have also been shown to be linked to micro-RNA (miR)-155, Thioredoxin-1 (TXN1), and Selenoprotein 1 (SEPP1) (246–256). Differential gene expression of *Mir155*, *Txn1,* and *Sepp1* therefore indicated an effect on T-cell effector functions as well.

A presumed hyperactivation and altered signalling upon XPR1 abrogation in stimulated CD4+ T cells was further validated by pathway analysis of the differentially expressed genes using the publicly available software program Panther (www.pantherdb.org), which revealed a 27.7-

fold enrichment in interleukin signalling pathway and 10.0-fold enrichment in inflammation mediated by chemokine and cytokine signalling pathway (Figure 10D).

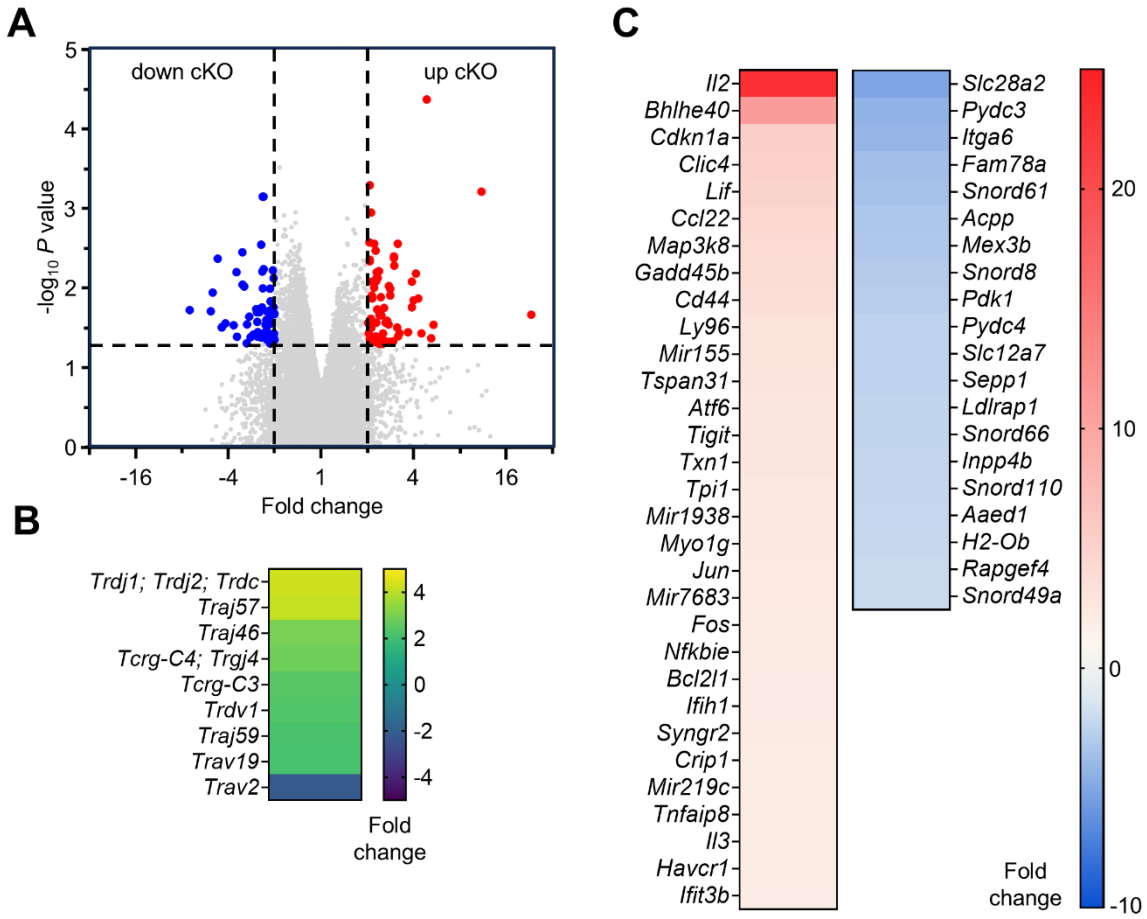

D

GO: 0005125 Cytokine activity

Pathway analysis (Panther version 19.0)	Fold enrichment	*P*-value	FDR
Interleukin signalling pathway	27.65	9.96×10^{-7}	8.02×10^{-5}
Inflammation mediated by chemokine and cytokine signalling pathway	10.04	1.34×10^{-4}	3.6×10^{-3}

Figure 10: Differential gene expression of stimulated cKO vs CTL CD4+ T cells. Naïve CD4+ T cells were isolated from CTL and cKO mice and stimulated for 6 h with 5 µg/mL α-CD3 and 1 µg/mL α-CD28. RNA was isolated and transcriptome analysis was done using the Clariom D mouse microarray. **A**: Differential gene expression between cKO and CTL samples shown in a volcano plot. Significant ($P < 0.05$) hits with a fold change >|2| are coloured in blue (higher expression in CTL cells) or red (higher expression in cKO cells). **B**: Heatmap showing the fold change of filtered TCR chain genes. **C**: Heatmap showing the fold change of remaining, filtered hits. **D**: Results of pathway analysis using gene ontology program Panther for GO: 0005125 cytokine activity. Data is from $n = 3$ independent experiments.

Taken together, RNA microarray data showed that XPR1 deficiency induces a hyperactivated expression profile in stimulated CD4+ T cells, especially pronounced by the elevated IL-2 expression. Effects on metabolism, differentiation, cytokine production, and TCR downstream

signalling are apparent. This is in line with the expression pattern of *ex vivo* isolated and *in vitro* stimulated CD4+ T cells lacking XPR1, confirming that XPR1 plays a role as negative regulator of T-cell hyperactivation.

4.2. Effector mechanisms of XPR1 deficient CD4+ T cells

Since section 4.1.5 shows a hyperactivated phenotype of XPR1 deficient CD4+ T cells in response to α-CD3/α-CD28 stimulation, we next addressed XPR1-dependent effector T-cell functions. For this, proliferation, differentiation into T-helper cell subtypes, cytokine production, and metabolism were analysed. Further, serum IgG and IgM levels were measured to identify potential autoimmunity in mice with XPR1 deficient CD4+ T cells.

4.2.1. XPR1 deficient CD4+ T cells are hyperproliferative

CD4+ T cells isolated from CTL and cKO mice were stained with a proliferation dye and stimulated with α-CD3/α-CD28, phorbol 12-myristate 13-acetate (PMA)/ionomycin, or staphylococcal enterotoxin B (SEB) for 72 h (Figure 11). While α-CD3/α-CD28 engages the TCR-CD3 complex and CD28 for T-cell stimulation, PMA activates protein kinase C (PKC), whereas ionomycin induces Ca^{2+} influx via its function as an ionophore (257–259). SEB is a superantigen and a potent activator of T cells by binding polyclonally to TCR-Vβ, MHC-II, CD28, and B7, leading to toxic shock, sepsis, and cytokine storm (260–264).

For the analysis, the intensity of the proliferation dye was compared between samples by flow cytometry. With each cell division, the intensity of the dye is diluted by half, leading to another population with lower fluorescence intensity. The lower the intensity of the proliferation dye is, the higher was the proliferation activity of analysed cells. T cells that underwent three division cycles or more were defined as populations with high proliferative capacity. The resulting gate is indicated in the representative histograms (Figure 11A).

Compared to CD4+ T cells from CTL mice, XPR1 deficiency significantly increased the proportion of cells with high proliferative capacity when stimulated with α-CD3/α-CD28 (Figure 11B). In contrast, stimulation with PMA/ionomycin (Figure 11C) and SEB (Figure 11D) did not lead to differences in proliferative capacity between CTL and cKO CD4+ T cells.

In summary, XPR1 deficiency increased proliferation of CD4+ T cells upon antibody-mediated stimulation *in vitro*, whereas overstimulation of TCR-mediated signalling pathways abrogated the proliferative advantage of cKO T cells.

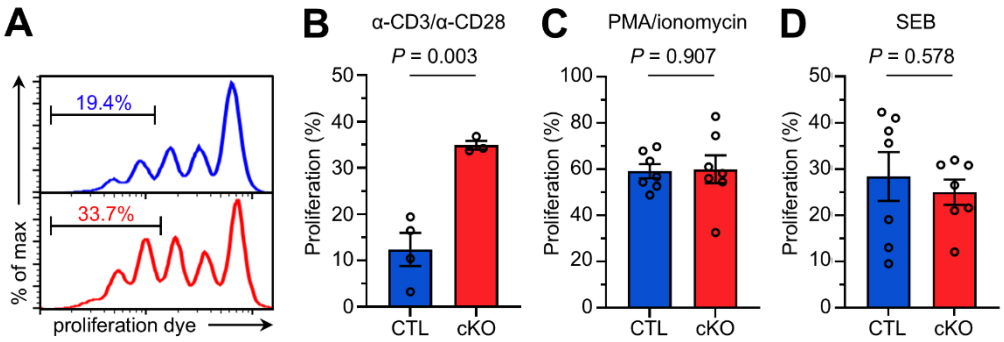

Figure 11: Antibody-mediated proliferation is increased in XPR1 deficient CD4+ T cells. CD4+ T cells were isolated from CTL and cKO mice, stained with eFluor450 cell proliferation dye, and stimulated for 72 h. **A**: Representative flow cytometry histograms of stimulation with α-CD3/α-CD28. **B, C, D**: Quantification of populations with high proliferative capacity. Stimulation was done with 5 µg/mL α-CD3 and 1 µg/mL α-CD28 (**B**), 50 µg/mL PMA and 1 µg/mL ionomycin (**C**), or 1 µg/mL SEB (**D**). Data are presented as mean ± SEM. Statistical analysis: Unpaired *t* test. *n* = 4, 3 (CTL, cKO) for **B**, *n* = 7 for **C** and **D**.

4.2.2. Cytokine expression levels are increased in CD4+ T cells

During stimulation of CD4+ T cells, the cytokine environment is affecting the differentiation into different T-helper cell subtypes like Th1-, Th2-, Th17 or iTreg cells. These subpopulations differ in their immunological functions (7, 36): Th1 and Th17 cells protect from bacterial and fungal infections, respectively. Th2 cells promote humoral immunity and drive allergic reactions. Regulatory T cells on the other hand are pivotal for antiinflammatory mechanisms that suppress hyperreactive immune responses that would otherwise cause detrimental tissue damage.

In order to address XPR1's role for regulation of T-helper cell differentiation, *in vitro* differentiation assays were performed. For this, CTL and cKO CD4+ T cells were isolated and stimulated with α-CD3/α-CD28. During stimulation and 72-120 h of cultivation, specific combinations of cytokines and antibodies were added to allow optimal skewing conditions for Th1-, Th2-, Th17-, or iTreg-cell differentiation. Characteristic transcription factors and cytokines were subsequently stained and analysed using flow cytometry.

As shown in Figure 12, expression levels of the proinflammatory cytokines TNF-α and IFN-γ were significantly increased upon Th1-cell differentiation of CD4+ T cells from cKO mice compared to CTL mice. In contrast, T-bet expression indicating *bona fide* Th1 cells was significantly decreased in CD4+ T cells lacking XPR1 compared to the control group.

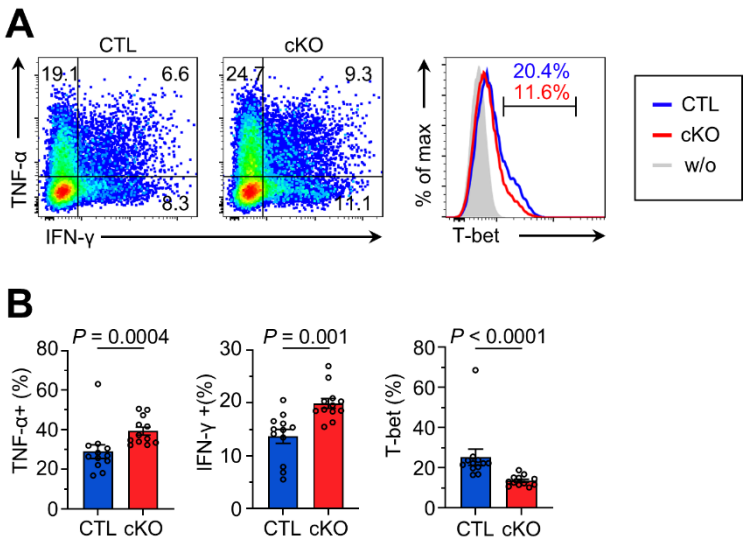

Figure 12: XPR1 deficiency increases TNF-α- and IFN-γ expression under Th1-skewing conditions. CD4+ T cells isolated from CTL and cKO mice were stimulated *in vitro* in the presence of Th1-skewing conditions. After 72 h, CD4+ T cells were restimulated and secretion of cytokines was blocked for four hours prior flow cytometric analysis. **A**: Representative dot plots and histograms with indicated gating of living CD4+ T cells expressing TNF-α and IFN-γ (left) and T-bet (right). Unstained samples are labelled as "w/o". **B**: Quantification of respective T-cell populations. Data are presented as mean ± SEM. Statistical analysis: Mann-Whitney test (TNF-α, T-bet); Unpaired *t* test (IFN-γ). *n* = 12 from four independent experiments.

For analysis of Th2-cell differentiation, the expression of IL-4, IL-5, and GATA-3 was assessed by flow cytometry, as shown in representative histograms (Figure 13A) and quantifications (Figure 13B). CD4+ T cells from cKO mice showed a tendency, albeit statistically not significant, towards reduced IL-4 expression upon Th2-cell differentiation, whereas IL-5 expression did not differ between cKO and CTL groups. Also, GATA-3 expression under Th2-skewing conditions was comparable in CD4+ T cells between cKO and CTL mice, suggesting that XPR1 deficiency does not have an impact on the differentiation of Th2 cells *in vitro*.

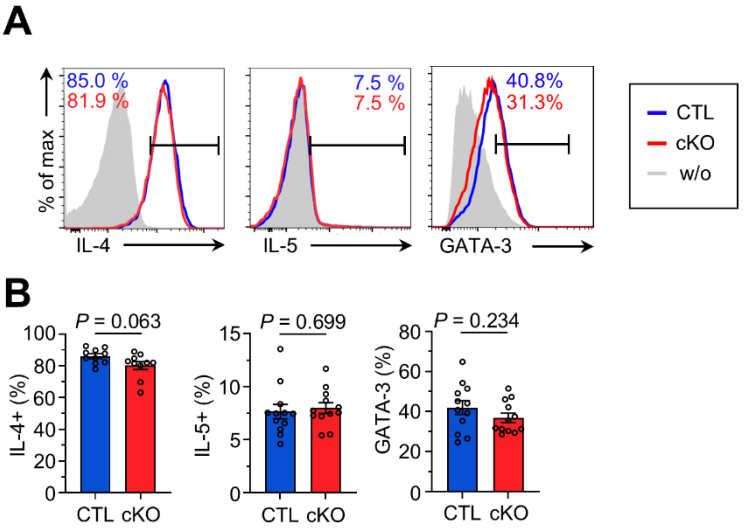

Figure 13: Th2-cell differentiation is not affected by XPR1 deficiency. CD4+ T cells isolated from CTL and cKO mice were stimulated *in vitro* in the presence of Th2-skewing conditions. After 72 h, CD4+ T cells were restimulated and secretion of cytokines was blocked for four hours prior flow cytometric analysis. **A**: Representative histograms with indicated gating of living CD4+ T cells expressing IL-4, IL-5, or GATA-3. Unstained samples are labelled as "w/o". **B**: Quantification of respective T-cell populations. Data are presented as mean ± SEM. Statistical analysis: Mann-Whitney test (IL-4); Unpaired *t* test (IL-5, GATA-3). *n* = 10 for IL-4; *n* = 12 for IL-5, GATA-3; from four independent experiments.

To investigate XPR1-dependent effects for Th17-cell differentiation, the proinflammatory cytokines IL-17a and IL-22, and the Th17-specific key transcription factor Ror-γt were analysed (Figure 14). Differentiation into Th17 cells *in vitro* was done with two different methods: using a ready-made and now discontinued kit by R&D systems that contained differentiation medium with unknown additives (Figure 14B), or using a differentiation protocol based on a mix of cytokines and antibodies in known concentrations in complete RPMI T cell medium similar to differentiation protocols used for Th1, Th2, and iTreg cells (Figure 14C).

The former protocol resulted in slightly decreased IL-17a expression in XPR1 deficient CD4+ T cells in comparison to controls (Figure 14B). However, expression of IL-22 was significantly increased by almost 2-fold in CD4+ T cells from cKO mice compared to CTL mice. In contrast, Ror-γt showed a significantly decreased expression in CD4+ T cells lacking XPR1 compared to controls when using this kit for Th17-cell differentiation.

Paradoxically, the latter differentiation protocol led to a significantly higher IL-17a expression in CD4+ T cells from cKO mice than in CD4+ T cells from CTL littermates (Figure 14C). The proportion of T cells expressing IL-22 tended to be increased in the cKO group compared to the CTL group. Notably, the overall frequency of IL-22+ T cells was lower using this differentiation protocol compared to the kit, irrespective of the genotype. Induction of Ror-γt was comparable between protocols but did not differ in CD4+ T cells from CTL and cKO mice under Th17-skewing conditions with defined antibody/cytokine supplementation.

Summarised, differential IL-17a and Ror-γt expression in CD4+ T cells with or without XPR1 deficiency was dependent on the *in vitro* differentiation method. However, both Th17-cell differentiation protocols revealed an increased expression of IL-22 in CD4+ T cells from cKO mice compared to CTL mice.

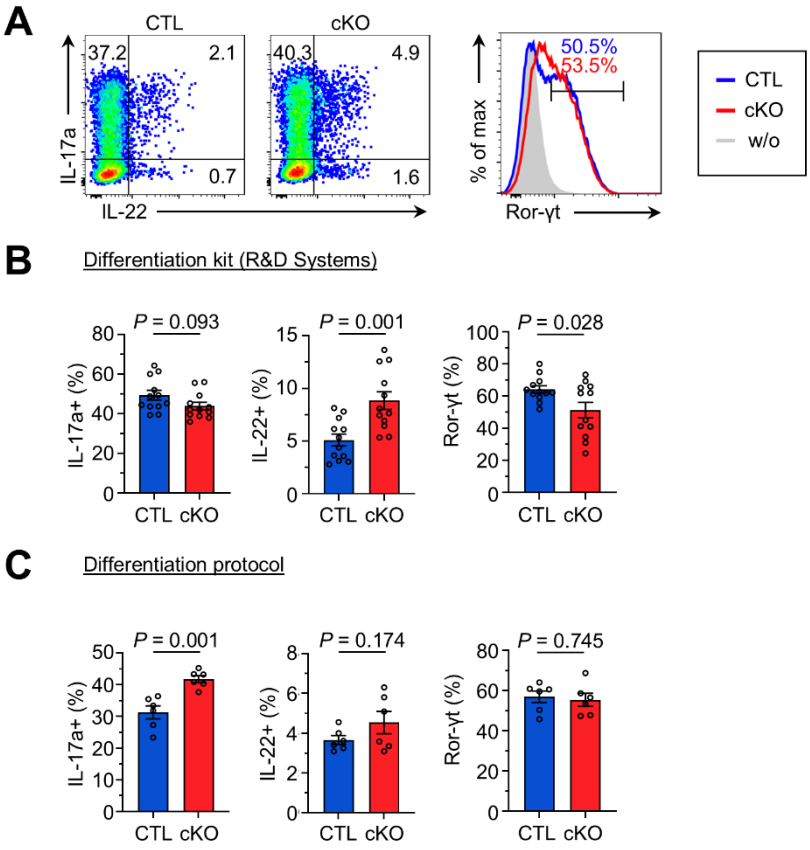

Figure 14: XPR1 deficiency increases IL-22 under Th17-skewing conditions. CD4+ T cells isolated from CTL and cKO mice were stimulated *in vitro* in the presence of Th17-skewing conditions. After 120 h, CD4+ T cells were restimulated and secretion of cytokines was blocked for four hours prior flow cytometric analysis. **A**: Representative dot plots or histograms with indicated gating of living CD4+ T cells expressing IL-17a, IL-22, or Ror-γt, after using the Mouse Th17 Cell Differentiation Kit for differentiation. Unstained samples are labelled as "w/o". **B, C**: Quantification of respective T-cell populations, either differentiated by using the Mouse Th17 Cell Differentiation Kit (**B**) or the differentiation protocol (**C**). Data are presented as mean ± SEM. Statistical analysis: Unpaired *t* test: **B** (IL-17a, IL-22), **C**; Welch's *t* test: **B** (Ror-γt). *n* = 12 for **B** from four independent experiments; *n* = 6 for **C** from three independent experiments.

In addition to differentiation into proinflammatory T-cell subsets, the impact of XPR1 deficiency on differentiation into antiinflammatory iTreg cells was investigated. Representative histograms and respective quantification of CD4+ T cells expressing CD25, IL-10 and Foxp3 after *in vitro* differentiation into iTreg cells are shown in Figure 15. While CD25 expression did not differ between CTL and cKO groups, the frequency of T cells from cKO mice that express IL-10 tended to be slightly increased in compared to T cells from CTL mice, but not significantly. In contrast, iTreg-skewing conditions induced significantly lower frequencies of Foxp3 expressing T cells from cKO mice than from CTL littermates.

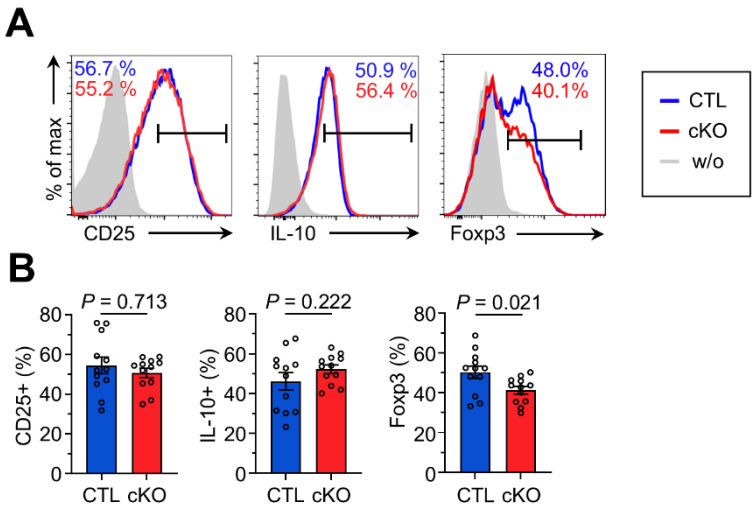

Figure 15: Differentiation into Foxp3+ iTreg cells is decreased in XPR1 deficient CD4+ T cells. CD4+ T cells isolated from CTL and cKO mice were stimulated *in vitro* in the presence of iTreg-skewing conditions. After 72 h, CD4+ T cells were restimulated and secretion of cytokines was blocked for four hours prior flow cytometric analysis. **A**: Representative histograms with indicated gating of living CD4+ T cells expressing CD25, IL-10, or Foxp3. Unstained samples are labelled as "w/o". **B**: Quantification of respective T-cell populations. Data are presented as mean ± SEM. Statistical analysis: Mann-Whitney test (CD25); Welch's *t* test (IL-10); Unpaired *t* test (Foxp3). *n* = 12.

Reduced transcription factor expression and concomitantly elevated cytokine production *in vitro* indicates a dysregulation of T-cell differentiation through *Xpr1* gene deletion. Since the gene expression array in section 4.1.5 showed that XPR1 deficiency significantly upregulated IL-2, a cytokine pivotal for T-cell activation and with a complex role in regulating T-cell differentiation programs, *e.g.* by priming and/or maintaining Th1- and Th2-differentiation (73), supernatants from *in vitro* differentiation experiments were analysed by IL-2 ELISA. IL-2 concentrations were determined in cell culture supernatants of CD4+ T cells from CTL or cKO mice collected after 72-120 h in respective skewing conditions (Figure 16).

In all differentiation conditions, IL-2 concentrations were significantly higher in supernatants of CD4+ T cells from cKO mice compared to those from CTL mice. This difference was most striking for the Th1- and Th17-cell differentiation, with about 5-fold increased IL-2 production in XPR1 deficient T cells compared to controls.

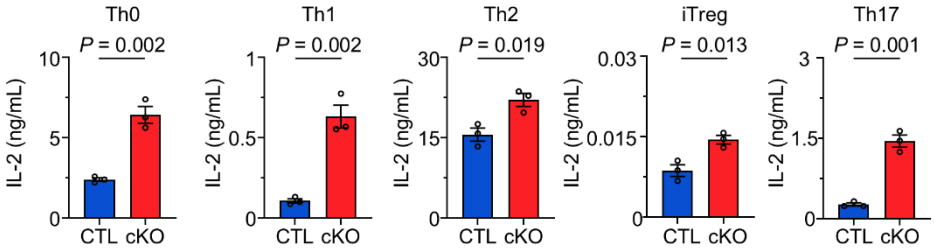

Figure 16: IL-2 concentration is increased in cKO CD4+ T-cell supernatants after differentiation. CD4+ T cells were isolated from CTL and cKO mice and treated with Th0, Th1, Th2, iTreg-, or Th17-skewing conditions for *in vitro* differentiation assays. Th17 differentiation was done using the Mouse Th17 Cell Differentiation Kit. After 72 h or 120 h, supernatants were collected and IL-2 concentration was determined by ELISA. Data are presented as mean ± SEM. Statistical analysis: Unpaired *t* test. *n* = 3.

Taken together, expression of characteristic cytokines of Th1 and Th17 subpopulations was significantly increased in XPR1 deficient CD4+ T cells under respective skewing conditions, namely IFN-γ, TNF-α, and IL-22. Characteristic cytokines of iTreg cells and Th2 cells were unaltered, while key transcription factor expression was slightly decreased in cKO cells compared to CTL cells. Additionally, XPR1 deficient CD4+ T cells released significantly more IL-2 compared to the control, which may delay their terminal differentiation or interfere with *bona fide* Th17 differentiation (265).

4.2.3. *XPR1* knockdown in Jurkat cells validated increased cytokine expression

Between mouse (NP_035403.1) and human (NP_004727.2) XPR1, there is a protein sequence homology of 95.3 %, making XPR1 a highly conserved protein. To address whether XPR1 deficiency promotes cytokine expression in human T cells as well, expression of *XPR1* was knocked down in Jurkat cells, an immortalised cell line derived from human T-cell leukaemia. Jurkat cells were treated with siRNA targeting *XPR1* transcripts (siXPR1) or scrambled control siRNA (siCtrl). Validation of a successful knockdown of XPR1 in siXPR1-treated Jurkat cells compared to siCtrl treatment is shown in Figure 17A and 17B: analysis of *XPR1* expression via qPCR 48 h after the transfection with siXPR1 revealed a reduction to 29.6 ± 3.8 % of the expression level in siCtrl treated Jurkat cells. Additionally, immunoblot analysis showed a reduced intensity of the XPR1 band at a height of 82 kDa 72 h after cells were transfected with siXPR1 compared to siCtrl treatment.

Establishing a knockdown of *XPR1*/XPR1 on gene and protein expression levels allowed for the subsequent investigation of cytokine gene expression in response to XPR1 reduction in Jurkat cells by qPCR (Figure 17C). 48 h after transfection, Jurkat cells treated with siXPR1 showed significantly increased expression of *TNFA*, *IFNG,* and *IL22* compared to cells treated with siCtrl. The highest increase was detected for *IFNG*, which displayed an about 2.75-fold elevated gene expression following XPR1 knockdown in Jurkat cells.

In summary, a siRNA-mediated knockdown of XPR1 in Jurkat cells led to increased expression of *TNFA*, *IFNG,* and *IL22*, matching the results of *in vitro* differentiation assays performed on XPR1 deficient CD4+ T cells from cKO mice.

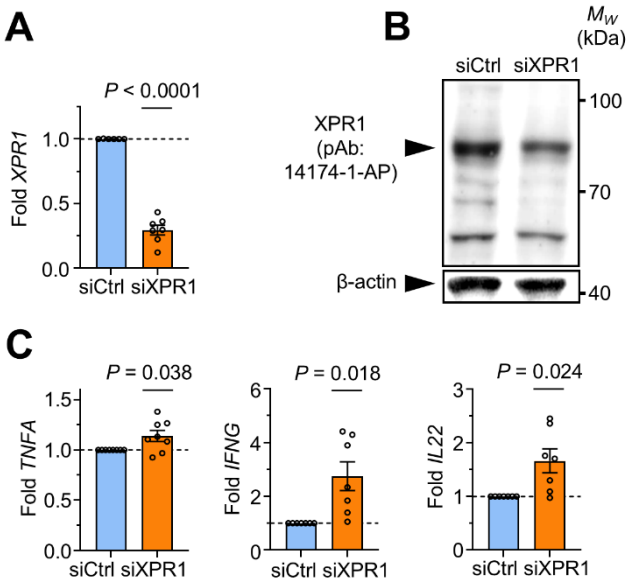

Figure 17: Knockdown of XPR1 in Jurkat cells promotes cytokine transcription. Knockdown of XPR1 in Jurkat cells was analysed. **A**: qPCR of *XPR1* transcription levels. **B**: Detection of XPR1 protein by immunoblotting with α-XPR1 polyclonal antibodies (14174-1-AP) 48 h and 72 h after transfection with indicated siRNAs, respectively. **C**: mRNA transcription levels of *TNFA*, *IFNG,* and *IL22* after siRNA transfection as in (**A),** analysed by qPCR. Data are presented as mean ± SEM. Statistical analysis: One sample *t* test. *n* = 7.

4.2.4. XPR1 deficient CD4+ T cells show increased glycolysis

CD4+ T-cell activation and differentiation are tightly linked with their metabolic activity. Changes in metabolism can either cause or be a result of specific differentiation and activation of CD4+ T cells, and affect their pro- or anti-inflammatory function (154). In order to address the impact of XPR1 deficiency on the metabolism of CD4+ T cells, Seahorse metabolic flux analysis was performed using the T cell metabolic profiling kit by Agilent. During this, the oxygen consumption rate (OCR) and the extracellular acidification rate (ECAR) are measured over time. OCR is mainly affected by oxygen consumption of the oxidative phosphorylation, while ECAR gets affected by acidification of the medium due to free protons arising from conversion of glucose to lactate in glycolysis. This allows for the distinct measurement of ATP production originating either from glycolysis or oxidative phosphorylation, hence referred to as glycoATP production and mitoATP production, respectively.

For the assay, three injections affect cell metabolism over time: oligomycin, BAM15, and rotenone/antimycin A. After measurement of the basal ATP production, addition of oligomycin inhibits the ATP synthase, and consequently, the production of ATP derived from oxidative phosphorylation (266). BAM15 is injected next, uncoupling the respiratory ATP production

(267). To match their energy demand, cells will then maximise the oxygen uptake. The resulting maximal respiratory capacity of OCR can be compared to the basal levels of OCR, with the increase from basal to maximal OCR quantified as the spare respiratory capacity. Rotenone/antimycin A get injected last, blocking complexes I and III of the respiratory chain (268, 269). This leads to the remaining respiration activity being only due to non-mitochondrial respiration (270–272).

Figure 19A and 19B depicts the kinetics of OCR and ECAR in response to indicated injections of reagents. For both genotypes, oligomycin injection caused a drop of OCR, which rose to a maximal respiration after BAM15 injection. Rotenone/antimycin A treatment reduced the OCR level to a minimum again. ECAR increased only slightly after oligomycin treatment. It further increased to a maximum after uncoupling due to BAM15, and decreased to the minimum due to rotenone/antimycin A treatment, similarly to the OCR measurements.

For OCR (Figure 19A), naïve cKO T cells showed a slightly higher basal and maximal OCR than naive CTL CD4+ T cells. Additionally, ECAR levels were slightly higher in the cKO group compared to the CTL group during the kinetic assay (Figure 19B).

A computational analysis of the OCR and ECAR was performed with the software provided by the manufacturer. This analysis revealed no significant difference between naïve CTL and cKO CD4+ T cells in their basal mitoATP production rate (Figure 19C), maximal respiration (Figure 19D), or spare respiratory capacity (Figure 19E). However, a significantly increased basal glycoATP production rate was found in cKO compared to CTL CD4+ T cells (Figure 19F). Further, the overall percentage of ATP production from glycolysis was significantly increased in naïve CD4+ T cells lacking XPR1 compared to the control (Figure 19G).

Taken together, a moderate shift towards increased glycolytic activity was detected in XPR1 deficient naïve CD4+ T cells in comparison to the control.

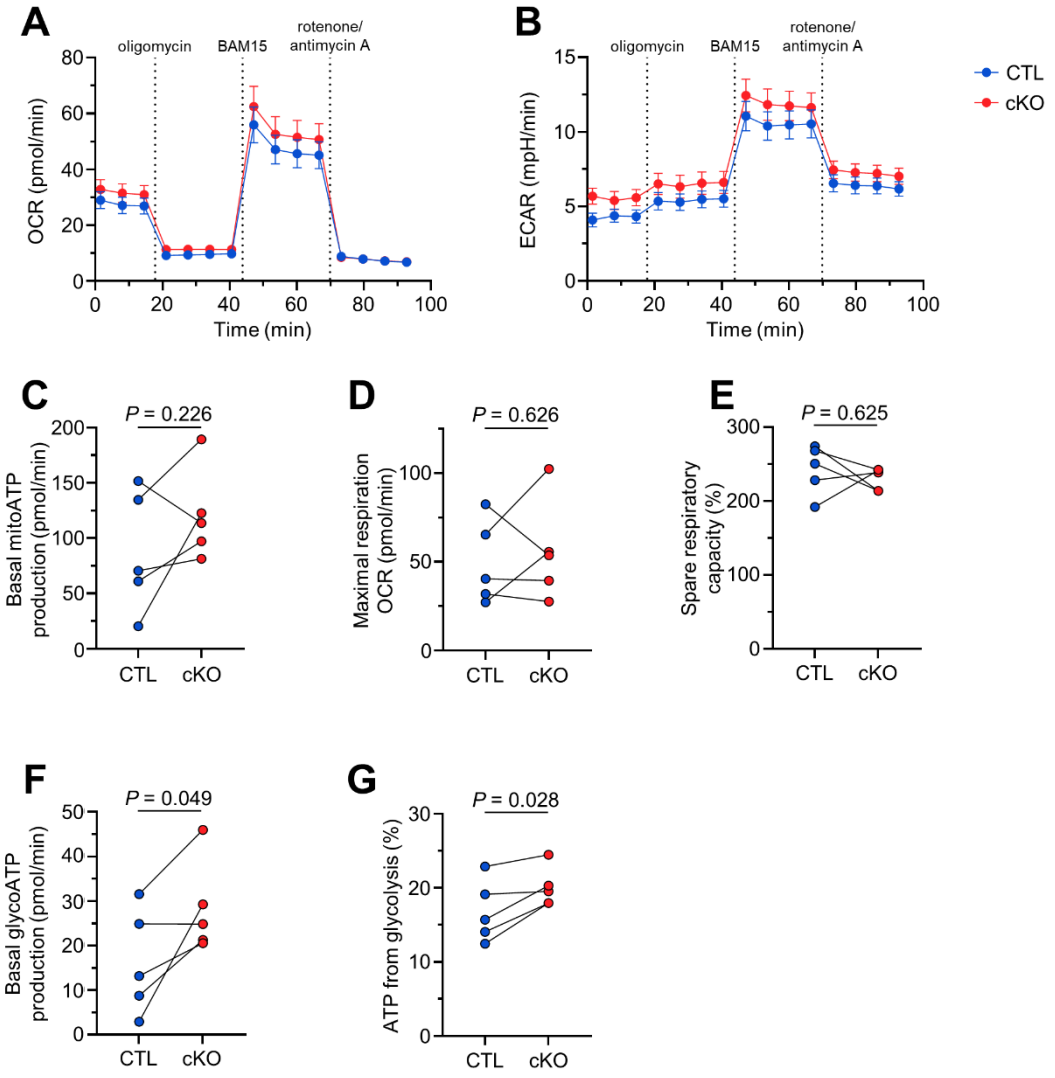

Figure 18: XPR1 deficiency moderately promotes glycolysis in CD4+ T cells. Naïve CD4+ T cells were isolated from CTL and cKO mice and analysed with Seahorse metabolic flux analysis using the Seahorse T Cell Persistence Assay of the T-cell metabolic profiling kit. **A**, **B**: Mean OCR (**A**) and ECAR (**B**) of all experiments over time. Injections of oligomycin, BAM15, and rotenone/antimycin A are indicated. **C-G**: Based on the measured OCR and ECAR kinetic, metabolic properties were determined using Agilent's analysis software: basal mitoATP production (**C**), maximal respiration (**D**), spare respiratory capacity (**E**), basal glycoATP production (**F**), and proportion of ATP from glycolysis (**G**). Data are presented as mean ± SEM. Statistical analysis: Paired *t* test (**C**, **D**, **F**, **G**); Wilcoxon matched-pairs signed rank test (**E**). *n* = 5.

4.2.5. Serum IgG and IgM levels are not altered in cKO mice

Antibody concentrations in serum increase during or after infections, or in the context of autoimmune diseases (273). IgM is the antibody isotype initially released in response to B-cell activation, with important functions for the complement system. IgG antibodies, the most common antibody isotype circulating in blood, are involved in pathogen clearing as well as immune system modulation, *e.g.* contributing to complement system activation (274). Since

CD4+ T cells from cKO mice display an hyperactivated phenotype, humoral immunity may be enhanced by increased T-cell responses. Furthermore, elevated T-cell activation can result in autoimmunity, which may be accompanied by increased production of autoantibodies.

To test this, serum of CTL and cKO mice was analysed by ELISA to determine IgM (Figure 19A) and IgG concentrations (Figure 19B). No significant differences for both IgM and IgG levels were detected in serum samples from CTL and cKO mice.

Taken together, these data argue against the development of autoimmunity in mice with XPR1 deficient CD4+ T cells, and corroborate the notion that Th2-related cytokines were unchanged in *in vitro* differentiation assays (Figure 13).

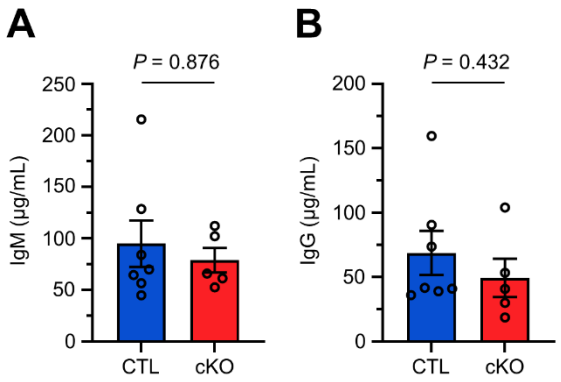

Figure 19: Serum IgG and IgM levels do not differ between CTL and cKO mice. Blood from CTL and cKO mice was collected by cardiac punction to obtain serum. Concentrations of IgM (**A**) and IgG (**B**) were determined using ELISAs. Data is presented as mean ± SEM. Statistical analysis: Mann-Whitney test. *n* = 7, 5 (CTL, cKO).

4.3. Signalling in XPR1 deficient CD4+ T cells

XPR1 deficient CD4+ T cells displayed increased proliferation, cytokine production, and glycolytic activity, which is in line with an overall hyperactivated phenotype in gene expression analysis. These data strongly suggest that signalling in response to TCR stimulation is altered in CD4+ T cells lacking XPR1 expression. In the following section, some of the central signalling pathways downstream of the TCR are analysed.

4.3.1. ERK signalling downstream of the TCR is impaired in XPR1 deficient CD4+ T cells

Following TCR stimulation, signalling pathways are activated by a cascade of kinases that phosphorylate target proteins. ERK1/2 is activated by phosphorylation and mediates the signal

transduction that controls T-cell activation, differentiation, and IL-2 expression (75, 275–277). To investigate changes in ERK1/2-mediated signalling by XPR1 deficiency, naïve CD4+ T cells from CTL, cHET and cKO mice were stimulated with α-CD3 antibodies for 0-60 min, and cell lysates were probed for differences in phosphorylated and total protein levels by immunoblotting. Representative immunoblots depicting the differential kinetics of ERK1/2 phosphorylation between genotypes are shown in Figure 20A.

Total protein levels and phosphorylated protein levels of ERK1/2 were detected as a double band at the height of 44 and 42 kDa for ERK1 and ERK2, respectively. In CTL samples of the representative blot, the intensity of the phospho(p)-ERK2 band increased strongly after 5 min, to an intensity maximum at 30 min. After that, the intensity decreased again. In contrast, the ERK2 phosphorylation in cHET CD4+ T-cell lysates was impaired, since an increased intensity of the p-p42 band in cHET CD4+ T-cell lysates appeared only after 30 min, and reached its intensity maximum after 60 min. In cKO CD4+ T cells, ERK2 phosphorylation was even more impaired, since the intensity of the p-ERK2 band only increased slightly after 60 min. Notably, the intensity after 60 min in cKO samples was strikingly lower than in CTL cells after 5 min. The p-ERK1 band intensity showed comparable levels over time in CTL cells, whereas a slight increase in cHET samples after 60 min was detected. In cKO cells, the p-ERK1 band intensity increased slightly after 5 min of stimulation.

As expected, the total protein levels for both ERK1 and ERK2 were unchanged irrespective of the stimulation time and the genotype.

For densitometric quantification after 5 min of stimulation, signals for each target protein were divided by the β-actin signal of the respective blot to compensate for variations in protein loading. p-ERK1/2 was divided by total ERK1/2, and relative intensity was normalised to values of CTL samples from each independent experiment. Quantification showed a significantly decreased ERK1/2 phosphorylation in cHET and cKO CD4+ T cells compared to CTL CD4+ T cells (Figure 20B). Notably, the fold change of p-ERK1/2/ERK1/2 ratios was comparable between cHET and cKO samples.

LAT is a membrane-associated adaptor protein that gets phosphorylated by ZAP-70 in one of the first steps of TCR-dependent CD4+ T-cell activation, and activated p-LAT then phosphorylates different adaptor proteins or enzymes, functioning as a signalling hub affecting different routes of TCR downstream signalling, one of which leads to ERK1/2 phosphorylation (278–280). To test whether impaired ERK1/2 phosphorylation in XPR1 deficient CD4+ T cells corresponds with changes in LAT phosphorylation, also LAT and p-LAT levels were analysed after TCR stimulation. Representative immunoblots are shown in Figure 20A.

LAT and its phosphorylated form p-LAT were detected as double bands at the height of 36 and 38 kDa. As expected, total LAT levels were comparable between all samples and genotypes. LAT phosphorylation in CTL samples increased slightly after 5 min compared to unstimulated samples; after that the p-LAT intensity remained constant. In cHET and cKO samples, p-LAT levels increased after 5 min as well, however with a slightly higher intensity compared to CTL samples. In cHET samples the p-LAT intensity was stable for 60 min, whereas in cKO samples, p-LAT intensity decreased after 5 min of stimulation.

Normalisation and data quantification of LAT activation after 5 min of TCR stimulation was done as described above. The pLAT/LAT ratio displayed a tendency towards increased LAT activation in cHET and cKO samples compared to CTL samples (Figure 20C). However, the data showed a high interexperimental variation, ranging from 0.5 to 2.5 for the p-LAT/LAT fold change in cHET and cKO samples.

Taken together, phosphorylation of ERK1/2 was strikingly reduced in cHET and cKO samples after 5 min of α-CD3 stimulation compared to control samples. In contrast, LAT phosphorylation was not significantly changed in TCR-stimulated naïve CD4+ T cells from cHET and cKO mice.

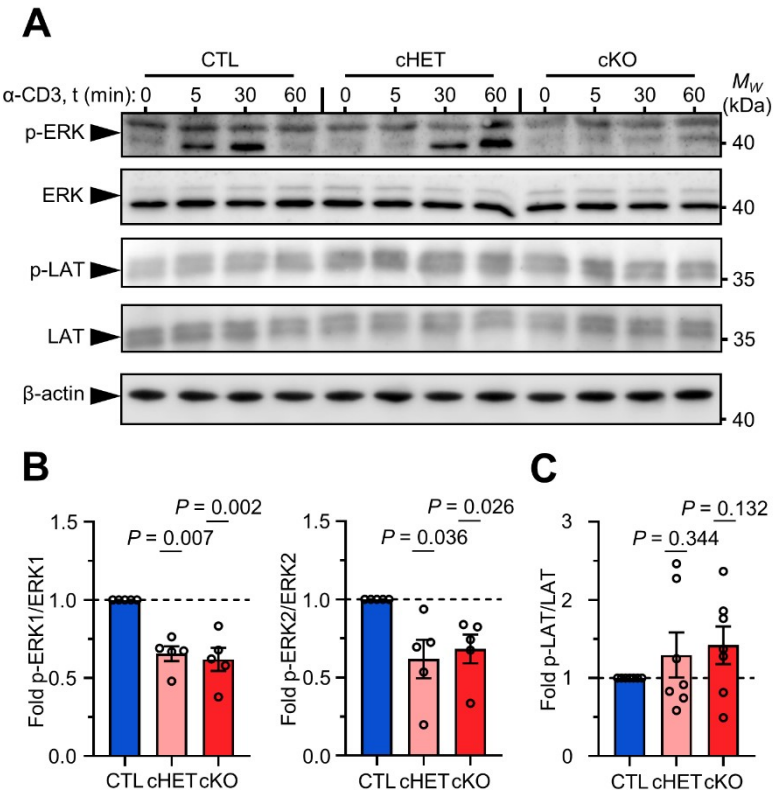

Figure 20: XPR1 deficient CD4+ T cells lack ERK phosphorylation after TCR stimulation. Naïve CD4+ T cells were isolated from CTL, cHET and cKO mice and stimulated with 5 µg/mL α-CD3 for 5, 30 or 60 min, or left unstimulated. **A**: Representative blots of phosphorylated and total protein levels of ERK1/2 and LAT from lysates analysed by immunoblotting. **B**, **C**: The ratio of phosphorylated protein by total protein for ERK1/2 (**B**) and LAT (**C**)

after 5 min of stimulation was determined using densitometric analysis of immunoblots. Intensities were adjusted by using the β-actin signal for each individual blot as a loading control. Data from three independent experiments were normalised to respective CTL values, presented as mean ± SEM. Statistical analysis: One sample *t* test. *n* = 5 (**B**); *n* = 7 (**C**); both from three independent experiments.

4.3.2. XPR1 deficient CD4+ T cells show an impaired Ca^{2+} response

In response to TCR stimulation, Ca^{2+} is rapidly released from intracellular stores into the cytosol of CD4+ T cells, which activates Ca^{2+}-dependent receptors that promote Ca^{2+} influx and regulate ERK1/2 phosphorylation (281). As ERK1/2 phosphorylation in response to α-CD3 stimulation is impaired in cKO CD4+ T cells, Ca^{2+} levels in CD4+ T cells were addressed next.

For this, live cell imaging using the ratiometric Ca^{2+} dye Fura-2 was performed in collaboration with Dr. Björn Diercks and Anette Rosche (Institute of Biochemistry and Molecular Cell Biology, UKE). Intracellular Ca^{2+} levels were quantified over time on a single-cell basis. The Ca^{2+} concentration in CTL or cKO naïve CD4+ T cells was calculated for 1 min before and 10 min after α-CD3 treatment. After subsequent treatment with the Sarcoplasmic/Endoplasmic Reticulum Calcium ATPase (SERCA) inhibitor thapsigargin, which blocks Ca^{2+} reuptake into intracellular stores (282), measurement was prolonged for another 4 min.

In Figure 21A, representative live cell imaging of Fura-2 stained CD4+ T cells with or without XPR1 expression is shown. Notably, intracellular Ca^{2+} levels increased more rapidly in the CTL CD4+ T cell, with a concentration peak already after 4 min, compared to 5.5 min for the cKO CD4+ T cell. Additionally, the maximum Ca^{2+} concentration during α-CD3 stimulation was higher in the CTL CD4+ T cell compared to the cKO cell. The Ca^{2+} concentration decreased again in both genotypes after 10 min. The time point at 13 min corresponded to the accumulation of Ca^{2+} into the cytosol in response to thapsigargin-mediated SERCA inhibition. The Ca^{2+} concentration was strikingly higher in the CTL CD4+ T cell after thapsigargin treatment compared to the cKO CD4+ T cell.

For each CD4+ T cell, the Fura-2 ratio was plotted over time, as shown for one representative experiment in Figure 21B. In total, 998 CTL and 794 cKO CD4+ T cells were analysed in three independent experiments. Mean Ca^{2+} concentrations over time as well as the area under the curve (AUC) per genotype were calculated for each sample. Data quantification for Ca^{2+} concentrations over time and the AUCs from three independent experiments in response to α-CD3 and thapsigargin treatment are shown in Figures 21C and 21D.

The Ca^{2+} response to α-CD3 stimulation (Figure 21C) was decreased in cKO CD4+ T cells compared to CTL CD4+ T cells. This is apparent by a lower maximum of mean Ca^{2+}

concentration. Additionally, the AUC was significantly lower in XPR1 deficient CD4+ T cells compared to controls with a decrease of about 2-fold.

When treated with thapsigargin (Figure 21D), Ca^{2+} levels in CTL cells peaked at a significantly higher Ca^{2+} concentration than cKO CD4+ T cells after 13.5 min of measurement. In line with this, the thapsigargin treatment led to a significant reduction of the AUC in cKO CD4+ T cells compared to CTL CD4+ T cells. Interestingly, the Ca^{2+} concentration still slowly increased in cKO CD4+ T cells until the end of the measurement at 15 min, whereas it reached a plateau in controls.

Taken together, XPR1 deficient CD4+ T cells displayed an impaired Ca^{2+} response compared to control CD4+ T cells. Further, they appeared to release less Ca^{2+} from intracellular stores upon thapsigargin treatment.

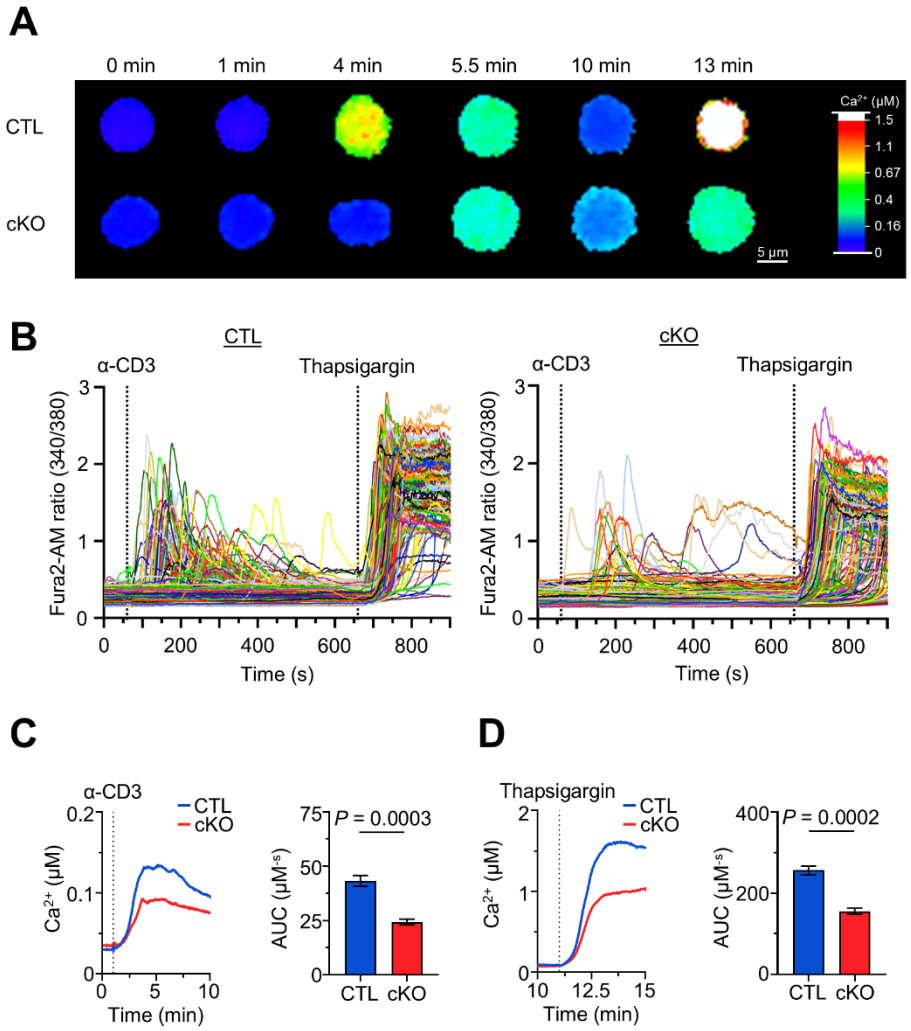

Figure 21: Ca^{2+} responses are impaired in XPR1 deficient CD4+ T cells. Naïve CD4+ T cells were isolated from CTL and cKO mice and stained with the Ca^{2+} sensor Fura2-AM for live cell imaging. Stimulation was done with 10 µg/mL α-CD3 after 1 min, and after 11 min of measurement, 1.67 µM thapsigargin were added. **A**: Representative single cells images of the measurement over time, with indication of cytosolic Ca^{2+} concentrations

using a heatmap (right). **B**: All single cell signals for CTL (left) and cKO T cells (right) from one representative experiment are shown, Fura2-AM ratio (340 nm/380 nm) is plotted against time. The application of α-CD3 and thapsigargin is indicated. **C**, **D**: Mean Ca^{2+} concentration over time (left) and AUC (right) after application of α-CD3 (**C**) or thapsigargin (**D**). Data are presented as mean ± SEM. Statistical analysis: Unpaired *t* test. Data were generated from *n* = 3 independent experiments with 998 (CTL) and 794 (cKO) single T cells analysed in total.

4.3.3. NFAT translocalisation to the nucleus is decreased in cKO CD4+ T cells

Ca^{2+} influx into a CD4+ T cell results in activation of calcineurin, which dephosphorylates NFAT and leads to translocation of NFAT to the nucleus. Inside the nucleus, NFAT controls the gene expression of transcription factors crucial for T-helper cell differentiation, or cytokines like IL-2 (219, 130, 283, 284). The decreased Ca^{2+} signalling in XPR1 deficient CD4+ T cells would also imply a reduced *Il2* gene expression, however RNA microarray analysis shown earlier (Figure 10) demonstrated markedly increased *Il2* expression. Therefore, we further addressed implications of XPR1 loss for downstream signalling of the Ca^{2+}-dependent pathway by investigating NFAT translocation to the nucleus using imaging flow cytometry.

For this, CD4+ T cells were stimulated for 10 min with or without α-CD3 or ionomycin, with the latter being used as a positive control for Ca^{2+} influx and NFAT translocalisation. After fixation, CD4+ T cells were stained with fluorophore-coupled antibodies detecting NFAT and CD4, as well as DAPI to visualise the nucleus. Fluorescence intensities as well as 60x magnified images of every event passing the laser were measured.

Representative images are shown in Figure 22A. The NFAT signal (green) in unstimulated cells was diffuse and not co-localised with DAPI (blue) or CD4 (red). When stimulated with α-CD3 or ionomycin, NFAT intensity increased, and the signal co-localised with the DAPI signal, observable by a cyan colour at sites of co-localisation in the overlay of all fluorescence channels.

To quantify the co-localisation between NFAT and DAPI, the Similarity Score was calculated using IDEAS' built-in analysis feature. Positive values of the Similarity Score indicate co-localisation, negative values indicate distinctive localisation of two compared channels. Representative histograms of the Similarity Score distribution are shown in Figure 22B. The used gate to quantify the frequency of cells with co-localisation between NFAT and DAPI is indicated in cyan. Unstimulated CTL or cKO CD4+ T cells displayed a low proportion of events with co-localisation between NFAT and DAPI, which increased after stimulation with α-CD3, and reached its maximum by ionomycin treatment.

Quantification of the frequency of cells with co-localisation between NFAT and DAPI is shown in Figure 22C. Unstimulated cells showed low co-localisation that did not differ between CTL and cKO CD4+ T cells. XPR1 deficient CD4+ T cells displayed a significantly lower proportion of cells with NFAT trans-localisation to the nucleus compared to CTL CD4+ T cells after stimulation with α-CD3. Notably, this frequency was also significantly decreased after treatment with the Ca^{2+} ionophore ionomycin, indicating not only a possibly impaired Ca^{2+} influx after TCR-dependent stimulation, but also an impaired signalling in response to artificially increased intracellular Ca^{2+} levels.

Taken together, NFAT trans-localisation to the nucleus in response to TCR-dependent or -independent Ca^{2+} influx is impaired in XPR1 deficient CD4+ T cells.

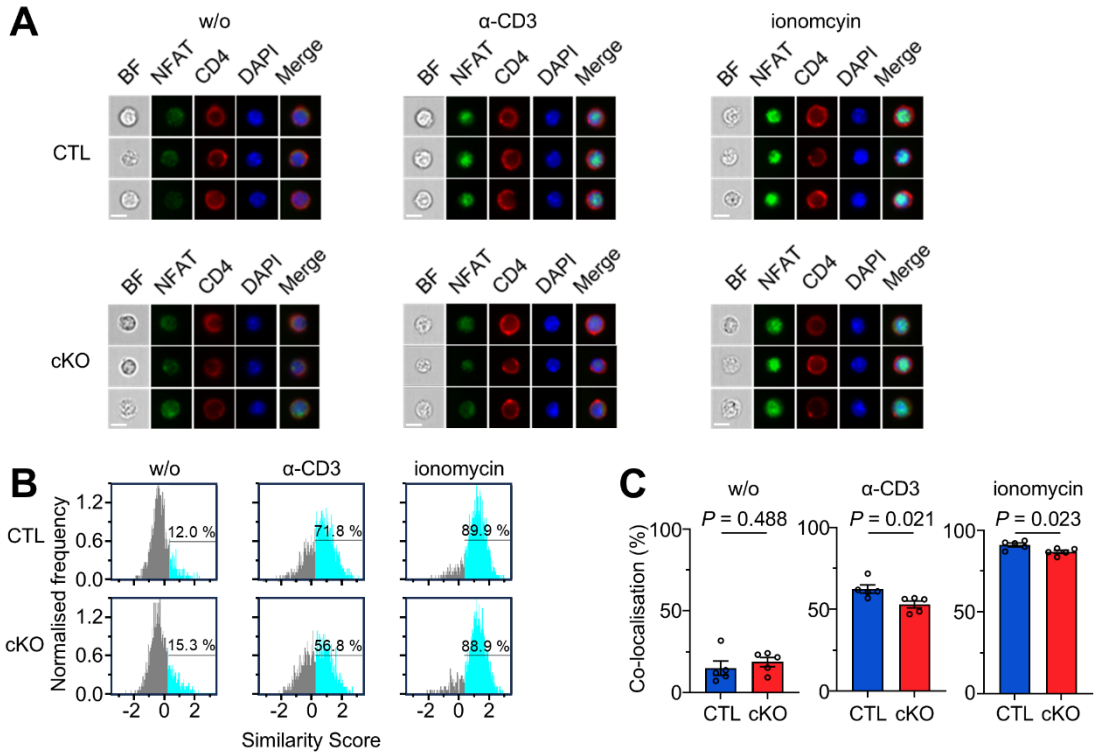

Figure 22: NFAT translocation to the nucleus is impaired in XPR1 deficient CD4+ T cells. CD4+ T cells were isolated from CTL and cKO mice with α-CD4-PE, and stimulated for 10 min with 5 µg/mL α-CD3, 1 µg/mL ionomycin, or left unstimulated. Cells were fixed, permeabilised, and stained with α-NFAT1-FITC and DAPI before subsequent analysis by imaging flow microscopy using the Amnis ImageStreamX MkII Imaging flow cytometer system. **A**: Representative image gallery with three CTL (upper panel) and cKO (lower panel) T cells left untreated (w/o, left), treated with α-CD3 (middle), and with ionomycin (right). Brightfield (BF), single fluorescence signals and merged images for NFAT, CD4, and DAPI stainings are shown in each gallery. Size bar corresponds to 7 µm. **B**, **C**: Using IDEAS analysis software, the Similarity Score feature of CD4+NFAT+DAPI+ single cells between NFAT and DAPI signals of the combined Intensity(Morphology(DAPI)) mask was calculated. Percentage of co-localisation between NFAT and DAPI was assessed by indicated gates in Similarity Score analyses. Representative histograms (**B**) and frequency of cells with co-localisation between NFAT and DAPI from *n* = 5 independent experiments are depicted (**C**). Data is presented as mean ± SEM. Statistical analysis: Unpaired *t* test.

4.3.4. mTOR signalling downstream of the TCR is increased in XPR1 deficient CD4+ T cells

ERK and Ca^{2+}/NFAT signalling only account for some of the signalling pathways activated by CD4+ T-cell stimulation. Another key regulator of cell homeostasis are the mTOR signalling complexes mTORC1 and mTORC2 (154, 285). AKT is a kinase upstream of mTORC1 and downstream of mTORC2, and important for linking co-stimulation to the TCR downstream signalling (285, 286). S6 is a ribosomal protein that gets phosphorylated by S6 kinase (S6K) downstream of the mTORC1 (285). Since AKT/mTOR activation can induce IL-2 expression independently of ERK or Ca^{2+} signalling (287), both AKT and S6 phosphorylation in the context of mTOR signalling were assessed in the following by immunoblotting. For this, CTL, cHET, and cKO naïve CD4+ T cells were stimulated with α-CD3 for 0-60 min, and ratios of phosphorylated to total protein levels for AKT and S6 were assessed.

Phosphorylated and total protein levels of AKT were detected as a band at the height of approximately 60 kDa (Figure 23A). In CTL samples, AKT phosphorylation increased slightly after 5 min, and more after 60 min. In the unstimulated cHET sample, p-AKT intensity was already comparable to the p-AKT intensity after 60 min of stimulation in the CTL sample. This effect was even more pronounced in the cKO samples, with an intensity peak after 5 min of stimulation. As expected, total AKT protein levels were constant for all genotypes and stimulation times.

Normalised to CTL samples, data quantification of p-AKT/AKT ratios after 5 min of stimulation showed significantly increased AKT phosphorylation in cHET and cKO CD4+ T cells compared to CTL samples (Figure 23B). Notably, the ratio in cKO samples increased by 1.8 ± 0.2-fold while the ratio in cHET samples increased only by 1.2 ± 0.1-fold.

Phosphorylated and total protein levels of S6 were detected as a band at the height of approximately 32 kDa (Figure 23A). S6 phosphorylation increased 5 min after start of the stimulation in CTL CD4+ T cells. In line with the results for AKT phosphorylation, the intensity of p-S6 in 5 min stimulated cHET and cKO CD4+ T cells was already markedly higher than the maximal p-S6 intensity detected across all time points in CTL samples. In cKO samples, the intensity of p-S6 was higher than in cHET samples at all four timepoints, with a pronounced sustained phosphorylation at 30 min and 60 min. In comparison, S6 phosphorylation in cHET and CTL CD4+ T cells decreased after the intensity peak at 5 min. In the representative blot, total S6 protein levels were lower in CTL cells with a stimulation time of 0, 5 and 30 min than in all other samples that showed a constant total S6 protein band intensity.

Normalised to CTL samples, data quantification of p-S6/S6 ratios after 5 min of stimulation revealed a significantly increased phosphorylation of S6 in cKO lysates by 2.2 ± 0.4 compared

to CTL lysates (Figure 23C). cHET cells displayed a fold change ratio comparable to the control.

In summary, increased AKT and S6 phosphorylation levels after 5 min of stimulation, but also in naïve CD4+ T cells, hint towards hyperactivation of the mTOR signalling complexes in XPR1 deficient CD4+ T cells in response to stimulation, but also in the naïve state.

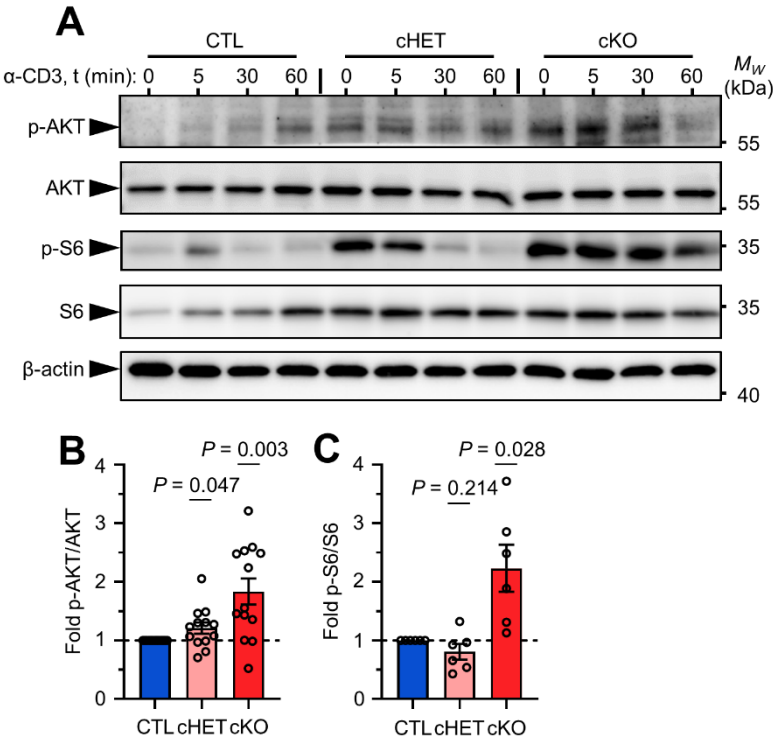

Figure 23: AKT and S6 phosphorylation is increased in XPR1 deficient CD4+ T cells. Naïve CD4+ T cells were isolated from CTL, cHET and cKO mice and stimulated with 5 µg/mL α-CD3 for 5, 30 or 60 min, or left unstimulated. **A**: Representative blots of phosphorylated and total protein levels of AKT and S6 from lysates analysed by immunoblotting. **B**, **C**: The ratio of phosphorylated protein by total protein for AKT (**B**) and S6 (**C**) after 5 min of stimulation was determined using densitometric analysis of immunoblots. Intensities were adjusted by using the β-actin signal for each individual blot as a loading control. Data from three independent experiments were normalised to respective CTL values, presented as mean ± SEM. Statistical analysis: One sample *t* test. *n* = 13 (**B**) pAKT/AKT; *n* = 6 (**C**); both from three independent experiments.

4.3.5. TCR-β surface expression decreases faster in XPR1 deficient CD4+ T cells after stimulation

Stimulation of the TCR results in internalisation of the TCR-CD3 complex (77, 83, 85, 86). Because XPR1 has been shown to be involved in endocytic trafficking of membrane-bound interaction partners (183, 184), we investigated internalisation of the TCR-CD3 complex.

For this, CTL and cKO CD4+ T cells were stimulated with α-CD3 or left untreated for 16 h. Surface levels of the TCR-β chain were analysed using flow cytometry. Representative histograms as well as quantification of the mean fluorescence intensity (MFI), normalised to untreated CTL CD4+ T cells, are shown in Figure 24. We detected no differences in surface levels of TCR-β between untreated CTL and cKO CD4+ T cells. Surface levels of TCR-β decreased in both CLT and cKO T cells, indicating successful TCR internalisation by α-CD3 stimulation. Importantly, after 16 h of stimulation cKO CD4+ T cells displayed a significantly decreased surface expression of TCR-β compared to CTL CD4+ T cells, indicating an altered kinetic for the internalisation of the TCR in stimulated CD4+ T cells lacking XPR1.

Taken together, XPR1 deficiency led to decreased surface levels of the TCR-CD3 complex in CD4+ T cells after stimulation compared to XPR1 expressing CD4+ T cells, indicating a possible role of XPR1 for TCR internalisation or trafficking, and possibly for altered signalling.

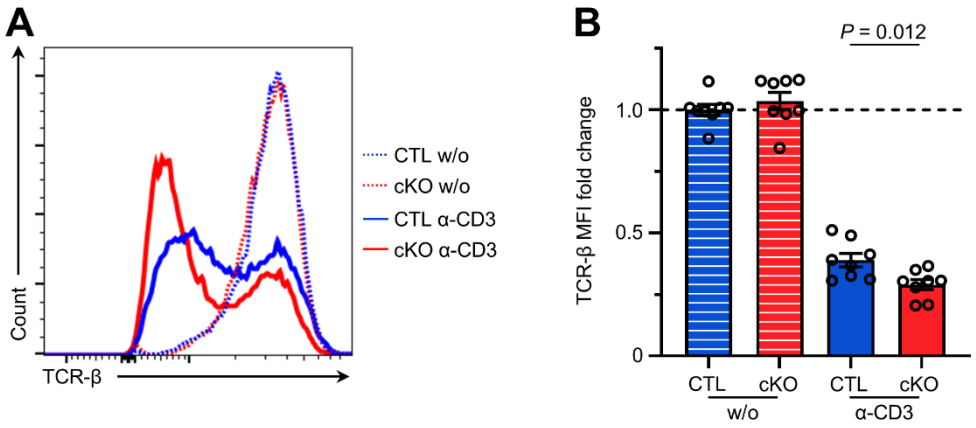

Figure 24: TCR-β internalisation is accelerated in XPR1 deficient CD4+ T cells. CD4+ T cells were isolated from CTL and cKO mice and stimulated with 3 µg/mL α-CD3 or left untreated. After 16 h, analysis of TCR-β was analysed flow cytometry. **A**: Representative histograms of TCR-β surface levels. **B**: Quantification of TCR-β surface levels from independent experiments, normalised to the mean value of untreated CTL sample, are shown. Data are presented as mean ± SEM. Statistical analysis: Unpaired *t* test. *n* = 8.

4.4. Pharmacological modulation and molecular interaction of XPR1 in CD4+ T cells

As XPR1 deficiency leads to a hyperactivated phenotype with enhanced proinflammatory effector functions in the analysed models, we investigated strategies to modulate XPR1 for enhancing CD4+ T-cell responses. Modulating XPR1's function in CD4+ T cells by pharmacological intervention could be a useful tool for invigorating insufficient responses during infections or in the tumour microenvironment. In order to test this, we used viral ligands that bind XPR1 on the cell surface and the inositol hexakisphosphate kinase 1 (IP6K1) inhibitor

UNC7467 that regulates inositol pyrophosphate (IP8)-mediated phosphate channelling by XPR1 to alter CD4+ T-cell reactivity. Proliferation assays were performed to determine whether treatment with any of these reagents induces hyperactivation that mimics the phenotype of XPR1 deficient T cells.

4.4.1. CD4+ T-cell proliferation is not affected by XPR1 binding of the viral ligand XVDL

XPR1 has been shown to act as an entry receptor for viruses like the murine leukaemia virus (MLV) (288). Later it was found that the phosphate exporter function of XPR1 can be inhibited by a retroviral envelop protein domain (289). Further research used the receptor binding domains (RBD) of xenotropic MLV (X-MLV) – and polytropic MLV (P-MLV) as a control – that were coupled with a His-Tag (Figure 25A), overexpressed in *E. coli*, and purified using affinity chromatography in HPLC, to block XPR1-mediated phosphate export in platelets, resulting in aggravated thrombus formation by polyP accumulation (180). To investigate the impact of these constructs that were termed xenotropic virus-derived ligand (XVDL) and polytropic virus-derived ligand (PVDL) on CD4+ T-cell responses, purification of recombinant viral ligands was performed analogously. Here, we used proliferation assays to elucidate whether inhibition of XPR1's phosphate exporter function by XVDL promotes CD4+ T-cell proliferation in comparison to controls.

Proliferation of CD4+ T cells stained with proliferation dye and stimulated with α-CD3/α-CD28 in the absence or presence of 20 µg/mL XVDL or PVDL was analysed by flow cytometry after 72 h (Figure 25B). CD4+ T cells that underwent three or more cell divisions were considered as cells with high proliferative activity, and the respective gates were analysed. Quantification revealed no significant difference in proliferation between untreated and XVDL or PVDL treated T cells.

These data suggest that XVDL binding to XPR1 does not affect CD4+ T-cell proliferation, and underscores that hyperactivity in cKO CD4+ T cells is independent of the XPR1 phosphate exporter function.

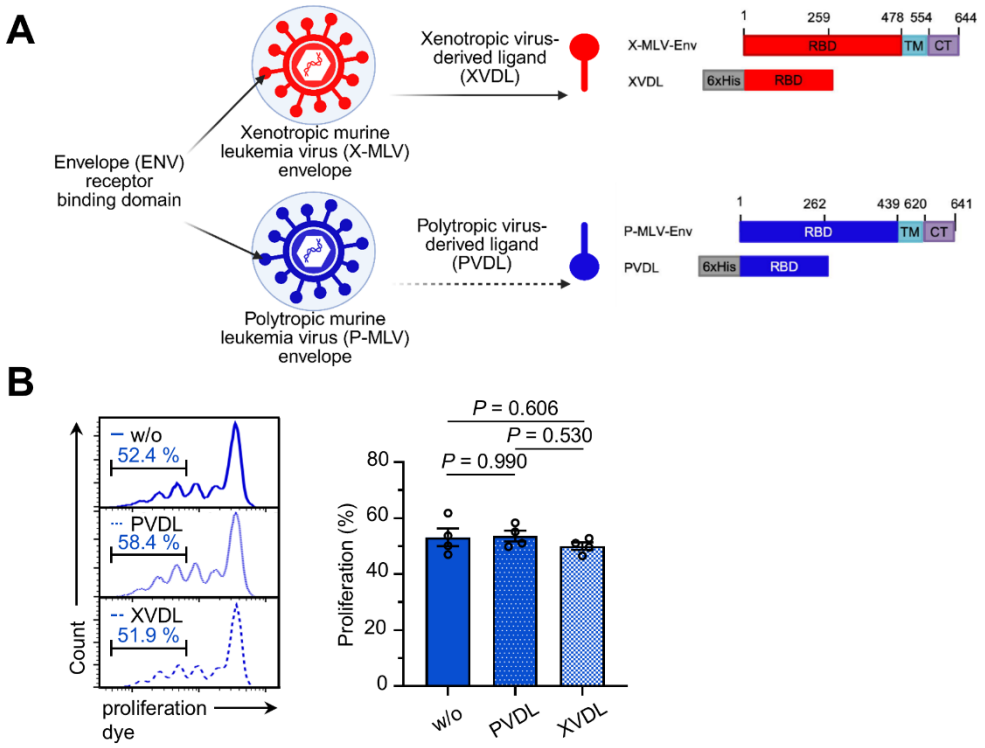

Figure 25: XVDL treatment does not affect proliferation of stimulated CD4+ T cells. A: Schematic representation of a xenotropic murine leukemia virus envelope (X-MLV-Env) and a polytropic (P-) MLV-Env (left). The envelopes of X-MLV and P-MLV consist of a receptor binding domain (RBD), a transmembrane domain (TM) and a cytoplasmic tail (CT) (right). Xenotropic virus derived ligand (XVDL) and polytropic virus derived ligand (PVDL) are derived from the xenotropic and polytropic MLV-Envs, respectively, and each consists of the first 259 or 262 amino acids of the corresponding RBD, coupled N-terminally with a 6x His-Tag. Figure created with BioRender.com and changed from (180). **B**: CD4+ T cells isolated from CTL mice, stained with CFSE cell proliferation dye, and stimulated with 5 µg/mL α-CD3 and 1 µg/mL α-CD28 were treated with 20 µg/mL PVDL, XVDL or left untreated. After 72 h of cultivation, cells were analysed by flow cytometry; representative histograms and indicated gating of highly proliferative CD4+ T cells (left) and quantified frequency of highly proliferating CD4+ T cells (right) are shown. Data are presented as mean ± SEM. Statistical analysis: Ordinary one-way ANOVA followed by Tukey's multiple comparisons test, $n = 4$.

4.4.2. CD4+ T-cell proliferation is decreased by IP6K1 inhibitor UNC7467 independently of XPR1 expression

XPR1 has been shown to control trafficking of its interaction partner and phosphate importer PiT1, thereby regulating recycling and degradation of PiT1 (184). IP8 is crucial for phosphate sensing of XPR1 by its interaction with XPR1's SPX domain, and without IP8, XPR1 mediated phosphate efflux as well as PiT1-mediated phosphate intake are impaired (183, 184). Li *et al.* used the novel IP6K1 inhibitor UNC7467, which deprives diphosphoinositol pentakisphosphate kinase type 1 (PPI5K1) of the substrate diphosphoinositol

pentakisphosphate (IP7) to generate IP8, resulting in decreased IP8 levels, which affects XPR1's functions in regards to phosphate efflux and trafficking of PiT1 (184, 290).

In this work, the effect of reduced IP8 levels by UNC7467 treatment was addressed in CD4+ T cells isolated from CTL and cKO mice to validate differences in proliferation specifically in the context of XPR1 deficiency. Similar to previous analyses, CTL and cKO CD4+ T cells were stained with proliferation dye, stimulated with α-CD3/α-CD28 antibodies in the presence of DMSO vehicle control or 1 µM UNC7467 treatment, and proliferation was assessed after 72 h by flow cytometry (Figure 26).

Representative histograms (Figure 26A) as well as the quantification of three independent experiments (Figure 26B) showed that the frequency of proliferating CTL CD4+ T cells treated with UNC7467 was significantly decreased compared to CTL CD4+ T cells treated with the DMSO vehicle control. However, we also observed a marked and significant reduced proliferation by UNC7467 treatment in comparison to the DMSO vehicle control treatment in cKO CD4+ T cells. Since the inhibitor UNC7467 is supposed to target XPR1 function by blockade of IP6K1, the treatment most likely caused off-target effects which disguised any potential effect of an altered XPR1 function for the modulation of CD4+ T-cell proliferation. This is corroborated by the plethora of cellular processes, such as metabolism and proliferation, in which IP6K1, but not necessarily XPR1, plays a role (291).

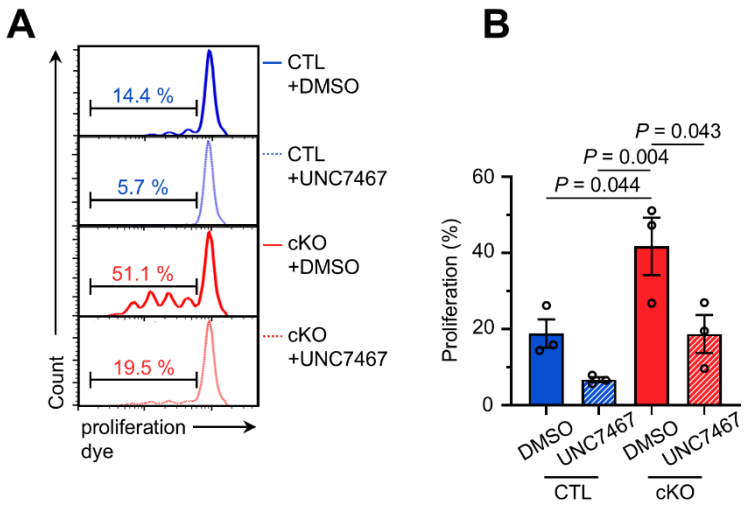

Figure 26: UNC7467 treatment inhibits proliferation of CD4+ T cells irrespective of the genotype. CD4+ T cells isolated from CTL and cKO mice, stained with eFluor450 cell proliferation dye, and stimulated with 5 µg/mL α-CD3 and 1 µg/mL α-CD28 were treated with 1 µM UNC7467 or the respective dilution of DMSO. After 72 h of cultivation, CD4+ T cells were analysed by flow cytometry. **A**: Representative histograms and indicated gates for proliferating T cells. **B**: Quantified frequency of proliferating CD4+ T cells. Data is presented as mean ± SEM. Statistical analysis: Ordinary one-way ANOVA followed by Tukey's multiple comparisons test. Comparisons that were not indicated correspond to $P > 0.05$. $n = 3$.

4.4.3. XPR1 interacts with Kidins220 in CD4+ T cells

Huttlin *et al.* identified putative interaction partners of XPR1 by mass spectrometry interaction complex screening in HEK293T cells. Among these XPR1 interaction partners are CTLA-4 (205, 206) and Kidins220, with the latter also reported by others (165, 166, 176, 201, 205, 206). Kidins220 is known to be involved in sustained ERK signalling in T cells via association with B-Raf, and interacts with the TCR (197). CTLA-4 is a TCR co-receptor transmitting co-inhibitory signals, and thereby is a key player for immune regulation in CD4+ T cells (292).

To address whether XPR1's function in CD4+ T cells depends on interactions with other membrane-associated or transmembrane proteins, we sought to validate these interactions in CTL CD4+ T cells. For this, proximity ligation assays (PLAs) were performed. This method is based on amplification of fluorophore-coupled DNA that is only possible when two antibodies generated from different host species are in spatial vicinity to each other. Here, four different antibody pairs were used, generated in rabbit (rb) & mouse, respectively: α-CD247 (rb) & α-Kidins220 (mouse), α-Kidins220 (rb) & α-XPR1 (mouse), α-XPR1 (rb) & α-CTLA-4 (mouse), and α-CTLA-4 (rb) & α-XPR1 (mouse). CTL CD4+ T cells were fixed, the PLA protocol was performed, and fluorescent spots were imaged by confocal microscopy. The number of fluorescent spots per CD4+ T cell was determined using ImageJ, and used as a relative measurement for interaction.

First, the respective isotypes for each antibody pair had to be used to account for potential unspecific interaction that would lead to a false positive signal. Each antibody pair was tested with the following three samples: I) specific (rb) & specific (mouse), II) specific (rb) & isotype control (mouse) and III) isotype control (rb) & specific (mouse). Representative images for the four antibody pairs as well as the quantifications of spots per CD4+ T cell are shown in Figure 27.

CD247/CD3ζ and Kidins220 are interaction partners in murine T-cell lines (197). Therefore, the first antibody pair CD247 & Kidins220 was used as a positive control to establish PLA protocols for this thesis (Figure 27A). A mean spot count of 6.1 ± 0.3 spots per cell was detected for the specific antibody combination, whereas in the controls significantly fewer spots were counted (4.4 ± 0.2 and 1.2 ± 0.1). This was considered a suitable example for positive protein association detected by this method and antibody combination.

Next, the interaction of XPR1 and Kidins220 was tested using the respective antibody combinations (Figure 27B). Applying specific antibodies resulted in a spot count of 22.4 ± 0.7 spots per CD4+ T cell. In both controls, when replacing respectively one specific antibody with an isotype, a strikingly and significantly lower spot count of 8.8 ± 0.7 and 1.8 ± 0.2 spots per CD4+ T cell was observed for α-Kidins220 & mouse isotype control and rb isotype

control & α-XPR1, respectively. The specific antibody combination was therefore deemed suitable to detect an association of Kidins220 and XPR1 using PLAs.

Lastly, the interaction between XPR1 and CTLA-4 was addressed using two different antibody pairs, generated in different species. For the first pair, rb α-XPR1 and mouse α-CTLA-4, the specific antibody combination did not differ from the α-XPR1 & mouse isotype control samples with 13.3 ± 0.7 and 11.6 ± 1.2 spots per CD4+ T cell, respectively (Figure 27C). However, the rb isotype control & α-CTLA-4 samples displayed a significantly lower spot count compared to the specific antibody combination with 2.2 ± 0.2 spots per CD4+ T cell.

For the other pair, mouse α-XPR1 and rb α-CTLA-4, a mean of 3.2 ± 0.5 spots per cell were counted in the specific antibody combination, whereas significantly fewer (1.4 ± 0.27) were detected in the α-CTLA-4 & isotype control samples (Figure 27D). However, in the isotype control & α-XPR1 samples, a mean of 5.1 ± 0.6 spots was counted, which was significantly more than in the specific antibody combination samples. Thus, for both antibody pairs addressing the interaction of CTLA-4 and XPR1, XPR1 antibodies generated either in rabbit or mouse in combination with respective isotype controls led to similar or more spots per cell. Consequently, an interaction of XPR1 and CTLA-4 in CD4+ T cells could not be validated by this method and respective antibodies.

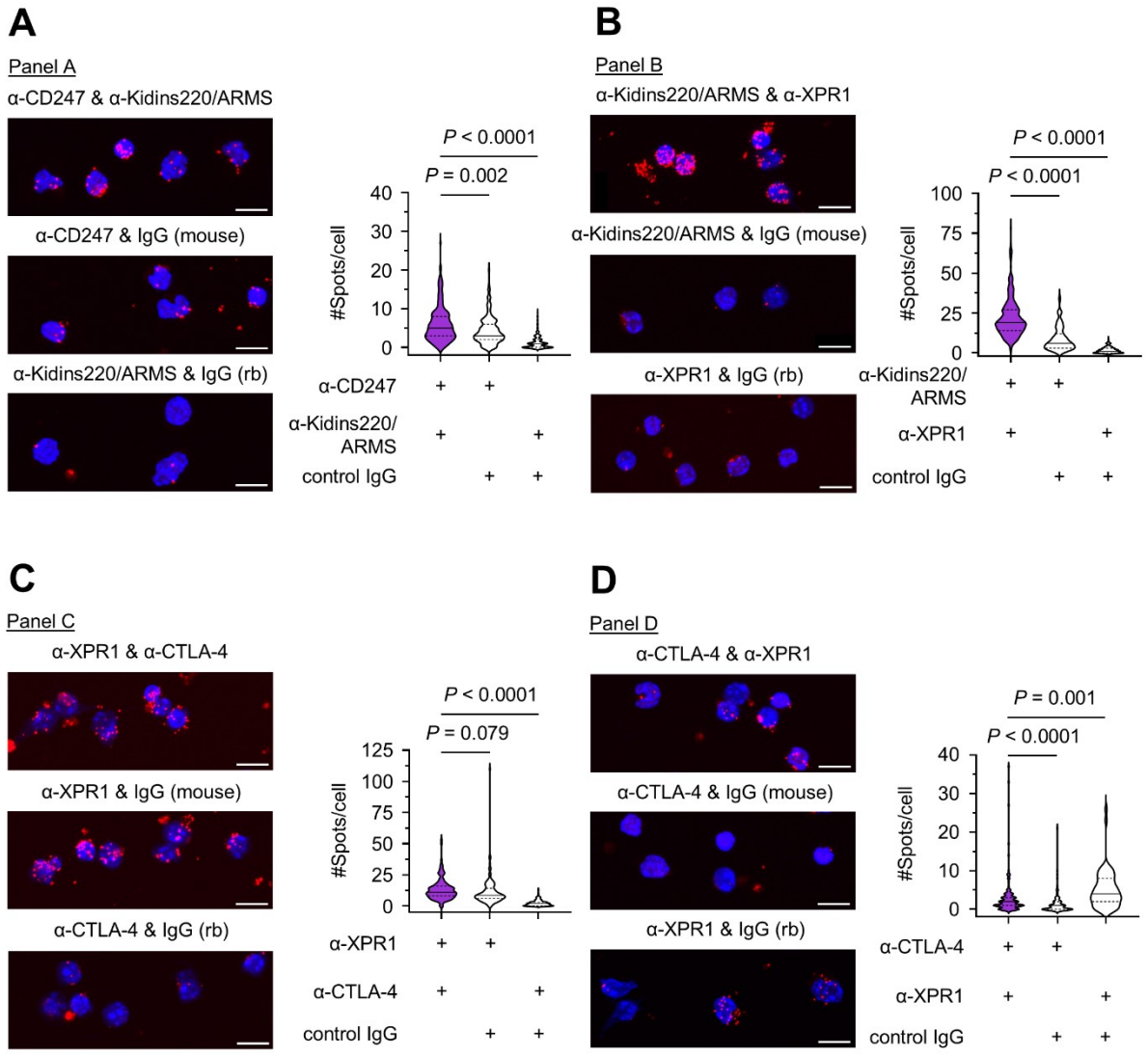

Figure 27: Interaction analyses with proximity ligation assays. CD4+ T cells were isolated from CTL mice using α-CD4-Biotin, seeded on fibronectin-coated glass coverslips and fixed. Proximity ligation assay (PLA) was performed using the Duolink In Situ PLA reagents. Confocal imaging was done and fluorescent interaction spots per T cell were counted for analysis. **A**-**D**: Representative images (left) and quantification (right) of spot counts per T cell. Size bar corresponds to 10 µm. Used antibody combinations: α-CD247 (rb) & α-Kidins220 (mouse) (**A**), α-Kidins220 (rb) & α-XPR1 (mouse) (**B**), α-XPR1 (rb) & α-CTLA-4 (mouse) (**C**), and α-CTLA-4 (rb) & α-XPR1 (mouse) (**D**). Data are presented as violin plots with median depicted as solid line, quartiles as dashed lines. Statistical analysis: Kruskal-Wallis test followed by Dunn's multiple comparisons test. Number of analysed cells corresponds to (**A**): 185 (α-CD247 & α-Kidins220), 225 (α-CD247 & mouse IgG), and 255 (α-Kidins220 & rb IgG); (**B**): 113 (α-Kidins220 & α-XPR1), 103 (α-Kidins220 & mouse IgG), and 66 (α-XPR1 & rb IgG); (**C**): 139 (α-XPR1 & α-CTLA-4), 110 (α-XPR1 & mouse IgG), and 223 (α-CTLA-4 & rb IgG); (**D**): 281 (α-CTLA-4 & α-XPR1), 107 (α-CTLA-4 & mouse IgG), and 153 (α-XPR1 & rb IgG). Data was collected in $n = 3$ (**A**, **B**) or $n = 2$ (**C**, **D**) independent experiments.

To investigate a potential relevance of CTLA-4 for the altered signalling in XPR1 deficient CD4+ T cells, particularly with a focus on protein trafficking, CTLA-4 surface expression was analysed by flow cytometry either in unstimulated or stimulated CTL and cKO CD4+ T cells.

Representative plots as well as gating for surface expression of CTLA-4 are shown in Figure 28A. For unstimulated (Figure 28B) as well as 72 h stimulated (Figure 28C) CD4+ T cells, cKO samples showed a tendency for increased frequency of CTLA-4+ CD4+ T cells compared to the CTL samples. Considering the high variance especially for the frequency in cKO CD4+ T cells (values from 3.0 % to 17.36 %), surface expression of CTLA-4 during T-cell stimulation was barely affected by the lack of XPR1.

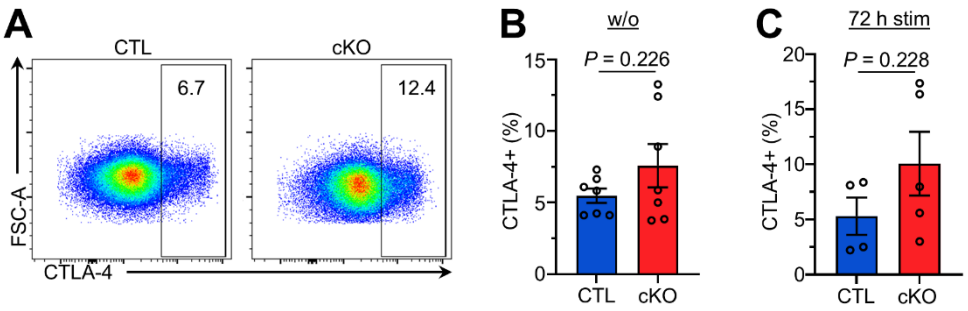

Figure 28: CTLA-4 surface expression on CTL and cKO CD4+ T cells. CD4+ T cells were isolated from CTL and cKO mice and either stimulated with 5 µg/mL α-CD3 and 1 µg/mL α-CD28 for 72 h, or analysed immediately. Surface expression of CTLA-4 was done by flow cytometry. **A**: Representative dot plots with indicated gating of CTLA-4+ CD4+ T cells. **B**, **C**: Frequency of CTLA-4+ CD4+ T cells when unstimulated (**B**) or stimulated for 72 h (**C**). Data are presented as mean ± SEM. Statistical analysis: Unpaired *t* test (**B**); Welch's *t* test (**C**). *n* = 7 (**B**), *n* = 4, 5 (CTL, cKO in **C**).

Taken together, an interaction of XPR1 with CTLA-4 could not be verified. Furthermore, CTLA-4 surface expression was not significantly altered in unstimulated or stimulated CD4+ T cells from CTL and cKO mice, suggesting that differential CTLA-4 signalling does not play a decisive role for hyperactivity in XPR1 deficient T cells. In contrast, the expected interaction between CD247 and Kidins220 was confirmed, and an interaction between XPR1 and Kidins220 in CD4+ T cells was successfully demonstrated using PLAs.

4.4.4. Membrane-permeable peptide Tat-X modulates XPR1-Kidins220 interaction

Recently, the interaction between XPR1 and Kidins220 has been shown in tumour cells and structural analyses (176, 165, 166). Especially the SPX domain as well as the C-terminal loop of XPR1 have been proposed to be essential for the interaction between these proteins (165, 166). To target the association of XPR1 with Kidins220 and/or a putative shared signalling/trafficking complex, we designed the peptide Tat-X that features the cell-penetrating peptide (CPP) derived from the Tat protein of human immunodeficiency virus 1 (HIV1), coupled with the C-terminal amino acids 671-695 of the murine XPR1 sequence (Figure 29A, top). This peptide's design strategy is based on work of Gamir-Morralla *et al.* who designed

the CPP-peptide Tat-K (293). Tat-K also features the CPP sequence of the Tat protein, coupled with amino acids 1699-1712 of the disordered C-terminal region of the murine Kidins220 sequence (Figure 29A, bottom). Tat-K features the calpain cleavage site of Kidins220, cutting between the second amino acid (asparagine) and the third amino acid (arginine). Treatment with Tat-K impaired Kidins220 cleavage by calpain in cortical neurons, which inhibits proteolysis of Kidins220, resulting in upheld ERK1/2 signalling and neuroprotection (293). Since Kidins220 is also involved in regulation of ERK1/2 signalling in the context of T cells and interacts with the TCR (197), we included Tat-K in our experimental setup to analyse molecular mechanisms of XPR1.

First, we tested whether treatment with Tat-K or Tat-X was able to alter the interaction of XPR1 and Kidins220. CD4+ T cells were treated with DMSO, Tat-K or Tat-X for 90 min, fixed, and then analysed using PLAs and confocal microscopy. Representative images as well as quantifications of spot counts per CD4+ T cell are shown in Figure 29B and 29C.

CD4+ T cells treated with the DMSO control displayed a mean spot count per cell of 20.9 ± 0.8. When treated with Tat-K, CD4+ T cells displayed a significantly higher spot count per cell of 26.3 ± 1.1, whereas treatment with Tat-X led to a significantly decreased spot count per cell of 15.1 ± 0.5. Since Gamir-Morralla *et al.* have shown that Tat-K treatment prevents calpain cleavage and stabilises Kidins220 expression levels (293), the increased spot count after Tat-K treatment in CD4+ T cells argues for an accumulation of Kidins220 that increases the interaction with XPR1. Strikingly, the treatment with Tat-X interfered with the spatial vicinity of XPR1 and Kidins220.

Taken together, treatment with Tat-K led to a significantly increased interaction spot count, whereas Tat-X treatment significantly decreased the interaction spot count, indicating that the interaction of XPR1 with Kidins220 or a Kidins220 containing interaction complex can be promoted by Tat-K treatment, but inhibited by Tat-X treatment.

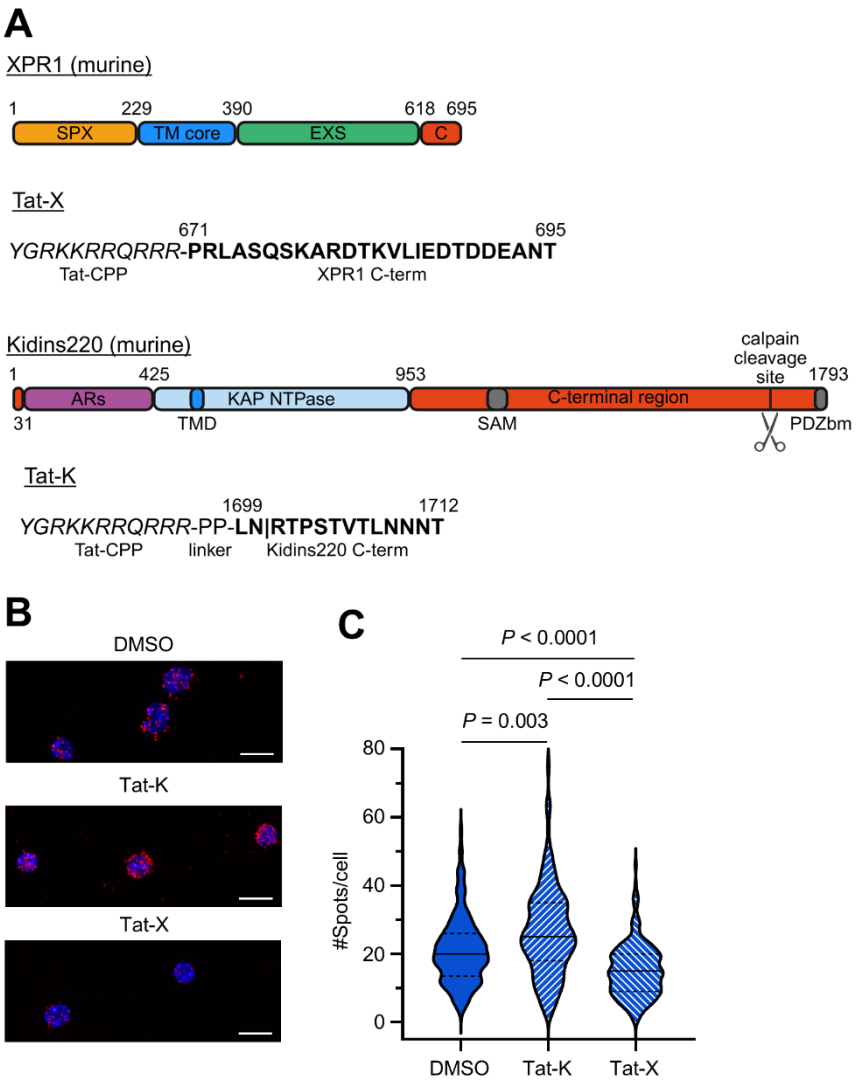

Figure 29: Membrane-permeable protein fragments interfere with the interaction of XPR1 and Kidins220. **A**: Cartoon representation of murine XPR1 (top) and Kidins220 (bottom) domains. Sequences of Tat-X and Tat-K are shown, with indication of the Tat sequence (italics), the protein-derived sequences (bold), and the calpain cleavage site of the Kidins220 sequence (indicated by "|"). Created with BioRender.com and changed from (165) and (293), with respect to species differences in the sequences. Used sequences for alignment: XPR1 murine (NP_035403.1), XPR1 human (NP_004727.2), Kidins220 murine (NP_001074847.1), Kidins220 human (NP_065789.1). SPX: SYG1/PHO/XPR1; TM: transmembrane; EXS: ERD1/XPR1/SYG1; C: C-terminal region; CPP: cell-penetrating peptide; ARs: ankyrin repeats; TMD: transmembrane domain; KAP NTPase: Kidins220/ARMS and PifA NTPase; SAM: sterile alpha domain; PDZbm: PDZ binding motif. **B**, **C**: CD4+ T cells were isolated from CTL mice using α-CD4-Biotin, treated with 3 µM Tat-K, Tat-K or DMSO for 90 min, seeded on fibronectin-coated glass coverslips and fixated. PLA was performed using the Duolink In Situ PLA reagents. Used antibody combination: α-Kidins220 (rb) & α-XPR1 (mouse). Confocal imaging was done and fluorescent interaction spots per cell were counted for analysis. **B**: Representative images of the specific antibody combination in CD4+ T cells treated as indicated. Size bar corresponds to 10 µm. **C**: Quantification of spot counts per cell for the specific antibody combination for different treatments. Data is presented as violin plots with median depicted as solid line, quartiles as dashed lines. Statistical analysis: Kruskal-Wallis test followed by Dunn's multiple comparisons test. Number of analysed cells corresponds to 157 (DMSO), 128 (Tat-K), and 219 (Tat-X). Data was generated in $n = 3$ independent samples.

4.4.5. Tat-X treatment emulates the XPR1 deficiency phenotype

To investigate whether an impaired Kidins220-XPR1 interaction induces hyperproliferation in CD4+ T cells from cKO mice, we used Tat-X treatment in both CTL CD4+ T cells, which displayed the protein interaction in PLAs, and as a control cKO CD4+ T cells, which are devoid of XPR1 complexes. Further, Tat-K treatment of CTL and cKO CD4+ T cells was done to address whether Kidins220's function in CD4+ T cells might be dependent on XPR1. Proliferation assays were used as a readout for the peptides' effect on CD4+ T cells that feature or lack XPR1 expression.

CTL and cKO CD4+ T cell were stained with cell proliferation dye, treated with Tat-K, Tat-X, or DMSO, and stimulated with α-CD3/α-CD28 for 72 h of cultivation. Representative flow cytometry histograms as well as data quantification of cell frequencies with a high proliferative capacity are shown in Figure 30.

The proportion of highly proliferating CTL CD4+ T cells increased significantly by about 2-fold upon Tat-K and Tat-X treatment compared to DMSO vehicle control samples. The increased proliferation frequencies in CTL CD4+ T cells treated with Tat-K and Tat-X reached a similar proliferation level as DMSO-treated cKO CD4+ T cells, strongly indicating an emulation of the hyperproliferative phenotype of XPR1 deficient CD4+ T cells by Tat-K and Tat-X treatment. Notably, the proliferation frequency increased slightly with Tat-K treatment in cKO T cells in comparison to the DMSO control, whereas Tat-X treatment had no effect.

Taken together, treatment with Tat-X, which prevents interaction of XPR1 with Kidins220, led to a XPR1 deficiency-like phenotype in CTL CD4+ T cells, implying a marked relevance of the XPR1-Kidins220 interaction for CD4+ T-cell activation and proliferation.

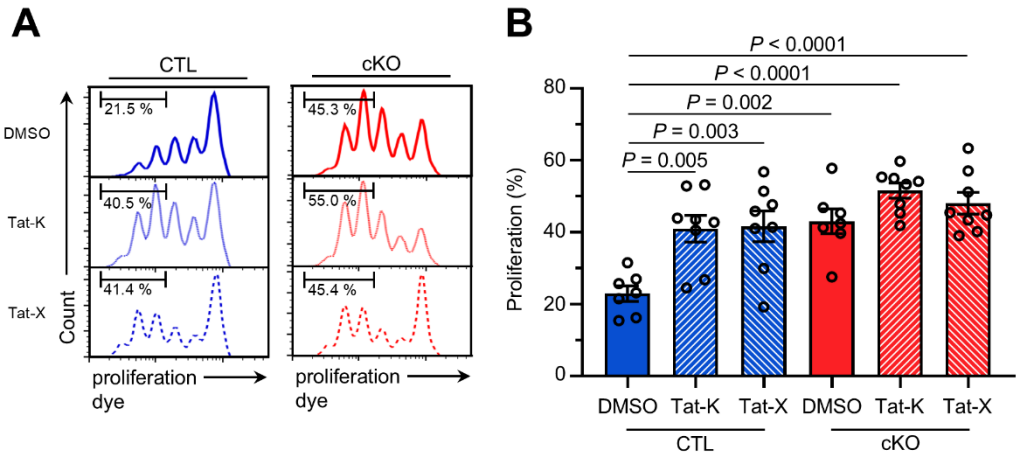

Figure 30: Tat-X treatment promotes proliferation of CTL, but not cKO CD4+ T cells. CD4+ T cells isolated from CTL (blue) and cKO (red) mice were stained with eFlour450 cell proliferation dye, treated with 3 µM Tat-K, Tat-K or DMSO vehicle control for 90 min, and then stimulated with 5 µg/mL α-CD3 and 1 µg/mL α-CD28. After 72 h, cells were analysed by flow cytometry. **A**: Representative histograms with indicated gating of highly

proliferative cells. **B**: Frequencies of highly proliferating CD4+ T cells. Data are presented as mean ± SEM. Statistical analysis: Ordinary one-way ANOVA, followed by Tukey's multiple comparisons test. Comparisons that were not indicated correspond to $P > 0.05$. $n = 7, 8, 8$ (DMSO, Tat-K, Tat-X).

4.5. XPR1 regulates CD28-dependent T-cell responses *in vitro* and *in vivo*

So far, the impact of XPR1 deficiency has been characterised in isolated CD4+ T cells that were analysed in *in vitro* assays for changes in functional and mechanistic parameters. Stimulation was done using α-CD3 and α-CD28, which bind to the CD3-TCR complex or CD28, respectively, inducing signal 1 and 2 of T-cell activation (294–296). In a physiological context however, CD4+ T cells get activated by antigen presentation to the TCR by an APC (75). To investigate the role of XPR1 in a more physiologically relevant setting, *Marilyn* mice that express a transgenic TCR were cross-bred with CD4+ T cell-specific *Xpr1* knockout mice. In detail, *Marilyn* mice carry a global knockout of *Rag2*, leading to abbreviated V(D)J recombination during T-cell development in addition to the transgenic *Tg(TcraH-Y,TcrbH-Y)1Pas* TCR that specifically recognises male H-Y antigen presented by MHC II I-A^{b29}. Due to limited positive selection in females, a reduced number of mature CD4+ T cells is present in the periphery, however with a monoclonal specificity for the cognate antigen. Furthermore, H-Y antigen expression leads to excessive negative selection of thymocytes in male *Marilyn* mice, resulting in a negligible number of mature T cells in the periphery. *Marilyn* mice have already been characterised before and have been shown to be a useful tool for studies investigating T-cell development and antigen recognition (297–300).

Henceforth, *Cd4-Cre*$^{-}$ *Xpr1*$^{fl/fl}$ *TCRtg*$^{+}$ *Rag2*$^{-/-}$ mice are called *Marilyn* CTL mice, and *Cd4-Cre*$^{+}$ *Xpr1*$^{fl/fl}$ *TCRtg*$^{+}$ *Rag2*$^{-/-}$ mice are called *Marilyn* cKO mice. *Marilyn* cKO mice did not show reduced life expectancy, an increased susceptibility for diseases, a health burden, or other abnormalities compared to *Marilyn* CTL mice.

4.5.1. Female *Marilyn* XPR1 cKO mice show increased activation marker and cytokine expression in peripheral T cells upon H-Y injection

First, CD4+ T cells from *Marilyn* CTL or cKO mice were challenged with antigen *in vivo*, and effector functions of thereby activated CD4+ T cells were compared. For this, recombinant protein, harbouring the T-cell epitope sequence of the H-Y protein was injected into female *Marilyn* CTL or *Marilyn* cKO mice intravenously, as schematically depicted in Figure 31A. After 6 days, mice were sacrificed, and splenic as well as lymph node (LN)-derived T cells were

analysed using flow cytometry, where TCR-Vβ6 (TRBV6) expression as part of the transgenic TCR in *Marilyn* mice was used to identify antigen-specific CD4+TRBV6+ T cells. The panel used for analyses assessed surface levels of immune checkpoint molecules (PD-1, CTLA-4), the proliferation marker Ki-67, activation markers (CD44, CD62L), key transcription factors (Ror-γt, Foxp3) and cytokines (IL-17a, IL-22, IFN-γ, TNF-α). Representative gating as well as expression levels are shown in Figure 31-33.

Analysis of immune checkpoint molecules CTLA-4 and PD-1 revealed strikingly and significantly increased CTLA-4 expression in CD4+TRBV6+ T cells from LNs of *Marilyn* cKO mice compared to control samples, as shown in Figure 31B and Figure 31C. Also, the proportion of CTLA-4+ CD4+TRBV6+ T cells tended to be increased in the spleen of *Marilyn* cKO mice compared to *Marilyn* CTL mice, however not significantly.

Similar to CTLA-4, the proportion of PD-1+ CD4+TRBV6+ T cells in LNs of *Marilyn* cKO mice was significantly increased compared to the control (Figure 31D), while there was only a tendency for an increased frequency in splenic CD4+TRBV6+ T cells from *Marilyn* cKO mice compared to those from *Marilyn* CTL mice (Figure 31E). The proportion of Ki-67+ T cells showed a trend to be increased in LNs from *Marilyn* cKO mice. In spleen, Ki-67+ T cells were very rare (0.01-0.10%), with no difference between samples from *Marilyn* CTL and cKO mice.

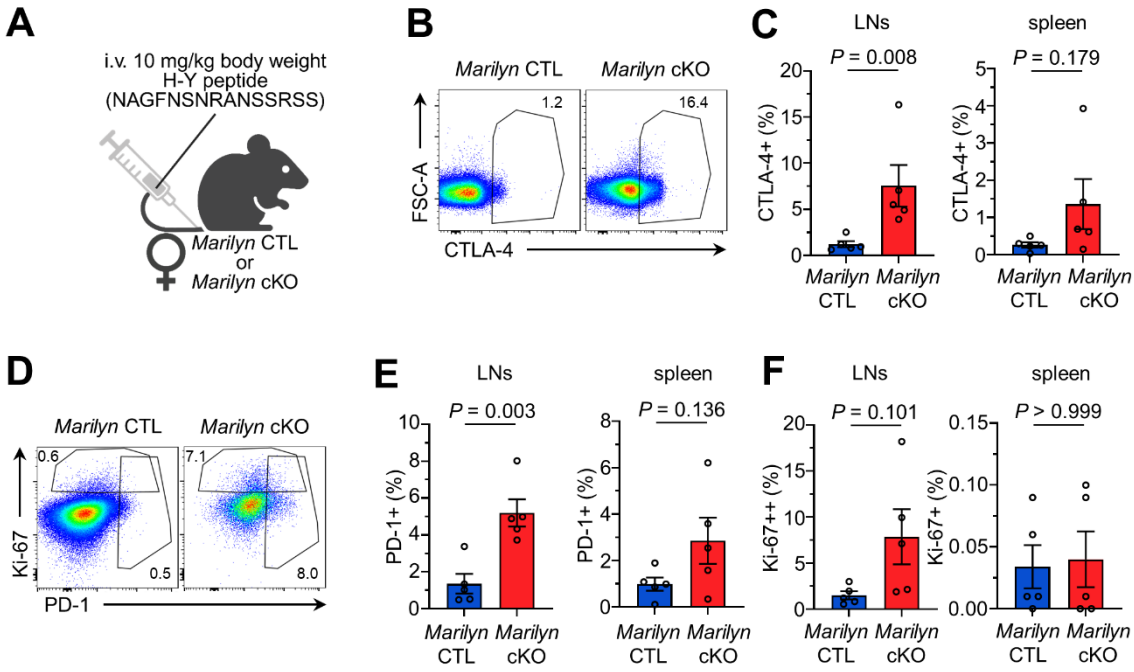

Figure 31: Differential expression of CTLA-4, PD-1, and Ki-67 in *Marilyn* CTL and cKO mice after H-Y injection. Female *Marilyn* CTL or *Marilyn* cKO mice were intravenously injected with 10 mg/kg bodyweight H-Y peptide in 100 µL 0.9 % saline. After 6 days, mice were sacrificed and spleen as well as lymph nodes (LNs: pool of inguinal, axillary, cervical and mesenteric LNs) were dissected and analysed by flow cytometry. Events within lymphocyte gates labelled as singlets, and viable CD4+TRBV6+ T cells were analysed. **A**: Schematic overview of

the experimental design. **B**, **C**: Representative dot plots with indicated gating of CTLA-4+ T cells in LNs from *Marilyn* CTL and cKO mice (**B**), and frequencies of CTLA-4+ T cells (**C**) in LNs and spleen. **D**-**F**: Representative dot plots with indicated gating of PD-1+ and Ki-67+ T cells in LNs from *Marilyn* CTL and cKO mice (**D**), and frequencies of PD-1+ (**E**) and Ki-67+ T cells (**F**) in LNs and spleen. Data are presented as mean ± SEM. Statistical analysis: Mann-Whitney test: **C** (LNs), **F** (spleen); Welch's *t* test: **C** (spleen), **E** (spleen); **F** (LNs); Unpaired *t* test: **E** (LNs). *n* = 5. Continued in Figure 32 and Figure 33.

Next, expression levels of CD44 and CD62L were analysed to assess T-cell activation as shown in Figure 32A. For this, the MFI instead of the frequency was compared to detect subtle expression level changes in populations. Surface levels of CD44 were significantly increased in LNs, and tended to be increased in the spleen of *Marilyn* cKO mice compared to *Marilyn* CTL mice (Figure 32B). For CD62L, neither in LNs nor spleen significant alterations between T cells from *Marilyn* CTL and cKO mice were observed (Figure 32C).

Additionally, the key transcription factors Ror-γt and Foxp3 were stained to analyse *bona fide* Th17 and Treg cell populations, respectively, as shown in Figure 32D. The proportion of Ror-γt CD4+TRBV6+ T cells showed a trend for an increase in LNs from *Marilyn* cKO mice compared to *Marilyn* CTL mice (Figure 32E), whereas no difference was apparent in the spleen where Ror-γt levels were very low in general (maximum of 0.01 %). The frequencies of Foxp3+ CD4+TRBV6+ T cells were unaltered between *Marilyn* CTL and cKO mice in the spleen, but significantly increased in LNs samples from *Marilyn* cKO compared to *Marilyn* CTL mice (Figure 32F).

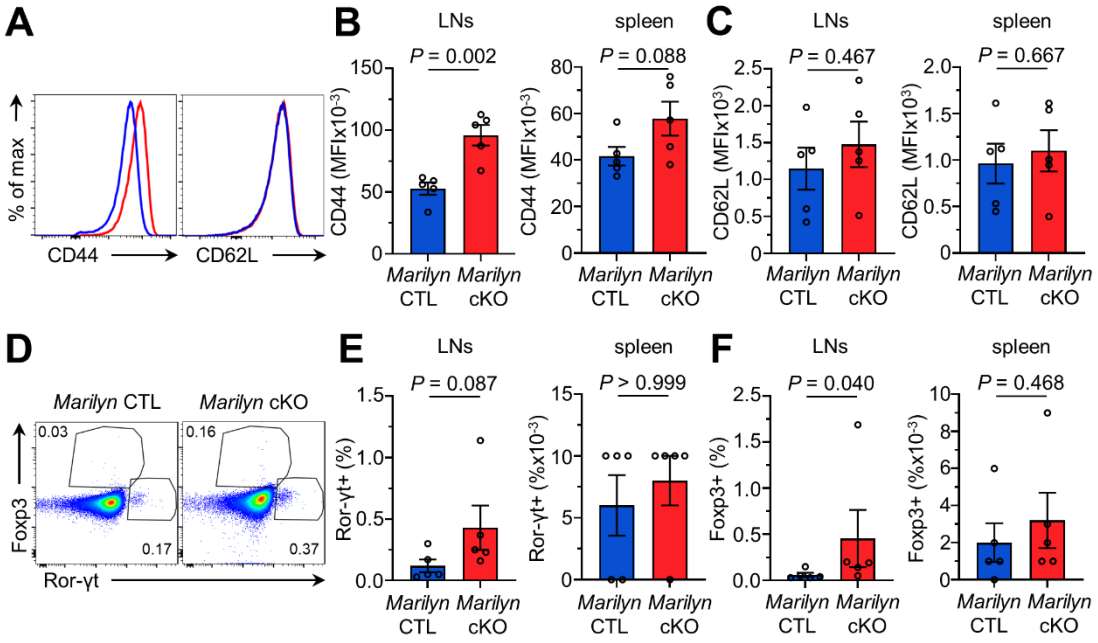

Figure 32: Analysis of CD44, CD62L, Ror-γt, and Foxp3 expression in CD4+ T cells from *Marilyn* CTL and cKO mice after H-Y injection. CD4+TRBV6+ T cells from CTL and cKO *Marilyn* mice treated as in Figure 31 were analysed by flow cytometry. **A**-**C**: Representative histograms in LNs from *Marilyn* CTL and cKO mice (**A**), and MFI of CD44 (**B**) and CD62L (**C**) from LNs and spleen. **D**-**F**: Representative dot plots with indicated gating in LNs from

Marilyn CTL and cKO mice (**D**), and frequencies of Ror-γt+ (**E**) and Foxp3+ T cells (**F**) from LNs and spleen. Data are presented as mean ± SEM. Statistical analysis: Unpaired *t* test: **B**, **C**; Mann-Whitney test: **E**, **F**. *n* = 5. Continued in Figure 33.

Lastly, cytokine expression was analysed with the respective gates for IL-17a and IL-22 shown in Figure 33A. The proportion of IL-17a+ CD4+TRBV6+ T cells in LNs and spleens of *Marilyn* cKO mice was strikingly increased (2- to 4-fold) compared to *Marilyn* CTL mice, however significance was only achieved for samples from spleen (Figure 33B). Also, the proportion of IL-22+ CD4+TRBV6+ T cells showed a trend to be increased by about 2-fold in LNs and spleen of *Marilyn* cKO mice compared to *Marilyn* CTL mice (Figure 33C).

TNF-α expression, assessed by the respective gates outlined in Figure 33D, was similar in CD4+TRBV6+ T cells from LNs samples of *Marilyn* CTL and cKO mice, however there was a tendency for decreased expression of TNF-α in spleen samples from *Marilyn* cKO mice compared to *Marilyn* CTL mice (Figure 33E). For IFN-γ, there was no significant difference between LNs or spleen samples from *Marilyn* CTL and cKO mice, but we detected a trend for increased IFN-γ expression for splenic CD4+TRBV6+ T cells from *Marilyn* cKO mice compared to *Marilyn* CTL mice (Figure 33F).

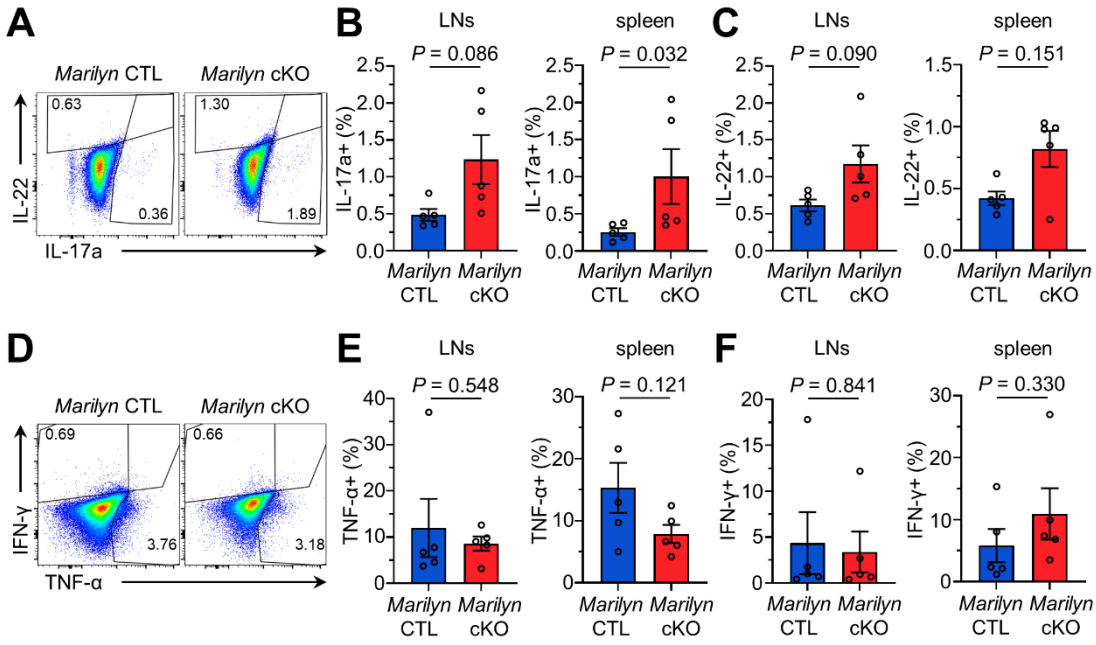

Figure 33: Cytokine expression in CD4+ T cells from *Marilyn* CTL and cKO mice after H-Y injection. CD4+TRBV6+ T cells from *Marilyn* CTL and cKO mice treated as in Figure 31 and Figure 32 were analysed by flow cytometry. For intracellular staining of cytokines, T cells were restimulated for 6 h with 50 ng/mL PMA and 1 µg/mL ionomycin, with addition of 1x Protein Transport Inhibitor Cocktail after the first two hours. **A-C**: Representative dot plots with indicated gating of IL-17A+ and IL-22+ T cells in LNs from *Marilyn* CTL and cKO mice (**A**), and frequencies of IL-17A+ (**B**) and IL-22+ T cells (**C**) in LNs and spleen. **D-F**: Representative dot plots with indicated gating of TNF-α+ and IFN-γ+ T cells in LNs from *Marilyn* CTL and cKO mice (**D**), and frequencies of

TNF-α+ (**E**) and IFN-γ+ T cells (**F**) in LNs and spleen. Data is presented as mean ± SEM. Statistical analysis: Welch's *t* test: **B** (LNs), **C** (LNs); Mann-Whitney test: **B**, **C** (spleen), **E**, **F** (LNs); Unpaired *t* test: **E**, **F** (spleen). *n* = 5.

In summary, H-Y injection induced significantly increased expression of immune checkpoint molecules CTLA-4 and PD-1, of the activation marker CD44, of the transcription factor Foxp3, and the proinflammatory cytokine IL-17a in T cells from lymph nodes of *Marilyn* cKO mice compared to *Marilyn* CTL mice, suggesting that XPR1 deficiency drives antigen-specific T-cell responses *in vivo*.

4.5.2. The lack of XPR1 impairs antigen-specific clonal expansion of CD4+ T cells *in vitro*

When H-Y was injected into *Marilyn* cKO mice, CD4+ T cells upregulated the expression of activation markers, cytokines, immune checkpoint molecules, and T-cell differentiation-associated transcription factors in comparison to the antigen-specific response in *Marilyn* CTL mice. Next, the competitive proliferation of CTL and cKO CD4+ T cells by antigen-specific stimulation was addressed.

For this objective, we did a clonal expansion experiment. Same numbers of *Marilyn* CTL and cKO CD4+ T cells were challenged by antigen while being cocultured *in vitro*. Initially, experiments were carried out by isolating naïve CD4+ T cells from female *Marilyn* CTL and *Marilyn* cKO mice, labelling them with the cell proliferation dyes eFluor450 and eFluor670, respectively, and injecting them intravenously into a male CTL mouse. However, low T-cell numbers in *Marilyn* mice required many mice to be sacrificed to get a sufficient amount of labelled naïve CD4+ T cells for the transfer into a male recipient, and their retrieval in secondary lymphoid tissues after 96 h was hampered (data not shown), possible due to T-cell exhaustion by high antigen load (301, 302). Therefore, the *in vitro* approach was chosen instead.

For this, naïve CD4+ T cells from female *Marilyn* CTL and *Marilyn* cKO mice were isolated and labelled with the cell proliferation dyes eFluor450 or eFluor670, respectively. These differentially labelled *Marilyn* CTL and cKO CD4+ T cells were mixed in a 1:1 ratio and co-cultured with splenocytes from male CTL mice in a 1:15 ratio for 72 h (Figure 34A).

CD4+TRBV6+ T cells that were stained with either proliferation dye were analysed regarding their clonal expansion upon stimulation by male splenocytes. Representative gating as well as frequencies of T cells with a high proliferative capacity are shown in Figures 34B and 34C. Surprisingly, *Marilyn* cKO CD4+ T cells showed a significantly decreased proliferative capacity compared to *Marilyn* CTL CD4+ T cells in competitive co-culture assays. Further, the

proportion of fluorescently labelled CD4+TRBV6+ T cells from *Marilyn* cKO mice was significantly and markedly decreased compared to controls after 72 h. This shows that upon direct competition with *Marilyn* CTL T cells, *Marilyn* cKO T cells display a proliferation disadvantage in response to antigen-specific stimulation *in vitro* (Figure 34C and 34D).

Notably, this competition assay may reflect the impaired Ca^{2+} signalling of *Marilyn* cKO T cells in response to male antigen, which could not be compensated by enhanced AKT/mTOR signalling as the supplementation with 1 µg/mL soluble α-CD28 was probably diluted by the presence of CD3+ T cells in male splenocyte populations.

Taken together, XPR1 deficient T cells have a disadvantage in proliferation when competing with CTL T cells in antigen-specific clonal expansion experiments *in vitro*, when co-stimulation signals are limited.

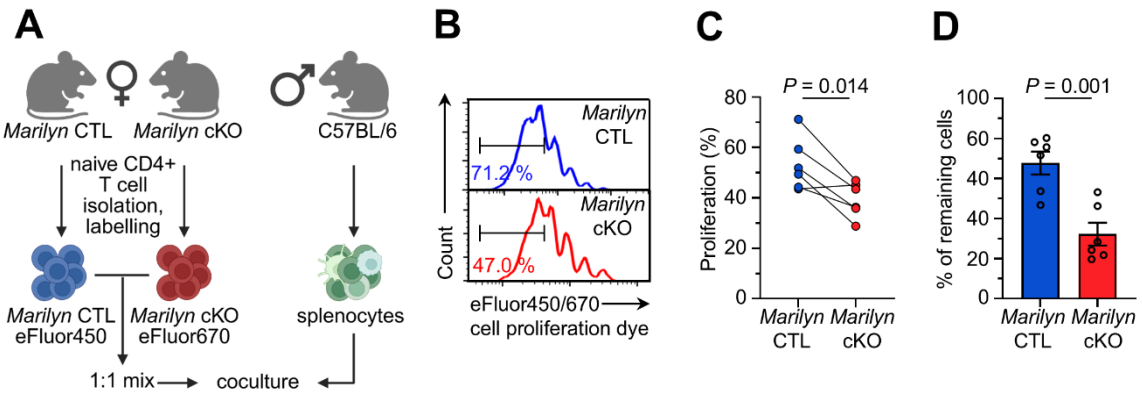

Figure 34: Clonal expansion of *Marilyn* cKO CD4+ T cells is decreased compared to *Marilyn* CTL CD4+ T cells *in vitro*. Naïve CD4+ T cells were isolated from female *Marilyn* CTL and *Marilyn* cKO mice and labelled with eFluor450 or eFluor670 cell proliferation dye. $5x10^4$ labelled, naïve CD4+ T cells of each genotype were mixed with each other, and cocultured with $1.5x10^6$ splenocytes from male CTL mice. Clonal expansion experiments were performed in X-VIVO 15, serum free medium, containing 1 µg/mL soluble α-CD28 for 72 h and analysed by flow cytometry. **A**: Schematic overview of the experimental design. **B**: Representative histograms with indicated gating of CD4+TRBV6+ T cells with high proliferative capacity. **C**: Frequency of T cells with high proliferative capacity. **D**: Proportion of labelled CD4+TRBV6+ T cells from *Marilyn* CTL and cKO mice after 72 h of culture. Data are presented as mean ± SEM. Statistical analysis: Ratio paired *t* test (**C**); Unpaired *t* test (**D**). *n* = 6 from three independent experiments.

4.5.3. Homeostatic expansion of XPR1 cKO CD4+ T cells is impaired *in vivo*

Initial analyses utilised co-stimulation by α-CD28 antibody treatment to assess effector functions and TCR signalling *in vitro*. In these experiments cKO T cells displayed a hyperactivated phenotype, while in competitive clonal expansion assays with limited

co-stimulation, *Marilyn* cKO CD4+ T cells proliferated less than XPR1 expressing *Marilyn* CTL CD4+ T cells. To confirm the relevance of CD28 signalling for XPR1-mediated changes in T-cell effector functions, we further investigated co-stimulation-independent proliferation of CTL and cKO CD4+ T cells using homeostatic expansion (303). Homeostatic expansion occurs independently of CD28 in situations of lymphopenia, like the neonatal period, a viral infection, or a therapeutic intervention with irradiation and cytotoxic drugs (304–307).

Naïve CTL and cKO CD4+ T cells labelled with eFluor450 and eFluor670 proliferation dye, respectively, were mixed 1:1, and injected intravenously into immunodeficient *Rag2*$^{-/-}$ mice, to enable CTL and cKO CD4+ T-cell expansion under lymphopenic conditions (Figure 35A). After 96 h, recipient mice were sacrificed and the proliferative activity of labelled T-cell populations retrieved from spleen was analysed by flow cytometry.

Representative gating is shown in Figure 35B, with CD4+ T cells that underwent at least one division are gated as proliferating CD4+ T cells. Frequencies of splenic CTL or cKO CD4+ T-cell proliferation from three independent experiments are summarised in Figure 35C. Compared to CTL T cells, a significantly and strikingly decreased proportion of proliferating cKO T cells was detected. This demonstrates that in the absence of CD28-mediated co-stimulation, XPR1 deficient CD4+ T cells have a proliferation disadvantage.

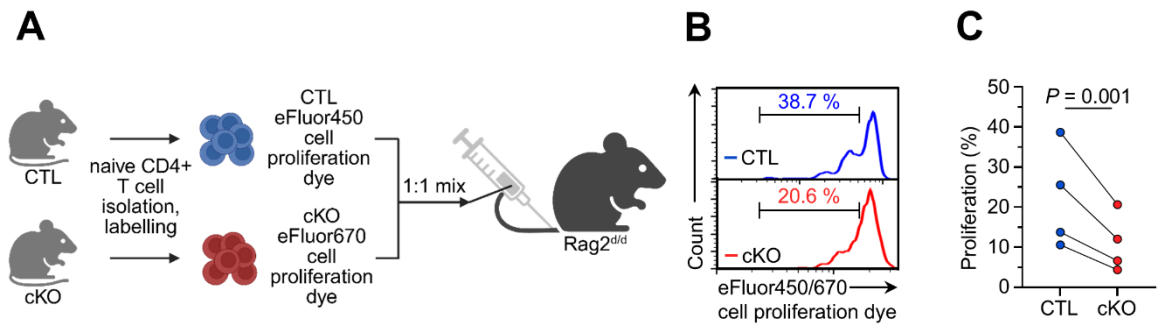

Figure 35: Co-stimulation-independent homeostatic expansion of cKO CD4+ T cells is impaired. Naïve CD4+ T cells isolated from CTL and cKO mice were labelled with eFluor450 and eFluor670 cell proliferation dye, respectively. A mixture of 1x10^6 labelled, naïve CD4+ T cells per genotype in 100 µL saline was transferred into *Rag2*$^{-/-}$ mice intravenously. After 96 h, recipient mice were sacrificed, spleens were dissected and analysed by flow cytometry. **A**: Schematic overview of the experimental design. **B**: Representative histograms with indicated gating of proliferating T cells. **C**: Frequency of proliferating T cells. Data are presented as mean ± SEM. Statistical analysis: Ratio paired *t* test. *n* = 4.

To further investigate the contribution of CD28 signalling to the hyperactivated phenotype of XPR1 deficient CD4+ T cells, proliferation in response to α-CD28 antibody treatment, but low concentrations or complete absence of α-CD3 antibody stimulation was assessed. For this, CTL and cKO CD4+ T cells stained with a proliferation dye were stimulated with plate-bound

antibody cocktails comprising of 1 or 5 µg/mL α-CD28, in combination with 0 or 0.5 µg/mL α-CD3. After 72 h of culturing, CD4+ T-cell proliferation was assessed by flow cytometry.

Representative dot plots for stimulation with 0 µg/mL α-CD3 and 1 µg/mL α-CD28 are shown in Figure 36A. Quantification of the frequency of proliferating T cells is shown in Figure 36B. In the absence of both α-CD3 and α-CD28 antibodies, only around 2 % of all CD4+ T cells were detected in the proliferation gate irrespective of the genotype. Strikingly, stimulation with 1 µg/mL and 5 µg/mL α-CD28 led to significantly increased proliferation frequencies in cKO CD4+ T cells compared to CTL T cells, although no α-CD3 stimulation or only low concentrations of 0.5 µg/mL α-CD3 were provided. In contrast, these conditions were not sufficient to induce proliferation in CTL CD4+ T cells, which showed similar background proliferation frequencies as the unstimulated negative control. Taken together, α-CD28 stimulation elicits a proliferative response in XPR1 deficient CD4+ T cells, even in the absence of α-CD3, indicating that XPR1 plays a regulatory function for CD28 signalling in CD4+ T cells.

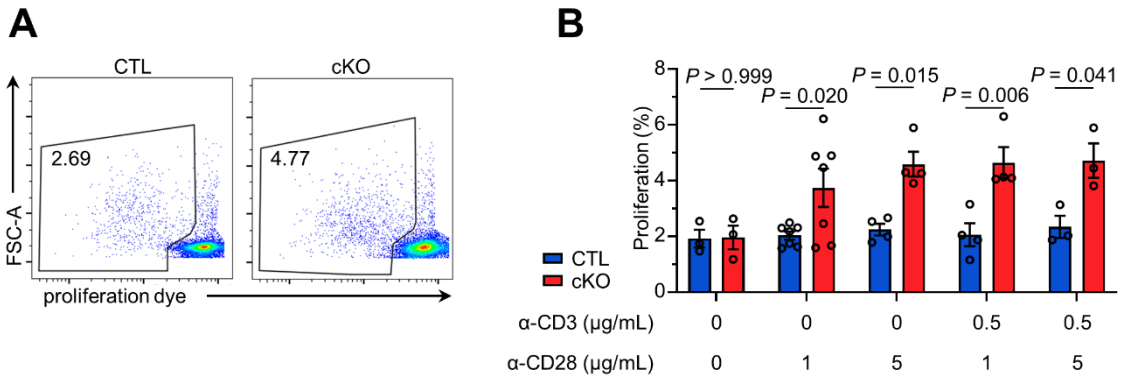

Figure 36: Treatment of α-CD28 is sufficient to induce proliferation of XPR1 deficient CD4+ T cells in the absence of α-CD3 stimulation. CD4+ T cells were isolated from CTL and cKO mice and stimulated for 72 h with the indicated concentrations of plate-bound α-CD3 and α-CD28 antibodies. **A**: Representative dot plots with indicated gating of proliferating T cells. **B**: Frequency of proliferated CD4+ T cells after 72 h of cultivation. Data are presented as mean ± SEM. Statistical analysis: Two-way ANOVA followed by Šidák's multiple comparisons test. For (α-CD3, α-CD28): *n* = 3 (0,0; 0.5,5); *n* = 7 (0,1); *n* = 4 (0,5; 0.5,1).

In summary, XPR1 deficiency in CD4+ T cells leads to a proliferation disadvantage during homeostatic expansion, indicating that CD28-dependent co-stimulation is indispensable for the hyperactivated phenotype of antibody-stimulated cKO T cells. This is further supported by the ability of cKO CD4+ T cells to proliferate even without α-CD3 stimulation by α-CD28 stimulation alone, highlighting an inhibitory function of XPR1 in CD4+ T-cell responses.

5. Discussion

5.1. Validation of conditional *Xpr1* gene knockout

XPR1 is a transmembrane protein and a phosphate exporter which is involved in the regulation of intracellular phosphate homeostasis in general and has specifically implications for polyP levels in platelets (165, 166, 180, 183, 184, 288, 289, 308, 309). Furthermore, XPR1 regulates trafficking and complex formation of adaptor proteins involved with T-cell stimulation (176, 185, 197). Therefore, the role of XPR1 in regulating CD4+ T cell-functions was addressed in this work.

Knockout mice with T cell-specific deletion of *Xpr1* were generated by crossing *Xpr1* floxed mice with the *Cd4-Cre* line that express transgenic Cre recombinase in all T cells due to its *Cd4*-derived promoter sequence. The analysis of these XPR1 deficient CD4+ T cells revealed that XPR1 regulates CD28-mediated T-cell responses.

The validation of the gene knockout by qPCR revealed moderately decreased *Xpr1* expression in cHET CD4+ T cells and severely decreased *Xpr1* expression in cKO CD4+ T cells in comparison to CTL* CD4+ T cells, that were phenotypically indistinguishable from CTL CD4+ T cells (data not shown) (Figure 5). Notably, *Xpr1* expression was not completely diminished in cKO CD4+ T cells. This is also supported by immunoblotting analysis, showing a decreased intensity, but not a total abolishment of XPR1 signal in cKO CD4+ T cell lysates (Figure 5). However, this is in line with previous reports with *Xpr1* deletion in the renal tubule (179) and platelets (180) and likely specifies the particular target gene sequence as T-cell isolations are constantly very pure (>95%), which excludes potential sample impurities as explanation. Similarly, when XPR1 was detected in Jurkat cells, the intensity of the XPR1 signal in immunoblots analysing siXPR1-treated cells was only moderately decreased compared to siCtrl treated cells, even though *XPR1* expression was decreased to 29.6 ± 3.8 % of the control expression levels, as shown in qPCR analysis (Figure 17), which may illustrate a slow turnover time of XPR1. Therefore, even though residual expression remains, reduction of XPR1 expression on protein level could be shown in the mouse model for cKO CD4+ T cells, and in the Jurkat cell culture model for siXPR1 treated cells, validating our models.

Immunoblots were done using a rabbit polyclonal (14174-1-AP) and a mouse monoclonal (2G8) antibody. Especially usage of the latter led to the detection of several bands at different molecular weights in immunoblot analysis. The rabbit polyclonal antibody 14174-1-AP also showed some unspecific bands in immunoblot analysis, though to a lesser extent. The structure of XPR1 is complex, since the protein features ten transmembrane helices (165, 162). Furthermore, cryo electron microscopy analysis done by several groups showed XPR1 to be present as a homodimer (162–166, 310). Due to this structural features, lysis, and

sample preparation for SDS PAGE that involves denaturing protein structures except for the primary structure might impede epitope recognition by the used antibodies. Different lysis buffers or sample preparation protocols that preserve the protein structure could be tested to optimise XPR1 detection in immunoblots (311, 312). An example for this might be Tsuji's work in which they analysed the impact of sample preparation for detection of the transmembrane iron transporter proteins SLC11A2 and SLC40A1, thereby revealing a strikingly improved detection efficiency in immunoblots if samples were not heated at 95 °C before SDS-PAGE (313). This could be tested to improve XPR1 detection with immunoblotting in the future.

A different approach to ensure antibody specificity against XPR1 for detection in immunoblots, immunofluorescence, flow cytometry, or other antibody-based methods could be to endogenously label XPR1 with a tag like V5, Halo, or others using a CRISPR-based approach (314–316). This could either be done in cell lines like Jurkat cells, or in mouse models. This approach also has the advantage of reliable detection of proteins with a low copy number. Further, interaction analyses based on immunoprecipitations could be enabled by using a tag for Pull-Down (317). However, the position for the tag insert needs to be chosen carefully, as interfering with interaction sites or the protein structure can critically affect stability, trafficking, and function of target proteins.

5.2. XPR1-mediated effects on thymic development

We found thymic development and selection processes to be dysregulated in XPR1 deficient CD4+ T cells (Figure 6). During development, T-cell progenitors enter the thymus being double negative for expression of CD4 and CD8 (DN). Even though CD4 protein expression is not apparent at the late DN stages DN3 (CD25-CD44+) and DN4 (CD25-CD44-), transcription of the *Cd4* gene locus starts at the DN3 stage (318, 319). Therefore, *Xpr1* deletion is likely effective starting at the DN3 stage of thymocytes.

During the DN3 stage, thymocytes undergo β-selection, rearranging their TCR-β chain (9, 10). Progression into DN4 and eventually DP cells requires the expression of a functional pre-TCR complex, comprised of a rearranged TCR-β chain, a pre-Tα chain, and CD3 (13–17). Pre-TCR signalling is crucial for the successful progression, as it controls proliferation, protection from apoptosis, and survival signals (13, 17–20). However, how exactly the pre-TCR drives β-selection is not fully understood to this day (13, 18, 320). Smid *et al.* proposed a model to study the pre-TCR by reconstituting it into non-immune cells (320). They showed that the pre-TCR can signal tonically, and that its internalisation and trafficking is largely independent of ligand binding to the TCR (320). This highlights the importance of trafficking and internalisation of the pre-TCR for T-cell development. Already in the DN3 stage, we observed a dysregulation

of thymic development due to XPR1 deficiency. The increased frequency of DN3 cells in cKO DN thymocytes compared to CTL DN thymocytes (Figure 6C) indicates a developmental block at the DN3 stage (207, 18). To properly address the developmental block at the DN3 stage, further experiments addressing the pre-TCR trafficking or the signalling in DN3 cells of cKO vs CTL mice would need to be conducted. However, we found differential TCR internalisation and signal transduction in CD4+ T cells from the periphery, indicating that similar aberrations may take place in the thymus.

Furthermore, analysis of the DP population revealed altered selection processes in XPR1 deficient thymocytes. Thymocytes undergo positive selection in the DP stage with CD69+TCR-β+ cells of the DP population delineating thymocytes that recently went through this selection (208, 209, 321). Hence, a decreased proportion of CD69+TCR-β+ thymocytes (Figure 6D) indicates that fewer cells recently passed the positive selection in the cKO DP population compared to the CTL DP population, highlighting a dysregulated positive selection process.

Another indication for developmental blockade is the differential upregulation of clonotypic genes encoding for TCR-α chains (Figure 10B). Hsieh *et al.* analysed the TCR repertoire of CD4+ T cells and found an overlap of TCR-α chain repertoire between natural thymic and peripherally developed Treg cells (322). In contrast, the overlap of natural thymic Treg cells and conventional T cells was not as large (322). They further discussed that Treg cells tend to express TCRs with higher avidity for recognising self-peptides (10, 322, 323). Therefore, differential expression of some TCR chain genes could indicate an altered TCR repertoire that arose due to altered selection processes, and might affect self-reactivity and/or differentiation of CD4+ T cells.

Moreover, we observed an increased expression of CD5 on DP thymocytes from cKO mice compared to CTL mice (Figure 6E). CD5 is a key player in functional tuning of the TCR signalling response, as CD5 negatively regulates the TCR signalling response (21, 22). During different developmental steps of thymocytes maturation, CD5 expression correlates with the avidity of the preTCR/TCR, thereby functionally tuning the TCR response (10, 21, 22). DP thymocytes that display high TCR avidity during positive selection upregulate CD5, whereas CD5 expression gets downregulated on DP thymocytes with a lower avidity (10, 21, 22). Therefore, increased CD5 expression in XPR1 deficient thymocytes could indicate two things: in scenario one, XPR1 deficiency directly upregulates CD5 expression, which affects functional tuning. Cells with a low avidity TCR would be more susceptible to apoptosis due to selection by neglect. In scenario two, XPR1 deficiency leads to increased TCR signalling, which in turn induces upregulation of CD5 to tune cells with a high TCR avidity. In this scenario,

a generally higher avidity of the TCR could also lead to increased selection due to high self-reactivity. Irrespective of the underlying molecular mechanism, the selection processes are shown to be affected in XPR1 deficient thymocytes, which is also supported by the decreased SP4 and SP8 frequencies as well as the increased DP frequency (Figure 6A).

Further, the functional tuning by CD5 also affects T-cell differentiation and effector functions of mature CD4+ T cells, as several studies found altered TCR downstream signalling, cytokine expression, and differentiation between CD4+ T cells expressing high versus low levels of CD5 (324–331). Concluding from this, differential CD5 expression during thymic development might be indicative for elevated effector functions in mature XPR1 deficient CD4+ T cells.

When relative frequencies in thymus analyses are compared, differences in frequencies between genotypes might not be in line with differences in absolute numbers. This can be the case if one or more of the analysed groups display an altered total thymus cell number. However, decreased frequencies also correlated to reduced absolute numbers of SP4 and SP8 thymocytes in XPR1 deficient thymi (Figure 6B). Moreover, decreased frequency and absolute number of SP4 thymocytes in XPR1 deficient mice also translate to the periphery, since CD4+ T-cell populations in spleen and mLNs are decreased by about 2-fold in cKO compared to CTL mice (Figure 7).

Taken together, thymic development and selection processes are altered in cKO mice compared to CTL and cHET mice, resulting in decreased numbers of mature peripheral CD4+ T cells. Further experiments would be required to properly address specific stages of development and selection to discover the mechanism of how XPR1 is affecting the thymic development of CD4+ T cells, *e.g.* through specific signalling pathways.

5.3. Hyperactivation of XPR1 deficient CD4+ T cells

We show that mature XPR1 deficient CD4+ T cells are hyperactivated. This is apparent by gene expression analysis of stimulated cKO vs. CTL CD4+ T cells (Figure 10), as well as surface protein expression analysis by flow cytometry using an activation marker panel (Figure 9), which will be discussed in the following section.

The most prominent hit in the gene expression array is *Il2*, the gene encoding IL-2, which is increased by 23.21-fold in α-CD3/α-CD28-stimulated cKO CD4+ T cells compared to the control (Figure 9, Table 23). IL-2 is a cytokine central for T-helper cell homeostasis and function, and acts by inducing proliferation and survival signals in lymphocytes (332, 333). IL-2 expression is rapidly upregulated once CD4+ T cells get activated (332, 333). The striking upregulation of *Il2* expression therefore indicates hyperactivation of XPR1 deficient CD4+

T cells, which is also supported by surface expression analyses of the activation markers CD44, CD62L, CD69, and CD25 on CD4+ T cells stimulated with α-CD3/α-CD28 for 72 h.

CD44 is an adhesion molecule expressed on the surface of different immune cells and has a pivotal role for CD4+ T-cell functions. During T-cell migration, CD44 surface expression increases and facilitates adhesion to the endothelium by interacting with ligands like hyaluronic acid, collagens, fibronectin, or others (334–336). Further, CD44 has been shown to increase stability of DC-T-cell interactions in the IS, and thereby facilitate TCR signalling, positively regulating the resulting proliferation and cytokine production (334, 337). CD44 is widely recognised as memory T-cell marker (215, 217). Upregulated *Cd44* gene expression by 3.65-fold (Figure 10, Table 23), as well as increased surface expression of CD44 (Figure 9) in α-CD3/α-CD28 stimulated CD4+ T cells of cKO compared to CTL mice both strongly argue for T-cell hyperactivation due to XPR1 deficiency.

CD25 is the alpha chain of the IL-2 receptor and widely used as surface marker for identification of Treg cells. However, conventional T cells upregulate CD25 also upon stimulation, which is therefore suited as a late activation marker (213, 338–342). We reported a trend for increased CD25 expression on unstimulated and stimulated XPR1 deficient CD4+ T cells (Figures 4.1.5), indicating hyperactivation. Similarly, CD69, which is an early marker of CD4+ T-cell activation (343, 344), was upregulated significantly without stimulation (Figures 4.1.5).

CD62L is another key adhesion molecule in CD4+ T-cell biology. Upon activation of T cells, CD62L is shed by ADAM17 from the cell surface, thereby controlling migration and homing to tissues (345–352). CD62L is expressed on naïve CD4+ T cells and on central memory cells, whereas effector memory cells are $CD62L^{low}$ (353–357, 214–216). Therefore, CD62L expression is commonly used as a marker to differentiate between naïve and effector memory T-cell populations (353–357, 214–216). We did not observe a significant difference in CD62L expression of unstimulated or stimulated cKO CD4+ T cells compared to CTL CD4+ T cells (Figure 9), which contrasts the differential expression of CD44. However, since unstimulated and stimulated cKO CD4+ T cells increased CD44 on gene expression and protein levels, in line with an elevated expression of activation markers CD25 and CD69, these data show that XPR1 deficiency leads to a hyperactivated T-cell phenotype, identifying XPR1 as a negative regulator of CD4+ T-cell activation.

Hyperactivated CD4+ T cells can be dangerous for the host if they facilitate proinflammatory effector functions for longer periods of time, promoting or contributing to chronic inflammation, autoimmunity, and tissue damage (7). To prevent this, antiinflammatory mechanisms downregulate CD4+ T-cell activation in order to dampen a harmful immune response. A

common mechanism to facilitate this is the engagement of immune checkpoint molecules whose expression gets induced by CD4+ T-cell stimulation (7, 68, 358).

We addressed the surface expression of immune checkpoint molecule PD-1 which inhibits TCR downstream signalling when engaged by its ligand PD-L1, and therefore serves as a common target for anti-tumour immune checkpoint therapy (31). The mechanism of PD-1 inhibiting CD4+ T-cell activation has been recently found to be driven by PD-1 inhibiting CD28-mediated co-stimulatory signals (30). PD-1 has further been shown to be a marker for T-cell exhaustion (7, 212). Nettersheim *et al.* show in a vaccination mouse model that PD-1 expression in CD4+ T cells is associated with self-specificity, and that antibody-mediated blockade of PD-1 on self-specific CD4+ T cells increased their proliferation when treated with vaccine (359). They deduce from their experiments that PD-1 is involved in controlling CD4+ T-cell responses to self by inhibition (359). We found significantly increased expression of PD-1 on naïve cKO compared to naïve CTL T cells, but not after stimulation for 72 h (Figure 9). This could indicate a higher self-specificity and/or tonic stimulation of XPR1 deficient CD4+ T cells. Therefore, it is possible that increased PD-1 expression in naïve cKO T cells is contributing to inhibit T-cell activation to counteract the observed hyperactivation phenotype. In line with this role of checkpoint molecule inhibition, we found increased expression of *Tigit* in cKO compared to CTL CD4+ T cells in our gene expression analysis (Figure 10, Table 23). TIGIT is an inhibitory receptor which is expressed on activated T cells, or other immune cells like DCs, macrophages and B cells (26, 224). Via interaction with its ligand CD155, TIGIT transduces inhibitory signals in T-helper cells (26, 224). This leads to the conclusion that upregulation of immune checkpoint molecules in XPR1 deficient CD4+ T cells might counteract hyperactivation of self-specificity, preventing autoimmunity or tissue damage.

In summary, analysis of XPR1 deficient CD4+ T cells displays XPR1 to be a negative regulator of CD4+ T-cell hyperactivation.

5.4. Effector functions in XPR1 deficient CD4+ T cells

Activated CD4+ T cells carry out a variety of effector functions: they proliferate, differentiate into T-helper subsets, and produce cytokines, regulating the immune system (7). In this work, proliferation, differentiation, and cytokine production was analysed to assess the impact of XPR1 deficiency on CD4+ T-cell effector functions.

5.4.1. Proliferation

Proliferation assays revealed increased proliferation of XPR1 deficient CD4+ T cells in response to α-CD3/α-CD28 stimulation (Figure 11B), which presents one major indication for increased effector functions.

Moreover, we performed proliferation assays with PMA/ionomycin treatment to stimulate CD4+ T cells independently of the TCR. PMA is a DAG analogue which activates PKC signalling, whereas ionomycin acts as a ionophore, inducing Ca^{2+} influx into the cytosol (257–259). Therefore, this method circumvents TCR or CD28 engagement to stimulate CD4+ T cells. Proliferation does not differ between CTL and cKO CD4+ T cells when stimulated with PMA/ionomycin (Figure 11C), indicating that the increased proliferation in XPR1 deficient CD4+ T cells depends on engagement of the TCR-CD3 complex and/or CD28.

Further, we performed proliferation assays using the toxic superantigen SEB to stimulate CD4+ T cells. The superantigen SEB is able to bind TCRVβ and MHC-II, as well as CD28 and B7, leading to rapid cytokine production, inflammation, and sepsis (360, 263, 361, 264). It has previously been found that SEB is even able to bind the TCR complex and CD28 independently of APCs, leading to T-cell activation and expression of proinflammatory cytokines in human CD4+ T cells (362). SEB treatment did not result in altered proliferation of cKO compared to CTL CD4+ T cells (Figure 11D). We conclude that SEB affects CTL and cKO CD4+ T cells to the same degree by inducing hyperactivation and excessive effector mechanism programs that elevate proliferation irrespectively of XPR1 expression.

5.4.2. Differentiation and cytokine production

In vitro differentiation assays revealed altered cytokine and transcription factor expression in cKO T cells compared to CTL T cells under Th1-, Th2-, Th17-, and iTreg-skewing conditions (Figures 12-15).

IFN-γ and TNF-α are characteristic proinflammatory cytokines expressed by Th1 cells (7, 35, 36). Both TNF-α and IFN-γ production significantly increased in cKO CD4+ T cells compared to controls under Th1-skewing conditions (Figure 12). This points towards increased signalling in XPR1 deficient T cells which promotes the induction of cytokines, *e.g.*, STAT1 (363). However, we also observed a trend for decreased expression of T-bet in cKO compared to CTL T cells (Figure 12), indicating decreased *bona fide* differentiation into Th1 cells. Since increased levels of TNF-α and IFN-γ have been shown to be associated with increased T-bet expression (364, 363), these results are puzzling and presumably reflect the insufficient Ca^{2+}

signalling in cKO T cells that is has been shown to be necessary for proper Th1 differentiation in human CD4+ T cells (365).

Th2 cells are involved with humoral immunity, allergies and important for mucus production at mucosal surfaces (7, 36, 43). Differentiation was not altered between cKO and CTL CD4+ T cells under Th2-skewing conditions, indicating a negligible role of XPR1 for this subset differentiation (Figure 13). This is also supported by comparable IgG and IgM levels in serum from CTL and cKO mice (Figure 19), as an increased Th2 differentiation would enhance the antibody production from B cells.

IL-17, the key proinflammatory cytokine produced by Th17 cells, is involved in host defence, and has been shown to aggravate autoimmunity or chronic inflammation (366). Further, Th17 cells express IL-22, a cytokine from the IL-10 family. IL-22 can also be expressed by other cells, *e.g.* innate lymphoid cells, natural killer cells, or the specialised Th22 subpopulation (56). Th22 cells are characterised by expression of IL-22, TNF-α, IL-13, IL-26 and granzyme B, but they do not express IL-17 (33, 58). Moreover, TGF-β has been shown to inhibit IL-22 expression (58, 59). Th22 cells and IL-22 have been shown to be involved in maintaining barrier function and mucosal homeostasis, but have also been shown to mediate both pro- and antiinflammatory immune responses in the context of host defence, cancer, or inflammatory diseases like SLE, RA, IBD, or atopic dermatitis (33, 54–57, 59–61, 367–369).

When XPR1 deficient CD4+ T cells were cultured under Th17-skewing conditions, two different protocols were used. Using the now discontinued kit, IL-22 expression was increased in XPR1 deficient CD4+ T cells (Figure 14B). Since high expression levels of IL-17a were present in both genotypes (40-50 % IL-17a+ CD4+ T cells), differentiation into a Th22 phenotype is unlikely. However, IL-17a levels did not differ between CTL and cKO CD4+ T cells. Furthermore, Ror-γt expression was decreased in XPR1 deficient CD4+ T cells. Lazarevic *et al.* showed that increased expression of T-bet mediated by the “alternative” Th17 type inhibits Ror-γt expression (370). Further, IL-22 expression was shown to be increased in “alternative” Th17 cells (7, 48–50, 371). Therefore, it is possible that XPR1 deficiency led to differentiation into a more pathological Th17 entity by dysregulated signalling when differentiated using the kit. Since IL-22 expression as well as the differentiation into “alternative” Th17 cells are inhibited by TGF-β, only a low concentration of TGF-β might be present in the kit.

In contrast to the differentiation using the kit, differentiation with a protocol including known concentrations of the cytokines IL-6, IL-23 and TGF-β led to significantly increased IL-17a production, but only a trend for increased IL-22 production in cKO compared to CTL cells (Figure 14C). This increased IL-17a expression highlights more proinflammatory

characteristics of XPR1 deficient Th17 cells compared to the control. Since increased IL-17a expression is usually due to increased expression of Ror-γt, the comparable levels of Ror-γt expression between CTL and cKO samples indicate that XPR1 deficiency increases cytokine production but not transcription factor expression. This suggests that increased IL-2 and/or CD28 signalling in XPR1 deficient T cells prevents the differentiation of *bona fide* Th17 cells (265, 372).

Irrespective of the plasticity of the Th17 differentiation response of CD4+ T cells when using different protocols, cKO cells always showed an increased expression of IL-17a or IL-22, or both. This highlights XPR1 deficiency to contribute to proinflammatory programs and/or dysregulated signalling. Since IL-22 expression seems to be regulated by XPR1, one could address XPR1's role for the differentiation into a Th22 subtype. Plank *et al.* established a protocol to culture CD4+ T cells under Th22-skewing conditions (58). As a readout for Th22 differentiation, one could assess Th22-characteristic cytokines, *e.g.* TNF-α, IL-22, or IL-13. Further, expression of AhR could be addressed, which represents the key transcription factor of the Th22 subpopulation (33).

Treg cells are downregulating the immune response to circumvent acute and/or chronic inflammation and autoimmunity (7, 68). When analysing XPR1 deficient T cells after differentiation under iTreg-skewing conditions, no differences for expression of CD25 or IL-10 were observed compared to controls (Figure 15). Foxp3 expression in Treg cells is associated with suppressive capacity (65, 373). Significantly downregulated Foxp3 expression in cKO CD4+ T cells compared to the control could therefore indicate decreased inhibitory functions of iTreg cells. In a physiological context, this would lead to aggravation of proinflammatory programs by insufficient inhibition of effector T-cells, most importantly Th1 and Th17 cells, which are prominently involved in the pathophysiology of autoimmune diseases (374–377). These data further highlight the imbalance of proinflammatory vs. antiinflammatory mechanisms in XPR1 deficient CD4+ T cells for T-cell subset differentiation.

Interestingly, IL-2 concentrations in the supernatants of Th0, Th1, Th2, Th17 and iTreg cells were consequently significantly increased in CD4+ T cells lacking XPR1 compared to controls (Figure 16). This indicates that increased *Il2* expression as determined by the gene expression array is uncoupled from T-helper cell differentiation, instead revealing an altered TCR downstream signalling effect by XPR1 deficiency for CD4+ T cells in general, not only for a specific T-helper cell subpopulation.

IL-2 supports differentiation into Th1- and Th2 cells, while it impairs differentiation into Th17 cells (69, 73, 74). IL-2 was added to the media used for *in vitro* differentiation into Th1-, Th2-, and Tregs, but not Th17 cells. This was done to ensure sufficient survival and proliferation of

the former three subpopulations (378, 379). Also, Th0 cells were cultured with IL-2 added to the culture medium. Measuring IL-2 levels after the *in vitro* differentiation could in theory detect supplemented IL-2 in supernatants of Th0, Th1, Th2, and Treg cells. However, IL-2 is rapidly consumed by proliferating T cells, and only in supernatants from Th0- and Th2-cell cultures was the IL-2 concentration higher than in Th17-cell cultures, which did not receive IL-2 supplementation. Thus, the observed differences in IL-2 secretion between CTL and cKO CD4+ T cells reflect rather an altered production than a differential uptake of IL-2.

Cytokine expression was also addressed in Jurkat cells as a means to put our findings into perspective for human T-cell responses. Strikingly, expression of *IFNG*, *TNFA*, and *IL-22* was increased in siXPR1-treated cells even without stimulation (Figure 17). This matches the increased expression of TNF-α, IFN-γ, and IL-22 in the *in vitro* differentiation experiments using the murine model (Figures 12 and 14). Other groups have shown that the expression of *TNFA*, *IFNG,* and *IL22* in Jurkat cells is very low without stimulation (380–385). Increased expression of *TNFA*, *IFNG*, and *IL22* might therefore indicate that Jurkat cells with reduced XPR1 expression exhibit dysregulated activation or signalling even in the unstimulated state. It might be interesting to analyse signalling or cytokine expression, on protein as well as mRNA level, after stimulation of Jurkat cells.

5.4.3. Antigen-specific activation of *Marilyn* T cells by H-Y injection

Stimulation with α-CD3/α-CD28 was done to induce activation, proliferation, and differentiation of T-helper cell populations. This mimics the interaction of a CD4+ T cell with a DC during antigen-presentation: plate-bound α-CD3 engages with the CD3-TCR complex, crosslinking the TCR, whereas α-CD28 induces co-stimulation via interaction with CD28 (294–296). However, *in vivo* stimulation of CD4+ T cells is achieved via antigen presentation by APCs in synergy with co-stimulation, leading to clonal expansion (7, 123). Antigen-specific activation of *Marilyn* CTL or cKO CD4+ T cells presents a more physiologically relevant approach to address XPR1 dependent CD4+ T-cell functions (297–300).

Injection of the cognate peptide H-Y into female *Marilyn* mice (Figure 31A) led to results similar to effector function analyses done *ex vivo*, with increased expression of the activation marker CD44 in cKO *Marilyn* mice (Figure 32B) supporting earlier evidence for hyperactivation. The trend for increased expression of Ki-67 in LNs of *Marilyn* cKO mice after H-Y injection (Figure 31F) also indicates increased proliferation in XPR1 deficient *Marilyn* CD4+TRBV6+ T cells (386, 387), which supports the results obtained in proliferation assays *ex vivo* using α-CD3/α-CD28 for stimulation (Figure 11B).

PD-1 expression was significantly increased in *Marilyn* cKO compared to *Marilyn* CTL mice as well (Figure 31E). As discussed in section 5.3, PD-1 is an exhaustion marker and gets expressed by cells to decrease the inflammatory response (7, 212, 30). Therefore, increased expression might either indicate exhaustion and/or immunoinhibitory mechanisms compensating for increased proinflammatory effector functions in XPR1 deficient *Marilyn* CD4+TRBV6+ T cells 6 days after peptide injection.

Contrary to findings in the *in vitro* differentiation assays (Figures 14 and 15), expression of Ror-γt as well as Foxp3 was increased in LNs of XPR1 deficient *Marilyn* mice after application of antigen stimulus (Figure 32D-F). This observation may indicate that additional signals are provided *in vivo* that promote the differentiation of XPR1 deficient Treg cells, which are lacking *in vitro*. This might also be the case for Th17-cell differentiation, indicated by increased Ror-γt expression as well as increased expression of IL-17a and IL-22 (Figure 33A-C), with the increased IL-22 levels hinting to a potentially more pathological Th17 phenotype (7, 48–51, 371, 388). Unexpectedly and contrary to data generated in *in vitro* differentiation assays, Th1 proinflammatory effector functions seem to be largely unaffected, since TNF-α and IFN-γ levels are not significantly altered between *Marilyn* CTL and *Marilyn* cKO mice (Figure 33D-F).

In summary, results of H-Y injection *in vivo* support a hyperactivated phenotype of XPR1 deficient CD4+ T cells undergoing clonal activation, with a putative key role of IL-17a and IL-22 expressed by Th17 cells eliciting proinflammatory effector functions. This is similar to earlier *in vitro* differentiation analyses.

5.5. Signalling in XPR1 deficient CD4+ T cells

XPR1 deficiency induced markedly dysregulated signalling in CD4+ T cells. Since we observed increased gene and protein expression of *Il2*/IL-2 (Figure 10, Figure 16, and Table 23), we analysed TCR downstream signalling that induces or regulates IL-2 expression.

5.5.1. Ca^{2+}-Calcineurin-NFAT- and ERK1/2-AP-1 pathways

A major signalling pathway leading to expression of *Il2* is the Ca^{2+}-Calcineurin-NFAT pathway. Since *Il2*/IL-2 expression is markedly increased in XPR1 deficient CD4+ T cells that were stimulated for 6 h with α-CD3/α-CD28, the impaired Ca^{2+} response to α-CD3 stimulation in XPR1 deficient CD4+ T cells is surprising (Figure 21). Ca^{2+} influx can be affected by a plethora of proteins or mediators, therefore we sought to address which upstream signalling molecules that couple TCR activation to Ca^{2+} release into the cytosol could be differentially regulated. We addressed LAT phosphorylation since LAT is upstream of the Ca^{2+}-calcineurin-NFAT

pathway. We did not observe significantly increased p-LAT levels upon stimulation of CD4+ T cells due to high variance of the samples (Figure 20). Activation of PLCγ1 as another upstream player was addressed by analysing PLCγ1 phosphorylation by immunoblots, however we were not successfully able to detect a signal for p-PLCγ1 (data not shown), leaving its role unknown. Further analyses of LAT and PLCγ1 would be beneficial to address proximal TCR signalling.

Ca^{2+} influx into the cytosol leads to translocation of NFAT into the nucleus (114). NFAT translocation to the nucleus is significantly decreased in XPR1 deficient CD4+ T cells after 10 min of α-CD3 stimulation (Figure 22), which is in line with the decreased upstream Ca^{2+} response (Figure 21). Interestingly, induction of Ca^{2+} influx into the cytosol by the ionophore ionomycin resulted in significantly less NFAT translocation to the nucleus in XPR1 deficient CD4+ T cells (Figure 22). Further, thapsigargin treatment of XPR1 deficient CD4+ appeared to cause a decreased concentration of Ca^{2+} to be released from intracellular stores (Figure 21). Even though the latter treatment might also indicate a dysregulation of STIM1/Orai1-mediated calcium release (389), reduced Ca^{2+} influx into the cytosol in XPR1 deficient CD4+ T cells mediated by both ionomycin and thapsigargin might indicate a dysregulated balance of Ca^{2+} complexes or dysregulated intracellular Ca^{2+} buffering (390, 391).

ERK1/2 activation can be induced by Ca^{2+} influx, and affects *Il2* expression via the RASGRP1-RAS-ERK1/2-AP-1 pathway (75, 281). Similar to decreased NFAT translocalisation after 10 min of α-CD3 stimulation, and an impaired Ca^{2+} response to α-CD3 stimulation, we observed significantly decreased ERK1/2 phosphorylation 5 min after α-CD3/α-CD28 stimulation in XPR1 deficient CD4+ T cells (Figure 20). Taken together, these three analysed targets show impaired TCR downstream signalling 5-10 min after stimulation in XPR1 deficient CD4+ T cells.

Inside the nucleus, NFAT induces gene expression in complex with other players, one of which is AP-1, which contains c-Fos and c-Jun. Both were found to be upregulated by 2.38-fold (*Jun*) and 2.32-fold (*Fos*) in XPR1 deficient CD4+ T cells compared to the control (Figure 10, Table 23). Since c-Fos is downstream of the RASGRP1-RAS-ERK1/2 pathway (232), this contrasts the immunoblot analysis of ERK1/2 phosphorylation. Another hit contrasting the decreased ERK1/2 phosphorylation in XPR1 deficient CD4+ T cells is *Map3k8* which was upregulated by 3.97-fold in XPR1 deficient CD4+ T cells (Figure 10, Table 23). MAP3K8 is a serine/threonine kinase involved in promoting activation of ERK1/2, NFAT, and the PI3K-AKT-mTOR pathway, thereby positively regulating expression of IL-2, TNF-α, IFN-γ, and T-bet, as

well as favouring Th1 differentiation (225–230). An increased *Map3k8* expression in cKO cells would therefore rather suggest increased instead of decreased ERK1/2 phosphorylation.

One possible explanation for the unexpected reduced ERK phosphorylation could be the time point of analyses. ERK1/2 activation can be achieved in a transient manner, mediated by Raf1, or in a sustained manner, mediated by B-Raf (392–394, 275–277, 197). Importantly, IL-2 expression is dependent on sustained ERK1/2 signalling (197, 275–277, 394). In the representative immunoblots analysis, cKO CD4+ T cells showed a delayed increase of ERK1/2 phosphorylation after 30-60 min of stimulation (Figure 20). Since quantifications of ERK1/2 phosphorylation were done after 5 min of stimulation, which corresponds to the ERK1/2 phosphorylation peak in control CD4+ T cells, it is possible that ERK1/2 signalling is delayed rather than diminished in XPR1 deficient CD4+ T cells. However, quantification and repeated analysis of time points other than 5 min of stimulation would be required.

Moreover, prolonged NFAT translocation to the nucleus might be relevant. AKT has been shown to inactivate GSK3, which is an inhibitor of NFAT's binding to DNA (148–150). Consequently, AKT inhibition of GSK3 leads to prolonged NFAT localisation to the nucleus (148–150, 75). Therefore, increased AKT phosphorylation in XPR1 deficient CD4+ T cells (Figure 23) might cause prolonged NFAT localisation to the nucleus, increasing *Il2* expression by a sustained nuclear localisation, even when showing an impaired transient response. Therefore, NFAT translocation to the nucleus at later time points could be addressed.

5.5.2. PI3K-AKT-mTOR pathway

Il2 expression is also induced via signalling by the PI3K-AKT-mTOR pathway, which operates independently of ERK or Ca^{2+} signalling (287), and is differentially activated in CD4+ T cells that do or do not express XPR1. Co-stimulation in CD4+ T cells leads to PI3K activation, which results in phosphorylation of AKT at Thr308 and mTOR activation (142–146). mTOR associates with different proteins to for the mTOR complexes (mTORC) mTORC1 and mTORC 2. mTORC1 activates S6K1, which phosphorylates S6 (395, 396). mTORC2 has been shown to facilitate AKT phosphorylation at Ser473 (397, 398). In CD4+ T cells, mTOR is important for regulating differentiation: Delgoffe *et al.* showed that Rheb-dependent mTORC1 signalling positively affects Th1 and Th17 differentiation, supported by *in vitro* and *in vivo* data of Rheb deficient mice who did not develop EAE (399). On the other hand, Lee *et al.* revealed that mTORC2 regulates differentiation into Th1 and Th2 cells, dependent on the mTOR-PKC and mTOR-AKT signalling pathways (147).

Phosphorylation of AKT (Ser473) and S6 was upregulated in XPR1 deficient CD4+ T cells after 5 min of α-CD3 (Figure 23), which indicates increased mTOR signalling, and activation of both mTORC1 and mTORC2. In addition to PI3K-mediated co-stimulatory signals, AKT can also be phosphorylated dependent on TCR downstream signals, *e.g.* by PKC-α (400). This might contribute to increased AKT phosphorylation after α-CD3 stimulation in the absence of an α-CD28-mediated co-stimulus. Interestingly, phosphorylation of AKT and S6 was already increased in unstimulated, naïve XPR1 deficient CD4+ T cells (Figure 23A). This indicates striking hyperactivation of the CD28-dependent PI3K-AKT-mTOR pathway in XPR1 deficient CD4+ T cells, further highlighting the role of XPR1 as a negative regulator of co-stimulatory signals. However, this was only apparent in representative blots, and quantification at this time point in several experiments needs to be done to solidify our findings. Addressing PI3K and AKT phosphorylation after stimulation with α-CD3 or α-CD3/α-CD28 by immunoblotting could shed light on the impact of co-stimulation on AKT phosphorylation.

The importance of XPR1 for the PI3K-AKT-mTOR signalling pathway is further supported by the 2.36-fold downregulation of *Inpp4b* (Figure 10, Table 23). Peng *et al.* showed recently that INPP4B acts as a suppressor of T-cell activation in the PI3K pathway (220). They overexpressed or knocked down *Inpp4b* in murine T cells, revealing effects on proliferation and production of the cytokines IFN-γ and TNF-α. Consequently, increased expression of IFN-γ and TNF-α under Th1-skewing conditions (Figure 12), as well as increased AKT and S6 phosphorylation (Figure 23) might be in part explained by the downregulation of *Inpp4b* in XPR1 deficient CD4+ T cells.

There are also other differentially expressed genes that indicate increased activation of the PI3K-AKT-mTOR pathway in the absence of XPR1 in CD4+ T cells (Figure 10, Table 23):

Lif is upregulated by 4.84-fold in XPR1 deficient CD4+ T cells (Figure 10, Table 23). Lif has been shown to be involved in tumorigenesis and cancer progression by upregulating mTORC1-S6K1 signalling (233), or mTOR-AKT signalling (234). Gao *et al.* showed that LIF expression is increased in Tregs of a BALC/c based allo-tolerance model (235). Moreover, LIF has been shown to promote Foxp3 expression and suppress Th17-dependent genes (236–238). Induction of Tregs and inhibition of Th17 cells deviates from our data (Figures 14 and 15), therefore LIF might contribute to mTOR signalling in a differentiation-independent way.

Further, *Tspan31* and *Tpi1* were upregulated by 2.96-fold and 2.55-fold in XPR1 deficient CD4+ T cells, respectively (Figure 10, Table 23). TSPAN31 has been shown to be involved in tumour progression in breast cancer and glioma by activating PI3K-AKT-mTOR signalling or fatty acid metabolism in humans (239, 240). TPI1 activates PI3K-AKT-mTOR signalling in

breast and bladder cancer, inducing tumour progression (241, 242). These hits hint towards increased mTOR activation.

Expression of *Itga6* is downregulated by 4.17-fold in XPR1 deficient CD4+ T cells (Figure 10, Table 23). Low levels of ITGA6 have been shown to inhibit the PI3K/AKT pathway in adult neurogenesis by Guo *et al.* (243), however, ITGA6 is also associated with PI3K/AKT/mTOR activation in tumour cells (401). Thus, our findings possibly show a cell type-dependent regulation of this integrin.

Interestingly, expression of *Pdk1* has been shown to be decreased by 2.86-fold in XPR1 deficient CD4+ T cells. PDK1 is a prominent player in PI3K downstream signalling, as it gets recruited together with AKT to the membrane upon PI3K activation, where AKT gets phosphorylated at Thr308 by PDK1 (145, 244, 245). PDK1 prominently induces NF-κB signalling during T-cell activation (138). Reduced *Pdk1* expression might indicate an altered signalling downstream of PI3K, favouring mTOR signalling over PDK1 pathways. Therefore, addressing NF-κB signalling might be of interest for XPR1-dependent TCR downstream signalling.

Taken together, differentially expressed genes and immunoblot analyses highlight that increased PI3K-AKT-mTOR signalling initiated by CD28-mediated co-stimulation might be crucial for hyperactivation and increased effector functions like proliferation and expression of proinflammatory cytokines in XPR1 deficient CD4+ T cells.

5.5.3. Metabolism

CD4+ T-cell activation induces aerobic glycolysis. This metabolic shift is regulated by mTOR signalling: Shi *et al.* showed mTOR to control upregulation of HIF1α, which is an important player for mediating glycolytic activity (402). mTORC1 inhibition has also been shown to decrease cellular ATP levels by Schieke *et al.* (403). Moreover, Düvel *et al.* demonstrated that HIF1α and SREBP1/2 promote mTORC1-mediated proliferation and protein synthesis through activating metabolic gene targets (404).

We found that the activation-induced metabolic shift is predominantly elevated in XPR1 deficient CD4+ T cells with increased basal glycoATP production and increased proportion of ATP production from glycolysis (Figure 18). This could be due to increased mTOR activation in naïve as well as stimulated CD4+ T cells, and points towards a metabolic phenotype of hyperactivated T cells with high energy demand.

This is supported by some hits of the gene expression assay that were associated with metabolism (Figure 10, Table 23):

Mir155 expression was upregulated by 3.13-fold in XPR1 deficient CD4+ T cells (Figure 10, Table 23). Cai *et al.* demonstrated that miR155 delivery into CD4+ T cells in an arthritis mouse model induced glycolysis and enhanced differentiation into Th1/Th17 cells while inhibiting Treg differentiation (246). Jung *et al.* identified increased miR155 expression in Th17 cells which correlated with a favourable outcome in chronic lymphocytic leukaemia (247). Therefore, upregulated miR155 levels might impact immunometabolism and differentiation into Th1/Th17 cells in our model.

Txn1 was upregulated by 2.72-fold in XPR1 deficient CD4+ T cells (Figure 10, Table 23). This gene encodes for TNX1, which is part of the antioxidant thioredoxin (TRX) pathway (248). Increased levels of TXN1 in T cells have been shown to be associated with increased proliferation, increased anti-tumour efficiency, and altered immunometabolism (249–252). SEPP1 is also involved in the TRX pathway, and a selenium transport protein responsible for its distribution in the body (253–255). Hu *et al.* showed in a healthy human cohort that selenium supplementation increased the proportion of activated Tregs, which was associated with increased SEPP1 serum concentration (256). We further observed decreased expression of *Sepp1* by 2.57-fold in XPR1 deficient CD4+ T cells (Figure 10, Table 23). This might indicate reduced differentiation into Tregs, matching our results from the *in vitro* differentiation assays (Figure 15).

Taken together, metabolism is dysregulated and shifted to glycolysis, indicating an activated phenotype of XPR1 deficient CD4+ T cells, and possibly an impact of metabolism on differentiation.

5.5.4. Impact of CD28-mediated co-stimulation

PI3K-AKT-mTOR signalling is dependent on co-stimulation of CD4+ T cells (75). Since we found several components of this signalling pathway to be hyperactivated, co-stimulation via CD28 was addressed.

We first addressed proliferation in a setup for clonal expansion of *Marilyn* CTL and cKO CD4+TRBV6+ T cells. Proliferation of *Marilyn* cKO CD4+ T cells was impaired in coculture with *Marilyn* CTL CD4+ T cells compared to the control (Figure 34). This was surprising, since we expected that α-CD28 treatment provides a sufficient co-stimulus to induce hyperproliferative activity in XPR1 deficient *Marilyn* CD4+TRBV6+ T cells. It is possible that most α-CD28 antibodies were bound to splenocytes instead of providing a co-stimulatory signal for the CD4+ T cells, since *Marilyn* CD4+ T cells were cocultured with male splenocytes in a ratio of 1:15. Consequently, without AKT/mTOR hyperactivation, the impairment of Ca^{2+}

influx, NFAT translocation, and ERK phosphorylation would have negatively affected the proliferative response and survival of XPR1 deficient T cells.

To test our hypothesis that APC-mediated co-stimulation would lead to an advantage of *Marilyn* cKO CD4+ T cells in a clonal expansion setup, labelled *Marilyn* T cells from female mice were injected into a male CTL mouse. However, labelled cells were not retrieved in spleen or LNs after 4 days in initial experiments, so these injection experiments could be repeated.

Our hypothesis is further supported by a homeostatic expansion experiment. Homeostatic expansion is a mechanism that leads to T-cell expansion during lymphopenia, restoring T-cell homeostasis. Lymphopenia can occur during the neonatal period, due to treatment of conditions with irradiation or cytotoxic drugs, or after a strong viral infection (304–307). Classic co-stimulation via CD28 is not required for this process, instead the co-stimulatory molecules OX40 and CD24 are important (405–407, 303). We observed decreased proliferation of cKO CD4+ T cells compared to CTL CD4+ T cells when injected into $Rag2^{-/-}$ mice in a homeostatic expansion experiment (Figure 35). This further supports that the observed impaired response of the Ca^{2+}-Calcineurin-NFAT and ERK1/2 pathways might be detrimental for cKO CD4+ T-cell survival and proliferation in the homeostatic expansion setting. Moreover, it highlights that CD28 stimulation is a key process mediating the observed hyperactivation and increased effector functions of XPR1 deficient CD4+ T cells.

IL-7 has been shown to be involved in regulation of homeostatic expansion, supporting the survival of T cells (408, 409). Increased activation of mTORC1 has been shown to impair the IL-7 mediated survival of T cells by Yan *et al.* (410). Therefore, a trend for increased AKT and S6 activation shown in representative blots analysing unstimulated, naïve XPR1 deficient CD4+ T cells (Figure 23) could negatively affect homeostatic expansion. However, a quantification of AKT and S6 phosphorylation in naïve CD4+ T cells would be required to support this claim.

To properly address the role of CD28-dependent co-stimulation for increased effector functions of XPR1 deficient CD4+ T cells, proliferation assays with α-CD28 treatment in the absence of α-CD3 were performed. In line with earlier findings, cKO, but not CTL CD4+ T cells proliferated during treatment with α-CD28 in the absence of α-CD3 (Figure 36).

Moreover, we found *Bhlhe40* expression to be upregulated by 10.99-fold (Figure 10, Table 23). BHLHE40/DEC-1 was shown to be a positive regulator of CD4+ T-cell activation and expression of IFN-γ and IL-2 by Martínez-Llordella *et al*. (222). Importantly, DEC-1 activation is induced by CD28, and involved in EAE development (221, 222). Further, Salmon *et al.* showed DEC-1 to be crucial for effective ICT using α-PD-1 or α-CTLA-4 antibodies, and

therefore to be a suited therapeutic target (223). These studies indicate that the transcriptional regulator DEC-1 could be central for XPR1's function in CD4+ T cells, and suggest an importance of XPR1-mediated T-cell responses for immunotherapy.

CD28 autonomous signalling, i.e. proinflammatory responses in the absence of TCR engagement, has also been addressed by others. Camperio *et al.* revealed increased expression of IL-17a and IL-6 in response to CD28 engagement without simultaneous TCR stimulation in CD4+ T cells of relapsing-remitting multiple sclerosis (RRMS) patients (411). RRMS is a disease characterised by a relapsing acute inflammatory response caused by autoreactive T cells targeting myelin-like structures in the central nervous system (411–414). Camperio *et al.* showed that the observed proinflammatory response was due to PI3K signalling (411). Similarly, Kunkl *et al.* showed that autonomous CD28 signalling in the absence of TCR stimulation upregulated expression and secretion of IL-22 in human CD4+ T cells (415). Both studies identified PI3K to be a central mediator of the proinflammatory effects induced by CD28 autonomous signalling (411, 415). Our data extend on this notion, as XPR1 deficiency in CD4+ T cells regulates CD28-dependent co-stimulation for cytokine expression and signalling processes as discussed earlier.

Taken together, we conclude that CD28-mediated co-stimulation and the downstream PI3K-AKT-mTOR pathway are severely upregulated in XPR1 deficient CD4+ T cells, and thereby drive the observed hyperactivation and increased effector functions. Our analyses strongly indicate a pivotal role of XPR1 for negatively regulating co-stimulatory signalling.

5.6. Molecular function and modulation of XPR1 in CD4+ T cells

Since we showed CD4+ T-cell activation and effector functions to be strikingly increased due to XPR1 deficiency, XPR1 could be a suitable target for the modulation of T-cell responses, *e.g.* for ICT. Current targets of ICT are predominantly co-inhibitory receptors modulating TCR downstream signalling (31). Prominent examples for ICT targets are CTLA-4, PD-1 and its ligand PD-L1, lymphocyte-Activation Gene 3 (LAG3), and TIGIT (31, 416–420). Resistance to ICT therapy is a major challenge in modern anti-tumour medicine (31), which is why combining XPR1 inhibition with other ICT treatments could be potentially beneficial to enhance T-cell functions.

We sought to induce a XPR1 deficiency-like phenotype by pharmacological interference with XPR1. By choosing different approaches to modulate XPR1's function in CD4+ T cells, we

further address the molecular mechanism by which XPR1 deficiency promotes a dysregulated status in CD4+ T cells.

5.6.1. XPR1 as a regulator of phosphate homeostasis

Malachite Green Assays and urea PAGE analysis revealed no differences in polyP content between unstimulated CTL, cHET and cKO CD4+ T cells (Figure 8). Arguably, since polyP accumulates in CD4+ T cells upon activation, a XPR1-dependent effect on polyP content and phosphate homeostasis could become relevant upon stimulation of CD4+ T cells.

However, when stimulated with α-CD3/α-CD28, XVDL treatment of CTL CD4+ T cells did not result in increased proliferation as a readout for CD4+ T-cell effector functions compared to PVDL treatment or no treatment (Figure 25). This result suggests that in CD4+ T cells the phosphate/polyP metabolism is not changed accordingly to platelets, and that T-cell effector functions are not altered by the inhibition of the XPR1 phosphate exporter function.

Another compound to modulate XPR1-mediated phosphate efflux was used by Li *et al.* in U2OS and Saos-2 cells (184): They showed that UNC7467 treatment leads to reduced XPR1-mediated phosphate efflux (184). Therefore, we concluded that if increased proliferation of XPR1 deficient CD4+ T cells was dependent on XPR1's function in regulating phosphate homeostasis, we would expect increased proliferation in UNC7467-treated CTL, but not cKO CD4+ T cells. Our finding of a genotype-independent decrease of CD4+ T-cell proliferation after 1 µM UNC7467 treatment was therefore unexpected (Figure 26). Notably, when treating CD4+ T cells with 10 µM UNC7467 as used by Li *et al.* (184), cell viability was markedly reduced in CTL and cKO samples (data not shown). We hypothesise that inhibition of IP6K1 impaired vital aspects of CD4+ T-cell biology, which prevented proliferation of α-CD3/α-CD28 stimulated CD4+ T cells. The UNC7467 target IP6K1 is involved in a plethora of cellular processes, among which are metabolism, trafficking, migration, cytoskeletal remodelling, DNA repair, and immunity (291). For instance, Lee *et al.* showed that IP6K1 knockout dysregulates immune responses in a tumour model, leading to accelerated tumour growth, mediated by decreased CD8+ T-cell infiltration into tumour tissue, which indicated impaired T-cell functions (421). However, in their study the gene for IP6K1 was globally knocked out, and they discussed that conditional IP6K1 knockout models in T cells have not been analysed yet (421).

To date, XPR1 is the only known exporter of inorganic phosphate in metazoans (289, 308, 309, 165). Still, regulation of phosphate homeostasis seems to be functional in CD4+ T cells, even with greatly reduced XPR1 expression. Li *et al.* showed that XPR1 controls trafficking of the phosphate importer PiT1, which results in degradation of PiT1 in absence of XPR1 and

XPR1-mediated phosphate efflux in U2OS and Saos-2 cells (184). The concomitant inhibition of PiT1-mediated phosphate influx when phosphate efflux is impaired due to XPR1 absence thereby restores phosphate homeostasis in a slightly delayed manner (184).

Based on data from Li *et al.*, we hypothesised a similar mechanism in CD4+ T cells to protect phosphate homeostasis from dysregulation. It is reasonable to assume that similar to osteosarcoma cells, the lack of XPR1-dependent phosphate export is accompanied by an impaired PiT1-dependent phosphate import in CD4+ T cells, which protects from dysregulated polyP homeostasis. Notably, the protective mechanism described by Li *et al.* in U2OS and Saos-2 cells cannot apply to phosphate homeostasis in platelets as systems biology analysis of phosphate transporters by Mailer *et al.* showed that PiT1 and PiT2 expression was absent on mRNA and protein levels in human platelets (180, 184). However, mature murine T cells have been shown to express PiT1 (422), which highlights a possible regulation mechanism for phosphate homeostasis in CD4+ T cells that is missing in platelets.

Further, other unknown mechanisms regulating phosphate homeostasis, *e.g.* based on a compensatory transporter or unknown transporters could support regulation of phosphate homeostasis in the absence of XPR1 in CD4+ T cells.

5.6.2. XPR1 as regulator of trafficking

Autosomal-dominant mutations in XPR1 that impair XPR1's phosphate transport function have been associated with PFBC (167–170). However, in PFBC patients, no immune system dysregulation or immune system associated disease has been reported (171). Therefore, the striking differences in CD4+ T-cell functions upon knockout of *Xpr1* are surprising.

Ramos *et al.* pointed out that the currently known XPR1 mutations detected in the context of PFBC are localised in the SPX domain of XPR1, affecting phosphate transport (171). This implies that brain calcification due to XPR1 dysfunction in PFBC is related to the SPX domain. This is supported by work by Xu *et al.* who reported a striking reduction of foetal growth and a calcification of placenta tissue in mice heterozygous for a global knockout of *Xpr1* (177). Further, Maheshwari *et al.* used mice heterozygous for a global knockout of *Xpr1*, and detected increased reactivity and proliferation of microglia in addition to calcification in the brain (178). Importantly, this microglia activation was not restricted to the sites of calcification, but was rather a widespread observation in other brain areas, *e.g.* the cortex, white matter, and the midbrain (178). Taken together, these studies suggest a role of XPR1 for the immune system that is not mediated via mutation sites of the SPX domain in PFBC.

Instead of SPX-regulated transport function, we hypothesised that interaction partners may bind to the EXS domain or the C-terminal region of XPR1, which could then act as an adapter protein, regulating localisation, trafficking, and/or protein conformation in CD4+ T cells. As earlier discussed, Li *et al.* showed PiT1 trafficking and degradation to be dependent on XPR1 in U2OS and Saos-2 cells (184). Involvement of XPR1 in trafficking processes in Jurkat cells was also shown by Tello-Lafoz *et al.*, who identified XPR1 in a pull-down with SNX27, a protein that is involved in cargo trafficking (185). Interestingly, Tello-Lafoz *et al.* revealed that SNX27 controls trafficking of the cell-cell junction protein ZO-2 during IS formation, identifying a striking relevance for T-cell biology (185). Further, Rodriguez-Rodriguez *et al.* showed SNX27 to regulate CD4 and LCK expression at the early stages of T-cell activation, and thereby, to contribute to T-cell functions (186).

XPR1's potential function in regulating trafficking of TCR signalling molecules is further demonstrated by increased TCR internalisation after 16 h of α-CD3 stimulation in XPR1 deficient CD4+ T cells (Figure 24). The localisation of the TCR complex could be directly affected by XPR1-mediated trafficking. Another possible cause for altered TCR internalisation could be XPR1 indirectly affecting internalisation through interaction with other proteins involved in regulation of TCR internalisation and trafficking. TC21/RRas2 is a RRas superfamily GTPase that associates with the TCR, and is further necessary for TCR internalisation (423). TC21 is also able to activate PI3K, thereby affecting survival pathways that are dependent on PI3K and AKT (83, 424–427, 423). TC21 possibly links increased AKT phosphorylation with decreased TCR surface levels in XPR1 deficient CD4+ T cells, and could be an interesting target to analyse further XPR1-mediated functions in CD4+ T cells.

5.6.3. XPR1 interaction networks

Since we hypothesised that XPR1 acts as an adaptor protein, we addressed possible interaction partners that could be relevant for CD4+ T-cell functions. Human XPR1 interaction networks have been studied by affinity capture-mass spectrometry and proximity label-mass spectrometry approaches (201, 203–206). XPR1 was shown to interact with lysosomal proteins (LAMP1, LAMP2, LAMP3, and five subunits of the lysosomal v-ATPase, H+ transporting, 16 kDa) (201, 203, 428), proteins in the Golgi apparatus and the trans Golgi network (TGN38, GLG1, GOLM1, GOLIM4) (205, 206, 201, 429–432), and proteins involved in endocytosis and trafficking (GOLT1B, VAPA, CLTC, KLC2, KLC4, KIF5B, KIF5C) (201, 204, 433–439). This is in line with a role of XPR1 in trafficking and/or degradation of proteins.

More importantly, these studies revealed interesting interaction partners of XPR1 which are associated with TCR signalling.

For the putative XPR1 interaction partner LAMTOR1 (201), Hosokawa *et al.* showed a crucial role in regulating CD4+ T-cell biology: LAMTOR1 deficient CD4+ T cells showed decreased differentiation into Th17 cells, decreased proliferation and IL-2 production, and decreased mTORC1 activation (440). Further, LAMTOR1 deficient Foxp3+ T cells showed severe autoimmunity due to decreased suppressive function and CTLA-4 expression (440). Go *et al.* detected interaction of XPR1 with LCK and LYN (203), which are both Src family kinases crucial for proximal TCR signalling (75, 441). Interaction with XPR1 of any of these players might lead to the observed upregulation of proliferation, differentiation, or cytokine production in XPR1 deficient CD4+ T cells.

Another XPR1 interactome hit is CD226 (205). CD226 can relay co-stimulatory signals via its ligand CD155 (25). CD155 can also transmit co-inhibitory signals via binding to TIGIT instead, which leads to a competitive relationship of CD226 and TIGIT (224). Gaud *et al.* revealed that CD226 triggers activation of VAV1, which is synergised by TCR activation (442). VAV1 gets recruited to the TCR complex upon stimulation and gets phosphorylated by LCK (442, 443). VAV1 has been shown to be involved in signalling of Ca^{2+}, ERK1/2, PI3K-AKT, and NF-κB using VAV1 deficient mouse models (442, 444–447). Gaud *et al.* showed that CD226 signalling through VAV1 increased ERK1/2 signalling and IL-17 production by human CD4+ T cells (442). Further, an autoimmune disease risk variant of CD226 was shown to increase ERK1/2 and VAV1 activation when the TCR and CD226 were synergistically stimulated (442). Impaired VAV1 activation might be related to impaired ERK1/2 signalling in XPR1 deficient CD4+ T cells, since we found upregulated expression of *Jun*, as discussed earlier (section 5.5.1).

Further, PD-1 was identified as an interaction partner of XPR1 (205, 206). PD-1's function as an immune checkpoint molecule has been discussed earlier. Since we detected elevated surface levels of PD-1 in unstimulated XPR1 deficient CD4+ T cells, XPR1's functions might be related to controlling trafficking of PD-1.

XPR1 has been shown to interact with CTLA-4 in affinity capture-mass spectrometry (205, 206). We hypothesised that XPR1's interaction with CTLA-4 might control localisation, trafficking, or recycling of the immune checkpoint molecule, regulating activity of CD4+ T cells by modulating co-inhibitory signals. However, in our study, we could not definitely validate the interaction of XPR1 and CTLA-4 in unstimulated murine CTL CD4+ T cells using PLAs with two different antibody combinations (Figure 27C and 27D). A problem could be low expression of CTLA-4 in unstimulated CD4+ T cells (448), pointed out by a general low spot count compared to the α-XPR1 & α-Kidins220 specific antibody combination. Further, unspecific binding of antibodies might be disadvantageous, since either no significant difference in spot

count between the specific antibody combination and one control antibody combination, or even a higher spot count in the control combination were observed.

Surface expression of CTLA-4 was not significantly altered on XPR1 deficient CD4+ T cells, as only a trend for increased expression with high variance was observed in naïve or 72 h α-CD3/α-CD28 stimulated CD4+ T cells (Figure 28). In contrast to this, CTLA-4 expression was significantly increased on CD4+ T cells isolated from LNs of H-Y-injected *Marilyn* cKO mice compared to the control (Figure 31C). This could be due to T-cell exhaustion, since cells were analysed 6 days after peptide injection, whereas *ex vivo* CTLA-4 analysis was done after 3 days of stimulation. Taken together, CTLA-4's role for XPR1-depedent T-cell functions remains unclear and probably depends on stimulation conditions and spatiotemporal analysis.

In summary, interaction of XPR1 with LAMTOR1, LYN, LCK, CD226, PD-1, or CTLA-4, and possible regulation of trafficking, localisation, or degradation of its interaction partners could indirectly have an impact on TCR signalling.

5.6.4. The XPR1-Kidins220 complex and modulation of XPR1 interactions

Kidins220 has been identified as an interaction partner of XPR1 in different affinity capture-mass spectrometry screenings (205, 206, 201), and in cryo electron microscopy analysis (165, 166). Kidins220 is involved in neuronal differentiation and development, neuroprotection, cancer pathogenesis, and regulation of immune responses (188–197, 185). Kidins220 has been shown to affect ERK1/2 signalling by acting as an adaptor or scaffolding protein for interaction partners, and mediate transport or complex assembly (197, 195, 186, 449). In T cells, Deswal *et al.* showed Kidins220 to interact with CD3-ζ/CD247 (197) which was confirmed in a reference experiment to validate our PLA setup for CD4+ T cells (Figure 27A). Stable knockdown of Kidins220 in T cells reduced ERK1/2 phosphorylation, Ca^{2+} influx, CD69 expression, and secretion of IL-2 and IFN-γ (197). Mechanistically, Deswal *et al.* propose that Kidins220's function in T cells is dependent on activating the Grb2-SOS-Ras-B-Raf pathway by interacting with the TCR, Grb2, and B-Raf, the latter of which mediates sustained ERK1/2 activation (197). We therefore hypothesised that XPR1's interaction with Kidins220 might be linked to the severely altered CD4+ T-cell functions in XPR1 deficient CD4+ T cells.

Recently, two different groups showed cryo EM analysis of the XPR1 interaction with Kidins220 and inositol pyrophosphate entities in the context of phosphate export in human cells (165, 166). Zuo *et al.* showed the structure of a XPR1 homodimer in interaction with IP6 and amino acids 1-432 of Kidins220 (166), while Wang *et al.* analysed the structure of a XPR1 homodimer in interaction with IP8 and amino acids 1-1,076 of Kidins220 (165). Even though

they proposed different mechanisms for XPR1-mediated phosphate export, both concluded that the interaction of XPR1 and Kidins220 is crucial for the regulation of it. This was also stated by Bondeson *et al.* who analysed ovarian and uterine cancer in a large-scale functional genomics study (176). They showed that Kidins220 is required for XPR1's phosphate efflux activity, and that inactivation or suppression of the *XPR1* gene led to decreased protein levels of Kidins220 (176). Moreover, Bondeson *et al.* validated data from other studies that suggest that the XPR1-Kidins220 complex is present in several subcellular departments, and possibly undergoes trafficking together (176, 450, 451).

We confirmed the interaction of XPR1 and Kidins220 *ex vivo* in CTL CD4+ T cells using a PLA (Figure 27B). Even though detection of XPR1 in immunoblots was not ideal (as discussed in section 5.1), the XPR1 antibodies were used to address interaction with other proteins in PLAs. In this method, XPR1 is present in its native state in fixed cells, and therefore, antibody binding could be improved in comparison to immunoblots. Furthermore, unspecific antibodies were used as control for each tested antibody pair used for PLAs. We only considered the interaction between two target proteins to be valid when the spot counts for the unspecific control pairs were significantly lower than the specific antibody combination. Therefore, we considered the XPR1 antibodies sufficiently suited for this method.

We next sought to disturb the interaction between Kidins220 and XPR1 in order to address the impact of their interaction on CD4+ T-cell functions. While XPR1's SPX domain has been shown to be essential for the interaction between XPR1 and Kidins220 (165), Wang *et al.* also described XRP1's C-terminal, unorganised loop to act as a hook for Kidins220, playing a significant role as a stabilising component in the interaction dynamic (165). Importantly, they pointed out that residues 654-696 of the XPR1 C-terminal loop are unoccupied and therefore accessible for interaction, which corresponds to residues 653-695 of murine XPR1 (165). Wang *et al.* propose the possibility of other interaction partners in the XPR1-Kidins220 complex via binding to the XPR1 C-terminal loop. Therefore, we focused on targeting the C-terminal loop to disturb interactions of XPR1 with Kidins220 and/or unknown interaction partners.

Based on the work of Gamir-Morralla *et al.* (293), we designed the cell-penetrating peptide Tat-X featuring the last 25 C-terminal amino acids of the murine XPR1 sequence (Figure 29A). Our aim was for Tat-X to competitively bind and block the interaction sites of XPR1's putative interaction partner(s) in CD4+ T cells that might modulate T-cell functions. We also used Tat-K (293), a cell-penetrating peptide featuring 14 amino acids around the calpain cleavage site at the C-terminal tail of Kidins220 that was shown to preserve ERK1/2 phosphorylation by inhibiting calpain-dependent Kidins220 downregulation in neurons (293). In CD4+ T cells, we

showed increased interaction of Kidins220 and XPR1 upon Tat-K treatment, possibly due to increased Kidins220 levels when protected from calpain-dependent degradation (Figure 29B and 29C). Further, proliferation was increased in CTL and cKO CD4+ T cells after Tat-K treatment, indicating an XPR1-independent effect (Figure 30). Based on Gamir-Morralla *et al.*'s results, and Deswal *et al.*'s analyses of Kidins220 affecting ERK1/2 signalling in T cells, we hypothesise that increased ERK1/2 activation due to decreased Kidins220 degradation might positively affect proliferation of CD4+ T cells when treated with Tat-K.

Treatment with Tat-X reduced interaction of XPR1 and Kidins220 (Figure 29B and 29C). As earlier discussed, the C-terminal loop of XPR1 is involved in stabilising the Kidins220-XPR1 interaction in humans during phosphate export, and might further interact with other unknown proteins while in complex with Kidins220 (165). Therefore, targeting putative interaction partners of XPR1's C-terminal loop with Tat-X leading to reduction of Kidins220-XPR1 interaction suggests that the C-terminal loop is crucial for the interaction of XPR1 and Kidins220 either directly or indirectly.

The increase in proliferation after Tat-X treatment of CTL CD4+ T cells was dependent on XPR1 expression, since we observed no difference in proliferation between DMSO- and Tat-X treated cKO CD4+ T cells (Figure 30). We conclude that XPR1's role for T-cell signalling and effector functions is regulated by crucial interactions at the C-terminal loop. Whether the interaction is directly dependent on Kidins220 or other adaptor protein associations remains to be clarified.

In order to rule out off-target effects, and to unravel XPR1's molecular mechanism as a regulator of CD4+ T-cell signalling and effector functions, further experiments could be insightful. Tat-X's effect on CD4+ T-cell differentiation, gene expression, or TCR downstream signalling can be used to validate findings of this work, and possibly link them to interaction mediated by XPR1's C-terminal loop.

Taken together, we discovered that XPR1 deficiency in CD4+ T cells leads to hyperactivation and increased effector functions independently of polyP homeostasis and XPR1's phosphate exporter function upon *ex vivo* α-CD3/α-CD28 stimulation of primary murine CD4+ T cells. We showed increased gene expression and secretion of *Il2*/IL-2, a moderate shift to glycolysis, and elevated expression of the proinflammatory cytokines TNF-α, IFN-γ, and IL-22 in *in vitro* differentiation assays using Th1- and Th17-skewing conditions. Increased expression of *TNFA*, *IFNG,* and *IL22* in Jurkat cells with a siRNA-mediated knockdown of *XPR1* underscored our findings in human T cells. Moreover, antigen-specific stimulation of CD4+ T cells in *Marilyn* mice by injection of the cognate H-Y antigen peptide revealed hyperactivation, increased expression of the immune checkpoint molecules PD-1 and CTLA-4, and of the

proinflammatory cytokines IL-17a and IL-22 in XPR1 deficient CD4+TRBV6+ T cells. TCR downstream signalling in XPR1 deficient CD4+ T cells was severely dysregulated, as evident by impaired ERK1/2 phosphorylation, a decreased Ca^{2+} response as well as impaired NFAT translocation to the nucleus, which was contrasted by strikingly increased AKT and S6 phosphorylation of the mTOR pathway. Homeostatic expansion experiments revealed a disadvantage of XPR1 deficient CD4+ T cells in a setup independent of CD28-mediated co-stimulation, while α-CD28-driven *ex vivo* proliferation assays in the absence of α-CD3 elicited a proliferative response in XPR1 deficient, but not control CD4+ T cells. Mechanistically, XPR1 interaction with the scaffolding protein Kidins220 was validated by PLAs, and treatment of CD4+ T cells with the cell-penetrating peptide of XPR1's C-terminal loop disrupted interaction of XPR1 with Kidins220 while simultaneously inducing an increase in proliferation, thereby phenocopying XPR1 deficient, hyperactivated CD4+ T cells. This work revealed that XPR1 is an important regulator for CD4+ T-cell signalling, indicated by hyperactive CD28-dependent co-stimulation and impaired Kidins220 functions by XPR1 deficiency and Tat-X treatment. Thus, XPR1 displays a potential target for novel immunotherapy approaches that aim to boost co-stimulatory signalling and to invigorate insufficient T-cell responses.

5.7. Outlook

In the present thesis, we addressed CD4+ T-cell hyperactivation, increased effector functions, and dysregulated TCR downstream signalling in a mouse model with conditional knockout of *Xpr1*. Moreover, we used a *Marilyn* mouse model with conditional knockout of *Xpr1* to address effector functions and activation of XPR1 deficient CD4+ T cells in a more physiological context of TCR stimulation. The data generated in both models display increased proinflammatory characteristics of *in vivo* and *in vitro* differentiated XPR1 deficient CD4+ T cells, which could be further validated in an OT-II/B16-OVA-based tumour model.

OT-II mice (*B6.Cg-Tg(TcraTcrb)425Cbn/J*) express a transgenic TCR that pairs with CD4, and that is specific for the chicken ovalbumin 323-339 (OVA) peptide when presented by MHC-II (452, 453). OT-II mice therefore express CD4+ T cells recognising the OVA peptide in the context of MHC-II (452, 453). B16-OVA melanoma cells that stably express the OVA peptide can be subcutaneously injected into C57BL/6 mice, which leads to formation of a tumour within 7-21 days (454). OT-II mice that were crossbred with CD4-Cre-XPR1-flox mice would generate XPR1 deficient or XPR1 wildtype OT-II mice. CD4+ OT-II cells can be intravenously injected into B16-OVA-bearing congenic mice, as described before (455). Tumour volume can be analysed after a given timepoint to compare the anti-tumour efficiency of XPR1 deficient

vs. XPR1 wildtype OT-II CD4+ T cells. Further, analysis of tumour-infiltrating CD4+ T cells addressing differentiation, cytokine expression, and activation status can be done to address XPR1's role in orchestrating CD4+ T-cell responses in the tumour microenvironment. The results in this work highlight that XPR1 deficiency in CD4+ T cells caused hyperactivation and increased secretion of proinflammatory cytokines TNF-α, IFN-γ, IL-17a, and IL-22, which are associated with a favourable outcome in the tumour microenvironment (456–458, 61, 459). Even though IL-22 has previously been discussed to contribute to cancer spread by supporting metastasis and immune evasion (55, 61, 369), we expect a decreased tumour size and increased cytokine expression as well as effector functions and activation status in XPR1 deficient tumour-infiltrating CD4+ lymphocytes.

We concluded from our signalling analyses that CD28-mediated co-stimulation is severely upregulated in XPR1 deficient CD4+ T cells, leading to hyperactivation of the PI3K-AKT-mTOR pathway of TCR downstream signalling. Further analysis of different players involved in this signalling pathway could also be conducted to unveil the molecular mechanism of XPR1-mediated regulation of CD4+ T-cell functions. Phosphorylation of PI3K as the main player upstream of AKT and mTOR could be addressed to solidify the role of CD28-dependent hyperstimulation of XPR1 deficient CD4+ T cells. PLCγ1 is a central player of TCR distal signalling whose activation status in XPR1 deficient CD4+ T cells remains elusive. Further, VAV1 could be interesting to analyse due to predicted XPR1-CD226 interaction and increased expression of *Tigit* in XPR1 deficient CD4+ T cells.

Establishing endogenously tagged XPR1 in a mouse model or Jurkat cells might be beneficial due to mediocre performance of the used α-XPR1 antibodies, *e.g.* in immunoblotting and for targeting XPR1 at the cell surface. Antibody-based approaches, *e.g.* Pull-Down based methods like Co-immunoprecipitation or Affinity Capture-mass spectrometry, or localisation/trafficking analyses using immunofluorescence staining-based confocal microscopy, could greatly benefit from endogenously tagged XPR1. These methods will be useful for unravelling XPR1's molecular mechanism based on interaction with and or/trafficking of signalling complexes.

Enhanced effector functions of XPR1 deficient CD4+ T cells makes XPR1 a potential target for anti-tumour immunotherapy. The cell-permeable Tat-X peptide featuring the 25 C-terminal amino acids of XPR1's sequence might represent a suitable construct to target XPR1. However, Tat-X's effect on CD4+ T-cell effector functions still needs to be characterised in greater detail. Further analyses of effector functions, signalling, and gene expression in Tat-X-treated CD4+ T cells will unveil whether blocking of potential binding sites of XPR1's C-

terminal loop is sufficient to phenocopy the co-stimulatory hyperactivity of XPR1 deficient CD4+ T cells.

6. Materials and Methods

6.1. Materials

6.1.1. Used antibodies (flow cytometry)

Table 1: Antibodies used for flow cytometry.

Description	Clone	Isotype	Fluorophor	Supplier	Cat. #	Application
α-mouse CD152	UC10-4B9	Hamster IgG1	APC	Miltenyi Biotec, Bergisch Gladbach	130-102-518	1:10
α-mouse CD2	RM2-5	Rat IgG2b, λ	FITC	BioLegend, San Diego	100105	1:200
α-mouse CD25	PC61	Rat IgG1, λ	BV421	BioLegend, San Diego	102043	1:160
α-mouse CD28	37.51	Syrian hamster IgG	PE/Cy7	BioLegend, San Diego	102125	1:333
α-mouse CD3	17A2	Rat IgG2b, κ	BV421	BioLegend, San Diego	100227	1:50
α-mouse CD3e	145-2C11	Armenian hamster IgG	PacificBlue	BioLegend, San Diego	100334	1:50
α-mouse CD4	GK1.5	Rat IgG2b, κ	PE	BioLegend, San Diego	100408	1:200-1:400
α-mouse CD4	GK1.5	Rat IgG2b, κ	APC	BioLegend, San Diego	100412	1:200-1:400
α-mouse CD4	GK1.5	Rat IgG2b, κ	APC/Cy7	BioLegend, San Diego	100414	1:200-1:400
α-mouse CD44	IM7	Rat IgG2b, κ	FITC	BioLegend, San Diego	103021	1:100
α-mouse CD44	IM7	Rat IgG2b, κ	APC	BioLegend, San Diego	103012	1:100
α-mouse CD5	53-7.3	Rat IgG2a, κ	PerCP/Cy5.5	BioLegend, San Diego	100623	1:80

(continued)

α-mouse CD62L	MEL-14	Rat IgG2a, κ	PerCP	BioLegend, San Diego	104429	1:80
α-mouse CD69	H1.2F3	Hamster IgG1	PE-Vio 770	Miltenyi Biotec, Bergisch Gladbach	130-103-944	1:10
α-mouse CD8a	53-6.7	Rat IgG2a, κ	PE	BD Biosciences, Franklin Lakes	561095	1:100
α-mouse Foxp3	FJK-16s	Rat IgG2a, κ	Alexa-Fluor488	ThermoFisher Scientific, Waltham	53-5773-82	1:100
α-mouse Foxp3	FJK-16s	Rat IgG2a, κ	APC	ThermoFisher Scientific, Waltham	17-5773-82	1:100
α-mouse Gata3	16E10 A23	Mouse IgG2b, κ	BV421	BioLegend, San Diego	653814	1:20
α-mouse IFN-γ	XMG1.2	Rat IgG1, κ	BV421	BioLegend, San Diego	505830	1:200
α-mouse IFN-γ	XMG1.2	Rat IgG1, κ	PE	ThermoFisher Scientific, Waltham	12-7311-82	1:80
α-mouse IL-10	JES5-16E3	Rat IgG2b, κ	PE/Cy7	BioLegend, San Diego	505025	1:80
α-mouse IL-17a	TC11-18H10	Rat IgG1, κ	FITC	Miltenyi Biotec, Bergisch Gladbach	130-102-262	1:10
α-mouse IL-22	Poly 5164	Goat IgG	PerCP/Cy5.5	BioLegend, San Diego	516411	1:20
α-mouse IL-4	11B11	Rat IgG1, κ	APC	BioLegend, San Diego	504106	1:20
α-mouse IL-4	11B11	Rat IgG1, κ	PerCP/Cy5.5	BioLegend, San Diego	504124	1:80
α-mouse IL-5	TRFK5	Rat IgG1, κ	PE	BioLegend, San Diego	504304	1:20

(continued)

α-mouse Ki67	REA183	Human IgG1	PE-Vio 770	Miltenyi Biotec, Bergisch Gladbach	130-120-559	1:50
α-mouse NFAT1	D43B1	Rabbit IgG	Alexa-Fluor488	Cell Signaling Technology, Danvers	14324	1:50
α-mouse Rorγt	Q31-378	Mouse IgG2a, κ	BV421	BD Biosciences, Franklin Lakes	562894	1:100
α-mouse Tbet	4B10	Mouse IgG1, κ	PerCP/Cy5.5	BioLegend, San Diego	644805	1:20
α-mouse TCRβ	H57-597	Armenian hamster IgG	FITC	BioLegend, San Diego	109206	1:50
α-mouse TNF-α	MP6-XT22	Rat IgG1, κ	BV421	BioLegend, San Diego	506327	1:20

6.1.2. Used antibodies (immunoblots)

Table 2: Antibodies used for immunoblot analysis.

Description	Clone	Species	Supplier	Cat. #	Application
α-His-Tag	-	Rabbit	Cell Signaling Technology, Danvers	2365	1:1,000
α-mouse AKT	11E7	Rabbit	Cell Signaling Technology, Danvers	4685	1:1,000
α-mouse ERK1/2	W15133B	Rat	BioLegend, San Diego	686901	1:1,000
α-mouse GAPDH	D16H11	Rabbit	Cell Signaling Technology, Danvers	5174	1:2,000
α-mouse IgG-HRP	polyclonal	Rabbit	Agilent, Santa Clara	P0260	1:10,000-1:20,000
α-mouse LAT	LAT1111	Mouse	BioLegend, San Diego	623901	1:500

(continued)

α-mouse phospho-AKT (Ser473)	D9E	Rabbit	Cell Signaling Technology, Danvers	4060	1:500
α-mouse phospho-ERK1/2 (Thr202/Thr204)	6B8B69	Mouse	BioLegend, San Diego	369501	1:500
α-mouse phospho-LAT (Tyr171)	A20005D	Mouse	BioLegend, San Diego	946601	1:1,000
α-mouse phospho-S6 (Ser235/Ser236)	polyclonal	Rabbit	MyBioSource, San Diego	MBS9404866	1:500
α-mouse S6	5G10	Rabbit	Cell Signaling Technology, Danvers	2217	1:1,000
α-mouse XPR1	2G8	Mouse	Sigma-Aldrich, St. Louis	SAB1402458	1:500
α-mouse XPR1	polyclonal	Rabbit	Proteintech, Rosemont	14174-1-AP	1:500
α-mouse β-actin	937215	Mouse	R&D Systems, Minneapolis	MAB8929	1:20,000
α-rabbit IgG-HRP	polyclonal	Goat	Jackson Immuno-Research, Cambridgeshire	111-035-045	1:10,000-1:20,000
α-rat IgG-HRP	polyclonal	Goat	Jackson Immuno-Research, Cambridgeshire	112-035-062	1:10,000-1:20,000

6.1.3. Used antibodies (other)

Table 3: Other antibodies.

Description	Clone	Species	Supplier	Cat. #
IgG1,κ Isotype control	P3.6.2.8.1	Mouse	ThermoFisher Scientific, Waltham	16-4714-85
IgG Isotype control	Polyclonal	Rabbit	Vectorlabs, Newark	I-1000-5
α-armenian hamster IgG H&L	Polyclonal	Goat	Abcam, Cambridge	Ab5738
α-mouse CD28	37.51	Syrian Hamster	BioLegend, San Diego	102102
α-mouse CD3	145-2C11	Armenian hamster	Antibodies.com, Stockholm	A86500
α-mouse CD4-Biotin	GK1.5	Rat	BioLegend, San Diego	100404
α-mouse CTLA4	037	Rabbit	ThermoFisher Scientific, Waltham	MA5-30444
α-mouse CTLA4	L4P2F5.F10	Mouse	NeoBiotechnologies, Union City	1493-MSM1-P0
α-mouse IFN-γ	XMG1.2	Rat	BioLegend, San Diego	505834
α-mouse IL-4	11B11	Rat	BioLegend, San Diego	504122
α-mouse Kidins220	polyclonal	Rabbit	ThermoFisher Scientific, Waltham	PA5-116475
α-mouse Kidins220	3-B6	Mouse	ThermoFisher Scientific, Waltham	MA5-32869
α-mouse PD-1	J43	Mouse	ThermoFisher Scientific, Waltham	14-9985-82
α-mouse TRBV6-TCR-Biotin	RR4-7	Rat	BD Biosciences, Franklin Lakes	553192

6.1.4. Used peptides

Table 4: Used peptides.

Description	Sequence	Supplier
H-Y	NAGFNSNRANSSRSS	ThermoFisher Scientific, Waltham
Tat-K	YGRKKRRQRRR-PPLNRTPSTVTLNNNT	GenScript, Piscataway
Tat-X	YGRKKRRQRRR-PRLASQSKARDTKVLIEDTDDEANT	GenScript, Piscataway

6.1.5. Used reagents and chemicals

Table 5: Used reagents and chemicals.

Reagent/chemical	Supplier	Cat. #
4′,6-Diamidino-2-phenylindole dihydrochloride (DAPI)	Sigma-Aldrich, St. Louis	D9542
2-Mercaptoethanol, 50 mM	ThermoFisher Scientific, Waltham	31350010
3-Morpholinopropanesulfonic acid (MOPS)	Sigma-Aldrich, St. Louis	475898-100GM
4′,6-diamidino-2-phenylindole (DAPI)	ThermoFisher Scientific, Waltham	D3571
Acetic acid (glacial)	Sigma-Aldrich, St. Louis	1.00063
Acrylamid/Bisacrylamid 29:1	Bio-Rad Laboratories, Hercules	1610156
Agarose	ThermoFisher Scientific, Waltham	16500500
Ammonium chloride	Carl Roth, Karlsruhe	K298.2
Ammonium persulfate (APS)	Bio-Rad Laboratories, Hercules	1610700
Ammonium sulphate	Carl Roth, Karlsruhe	9212.1
Ampicillin sodium salt	Sigma-Aldrich, St. Louis	A9518
Antifect	Schülke&Mayr, Norderstedt	113940
Anti-PE MicroBeads Ultra Pure	Miltenyi Biotec, Bergisch Gladbach	130-105-639

(continued)

Aqua ad injectabilia	B. Braun, Melsungen	2351744
Boric acid	Sigma-Aldrich, St. Louis	B0394
Bovine serum albumin (BSA)	Sigma-Aldrich, St. Louis	A3294-100G
Cell Proliferation Proliferation Dye eFluor 450	ThermoFisher Scientific, Waltham	65-0842-85
Cell Proliferation Proliferation Dye eFluor 670	ThermoFisher Scientific, Waltham	65-0840-90
Chloroform	Lohmann Laborservice, Marxen	7386.1000
Comassie Brilliant Blue R-250 Solution	Bio-Rad Laboratories, Hercules	1610436
cOmplete™ ULTRA Tablets, EDTA-free Protease Inhibitor cocktail	Sigma-Aldrich, St. Louis	5892953001
Dimethyl sulfoxide (DMSO)	Sigma-Aldrich, St. Louis	D5879
Dulbecco's PBS	ThermoFisher Scientific, Waltham	14190094
Duolink In Situ Detection Reagents Red	Sigma-Aldrich, St. Louis	DUO92008-30RXN
Duolink In Situ Mounting Medium with DAPI	Sigma-Aldrich, St. Louis	DUO82040-5ML
Duolink In Situ PLA Probe Anti-Mouse MINUS	Sigma-Aldrich, St. Louis	DUO92004-30RXN
Duolink In Situ PLA Probe Anti-Rabbit PLUS	Sigma-Aldrich, St. Louis	DUO92002-30RXN
Duolink In Situ Wash Buffers, Fluorescence	Sigma-Aldrich, St. Louis	DUO82049-4L
Ethanol absolute	Th. Geyer, Renningen	2273-5L
Ethylenediaminetetraacetic acid (EDTA)	Sigma-Aldrich, St. Louis	ED2SS-50G
Fetal calf serum (FCS)	ThermoFisher Scientific, Waltham	A5256801
Glycerol	ThermoFisher Scientific, Waltham	15514011
Glycine	Sigma-Aldrich, St. Louis	G712-1kg
Halt Protease and Phosphatase Inhibitor Cocktail, EDTA-free, 100X	ThermoFisher Scientific, Waltham	78441

(continued)

HEPES, 1 M	ThermoFisher Scientific, Waltham	15630080
Hydrochloric acid, 4 M	Lohmann Laborservice, Marxen	824.1011
Imidazole	Sigma-Aldrich, St. Louis	56749
Ionomycin	Sigma-Aldrich, St. Louis	I0634-1MG
Isoflurane (Sedaconda)	Sedana Medical, Wolfratshausen	3000 225-2109
Isopropyl alcohol	Sigma-Aldrich, St. Louis	190764-2.5L
Isopropyl β-D-1-thiogalactopyranoside (IPTG)	Sigma-Aldrich, St. Louis	I6758-10G
KAPA2G Fast HotStart Readymix 2x	Sigma-Aldrich, St. Louis	KK5603
Laemmli Sample Buffer, 4X	Bio-Rad Laboratories, Hercules	1610747
LB Agar	Carl Roth, Karlsruhe	X965.1
LB Medium	Carl Roth, Karlsruhe	X968.1
L-Glutamine, 200 mM	ThermoFisher Scientific, Waltham	25030-081
Lipofectamine RNAiMAX transfection reagent	ThermoFisher Scientific, Waltham	13778075
MACS buffer	Miltenyi Biotec, Bergisch Gladbach	130-091-221
Methanol	Lohmann Laborservice, Marxen	BAK.8045. 1000.GF
Minimal essential medium, non essential amino acid solution (MEM NEAA), 100x	Sigma-Aldrich, St. Louis	11140-050
N-2-Hydroxyethylpiperazine-N'-2-ethane sulphonic acid (HEPES)	Sigma-Aldrich, St. Louis	GH9136
Opti-MEM, reduced serum medium, no phenol red	ThermoFisher Scientific, Waltham	11058021
Oxygen, medical grade	Sol, Krefeld	22-202120
PageRuler Plus Prestained Protein Ladder, 10 to 250 kDa	ThermoFisher Scientific, Waltham	26620
Paraformaldehyde (PFA)	SERVA Electrophoresis, Heidelberg	31628

(continued)

Penicillin-Streptomycin 10.000 U/mL	ThermoFisher Scientific, Waltham	15140122
Permeabilization buffer	ThermoFisher Scientific, Waltham	00-8333-56
Phenol, TE-saturated	Sigma-Aldrich, St. Louis	77607
Phorbol myristate acetate (PMA)	Abcam, Cambridge	ab120297
Protein Transport Inhibitor Cocktail, 500x	ThermoFisher Scientific, Waltham	00-4980-03
Purified Rat Anti-Mouse CD16/CD32	BD Biosciences, Franklin Lakes	553142
Recombinant human IL-2	BioLegend, San Diego	589102
Recombinant human TGF-β 1	ThermoFisher Scientific, Waltham	AF100-21C
Recombinant mouse IL-12	BioLegend, San Diego	577002
Recombinant mouse IL-23	BioLegend, San Diego	589002
Recombinant mouse IL-4	BioLegend, San Diego	574302
Recombinant mouse IL-6	BioLegend, San Diego	575702
RIPA lysis buffer	ThermoFisher Scientific, Waltham	89900
ROTI Phenol Chloroform/Isoamylalcohol	Carl Roth, Karlsruhe	A156.1
RPMI 1640 Medium, GlutaMax Supplement	ThermoFisher Scientific, Waltham	72400021
S.O.C. Medium	ThermoFisher Scientific, Waltham	15544034
Saline, injection ready (Sodium chloride, 0.9 %, isotonic solution)	B. Braun, Melsungen	3570310
Seahorse XF Glucose Solution, 1 M	Agilent, Santa Clara	103577-100
Seahorse XF Glutamine Solution, 200 mM	Agilent, Santa Clara	103579-100
Seahorse XF Pyruvate Solution, 100 mM	Agilent, Santa Clara	103578-100
Seahorse XF RPMI Medium, pH 7.4	Agilent, Santa Clara	103576-100
Sodium acetate	Carl Roth, Karlsruhe	X891.1
Sodium carbonate	Sigma-Aldrich, St. Louis	S2127
Sodium chloride	ThermoFisher Scientific, Waltham	S9625-1Kg
Sodium dihydrogen phosphate dihydrate	Sigma-Aldrich, St. Louis	1.06342

(continued)

Sodium dodecyl sulfate, 20 % solution	SERVA Electrophoresis, Heidelberg	20767.03
Sodium hydrogen carbonate	Sigma-Aldrich, St. Louis	1063290500
Sodium hydroxide, 4 M	Carl Roth, Karlsruhe	T198.1
Sodium pyruvate, 100 mM	ThermoFisher Scientific, Waltham	11360070
Staphylococcal enterotoxin B (SEB) from *Staphylococcus aureus*	Sigma-Aldrich, St. Louis	S4881-1MG
Streptavidin Alexa Fluor 647	BioLegend, San Diego	405237
Streptavidin BV421	BioLegend, San Diego	405226
Streptavidin DyLight 488	ThermoFisher Scientific, Waltham	405218
Streptavidin MicroBeads	Miltenyi Biotec, Bergisch Gladbach	130-048-102
Streptavidin PE	BioLegend, San Diego	405203
Sulfric acid, 1 M	Carl Roth, Karlsruhe	X873.1
SYBR Safe Green	ThermoFisher Scientific, Waltham	S33102
TaqMan™ Universal Master Mix II, no UNG	ThermoFisher Scientific, Waltham	4440047
TBE urea sample buffer	ThermoFisher Scientific, Waltham	J60186.AC
Tetramethylethylenediamine (TEMED)	Sigma-Aldrich, St. Louis	T9281
Thapsigargin	Merck, Darmstadt	T9033
Tris	Th. Geyer, Renningen	8085-1KG
Trypan Blue solution (0.4 %)	ThermoFisher Scientific, Waltham	15250061
TWEEN 20	Sigma-Aldrich, St. Louis	P1379-500mL
UNC7467, 10 mM in DMSO	MedChemExpress, Monmouth Junction	HY-150607
Urea	Sigma-Aldrich, St. Louis	U6504
X-VIVO 15, serum-free	Biozym, Hessisch Oldendorf	881024

6.1.6. Used primers

Table 6: Used primers.

Description	Sequence	Supplier
Cd4 olMR1084_for primer	5' GCGGTCTGGCAGTAAAAACTATC 3'	Eurofins, Hamburg
Cd4 olMR1085_rev primer	5' GTGAAACAGCATTGCTGTCACTT 3'	Eurofins, Hamburg
HY1 Marilyn Ia2-b4 primer	5' GCAGAGGAACCTGGGAGCTGT 3'	Eurofins, Hamburg
HY1 Marilyn Samaup primer	5' GCTGTCTGTACCACCAGAAATAC 3'	Eurofins, Hamburg
Rag2 Common primer	5' CCATGTTGCTTCCAAACCAT 3'	Eurofins, Hamburg
Rag2 mut fw primer	5' AATTCGCCAATGACAAGACG 3'	Eurofins, Hamburg
Rag2 wt fw primer	5' CTGACTGCCTACCCCATGTT 3'	Eurofins, Hamburg
Xpr1 Forward primer	5' ATGTAGGCCCAGTGTTTATCTTTAGGAT 3'	Eurofins, Hamburg
Xpr1 Reverse primer	5' ATGGGAAAATGAAGACACACCTGAA 3'	Eurofins, Hamburg

6.1.7. Used plasmids

Table 7: Used plasmids.

Description	Supplier
pTrcHisB	ThermoFisher Scientific, Waltham
pTrcHisB-PVDL	Designed and purified at the Institute for Clinical Chemistry and Laboratory Medicine UKE Hamburg
pTrcHisB-XVDL	Designed and purified at the Institute for Clinical Chemistry and Laboratory Medicine UKE Hamburg

6.1.8. Used *TaqMan* probes and siRNA

Table 8: Used *TaqMan* probes and siRNA.

Description	Fluorophore	Supplier	ID # and Cat. #
HPRT1-probe (human)	FAM-MGB	ThermoFisher Scientific, Waltham	Hs02800695_m1 Cat. #4331182
Hprt1-probe (mouse)	FAM-MGB	ThermoFisher Scientific, Waltham	Mm00446968_m1 Cat. #4331182
IFNG-probe (human)	FAM-MGB	ThermoFisher Scientific, Waltham	Hs00989291_m1 Cat. #4331182
IL22-probe (human)	FAM-MGB	ThermoFisher Scientific, Waltham	Hs01574154_m1 Cat. #4331182
IL2-probe (human)	FAM-MGB	ThermoFisher Scientific, Waltham	Hs00174114_m1 Cat. #4331182
TNFA-probe (human)	FAM-MGB	ThermoFisher Scientific, Waltham	Hs00174128_m1 Cat. #4331182
XPR1-probe (human)	FAM-MGB	ThermoFisher Scientific, Waltham	Hs00173707_m1 Cat. #4331182
Xpr1-probe (mouse)	FAM-MGB	ThermoFisher Scientific, Waltham	Mm00495501_m1 Cat. #4331182
Silencer Select Negative Control No. 1 siRNA	-	ThermoFisher Scientific, Waltham	Cat. #4390843
Silencer Select siXPR1	-	ThermoFisher Scientific, Waltham	s17614 Cat. #4392420

6.1.9. Used buffers and media

Table 9: Used buffers and media.

Description	Formulation
Assay diluent ELISA	PBS, pH 7.4 1 % (m/v) BSA
Binding buffer	ddH_2O, pH 7.4 20 mM NaH_2PO_4 500 mM NaCl 20 mM Imidazol

(continued)

Ca^{2+} buffer	ddH_2O, pH 7.4 140 mM NaCl 5 mM KCl 1 mM $MgSO_4$ 1 mM $CaCl_2$ 20 mM HEPES 1 mM NaH_2PO_4 5.5 mM glucose
Coating buffer ELISA	ddH_2O, pH 9.5 100 mM $NaHCO_3$ 34 mM Na_2CO_3
Comassie destaining buffer	ddH_2O 10 % (v/v) ethanol 7.5 % (v/v) acetic acid (glacial)
Elution buffer	ddH_2O, pH 7.4 20 mM NaH_2PO_4 500 mM NaCl 500 mM Imidazol
Jurkat medium	RPMI1640 +GlutaMax 10 % (v/v) FCS 100 U/mL Penicillin/Streptomycin
ME buffer	ddH_2O, pH 7.8 25 mM MOPS 2.5 mM EDTA
Negative DAPI solution	ddH_2O, pH 8-10.5 5 % (v/v) glycerol 25 % (v/v) methanol 25 ng/mL DAPI
RBC lysis buffer	ddH_2O, pH 7.0 155 mM NH_4Cl 0.1 mM EDTA 12 mM $NaHCO_3$

(continued)

Running buffer (1x)	ddH_2O 50 mM Tris 200 mM Glycine 0.02 % (v/v) SDS
SDS lysis buffer	ddH_2O 50 mM Tris 0.5 % (v/v) SDS
Seahorse Assay Medium	Seahorse XF RPMI Medium, pH 7.4 10 mM Seahorse XF Glucose 1 mM Seahorse XF Pyruvate 2 mM Seahorse XF L-Glutamine
Separation gel buffer	ddH_2O, pH 8.8 1.5 M Tris
Stacking gel buffer	ddH_2O, pH 6.8 1.0 M Tris
TBE (10x)	ddH_2O 1 M Tris 1 M boric acid 20 mM EDTA
TBS (1x)	ddH_2O, pH 7.6 2.5 mM Tris 15 mM NaCl
TBS-T (1x)	ddH_2O, pH 7.6 2.5 mM Tris 15 mM NaCl 0.005 % (v/v) TWEEN 20
T-cell medium complete	RPMI1640 +GlutaMax 10 % (v/v) FCS 100 U/mL Penicillin/Streptomycin 10 mM HEPES 2 mM L-Glutamine 1 mM Sodium Pyruvate 1 mM MEM NEAA 50 µM β-Mercaptoethanol

(continued)

TE buffer	ddH_2O, pH 7.8 10 mM Tris 1 mM EDTA
Transfer buffer (1x)	ddH_2O 20 % (v/v) methanol 50 mM Tris 200 mM Glycine
Wash Buffer ELISA	PBS, pH 7.4 0.05 % (v/v) TWEEN 20

6.1.10. Used kits

Table 10: Used kits.

Kit	Supplier	Cat. #
blackPREP Rodent Tail DNA Kit	Th. Geyer, Renningen	845-BP-0010250
CellTrace CFSE Cell Proliferation Kit	ThermoFisher Scientific, Waltham	C34554
Clariom D assay, mouse	ThermoFisher Scientific, Waltham	902513
ECL Select Western Blotting Detection Reagent	Sigma-Aldrich, St. Louis	GERPN2235
ELISA MAX Standard Set Mouse IL-2	BioLegend, San Diego	431001
Foxp3/Transcription factor staining kit	ThermoFisher Scientific, Waltham	00-5523-00
IgG (Total) Mouse Uncoated ELISA Kit with Plates	ThermoFisher Scientific, Waltham	88-50400
IgM Mouse Uncoated ELISA Kit with Plates	ThermoFisher Scientific, Waltham	88-50470
LIVE/DEAD Fixable Aqua Dead Cell Stain Kit, for 405 nm excitation	ThermoFisher Scientific, Waltham	L34957
Mouse Th17 Cell Differentiation Kit	R&D Systems, Minneapolis	CDK017
Naïve CD4+ T cell isolation Kit, mouse	Miltenyi Biotec, Bergisch Gladbach	130-104-453
Phosphate Assay Kit (Colorimetric)	Abcam, Cambridge	ab65622

(continued)

Pierce BCA Protein Assay Kit	ThermoFisher Scientific, Waltham	23225
QIAprep Spin Miniprep kit (250)	Qiagen, Hilden	27106
RNeasy Micro Kit	Qiagen, Hilden	74004
RNeasy Mini Kit	Qiagen, Hilden	74104
Seahorse XFp T Cell Metabolic Profiling Kit	Agilent, Santa Clara	103771-100
SuperScript IV VILO Master-Mix	ThermoFisher Scientific, Waltham	11756050
TMB Substrate Set	BioLegend, San Diego	421101
Zombie Violet Fixable Viability Kit	BioLegend, San Diego	423113

6.1.11. Used cells

Table 11: Used cells.

Cells	Supplier	Cat. #
E. coli BL21 (DE3) Competent cells	New England Biolabs	C2527
Jurkat (E6-1)	ATCC	TIB-152

6.1.12. Used animals

Table 12: Used animal strains.

Strain	Description	Reference
CD4-Cre	B6.Cg-Tg(Cd4-cre)1Cwi/BfluJ	Strain #022071 (Jackson Laboratories)
Marilyn	B6.Cg-Ptprc^{a} Rag2tm^{1Fwa} Tg(TcraH-Y,TcrbH-Y)1Pas/PasOrl	Strain #EM:00133 (EMMA)
XPR1-flox	C57BL/6-*Xpr1*$^{tm1.1Frsv}$/J	Strain #037220 (Jackson Laboratories)

6.1.13. Used instruments

Table 13: Used instruments.

Model	Supplier
ABS 120-4N analysis balance	Kern&Sohn, Balingen-Frommern
Äkta start HPLC system	Cytiva, Marlborough
Amnis ImageStreamX MkII Imaging flow cytometer system	Cytek Biosciences, Frankfurt a. Main
BioPhotometer	Eppendorf, Hamburg
BrandTech accu-jet pro pipet controller	ThermoFisher Scientific, Waltham
BVC professional Fluid aspiration system	Vacuubrand, Wertheim
ChemiDoc MP Imaging system	Bio-Rad Laboratories, Hercules
Color Sprout Plus mini centrifuge	Biozym Scientific, Hessisch Oldendorf
DM IRBE inverted microscope	Leica Microsystems, Wetzlar
EMB 600-2 balance	Kern&Sohn, Balingen-Frommern
FACSCanto II Flow cytometer system	BD Biosciences, Franklin Lakes
FM-120 KE-50-HCN ice machine	Hoshizaki Europe, Amsterdam
GeneChip Scanner 3000 6G	ThermoFisher Scientific, Waltham
Heracell VIOS 160i CO2 incubator	ThermoFisher Scientific, Waltham
Heraeus Megafuge 40R centrifuge	ThermoFisher Scientific, Waltham
Heraeus Megafuge 8 centrifuge	ThermoFisher Scientific, Waltham
HERAsafe HS18 laminar flow system	ThermoFisher Scientific, Waltham
Infors HT Ecotron incubator shaker	Profcontrol, Schönwalde-Glien
InoLab pH 7110 pH meter set	Carl Roth, Karlsruhe
MACS Multistand	Miltenyi Biotec, Bergisch Gladbach
Mikro 220 R centrifuge	Hettich, Tuttlingen
Mini Trans-Blot Cell blotting system	Bio-Rad Laboratories, Hercules
Mini-PROTEAN Tetra Cell electrophoresis system	Bio-Rad Laboratories, Hercules
MiniShaker MS2 vortex shaker	IKA-Werke, Staufen
NanoDrop 1000 Spectrophotometer	ThermoFisher Scientific, Waltham
NovoCyte Quanteon Flow cytometer system	Agilent, Santa Clara
Olympus Fluoview FV3000 convocal microscope	Evident Europe, Hamburg
Polymax 1040 3D shaker	Heidolph Scientific Products, Schwabach

(continued)

PowerPac Basic power supply	Bio-Rad Laboratories, Hercules
Primovert inverted cell culture microscope	Carl Zeiss Microscopy, Oberkochen
ProFlex Applied Biosystems PCR system	ThermoFisher Scientific, Waltham
PURELAB flex 2 water purification system	ELGA LabWater, Celle
RTC basic magnetic stirrer	IKA-Werke, Staufen
Seahorse XF HS Mini	Agilent, Santa Clara
SHHD1619DG orbital shaker	Ohaus, Parsippany
Sigma 4-16K centrifuge	ThermoFisher Scientific, Waltham
Sonoplus HD 2200 ultrasonic disintegrator set	Bandelin electronic, Berlin
Sonorex RK 102 H ultrasonic bath	Bandelin electronic, Berlin
Sorvall LYNX 4000 Superspeed Centrifuge	ThermoFisher Scientific, Waltham
Spark 10M Luminescence multi-mode microplate reader	Tecan Group, Männedorf
StepOnePlus Realtime PCR system	ThermoFisher Scientific, Waltham
T12 incubator	Heraeus Holding, Hanau
Tabletop Anesthesia System	Harvard Apparatus, Holliston
ThermoMixer C	Eppendorf, Hamburg
TubeRoller Rocking Roller	Benchmark Scientific, Sayreville
Water bath	GFL, Burgwedel

6.1.14. Used software

Table 14: Used software.

Software	**Source**
4D v20	4D SAS, Le Pecq
BD FacsDiva v8	Becton Dickinson, Franklin Lakes
BioRender	BioRender, Toronto
Citavi 6	Swiss Academic Software, Wädenswil
FlowJo v10	Becton Dickinson, Franklin Lakes
GraphPad Prism v9	GraphPad Software, La Jolla
IDEAS v6.2	Merck, Darmstadt
ImageJ	National Institutes of Health, Bethesda
ImageLab v6	Bio-Rad Laboratories, Hercules
Microsoft Office 2016	Microsoft Corporation, Redmond

(continued)

NovoExpress v1.6	Agilent, Santa Clara
Spark control v2.3	Tecan Group, Männedorf
StepOne v2.3	Life Technologies, Carlsbad
TAC 4.0	ThermoFisher Scientific, Waltham
Wave Pro v10.1	Agilent, Santa Clara

6.1.15. Used consumables

Table 15: Used consumables.

Description	Supplier	Cat. #
12 % Mini-PROTEAN TGX Precast Protein Gels, 15-well	Bio-Rad Laboratories, Hercules	4561046
7.5 % Mini-PROTEAN TGX Precast Protein Gels, 15-well	Bio-Rad Laboratories, Hercules	4561026
96 well multiply Fast PCR plate	Sarstedt, Nümbrecht	72.1981.010
Blotting paper, 195 g/m²	Th. Geyer, Renningen	11830403
Cell Culture Flask T-25	Sarstedt, Nümbrecht	83.3910.002
Cell Culture Flask T-75	Sarstedt, Nümbrecht	83.3911.002
Cell strainer 100 µm	Sarstedt, Nümbrecht	83.3945.100
Culture plates 12 well	Sarstedt, Nümbrecht	83.3821
Culture plates 24 well	Corning, Corning (New York)	353226
Culture plates 48 well	Corning, Corning (New York)	353230
Culture plates 6 well	Sarstedt, Nümbrecht	83.3920.005
Culture plates 96 well	Sarstedt, Nümbrecht	83.3924
Flow cytometry tubes, 5 mL	Sarstedt, Nümbrecht	55.1579
HistoBond Microscope slides, 76x26x1 mm	Paul Marienfield, Lauda-Königshofen	0810000
HisTrapFF column 5 mL	Cytiva, Marlborough	17525501
LS columns	Miltenyi Biotec, Bergisch Gladbach	130-042-401
Micro test plate 96 well, conical bottom	Sarstedt, Nümbrecht	82.1583.001
Micro test plate 96 well, flat bottom	Sarstedt, Nümbrecht	82.1581
Micro tube, 1.5 mL	Sarstedt, Nümbrecht	72.706

(continued)

Micro tube, 2 mL	Sarstedt, Nümbrecht	72.695.500
Nunc MaxiSorp ELISA plates, uncoated	BioLegend, San Diego	423501
Parafilm M	Merck, Darmstadt	P6543
Pasteur pipette glass 230 mm	Th. Geyer, Renningen	7691061
Petri dishes	Greiner Bio-One, Frickenhausen	633180
Pipet tips, 1 mL	Sarstedt, Nümbrecht	70.3050.200
Pipet tips, 1 mL, filter	Sarstedt, Nümbrecht	70.3050.355
Pipet tips, 100 µL, filter	Sarstedt, Nümbrecht	70.3030.355
Pipet tips, 20 µL	Sarstedt, Nümbrecht	70.3010.200
Pipet tips, 20 µL, filter	Sarstedt, Nümbrecht	70.1114.210
Pipet tips, 200 µL	Sarstedt, Nümbrecht	70.3030.100
Pipet tips, 200 µL, filter	Sarstedt, Nümbrecht	70.3031.355
Reagent reservoir	ThermoFisher Scientific, Waltham	8086
Scalpel No. 11	Dahlhausen Medizintechnik, Köln	1100000711
Screwcap tube, 15 mL	Sarstedt, Nümbrecht	62.554.502
Screwcap tube, 50 mL	Sarstedt, Nümbrecht	62.547.254
Seahorse XFp Cell Culture Miniplates	Agilent, Santa Clara	103025-100
Seahorse XFp FluxPaks	Agilent, Santa Clara	103022-100
Sealing tape, optically clear	Sarstedt, Nümbrecht	95.1994
Serological pipette 10 mL	Sarstedt, Nümbrecht	86.1254.001
Serological pipette 25 mL	Sarstedt, Nümbrecht	86.1685.001
Serological pipette 5 mL	Sarstedt, Nümbrecht	86.1253.001
Serological pipette 50 mL	Sarstedt, Nümbrecht	86.1256.001
Slide-A-Lyzer G3 dialysis cassette 10 K MKCO, 15 mL	ThermoFishe Scientific, Waltham	A52972
Sterican 100, ø 0.40 x 20 mm, 26G x ¾" needles	B. Braun, Melsungen	4657705
Syringe 1 mL	B. Braun, Melsungen	9166017V
Syringe 30 mL	BD Biosciences, Franklin Lakes	301229
Syringe filter, 0.2 µm pore size	Sarstedt, Nümbrecht	83.1826.001

(continued)

Transfermembrane Immobilon-P, PVDF, 0.45 µm	Carl Roth, Karlsruhe	T831.1
VWR Coverslips, Round, 9 mm diameter	Avantor, Radnor	631-0169
Waste disposal bags	Th. Geyer, Renningen	7696994

6.2. Methods

6.2.1. Animals

6.2.1.1. General handling

All animals were kept in individually ventilated cages and under pathogen-free conditions. The breeding and general care for the animals was done at the animal facility of the University Medical Center Hamburg-Eppendorf. This study was carried out in accordance with the recommendations of Directive 2010/63/EU of the European Parliament on the protection of animals used for scientific purposes. The protocol was approved by the Behörde für Justiz und Verbraucherschutz der Freien und Hansestadt Hamburg (permit numbers: ORG1099; N016/24). Mice were sacrificed by cervical dislocation after anaesthesia in an isoflurane chamber.

6.2.1.2. Breeding

All mice were bred in-house on the C57BL/6J background. CD4-Cre mice (B6.Cg-Tg(*Cd4-cre*)1Cwi/BfluJ, Jackson Laboratories strain #022071) and XPR1-flox mice (C57BL/6-*Xpr1*$^{tm1.1Frsv}$/J, Jackson Laboratories strain #037220) were crossed, resulting in the CD4-Cre-XPR1-flox line. *Marilyn* mice (B6.Cg-*Ptprc*^{a} *Rag2*^{tm1Fwa} Tg(*TcraH-Y,TcrbH-Y*) 1Pas/PasOrl, EMMA strain #EM:00133), characterised by knockout of *Rag2* and the transgenic T-cell receptor specific for the H-Y antigen (TCR-H-Y), were cross-bred with the CD4-Cre-XPR1-flox line to produce *Marilyn*-CD4-Cre-XPR1-flox mice. Rag2$^{-/-}$ mice were presented as animals of the *Marilyn*-CD4-Cre-XPR1-flox line negative for genetic alterations except for knockout of *Rag2*.

6.2.1.3. Injections and serum collection

Injections of cells or peptides were done intravenously into the tail vein. Injections were done in 100 µL 0.9 % saline. Either $2x10^6$ cells or 10 mg/kg bodyweight H-Y peptide were injected per animal.

Blood was collected retroorbitally or by cardiac puncture. For generation of serum, collected blood was incubated for 20 min at room temperature (rt) to allow for blood clotting. After centrifugation for 10 min at 1,500 *g* and 4 °C, serum was collected and stored at -20 °C until further analysis.

6.2.2. Genotyping of transgenic mice

To identify the genotype of transgenic mice, genotyping polymerase chain reactions (PCRs) of regions of interest were performed. A tail biopsy was prepared within the first weeks of life by the animal technicians of the UKE's animal facility.

DNA from the tail biopsies was prepared using the blackPREP Rodent Tail DNA Kit (Th. Geyer), according to the manufacturer's instructions. First, the tail biopsies were lysed for 3 h at 37 °C in Lysis Solution QPT, which contained Protein Kinase K. After centrifugation at 10,000 *g* and rt for 30 s, the supernatant was mixed with SBS Binding Solution, transferred into a spin filter tube, and centrifuged for 2 min at 10,000 *g* and rt. The DNA was washed with MS Washing Solution twice at 10,000 *g* and rt for 2 min, followed by another centrifugation step without any applied buffer to remove residual ethanol. Elution was done with ddH_2O for 1 min at 8,000 *g* and rt. The prepared DNA was analysed by PCR using the KAPA2G Fast HotStart Readymix 2x PCR mix, which contains polymerase, dNTPs, essential ions and a suited buffer. CD4-Cre-XPR1-flox mice were genotyped using 0.5 µM primers (Table 6) and programs (Table 16) for *Cd4* and *Xpr1*. *Marilyn*-CD4-Cre-XPR1-flox mice were genotyped using 0.5 µM primers and programs for *Cd4*, *Xpr1*, *Rag2* and *TCR-HY*.

Table 16: Used cycler programs and primers used for genotyping PCRs.

Amplified Target	Temperature	Time	# cycles
Cd4	95 °C	4 min	
	95 °C	30 s	35
	60 °C	30 s	
	72 °C	60 s	
	72 °C	10 min	

(continued)

Xpr1	95 °C	4 min	
	95 °C	30 s	35
	62 °C	35 s	
	72 °C	35 s	
	72 °C	5 min	
Rag2,	94 °C	3 min	
TCR-HY	94 °C	40 s	10
	65 °C; -0.5°C/cycle	40 s	
	68 °C	40 s	
	94 °C	40 s	28
	60 °C	40 s	
	72 °C	40 s	
	72 °C	5 min	

After completion of the PCR program, the amplified samples were stored at 4 °C until further analysis by agarose gel electrophoresis. For visualisation of the DNA, 9 µL SYBR Safe Green per 150 mL 2 % agarose solution were added to the gel during casting. Imaging was performed at the ChemiDoc MP Imaging System (Bio-Rad Laboratories).

6.2.3. Cell culture

Cells were cultured at 37 °C, 5 % CO_2 and 85-90 % relative humidity. All procedures on cells were carried out under sterile conditions using a laminar air flow workbench.

Primary murine T cells or splenocytes were cultured in T-cell medium complete or X-VIVO 15 (serum-free). Jurkat cells (E6-1) were cultured in Jurkat medium, with passaging every 2-5 days.

Jurkat cells could be frozen to maintain an adequate cell stock. For freezing of Jurkat cells, 1-2 x10^6 cells were resuspended in FBS + 10% (v/v) DMSO, immediately cooled at 4 °C for 1 min, and then transferred to -80 °C overnight before long-term storage in liquid nitrogen. For thawing of Jurkat cells, 1-2x10^6 frozen cells were resuspended in prewarmed Jurkat medium, immediately centrifuged for 300 *g* and 5 min, and resuspended in fresh Jurkat medium to remove the DMSO containing freezing medium.

6.2.4. Overexpression and purification of viral ligands

XPR1 acts as an entry receptor for X-MLV. The RBDs of X-MLV and P-MLV were previously cloned into the pTrcHisB expression vector (180). P-MLV and X-MLV share high sequence homology, however their activities differ (460, 289, 180). In this work, the RBD of P-MLV was used as a negative control while the RBD of X-MLV was used to assess the effect of viral ligand interaction with XPR1 on CD4 T cell biology. For expression of the His-tagged Xenotropic Virus Derived Ligand (XVDL) and Polytropic Virus Derived Ligand (PVDL), the respective plasmids were transformed into ultracompetent *E. coli BL21*. XVDL or PVDL were purified using affinity chromatography in a high performance liquid chromatography (HPLC) system.

For one transformation, 50 µL *E. coli BL21* were thawed on ice for 10 min. 1 pg-100 ng plasmid DNA in 1-5 µL were added to the cell suspension. The DNA-cell suspension was mixed carefully and incubated on ice for 30 min. A heat shock for 10 s at 42 °C was applied to the mixture in order to facilitate transformation of the plasmid. After 5 min of incubation at 4 °C, 950 µL prewarmed SOC medium was added to the mixture. The bacteria were precultured for 60 min at 37 °C and 250 rpm in a heating block. A serial 1:10 dilution from 10^0 to 10^7 was prepared, and three way streaking onto agar plates containing 100 µg/mL Ampicillin was performed for each dilution.

The culture plates were incubated overnight at 37 °C, and the next day, a suited single colony was picked and used to inoculate a liquid culture of 100 mL LB medium (+100 µg/mL Ampicillin). The bacteria suspension was cultured overnight at 37 °C and 180 rpm. Once the suspension reached an optical density of 0.6 at 600 nm (OD_{600}), overexpression expression of XVDL or PVDL was induced using 1 mM IPTG. After 4 h of incubation at 37 °C and 180 rpm, the bacteria were centrifuged at 4,000 *g* and 4 °C for 20 min.

The cells were lysed in binding buffer (+EDTA-free cOmplete protease inhibitor tablets), with the lysis process being supported by 5x 15 s sonification at 20 % power with an ultrasound disintegrator. Cell debris and still intact bacteria as well as insoluble components were separated from the protein suspension by centrifugation for 20 min at 12,000 *g* and 4 °C.

In order to purify the protein of interest from other proteins present in the cell lysate, affinity chromatography was performed. A Ni-sepharose column (HisTrap) was used in the Äkta start HPLC system (Cytiva). First, the HPLC system and the used column were washed and equilibrated. Next, the cell lysate was introduced into the system. After three times of reapplying the flow-through onto the column to account for optimal binding, the column was washed. The bound protein was eluted with elution buffer containing a high imidazole

concentration, which competes with the His-Tag fused to the proteins of interest for the Ni^{2+} cations and replaces the tagged protein.

Dialysis was used to change the buffer of XVDL or PVDL to PBS. For this, Slide-A-Lyzer G3 dialysis cassettes (10K MWCO, 15 mL) were loaded with 5-15 mL of the protein eluate and incubated in 2 L PBS overnight.

6.2.5. Isolation of primary murine T cells

Murine CD4+ T cells can be isolated from the secondary lymphoid tissue of mice, i.e. spleen or lymph nodes, using magnetic activated cell sorting (MACS). Either positive or negative selection was used. For positive selection, cells of interest were labelled with an antibody, whereas for negative selection, all cells except for the cells of interest were labelled with an antibody cocktail. The antibodies used for labelling were bound by magnetic microbeads. Using columns inserted into a magnetic field, the cells of interest were separated from other cell types of the suspension.

Mice were sacrificed, and the spleen and/or lymph nodes were dissected and pushed through a 100 µm cell strainer using the plunger of a 1 mL syringe. The following protocols were used for roughly $1x10^8$ cells, which amounts to the number of splenocytes found in one spleen of an adult mouse.

The cell strainer was washed with PBS and the cell suspension was centrifuged at 500 *g* and rt for 12 min. To remove erythrocytes from the cell suspension, the cells were resuspended in 3 mL red blood cell (RBC) lysis buffer and incubated for 3.5 min at rt. 25 mL PBS were added to the suspension and the cells were washed using a centrifugation at 500 *g* and rt for 6 min. Next, either positive or negative selection could be applied.

6.2.5.1. Positive selection of CD4+ T cells

For positive selection, the cells were resuspended in 2 mL ice-cold MACS buffer and 10 µL α-CD4 (coupled to PE or Biotin) were added. After 15-30 min of incubation at 4 °C, 10 mL MACS buffer were added and the cells were washed at 500 *g* and 4 °C for 6 min. Next, the cells were resuspended in 900 µL MACS buffer and 100 µL microbeads, coupled with α-PE or streptavidin, were added to the suspension. After 15-30 min of incubation at 4 °C, the cells were centrifuged for 6 min at 500 *g* and 4 °C. The supernatant was discarded and the cells were washed with 20 mL MACS buffer for 6 min at 500 *g* and 4 °C. The sedimented cells were resuspended in 1 mL MACS buffer and applied onto an equilibrated LS column placed in a

magnetic field. Once the cell suspension had wholly entered the column bed, 3 mL MACS buffer were applied to wash the column.

The flow-through contained CD4- cells. The column was removed from the magnetic field and placed into a 15 mL reaction tube. 5 mL MACS buffer were applied onto the column and the liquid was pushed through with a plunger. The resulting cell suspension contained CD4+ cells and was changed to an appropriate buffer or medium and counted with a Neubauer cell counting chamber.

6.2.5.2. Negative selection of naïve CD4+ T cells

For negative selection, the Naïve CD4+ T cell isolation Kit was used. Splenocytes were resuspended in 400 µL MACS buffer and supplemented with 100 µL Biotin-Antibody cocktail (Naïve CD4+ T cell isolation kit, mouse). After 5 min incubation at 4 °C, 200 µL MACS buffer, 200 µL Anti-Biotin MicroBeads and 100 µL CD44 MicroBeads were added. The cell suspension was mixed and incubated for 10 min at 4 °C. Afterwards, 2 mL MACS buffer were added, and cells were centrifuged at 500 *g* and 4 °C for 6 min. The sedimented cells were resuspended in 1 mL MACS buffer and applied onto an equilibrated LS column placed in a magnetic field. Once the cell suspension had wholly entered the column bed, 3 mL MACS buffer were applied to wash the column.

The flow-through contained unlabelled naïve CD4+ T cells, and was therefore collected and centrifuged at 500 *g* and 4 °C for 6 min. Subsequently, the cells were resuspended in a suiting buffer or medium and counted with a Neubauer cell counting chamber. CD4- or non-naïve CD4+ T cell populations were retained in the column and could be collected by applying 5 mL MACS buffer to the column and pushing the liquid through it with a plunger.

6.2.6. Ca^{2+} measurements

In T cells, Ca^{2+} is an important second messenger that gets released into the cytosol upon stimulation. In order to study this Ca^{2+} response, the ratiometric Ca^{2+} reporter dye Fura2-AM was used.

Ca^{2+} measurements were performed in collaboration with Dr. Björn Diercks (Institute for Biochemistry and Molecular Cell Biology, University Medical Centre Hamburg-Eppendorf). In brief, naïve murine CD4+ T cells were freshly isolated and loaded with 4 µM Fura2-AM. After incubation for 40 min at 37 °C, the cells were washed two times and resuspended in Ca^{2+} buffer. During live cells imaging, T cells were stimulated after 1 min with 10 µg/mL α-CD3. This

was followed by addition of 1.67 µM thapsigargin after 11 min to accumulate cytosolic Ca^{2+} by blocking sarcoplasmic/endoplasmic reticulum Ca^{2+} ATPase (SERCA).

The live cell imaging was performed with a Leica IRBE microscope at 40x magnification and exposure of 25 ms, using Volocity v6.6.2 for acquisition. The acquisition frame rate was set to 1 frame every 2 s in 16-bit mode. Two excitation filters (HC 340 nm/26 nm and HC 387 nm/11 nm), one beamsplitter (4000 DLCP) and an emission filter (510 nm/84 nM) were used. Fiji 2v (ImageJ) was used for background correction, splitting of fluorescence channels and selection of cells. To calculate the Ca^{2+} concentration, a calibration was obtained by measuring the maximal ratio value Rmax and the minimal ratio value Rmin. Using this, the mean Ca^{2+} concentration over time and the area under the curve (AUC) were calculated.

6.2.7. Seahorse metabolic flux analysis

To analyse metabolic activity in CD4+ cells, the Seahorse XF HS Mini analyser (Agilent) was used. Naïve CD4+ T cells were isolated using negative selection, and the XFp T Cell Metabolic profiling kit was used according to the manufacturer's instruction. In brief, 200,000 cells in Seahorse Assay Medium were seeded per well of a preheated XF PDL miniplate in technical triplicates. After calibration, oxygen consumption rate (OCR) and extracellular acidification rate (ECAR) were measured. The experimental compounds oligomycin A, BAM15 and rotenone/antimycin A (provided by the manufacturer's kit) were injected by the instrument during the assay, with three to four measurement cycles per injection.

Analysis was done using Seahorse Wave Pro 10.1.0 software (Agilent), and the manufacturer's analysis website seahorseanalytics.agilent.com. By this, spare respiratory capacity, maximal respiration, % ATP from glycolysis and basal rates of ATP production (glycoATP and mitoATP production rate) were calculated.

6.2.8. Treatment of cells

The peptides Tat-K (YGRKKRRQRRRPPLNRTPSTVTLNNNT) and Tat-X (YGRKKRRQRRRPRLASQSKARDTKVLIEDTDDEANT) were used to disrupt the putative interaction of XPR1's and KIDINS220's PDZ binding motifs with PDZ domain containing interaction partners. For this, freshly isolated CD4+ T cells (optionally stained with proliferation dye) were treated with 3 µM Tat-K, Tat-X or DMSO and seeded. After 90 min of culturing at 37 °C, the medium was changed.

Treatment with the IP6K1 inhibitor UNC7467 was done to attenuate the intracellular IP8 pool to address XPR1's trafficking role in the endosomal/lysosomal compartment under the condition of inhibited phosphate transporter function (183, 184). Further, treatment with XVDL and PVDL (see 6.2.4) was done to a assess the effect of viral ligand binding to XPR1. CD4+ T cells were treated with 1 µM UNC7467 or 20 µg/mL XVDL or PVDL.

6.2.9. Stimulation of primary murine T cells

T cells can be stimulated using phorbol 12-myristate 13-acetate (PMA) and Ionomycin, which activate protein kinase C (PKC) and act as a Ca^{2+} ionophore, respectively. This combination allows for the stimulation of T cells without engagement of the TCR complex (258, 259). To achieve this, T cells were treated with 50 ng/mL PMA and 1 µg/mL Ionomycin, which were applied to the cell culture medium during seeding. SEB is a bacterial toxin and superantigen, which can interact with the TCR complex as well as CD28, and their respective ligands on APCs, inducing hyperactivation, sepsis, cytokine storm, and toxic shock (260–264). Treatment was done using 1 ug/mL SEB.

A more physiologic stimulus can be achieved by using antibodies directed against CD3 and CD28 to engage with the TCR complex and the co-stimulatory receptor CD28, respectively (257). For this stimulation method, cell culture plates were coated with α-CD3 (2-5 µg/mL) and α-CD28 (0.5-1 µg/mL) antibodies. To achieve this, the antibodies were diluted to the required concentration in PBS and applied onto cell culture plates in suitable volumes. The cell culture plates were incubated either at 37 °C for at least 1 h or at 4°C overnight. Before seeding cells onto the coated plates, the coating solution was discarded and the wells were washed twice with PBS.

6.2.10. Small interfering RNA (siRNA) transfection

Gene expression can be modulated using small interfering RNAs (siRNAs) which interact and thereby interfere with mRNA. siRNA targeting mRNA coding for XPR1 was used in cell culture experiments to transfect Jurkat cells, thereby downregulating the XPR1 expression. Scrambled siRNA served as a negative control for unaltered XPR1 expression.

24 h before the transfection with siRNA, 300,000 Jurkat cells per well of a 6-well plate were seeded in 1.5 mL Jurkat medium. 30 min prior to the transfection, the medium was changed to 1.5 mL OptiMEM. Per single reaction, 125 µL OptiMEM containing 7.5 µL Lipofectamin RNAiMAX were mixed with 75 pmol siRNA (siXPR1 or scrambled control siRNA (siCtrl)) in 125 µL OptiMEM. The resulting transfection mix was incubated for 5 min at rt, and then 250 µL

were applied to the cells, dropwise. Subsequently, the plate was swayed gently to spread the transfection mix. After 4 h of transfection, the medium was changed back to 1.5 mL Jurkat medium per well. In order to achieve an adequate transfection efficiency, cells were retransfected 24 h after the initial transfection, following the same instructions described above. Analysis was performed 48 h or 72 h after the initial transfection.

6.2.11. *In vitro* differentiation assays

Depending on the cytokine environment, stimulated CD4+ T cells differentiate into T helper (Th) cell subpopulations. *In vitro*, different combinations of cytokines and antibodies can be used to emulate Th1-, Th2-, Th17 or iTreg-skewing conditions. Stimulated, primary murine CD4+ T cells can then differentiate into the respective Th-cell subpopulations. As a control, Th0-skewing conditions represent a stimulation without a specific subpopulation arising.

For Th0-, Th1-, Th2- and iTreg differentiation, 24-well cell culture plates were coated with α-CD3 (2 µg/mL) and α-CD28 (0.5 µg/mL). For Th17 differentiation, cell culture plates were coated with α-CD3 only (5 µg/mL). Freshly isolated primary murine CD4+ T cells were counted and seeded onto the coated plates. For Th0-, Th1-, Th2- or Treg differentiation, $1x10^6$ T cells were seeded per coated well in 1 mL Th0-, Th1-, Th2- or Treg differentiation medium. For Th17 differentiation, $1x10^6$ T cells per well were seeded onto coated plates in 500 µL Th17 differentiation medium, either by the recipe shown below or by the differentiation medium provided by the Mouse Th17 Cell Differentiation kit. The compositions of the differentiation media are shown in Table 17.

Cells cultured under Th0-, Th1-, Th2- or iTreg-skewing conditions were analysed after 72 h of culture. For cells cultured under Th17-skewing conditions, 500 µL fresh Th17 differentiation medium was added to the wells after 72 h of culture. Cells were analysed after another 48 h of culture.

Table 17: Cytokine and antibody concentrations in Th subset differentiation media.

subpopulation	Th0	Th1	Th2	Th17	iTreg
Reagent	**Concentration in medium**				
IL-2	1 µg/mL	1 µg/mL	1 µg/mL		2 µg/mL
IL-12		5 ng/mL			
IL-4			4 ng/mL		
TGF-β				1 ng/mL	10 ng/mL
IL-6				50 ng/mL	
IL-23				5 ng/mL	
α-IL-4		10 µg/mL		10 µg/mL	1 µg/mL
α-IFN-γ			10 µg/mL	10 µg/mL	1 µg/mL
α-CD28				5 µg/mL	

6.2.12. Proliferation assays

T cell proliferation can be tracked over time using proliferation dyes. Those fluorescent dyes covalently bind to cellular proteins with primary amines. With every cell division, the dye is distributed equally between resulting daughter populations. Using a flow cytometer to quantify the fluorescence intensities for each cell, the frequency of cells in each generation can be determined and therefore, proliferation activities can be compared between samples.

Freshly isolated, primary murine CD4+ T cells were labelled with proliferation dyes. For this, $1x10^6$ cells in 500 µL warm PBS were mixed with 500 µL of a 2x concentrated solution of the used proliferation dye in warm PBS and vortexed immediately. After 20 min incubation at 37 °C, protected from light, the labelling process was stopped with 500 µL FCS. The suspension was incubated for 5 min at 37 °C, protected from light. Next, the cells were centrifuged at 500 *g* and rt for 6 min. Afterwards, the cells were resuspended in a suiting medium and either injected intravenously, or seeded onto a 48-well cell culture plate, with $1x10^6$ T cells in 500 µL medium per well with stimulation for 72 h.

CFSE was used in a final concentration of 2.5 µM, eFluor450 and eFluor670 were used in a final concentration of 1.25-2.5 µM.

6.2.13. Flow cytometry

Flow cytometry can be used to analyse protein expression and morphological characteristics of cells. The method is based on cells or other small particles passing different lasers individually, allowing analysis on a single-cell level. Morphological properties, i.e. cell size and

granularity/complexity of cells, are addressed by analysis of light refraction and scattering, respectively. For this, detectors angled 180° or 90° to the laser direction are used, and the readouts are termed forward scatter (FSC) or sideward scatter (SSC), respectively. Flow cytometers are equipped with different lasers and filter systems, allowing for detection of fluorescence intensity in several channels. The intensity of detected light in a channel is proportional to the relative abundance of the target. Therefore, protein expression can be analysed by labelling different targets of interests with *e.g.* using fluorophore-coupled antibodies. Targets can be stained on the cell surface and intracellularly.

6.2.13.1. Preparation for flow cytometry staining of cytokines

In case cytokine expression was analysed by flow cytometry, cells were pretreated to prevent the secretion of produced cytokines, causing them to be retained in the Golgi network instead. For this, cells were stimulated with PMA/ionomycin for 2 h before adding 1x Protein Transport Inhibitor Cocktail to the cells. After another at least 4 h, cells were subjected to flow cytometry staining.

6.2.13.2. Flow cytometry staining

For staining of cells with fluorophore-coupled antibodies, 0.2 to 2x10^6 cells per sample were transferred into the wells of a 96-well V-bottom plate. After centrifugation for 5 min at 500 *g* and 4 min, the supernatant was discarded and the cells were resuspended in 200 µL PBS. The cells were washed twice with PBS using the same centrifugation conditions, and the cells were resuspended in 10 µL of antibody mix directed against extracellularly expressed targets. Additionally, to prevent immune cells binding the constant domain of applied antibodies, Fc receptors were blocked by adding 1:200 TruStain FcX to the extracellular antibody solution. After 15-30 min of incubation at 4 °C, cells were washed twice with PBS.

For immediate measurement, cells were resuspended in PBS. For measurement later, cells were fixed using the Foxp3/Transcription Factor Staining Buffer Set (ThermoFisher Scientific) according to the manufacturer's instruction. Fixation was performed in 50 µL of a 1:4 mixture of Fixation/Permeabilization Concentrate and Fixation/Permeabilization Diluent for 10 min at 4 °C. After the incubation, cells were washed twice with 200 µL 1x Permeabilization Buffer. Fixed cells were stored in a suited volume of PBS at 4 °C until measurement, but not longer than 1 week.

For intracellular staining, fixed cells were resuspended in appropriately diluted antibodies for 15-30 min at 4 °C, followed by two washing steps in 1x Permeabilization buffer. Readily stained cells were then resuspended in PBS and either measured or stored, as indicated above.

For target-specific antibodies without a fluorophore, species-specific, secondary antibodies coupled to a fluorophore were applied in an extra step. This is also applicable for biotin-coupled, target-specific antibodies, which were then stained with streptavidin-fluorophore constructs. For this, cells that were already stained with the target-specific antibody and washed twice were resuspended in the secondary antibody or streptavidin construct, diluted in the appropriate buffer. After 15-30 min of incubation at 4 °C, cells were washed twice and the staining protocol was resumed accordingly.

Cell analysis using flow cytometry was performed at the cell analyser systems FACSCanto II (BD Bioscience) or NovoCyte Quanteon (Agilent) of the Cytometry and Cell Sorting Core Facility at the University Medical Centre Hamburg-Eppendorf. Analysis was done using FlowJo v10. For creation of a compensation matrix, samples stained with antibodies detectable in only one channel were used. Isotype controls were used for validation of antibody applicability.

6.2.13.3. General gating strategy for CD4+ T cells

In a first step, the target cells were gated in an SSC-A/FSC-A plot according to the cells' size and granularity (Figure 37A). Next, doublet discrimination was performed by setting a gate in the FSC-H/FSC-A plot (Figure 37B). The resulting single-cell population was further gated for living CD4+ T cells using a viability dye and an α-CD4 antibody (Figure 37C).

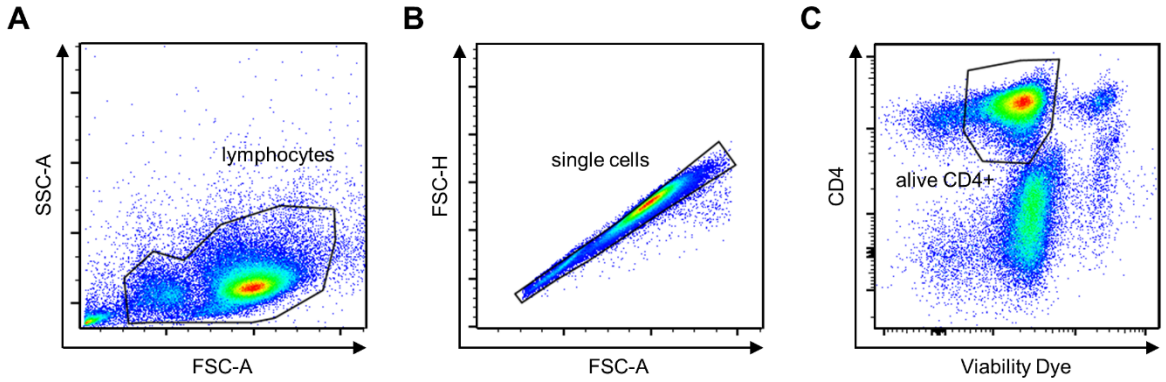

Figure 37: General gating strategy for flow cytometry analysis of CD4+ T cells. A: Size and granularity were used to identify the lymphocyte population in an SSC-A/FSC-A plot. **B**: The single cell population was gated using

an FSC-H/FSC-A plot to remove debris and doublets. **C**: Living CD4+ T cells were gated in a CD4/Viability Dye plot. The Viability Dye either corresponded to the LIVE/DEAD Fixable Aqua Dead Cell Stain Kit, for 405 nm excitation or the Zombie Violet Fixable Viability Kit.

6.2.13.4. Gating strategy for proliferation tracing

After gating for living CD4+ cells according to 6.2.13.3, proliferated cells were gated in an FSC-A/Proliferation Dye gate (Figure 38A): the population with the highest intensity of the proliferation dye corresponds to the population of not proliferated cells. All cells with a lower intensity were therefore gated as proliferated cells. For an optional more detailed proliferation analysis, the local maxima of the proliferation dye intensities were assigned to the proliferation cycle in a histogram plot (Figure 38B). Cells with a high proliferative activity were considered all cells in cycle #3 or more.

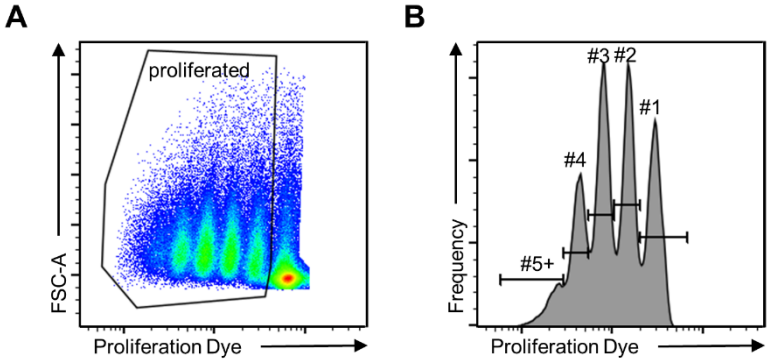

Figure 38: Gating strategy for proliferation tracing. A: Debris removed from the living CD4+ T cells gate using an FSC-A/Proliferation Dye plot. **B**: The FSC-A/Proliferation Dye plot was further used for gating all proliferated cells. **C**: In a histogram of the Proliferation Dye intensities, the proliferation cycle number were assigned to local maxima. The Proliferation Dye either corresponded to the CellTrace CFSE Cell Proliferation Dye, the Cell Proliferation Dye eFluor450 or the Cell Proliferation Dye eFluor670.

6.2.13.5. Gating strategy for *Marilyn* T cell phenotyping panel

Cells that were isolated from *Marilyn* mice and gated into single cells according to 6.2.13.3 were further gated for living cells in an SSC-A/Viability Dye plot (Figure 39A). Living cells were gated into H-Y antigen-specific CD4+ T cells expressing TCR TRBV6 (TRBV6) as indicated in Figure 39B.

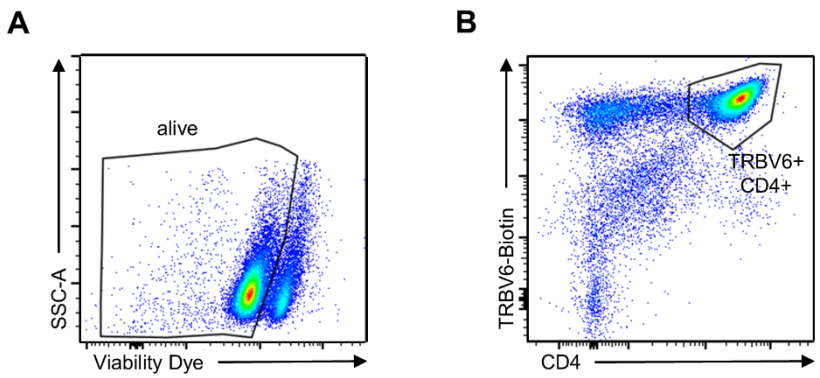

Figure 39: General gating strategy for *Marilyn* CD4+ T cells. A: Living *Marilyn* single cells were gated in an SSC-A/Viability Dye plot. **B**: Antigen-specific *Marilyn* CD4+ T cells were further gated as TRBV6+CD4+ in a TRBV6/CD4 plot. The used TRBV6-TCR antibody was coupled with biotin and therefore visualised using fluorophore-coupled streptavidin. Representative plots are from analysis of lymph nodes.

6.2.13.6. Microscopy in flow

Amnis ImageStream^X (Cytek) flow cytometers combine the benefits of flow cytometry and microscopy: Cells are passing different lasers individually, and SSC as well as fluorescence intensities in up to 10 channels are measured. Additionally, every event is imaged in bright field and all fluorescent channels with a magnification of 20x, 40x or 60x. This allows for a spatial correlation of detected signals.

In this thesis, the ImageStream method was used to analyse NFAT translocation into the nucleus after stimulation. For this, cells were permeabilised and stained intracellularly with a fluorophore-coupled NFAT1-antibody, and with DAPI for nuclear staining. About 2,000 events per sample of the target population were recorded with low flow rate and 60x magnification at the Amnis ImageStreamX MkII Imaging flow cytometer system (Cytek).

Analysis was done with IDEAS v6.2. Cells were gated for single cells in focus that were positive for CD4+, NFAT+ and DAPI+, according to Figure 40. To get a readout for co-localisation of NFAT signal and the nucleus, the Similarity Score feature was used, which calculates the log transformed Pearson's Correlation Coefficient. The Similarity Score describes the linear correlation between two channels within a masked region. Masks are sets of pixels defined by built-in functions, and are used to isolate areas of interest from background signals or irrelevant regions. A mask for the nucleus region was created by narrowing down the DAPI signal using the Morphology function mask and the Intensity function mask. The Similarity Score between the NFAT and DAPI signal was then calculated for each gated cell in the Morphology-Intensity-Mask. Cells with a high Similarity Score between NFAT and DAPI

were considered to have undergone NFAT trafficking to the nucleus, and were gated accordingly.

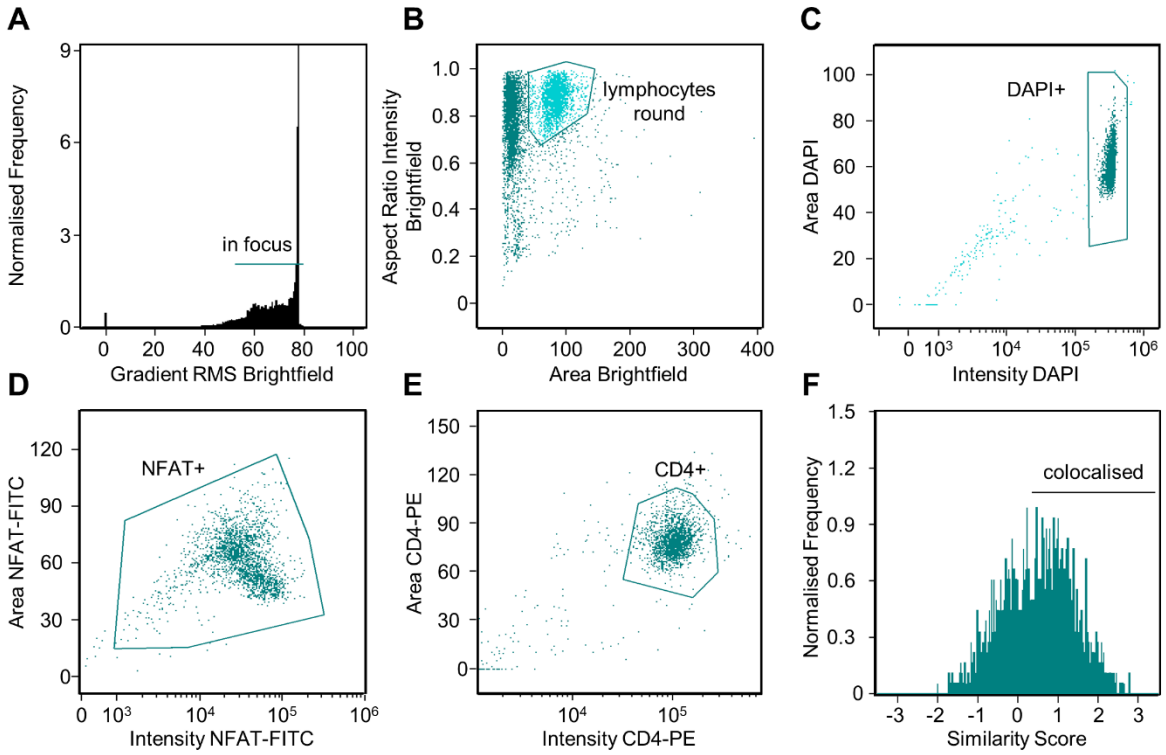

Figure 40: Gating strategy for analysis of NFAT-DAPI co-localisation. A: All unfocused events were removed from analysis by application of a gate in a Gradient Root Mean Square (RMS) histogram of the brightfield channel. **B**: Spherical lymphocytes were identified in plot with the Aspect Ratio Intensity of the brightfield channel plotted over the Area of the brightfield channel. **C-E**: Only cells with a sufficiently positive signal for DAPI, NFAT and CD4, respectively, were gated using plotting of the signal area over the signal intensity. **F**: Co-localised cells were gated as cells with a Similarity Score of ≥0.25. The Similarity Score between DAPI and NFAT was calculated by IDEAS' built-in Similarity Score feature in the Intensity(Morphology(DAPI)) mask.

6.2.14. Cell harvest and lysis

Primary murine T cells or Jurkat cell suspensions were centrifuged for 5 min at 500 *g* and 4 °C. Cell culture supernatants were collected and centrifuged for 20 min at 13,000 *g* and 4 °C to remove cells or debris. Until further analysis, the supernatants were stored at -20 °C.

Cells were washed twice with PBS for 5 min at 500 *g* and 4 °C, and then lysed using RIPA lysis buffer with supplementation of Halt Protease and Phosphatase Inhibitor Cocktail. After at least 30 min on ice with vortexing frequently, the lysate was sonicated thrice for 5 min in an ultrasound bath to improve the lysis process. Non-solubilised fractions were removed by centrifugation for 20 min at 13,000 *g* and 4 °C.

6.2.15. Measurement of protein concentration

Protein concentration in lysates was determined with the bicinchoninic acid (BCA) assay using the Pierce BCA Protein Assay kit (ThermoFisher Scientific) according to the manufacturer's instructions. The assay was performed using the microplate procedure. A bovine serum albumin (BSA) standard with a concentration range of 2-0.025 µg/mL was included in the kit. For the assay, 10 µL sample or standard were transferred into the wells of a 96-well flat-bottom plate. BCA reagent was prepared by mixing reagent A and B in a 50:1 dilution, and 200 µL of the reagent were added to each well. After 30 min of incubation at 37 °C, absorbance at 562 nm was read at the Spark 10M Luminescence multi-mode microplate reader (Tecan). For calculation of the protein concentration linear regression analysis was performed.

6.2.16. Sodium dodecyl-sulfate polyacrylamide gel electrophoresis (SDS-PAGE)

For separation of proteins according to their size, sodium dodecyl-sulfate polyacrylamide gel electrophoresis (SDS-PAGE) was performed.

Lysates were diluted 4:1 with 4x Laemmli sample buffer, containing β-mercaptoethanol and SDS, among other reagents, and then incubated for 10 min at 95 °C. By this, secondary and tertiary structures were denatured, and an evenly distributed negative charge was achieved.

Polyacrylamide gels were either purchased or prepared. If gels were produced in the lab, the separation gel was cast first and blanketed with a layer of isopropanol. Upon hardening of the separation gel after 20-30 min, the isopropanol was discarded and the space above the gel was washed with ddH_2O. Next, the stacking gel was cast on top of the separation gel and combs were applied to create 10 or 15 wells. Hardened gels were either used directly or stored at 4 °C, wrapped up in wet towels.

The recipes for used gels with different acrylamide proportions are listed in Table 18. Initially, all ingredients were mixed, except for ammonium persulfate (APS) and tetramethylethylenediamine (TEMED), which are applied to start the radical chain polymerisation reaction leading to the polymerisation of acrylamide.

Table 18: Polyacrylamide gel recipes used for SDS-PAGE.

	Separation gel (1.0 mm)			Stacking gel (1.0 mm)
Acrylamide proportion (final)	**8 %**	**10 %**	**12 %**	**3 %**
Acrylamide/Bisacrylamide 30 % (29:1)	2.025 mL	2.475 mL	3.000 mL	0.650 mL
Separation gel buffer	1.875 mL	1.875 mL	1.875 mL	-
Stacking gel buffer	-	-	-	1.875 mL
ddH_2O	3.600 mL	3.150 mL	2.625 mL	3.750 mL
SDS 20 %	37.5 µL	37.5 µL	37.5 µL	25.0 µL
TEMED	10.0 µL	10.0 µL	10.0 µL	7.5 µL
10 % APS	37.5 µL	37.5 µL	37.5 µL	30.0 µL

Gels were fixed in chambers filled with 1x running buffer. A mass of 0.5-10 µg per prepared sample as well as 4 µL PageRuler™ Plus Prestained Protein Ladder (10 to 250 kDa) were loaded into the wells. A voltage of 50-120 V was applied until the running front reached the bottom of the gel or until the regions of interest were sufficiently separated.

To visualise proteins on a SDS gel, it was stained with coomassie brilliant blue R-250 for 30 min. Unbound dye was removed with coomassie destaining solution overnight. Pictures of the gel were recorded using the Chemidoc MP Imaging System (Bio-Rad Laboratories) and analysed with ImageLab.

6.2.17. Immunoblotting

Proteins separated by SDS-PAGE were detected using immunoblotting, also known as the western blot method. In this method, proteins separated by SDS PAGE get blotted onto a membrane, specifically stained with antibodies, and visualised by chemiluminescence.

For this process, a blotting sandwich with different layers was prepared in 1x Transfer buffer: two Whatman filter papers were soaked in 1x Transfer buffer and placed on the bottom of the sandwich. A polyvinylidene fluoride PVDF membrane of suited size was pre-incubated in methanol for 30-60 s and then placed on top of the prepared filter papers, followed by the SDS gel and another two Whatman filter papers. The assembled sandwich was clamped into a blotting chamber and filled with ice-cold 1x Transfer buffer, with the membrane facing the

anode. By applying a constant voltage of 100 V for 75-90 min at 4 °C, the proteins were transferred onto the surface of the PVDF membrane.

Blocking of unspecific binding was achieved by rolling the membrane in 3 % BSA/TBS-T. After 1 h, the membrane was transferred into a reaction tube with the primary antibody, diluted appropriately in 3 % BSA/TBS-T, and rolled overnight at 4 °C. The next day, the membrane was washed thrice with TBS-T for 10 min at rt. Afterwards, the membrane was rolled for 1 h at rt in a secondary antibody specific for the species-specific constant region of the primary antibody, diluted 1:10,000 in TBS. After washing the membrane thrice in TBS-T for 10 min at rt again, the membrane was incubated for 1-5 min in ECL Select Western Blotting Detection Reagent (Sigma-Aldrich), prepared according to the manufacturer's instructions. The membrane was developed for a suited time using the ChemiDoc MP Imaging System (Bio-Rad Laboratories). Densitometric analysis for quantification of intensities was done using ImageLab.

6.2.18. Enzyme-linked immunosorbent assays (ELISA)

The concentration of murine IL-2 in cell culture supernatants was measured using the ELISA MAX Standard Set Mouse IL-2 (BioLegend) according to the manufacturer's instructions. The concentration of IgG and IgM in murine serum was determined using the IgG (Total) Mouse Uncoated ELISA Kit and the IgM Mouse Uncoated ELISA Kit (ThermoFisher Scientific) according to the manufacturer's instructions. The method is briefly described for the example of the Mouse IL-2 ELISA MAX Standard Set, as all three kits follow a similar workflow.

The day prior to the assay, capture antibody in coating buffer was applied to the wells of an uncoated Nunc MaxiSorp ELISA 96 well plate, and the plate was incubated overnight at 4 °C. The next day, the wells were washed four times with wash buffer. Assay diluent for blocking of unspecific binding sites was added to the wells, and the plate was incubated for 1 h at rt and 300 rpm on a horizontal shaker. After washing four times, diluted samples and standards were added in duplicates. The plate was incubated for 2 h at rt and 300 rpm. Subsequently, the wells were washed four times and detection antibody was applied to each well. After an incubation for 1 h at rt and 300 rpm, the wells were washed four times again, and avidin-HRP solution in assay diluent was applied onto the wells. The plate was incubated for 30 min at rt and 300 rpm, and after washing the plate five times, TMB substrate was added to each well to start the photometric reaction. After 10-30 min, the reaction was stopped using 1 M H_2SO_4. The absorbance at 450 nm and 570 nm was measured at the Spark 10M Luminescence multi-mode microplate reader (Tecan) within 15 min after the reaction stop. The absorbance at

570 nm was subtracted from the absorbance at 450 nm, and a linear regression or quadratic function was fitted using Excel 2016 to determine the unknown protein concentrations.

Following standard ranges were available in the used kits: 2-125 pg/mL (IL-2), 1.6-100 ng/mL (IgG), and 0.4-25 ng/mL (IgM).

6.2.19. Proximity ligation assay (PLA)

Protein-protein interactions can be visualised and quantified using a proximity ligation assay (PLA). In this method, two primary antibodies directed against the two respective proteins of interest, whose interaction is to be addressed, are used. The two antibodies are generated in different species, *e.g.* in mouse and rabbit. Species-specific secondary antibodies, coupled with PLUS or MINUS DNA oligos – termed PLA probes – bind to the primary antibodies. If the targets are in vicinity to each other, the oligos can be ligated to circular DNA, which is then amplified in a PCR-like reaction. By using fluorescent dNTPs in the amplification step, the produced, fluorescent DNA can be visualised and quantified using different techniques, *e.g.* confocal microscopy or flow cytometry.

In this thesis, CD4+ T cells were subjected to a PLA and then analysed using confocal microscopy. For this, CD4+ T cells were first attached to coverslips and fixed. Glass coverslips (ø=9 mm) were coated with fibronectin (1:50 in PBS) in 48-well or 24-well cell culture plates for 1 h at 37 °C or overnight at 4 °C. After washing the coverslips twice with PBS, CD4+ T cells were seeded in appropriate numbers (0.9-1.1 x10^6 cells/cm²) and incubated for 45-90 min. To support the attachment of the suspension cells to the surface of the coverslips, the cell culture plate was centrifuged at 300 *g* and rt for 1 min. The supernatant was discarded carefully, the cells were washed once with PBS, and fixation was performed by incubating the cells in 4 % PFA/PBS for 15 min at 37 °C. After discarding of the fixation solution, cells were washed twice with PBS.

The PLA was performed using the Duolink In Situ PLA reagents (Sigma-Aldrich) according to the manufacturer's instructions. A humid chamber was prepared, laid out with parafilm, and prewarmed in an incubator at 37 °C. The sample coverslips were transferred onto individual Duolink Blocking Solution drops on the parafilm, and the humid chamber was incubated for 1 h at 37 °C. Primary antibodies were diluted appropriately in Duolink Antibody Diluent. Each sample was incubated in a mix of two different antibodies from different species. The used concentrations are depicted in Table 19. Additionally, control samples incubated with an antibody from species A and the suited antibody isotype control from species B in the same concentration as the respective specific antibody were set up, as well as the other way around.

The coverslips were applied onto drops of 10-15 µL antibody mixtures, and the humid chamber was incubated overnight at 4 °C. The next day, coverslips were transferred into a 24-well plate and washed twice in 1x Wash Buffer A for 5 min. A new humid chamber was prewarmed and prepared with 10-12 µL drops of Duolink Antibody Diluent, containing 1:5 Duolink In Situ PLA Probe Anti-Rabbit PLUS and 1:5 Duolink In Situ PLA Probe Anti-Mouse MINUS. The washed coverslips were spotted top-down onto the PLA probe drops and incubated for 1 h at 37 °C. Subsequently, the coverslips were washed twice in a 24-well plate with 1x Wash Buffer A for 5 min at rt again. Ligase was diluted 1:40 in 1x Duolink Ligation Buffer and 10-15 µL drops were applied onto the parafilm of the humid chamber. Coverslips were spotted top-down onto the ligase drops, and after 30 min of incubation at 37 °C, the coverslips were washed twice with 1x Wash Buffer A. Duolink In Situ Detection Reagents Red were used for the amplification. Polymerase was diluted 1:80 in Duolink 1x Amplification Buffer, and coverslips were transferred onto them. The humid chamber was incubated for 100 min at 37 °C. Subsequently, the coverslips were washed twice for 10 min at rt in 1x Wash Buffer B, and once for 1 min at rt in 0.01x Wash Buffer B. Excess wash buffer was tapped off carefully, and microscopy slides were mounted with a coverslip using 5-8 µL of Duolink In Situ Mounting Medium with DAPI. The coverslips were fixated on the microscopy slides using nail polish since the mounting medium supplied by the kit does not harden. Slides were stored for a maximum of 2 months at -20 °C. Confocal microscopy imaging was performed in collaboration with the UKE Microscopy Imaging Facility at the Olympus Fluoview FV3000 (Evident Europe) using a 60x objective. Analysis was performed using the Cell Counter plugin of ImageJ, quantifying the interaction spots per cell.

Table 19: Antibody concentrations for PLA assays.

Antibody	Species	Stock concentration	End concentration
α-mouse CD247	Rabbit	0.8 mg/mL	8 µg/mL
α-mouse Kidins220	Mouse	2 mg/mL	20 µg/mL
α-mouse Kidins220	Rabbit	1 mg/mL	10 µg/mL
α-mouse XPR1	Mouse	0.5 mg/mL	10 µg/mL
α-mouse XPR1	Rabbit	0.7 mg/mL	10 µg/mL
α-mouse CTLA-4	Mouse	0.2 mg/mL	2 µg/mL
α-mouse CTLA-4	Rabbit	1 mg/mL	10 µg/mL
IgG isotype control	Rabbit	5 mg/mL	Adjusted to specific antibody
IgG1,κ isotype control	Mouse	1 mg/mL	Adjusted to specific antibody

6.2.20. Reverse transcription and quantitative polymerase chain reaction (qPCR)

Relative gene expression was analysed using quantitative polymerase chain reaction (qPCR).

First, cells were harvested and washed twice with ice-cold PBS at 500 *g* and 4 °C for 5 min. For isolation of mRNA, the RNeasy mini kit (Qiagen) was used according to the manufacturer's protocol. In brief, cells were resuspended in 350 µL RLT Buffer (+1 % (v/v) β-mercaptoethanol). The suspension was mixed with 350 µL 70 % ethanol and transferred immediately onto a spin column. After centrifugation for 15 s at 8,000 *g* and rt, the flow-through was discarded, 700 µL Buffer RW1 were added, and the spin column was centrifuged again. The samples were washed twice with 500 µL Buffer RPE, using centrifugation at 8,000 *g* and rt for 15 s and 2 min, respectively. Next, the spin column was placed into a fresh 2 mL collection tube, and the membrane was dried by a centrifugation for 1 min at 15,000 *g* and rt. RNA was eluted by applying 40 µL RNase free ddH_2O onto the membrane and centrifugation for 1 min at 8,000 *g* and rt. RNA concentration was then determined using the NanoDrop 1000 Spectrophotometer (ThemoFisher Scientific). If a concentration higher than 80 ng/mL was measured, the RNA was considered qualified for cDNA generation and qPCR.

For reverse transcription of the isolated mRNA to cDNA, 16 µL RNA were mixed with 4 µL SuperScript VILO Master Mix. The mix was incubated for 10 min at rt for primer annealing, then for 10 min at 50 °C for the transcriptase reaction, and finally for 5 min at 85 °C for denaturation of the transcriptase.

For the qPCR, 0.25-1.0 µL of the obtained cDNA were mixed with 10 µL TaqMan Universal Master Mix II, no UNG, 1 µL FAM-MGB-TaqMan probes, and 8.0-8.75 µL ddH_2O and transferred into the wells of a 96-well qPCR plate. Each reaction was run in triplicates, and for each sample, a housekeeping gene probe was used for analysis in addition to all the genes of interest. The used TaqMan probes are listed in Table 8. The plate was measured in the StepOnePlus Realtime PCR system (ThermoFisher Scientific), using the program described in Table 20.

Table 20: Program settings used for qPCR.

Temperature	Time	# cycles
50 °C	2 min	-
95 °C	10 min	-
95 °C	15 s	40
60 °C	1 min	

6.2.21. Transcriptome analysis

To analyse the transcriptional changes in samples, whole transcriptome analysis was performed. For this, primary naïve murine CD4+ T cells were stimulated for 6 h with 5 µg/mL α-CD3 (plate-bound) and 1 µg/mL α-CD28 (soluble). Cells were washed once with ice-cold PBS (450 *g*, 6 min, 4 °C), and RNA was isolated from the samples using the RNeasy Micro kit. In brief, cells were resuspended in 350 µL RLT buffer (+1 % (v/v) β-mercaptoethanol) and homogenised. Next, 350 µL 70 % ethanol were added and the suspension was mixed briefly by pipetting. Immediately afterwards, the sample was transferred into a RNeasy MinElute spin column, placed in a 2 mL collection tube, and centrifuged for 15 s at 8,000 *g* and rt. The flow-through was discarded, and DNase I incubation mix was added to the spin column filter membrane. Samples were incubated for 15 min at rt. After the DNA digestion, the filter tube was washed with 350 µL Buffer RW1 for 15 s at 8,000 *g* and rt. The filter column was then inserted into a fresh 2 mL collection tube, 500 µL Buffer RPE were applied to the membrane, and the tube was centrifuged for 15 s at 8,000 *g* and rt. After discarding the flow-through, 500 µL 80 % ethanol were added to the spin column, and the sample was centrifuged for 2 min at 8,000 *g* and rt. Next, the spin filter column was placed into a new collection tube, and the filter was spun dry for 5 min at 15,000 *g* and rt. Last, the spin column was placed into a 1.5 mL reaction tube, 14 µL RNase-free ddH_2O were applied onto the filter, and the sample was centrifuged for 1 min at 15,000 *g* and rt to collect the RNA in the new reaction tube.

After measuring the RNA concentration at the NanoDrop 1000 Spectrophotometer (ThermoFisher Scientific), whole transcriptome analysis was performed in collaboration with Dr. Timur Yorgan (Institute for Osteology and Biomechanics, University Medical Centre Hamburg-Eppendorf). For this, Clariom D mouse microarrays (ThermoFisher Scientific) were used according to the manufacturer's GeneChip WT PLUS reagent kit manual. Per sample, 100 ng of RNA were amplified and labelled. For the array, 5 µg of fragmented, labelled cDNA were used per sample. The Fluidics Station 450 was used for washing and staining. A GeneChip Scanner 3000 7G (ThermoFisher Scientific) was used for scanning of the microarrays. For analysis, the Transcriptome Analysis Console Software TAC 4.0 was used with default analysis settings (version2) and Gene+Exon-SST-RMA for summarisation. Additionally, pathway analysis based on the WikiPathways database was performed in TAC 4.0.

6.2.22. Malachite Green Assay

For quantification of polyphosphate (polyP) and phosphate levels, the Malachite Green Assay was used. In this photometry-based method, malachite green forms complexes with free

orthophosphate, which can be used to determine phosphate levels in relation to a provided phosphate standard.

Prior to the Malachite Green Assay, polyP was extracted according to the protocol by Christ and Blank (461). For this, cells were harvested and washed twice with 50 mM Tris buffer for 5 min at 500 *g* and 4 °C. Afterwards, the pellet was resuspended in 40 µL ME buffer and 30 µL phenol-saturated TE buffer. The samples were thoroughly mixed, lysed for 10 min at 45 °C, followed by 2 min of incubation at 4 °C. 100 µL chloroform were added and, after 20 s of vortexing, 100 µL TE buffer. After centrifugation at 12,000 *g* and 4 °C for 5 min, the aqueous phase containing polyP and free phosphate was retrieved and analysed with the Phosphate Assay Kit (Abcam) according to the manufacturer's instructions.

For the assay, every sample was split in half. One half was lysed for 10 min at 95 °C by adding 4 M HCl to a working concentration of 1 M. After the lysis, an equal volume of 4 M NaOH was added. Both the unlysed and the lysed part of every sample were diluted with ddH_2O to a volume of 400 µL. 200 µL in duplicates were added to the wells of a 96 well plate. Phosphate standard supplied by the kit was added in duplicates (standard range: 0-25 µM phosphate). To start the reaction, 30 µL of the Malachite Green Assay reagent were added to each well. After incubation for 30 min in the dark at rt, absorption at 650 nm was measured at the Spark 10M Luminescence multi-mode microplate reader (Tecan). Linear regression analysis was used to determine the unknown phosphate concentrations in the unlysed samples. The difference of free phosphate between lysed and unlysed samples corresponds to the polyP concentration of each sample.

6.2.23. Urea PAGE

PolyP can be visualised on a urea gel by negative DAPI staining: upon UV light exposure, DAPI disintegrates in the vicinity of polyP, but not in the vicinity of protein, DNA or RNA that were present in the samples. This leads to a black smear visible in the gel where polyP is present.

Prior to the urea page, polyP was extracted according to the protocol by Smith and Morrissey (462). For this, cells were harvested and washed twice with 50 mM Tris buffer for 5 min at 500 *g* and 4 °C. Afterwards, the pellet was resuspended in SDS lysis buffer and incubated for 10 min at rt. The QIAprep Spin Miniprep kit (Qiagen) was used for DNA extraction according to the manufacturer's instructions. In brief, the lysed cells were treated with N3, and by centrifugation for 10 min at 13,000 *g* and rt, debris and SDS were removed. The supernatant was transferred onto a QIAprep2.0 spin column and centrifuged. The polyP containing flow-

through was mixed 1:1 with phenol-chloroform isoamylalcohol and after centrifugation for 5 min at 10,000 *g* and rt, the aquaeous phase was collected. The organic phase was washed once with 20 mM Tris, while the thereby generated aquaeous phase was united with the initially recovered aquaeous phase. After another phenol-chloroform isoamylalcohol extraction and washing step, the polyP containing fraction was mixed 1:1 with chloroform. PolyP was precipitated with 20 mM ammonium sulphate, 0.3 M sodium acetate and 100 % cold ethanol. Pellets were air dried overnight and subsequently used for urea PAGE analysis.

For urea PAGE, 7.5 % 8 M urea PAGE gels were cast using the composition shown in Table 21. Initially, all ingredients were mixed, except for APS and TEMED, which are applied to start the radical chain polymerisation reaction leading to the polymerisation of acrylamide.

Table 21: 7.5 % 8 M Urea gel recipe used for urea PAGE.

Component	Amount
Urea	9.45 g
10x TBE	2.25 mL
Acrylamide/Bisacrylamide 30 % (29:1)	6.0 mL
ddH_2O	6.5 mL
TEMED	9 µL
10 % APS	225 µL

PolyP pellets were resuspended in 50 mM Tris and mixed with 2x TBE urea sample buffer. The chamber was prepared and the urea gel was pre-run in 1x TBE for 30 min at 100 V in order to remove undissolved urea. Before loading the samples, the pockets of the gel were washed with 1x TBE. Once samples were loaded, the gel was run with 120 V for size-dependent separation of the polyP molecules. Afterwards, the gel was stained in 2.5 µg/mL DAPI for 30 min and washed with negative DAPI solution for 1 h. For imaging after photobleaching, the ChemiDoc MP Imaging System (Bio-Rad Laboratories) was used.

6.2.24. Statistical analysis

Statistical analysis was performed using GraphPad Prism 9.5.

First, data sets were checked for normal distribution with the Shapiro-Wilk test. If the Shapiro-Wilk test indicated normal distribution, parametric tests were used. Else, nonparametric tests were used.

When comparing means of two unpaired, normally distributed datasets, a F test to compare variances between the data sets was conducted. If the variances differed significantly, a Welch's t test was conducted. If they did not differ significantly, an unpaired t test was conducted instead. As the corresponding nonparametric test, the Mann-Whitney test was used.

When comparing means of two paired, normally distributed data sets, either a paired t test or a ratio paired t test was conducted. In order to choose between these two, the ratio between paired values as well as the difference between paired values was calculated. If the ratios were consistent, a ratio paired t test was conducted. If the differences were consistent, a paired t test was conducted instead. As the corresponding nonparametric test, the Wilcoxon matched-pairs signed rank test was used.

If data was normalised to a control group before statistical analysis, all other groups were compared with a theoretical mean of 1 using either the One sample t test or the Wilcoxon Signed Rank test, for normally distributed or not normally distributed data, respectively.

When comparing means between more than two unpaired, normally distributed datasets, a Brown-Forsythe test to compare variances was performed. If the variances differed significantly, a Welch's analysis of variance test (ANOVA) was performed. If they did not differ significantly, an ordinary one-way ANOVA was performed. As the nonparametric alternative test to the one-way ANOVA, the Kruskal-Wallis test was performed.

If ANOVA results indicated a significant difference between datasets, a follow-up test with multiple comparisons was performed. For this, either the Tukey's, the Dunnett's T3 or the Dunn's multiple comparisons tests was used to follow up on the ordinary one-way ANOVA, the Welch's ANOVA or the Kruskal-Wallis test, respectively.

In order to analyse grouped data, statistical analysis was done using an ordinary two-way ANOVA. For follow-up analysis, Šidák's multiple comparisons test was used.

Significance was defined as $p \leq 0.05$. Data is summarised in the text as mean ± standard error of the mean (SEM). Number of independent biological samples is presented as N.

7. References

1. Han, L., Wu, T., Zhang, Q., Qi, A., and Zhou, X. (2025) Immune Tolerance Regulation Is Critical to Immune Homeostasis. *Journal of immunology research* **2025**, 5006201 10.1155/jimr/5006201 PMID 39950084

2. Wang, R., Lan, C., Benlagha, K., Camara, N. O. S., Miller, H., Kubo, M., Heegaard, S., Lee, P., Yang, L., Forsman, H., Li, X., Zhai, Z., and Liu, C. (2024) The interaction of innate immune and adaptive immune system. *MedComm* **5**, e714 10.1002/mco2.714 PMID 39286776
3. Li, D., and Wu, M. (2021) Pattern recognition receptors in health and diseases. *Signal transduction and targeted therapy* **6**, 291 10.1038/s41392-021-00687-0 PMID 34344870
4. Takeuchi, O., and Akira, S. (2010) Pattern recognition receptors and inflammation. *Cell* **140**, 805–820 10.1016/j.cell.2010.01.022 PMID 20303872
5. Carter, R. H. (2006) B cells in health and disease. *Mayo Clinic proceedings* **81**, 377–384 10.4065/81.3.377 PMID 16529141
6. Inoue, T., and Kurosaki, T. (2024) Memory B cells. *Nature reviews. Immunology* **24**, 5–17 10.1038/s41577-023-00897-3 PMID 37400644
7. Sun, L., Su, Y., Jiao, A., Wang, X., and Zhang, B. (2023) T cells in health and disease. *Signal transduction and targeted therapy* **8**, 235 10.1038/s41392-023-01471-y PMID 37332039
8. Hu, Y., Hu, Q., Li, Y., Lu, L., Xiang, Z., Yin, Z., Kabelitz, D., and Wu, Y. (2023) γδ T cells: origin and fate, subsets, diseases and immunotherapy. *Signal transduction and targeted therapy* **8**, 434 10.1038/s41392-023-01653-8 PMID 37989744
9. Ashby, K. M., and Hogquist, K. A. (2024) A guide to thymic selection of T cells. *Nature reviews. Immunology* **24**, 103–117 10.1038/s41577-023-00911-8 PMID 37464188
10. Baldwin, I., and Robey, E. A. (2024) Adjusting to self in the thymus: CD4 versus CD8 lineage commitment and regulatory T cell development. *The Journal of experimental medicine* **221** 10.1084/jem.20230896 PMID 38980291
11. Mariuzza, R. A., Agnihotri, P., and Orban, J. (2020) The structural basis of T-cell receptor (TCR) activation: An enduring enigma. *The Journal of biological chemistry* **295**, 914–925 10.1074/jbc.REV119.009411 PMID 31848223
12. Jung, D., and Alt, F. W. (2004) Unraveling V(D)J recombination; insights into gene regulation. *Cell* **116**, 299–311 10.1016/s0092-8674(04)00039-x PMID 14744439
13. Wang, X., Jiao, A., Sun, L., Li, W., Yang, B., Su, Y., Ding, R., Zhang, C., Liu, H., Yang, X., Sun, C., and Zhang, B. (2022) Zinc finger protein Zfp335 controls early T-cell development and survival through β-selection-dependent and -independent mechanisms. *eLife* **11** 10.7554/eLife.75508 PMID 35113015
14. Boehmer, H. von, and Fehling, H. J. (1997) Structure and function of the pre-T cell receptor. *Annual review of immunology* **15**, 433–452 10.1146/annurev.immunol.15.1.433 PMID 9143695
15. Dudley, E. C., Petrie, H. T., Shah, L. M., Owen, M. J., and Hayday, A. C. (1994) T cell receptor beta chain gene rearrangement and selection during thymocyte development in adult mice. *Immunity* **1**, 83–93 10.1016/1074-7613(94)90102-3 PMID 7534200
16. Malissen, B., Ardouin, L., Lin, S. Y., Gillet, A., and Malissen, M. (1999) Function of the CD3 subunits of the pre-TCR and TCR complexes during T cell development. *Advances in immunology* **72**, 103–148 10.1016/s0065-2776(08)60018-8 PMID 10361573
17. Hoffman, E. S., Passoni, L., Crompton, T., Leu, T. M., Schatz, D. G., Koff, A., Owen, M. J., and Hayday, A. C. (1996) Productive T-cell receptor beta-chain gene rearrangement: coincident regulation of cell cycle and clonality during development in vivo. *Genes & development* **10**, 948–962 10.1101/gad.10.8.948 PMID 8608942
18. Wikström, I., Forssell, J., Penha-Goncalves, M. N., Bergqvist, I., and Holmberg, D. (2008) A role for E2-2 at the DN3 stage of early thymopoiesis. *Molecular immunology* **45**, 3302–3311 10.1016/j.molimm.2008.02.012 PMID 18384878
19. Aifantis, I., Buer, J., Boehmer, H. von, and Azogui, O. (1997) Essential role of the pre-T cell receptor in allelic exclusion of the T cell receptor beta locus. *Immunity* **7**, 601–607 10.1016/s1074-7613(00)80381-7 PMID 9390684
20. Kruisbeek, A. M., Haks, M. C., Carleton, M., Michie, A. M., Zúñiga-Pflücker, J. C., and Wiest, D. L. (2000) Branching out to gain control: how the pre-TCR is linked to multiple functions. *Immunology today* **21**, 637–644 10.1016/s0167-5699(00)01744-8 PMID 11114425

21. Azzam, H. S., DeJarnette, J. B., Huang, K., Emmons, R., Park, C. S., Sommers, C. L., El-Khoury, D., Shores, E. W., and Love, P. E. (2001) Fine tuning of TCR signaling by CD5. *Journal of immunology (Baltimore, Md. : 1950)* **166**, 5464–5472 10.4049/jimmunol.166.9.5464 PMID 11313384
22. Azzam, H. S., Grinberg, A., Lui, K., Shen, H., Shores, E. W., and Love, P. E. (1998) CD5 expression is developmentally regulated by T cell receptor (TCR) signals and TCR avidity. *The Journal of experimental medicine* **188**, 2301–2311 10.1084/jem.188.12.2301 PMID 9858516
23. Qin, Z., and Xu, T. (2025) Deciphering the deterministic role of TCR signaling in T cell fate determination. *Frontiers in immunology* **16**, 1562248 10.3389/fimmu.2025.1562248 PMID 40469304
24. Curtsinger, J. M., and Mescher, M. F. (2010) Inflammatory cytokines as a third signal for T cell activation. *Current opinion in immunology* **22**, 333–340 10.1016/j.coi.2010.02.013 PMID 20363604
25. Bottino, C., Castriconi, R., Pende, D., Rivera, P., Nanni, M., Carnemolla, B., Cantoni, C., Grassi, J., Marcenaro, S., Reymond, N., Vitale, M., Moretta, L., Lopez, M., and Moretta, A. (2003) Identification of PVR (CD155) and Nectin-2 (CD112) as cell surface ligands for the human DNAM-1 (CD226) activating molecule. *The Journal of experimental medicine* **198**, 557–567 10.1084/jem.20030788 PMID 12913096
26. Harjunpää, H., and Guillerey, C. (2020) TIGIT as an emerging immune checkpoint. *Clinical and experimental immunology* **200**, 108–119 10.1111/cei.13407 PMID 31828774
27. Krummey, S. M., and Ford, M. L. (2014) Braking bad: novel mechanisms of CTLA-4 inhibition of T cell responses. *American journal of transplantation : official journal of the American Society of Transplantation and the American Society of Transplant Surgeons* **14**, 2685–2690 10.1111/ajt.12938 PMID 25387592
28. Rowshanravan, B., Halliday, N., and Sansom, D. M. (2018) CTLA-4: a moving target in immunotherapy. *Blood* **131**, 58–67 10.1182/blood-2017-06-741033 PMID 29118008
29. van der Merwe, P. A., Bodian, D. L., Daenke, S., Linsley, P., and Davis, S. J. (1997) CD80 (B7-1) binds both CD28 and CTLA-4 with a low affinity and very fast kinetics. *The Journal of experimental medicine* **185**, 393–403 10.1084/jem.185.3.393 PMID 9053440
30. Hui, E., Cheung, J., Zhu, J., Su, X., Taylor, M. J., Wallweber, H. A., Sasmal, D. K., Huang, J., Kim, J. M., Mellman, I., and Vale, R. D. (2017) T cell costimulatory receptor CD28 is a primary target for PD-1-mediated inhibition. *Science (New York, N.Y.)* **355**, 1428–1433 10.1126/science.aaf1292 PMID 28280247
31. Sharma, P., Goswami, S., Raychaudhuri, D., Siddiqui, B. A., Singh, P., Nagarajan, A., Liu, J., Subudhi, S. K., Poon, C., Gant, K. L., Herbrich, S. M., Anandhan, S., Islam, S., Amit, M., Anandappa, G., and Allison, J. P. (2023) Immune checkpoint therapy-current perspectives and future directions. *Cell* **186**, 1652–1669 10.1016/j.cell.2023.03.006 PMID 37059068
32. Luckheeram, R. V., Zhou, R., Verma, A. D., and Xia, B. (2012) $CD4^+$T cells: differentiation and functions. *Clinical & developmental immunology* **2012**, 925135 10.1155/2012/925135 PMID 22474485
33. Jiang, Q., Yang, G., Xiao, F., Xie, J., Wang, S., Lu, L., and Cui, D. (2021) Role of Th22 Cells in the Pathogenesis of Autoimmune Diseases. *Frontiers in immunology* **12**, 688066 10.3389/fimmu.2021.688066 PMID 34295334
34. Hayden, M. S., and Ghosh, S. (2014) Regulation of NF-κB by TNF family cytokines. *Seminars in Immunology* **26**, 253–266 10.1016/j.smim.2014.05.004
35. Lee, J., Lozano-Ruiz, B., Yang, F. M., Fan, D. D., Shen, L., and González-Navajas, J. M. (2021) The Multifaceted Role of Th1, Th9, and Th17 Cells in Immune Checkpoint Inhibition Therapy. *Frontiers in immunology* **12**, 625667 10.3389/fimmu.2021.625667 PMID 33777008
36. Wan, Y. Y., and Flavell, R. A. (2009) How diverse--CD4 effector T cells and their functions. *Journal of molecular cell biology* **1**, 20–36 10.1093/jmcb/mjp001 PMID 19482777
37. Davidson, N. J., Leach, M. W., Fort, M. M., Thompson-Snipes, L., Kühn, R., Müller, W., Berg, D. J., and Rennick, D. M. (1996) T helper cell 1-type CD4+ T cells, but not B cells, mediate colitis in

interleukin 10-deficient mice. *The Journal of experimental medicine* **184**, 241–251 10.1084/jem.184.1.241 PMID 8691138
38. Hu, H. Z., Li, G. L., Lim, Y. K., Chan, S. H., and Yap, E. H. (1999) Kinetics of interferon-gamma secretion and its regulatory factors in the early phase of acute graft-versus-host disease. *Immunology* **98**, 379–385 10.1046/j.1365-2567.1999.00881.x PMID 10583597
39. Leung, B. P., McInnes, I. B., Esfandiari, E., Wei, X. Q., and Liew, F. Y. (2000) Combined effects of IL-12 and IL-18 on the induction of collagen-induced arthritis. *Journal of immunology (Baltimore, Md. : 1950)* **164**, 6495–6502 10.4049/jimmunol.164.12.6495 PMID 10843707
40. Pakala, S. V., Chivetta, M., Kelly, C. B., and Katz, J. D. (1999) In autoimmune diabetes the transition from benign to pernicious insulitis requires an islet cell response to tumor necrosis factor alpha. *The Journal of experimental medicine* **189**, 1053–1062 10.1084/jem.189.7.1053 PMID 10190896
41. Parronchi, P., Romagnani, P., Annunziato, F., Sampognaro, S., Becchio, A., Giannarini, L., Maggi, E., Pupilli, C., Tonelli, F., and Romagnani, S. (1997) Type 1 T-helper cell predominance and interleukin-12 expression in the gut of patients with Crohn's disease. *The American journal of pathology* **150**, 823–832 PMID 9060820
42. Wang, B., André, I., Gonzalez, A., Katz, J. D., Aguet, M., Benoist, C., and Mathis, D. (1997) Interferon-gamma impacts at multiple points during the progression of autoimmune diabetes. *Proceedings of the National Academy of Sciences of the United States of America* **94**, 13844–13849 10.1073/pnas.94.25.13844 PMID 9391115
43. Kokubo, K., Onodera, A., Kiuchi, M., Tsuji, K., Hirahara, K., and Nakayama, T. (2022) Conventional and pathogenic Th2 cells in inflammation, tissue repair, and fibrosis. *Frontiers in immunology* **13**, 945063 10.3389/fimmu.2022.945063 PMID 36016937
44. Singh, A. K., Khare, P., Obaid, A., Conlon, K. P., Basrur, V., DePinho, R. A., and Venuprasad, K. (2018) SUMOylation of ROR-γt inhibits IL-17 expression and inflammation via HDAC2. *Nature communications* **9**, 4515 10.1038/s41467-018-06924-5 PMID 30375383
45. Kumar, R., Theiss, A. L., and Venuprasad, K. (2021) RORγt protein modifications and IL-17-mediated inflammation. *Trends in immunology* **42**, 1037–1050 10.1016/j.it.2021.09.005 PMID 34635393
46. Ivanov, I. I., McKenzie, B. S., Zhou, L., Tadokoro, C. E., Lepelley, A., Lafaille, J. J., Cua, D. J., and Littman, D. R. (2006) The orphan nuclear receptor RORgammat directs the differentiation program of proinflammatory IL-17+ T helper cells. *Cell* **126**, 1121–1133 10.1016/j.cell.2006.07.035 PMID 16990136
47. McGeachy, M. J., Bak-Jensen, K. S., Chen, Y., Tato, C. M., Blumenschein, W., McClanahan, T., and Cua, D. J. (2007) TGF-beta and IL-6 drive the production of IL-17 and IL-10 by T cells and restrain T(H)-17 cell-mediated pathology. *Nature immunology* **8**, 1390–1397 10.1038/ni1539 PMID 17994024
48. Ghoreschi, K., Laurence, A., Yang, X.-P., Tato, C. M., McGeachy, M. J., Konkel, J. E., Ramos, H. L., Wei, L., Davidson, T. S., Bouladoux, N., Grainger, J. R., Chen, Q., Kanno, Y., Watford, W. T., Sun, H.-W., Eberl, G., Shevach, E. M., Belkaid, Y., Cua, D. J., Chen, W., and O'Shea, J. J. (2010) Generation of pathogenic T(H)17 cells in the absence of TGF-β signalling. *Nature* **467**, 967–971 10.1038/nature09447 PMID 20962846
49. Peters, A., Lee, Y., and Kuchroo, V. K. (2011) The many faces of Th17 cells. *Current opinion in immunology* **23**, 702–706 10.1016/j.coi.2011.08.007 PMID 21899997
50. Akdis, M., Palomares, O., van de Veen, W., van Splunter, M., and Akdis, C. A. (2012) TH17 and TH22 cells: a confusion of antimicrobial response with tissue inflammation versus protection. *The Journal of allergy and clinical immunology* **129**, 1438-49; quiz1450-1 10.1016/j.jaci.2012.05.003 PMID 22657405
51. Mufazalov, I. A., Schelmbauer, C., Regen, T., Kuschmann, J., Wanke, F., Gabriel, L. A., Hauptmann, J., Müller, W., Pinteaux, E., Kurschus, F. C., and Waisman, A. (2017) IL-1 signaling is critical for expansion but not generation of autoreactive GM-CSF+ Th17 cells. *The EMBO journal* **36**, 102–115 10.15252/embj.201694615 PMID 27827809

52. Yen, D., Cheung, J., Scheerens, H., Poulet, F., McClanahan, T., McKenzie, B., Kleinschek, M. A., Owyang, A., Mattson, J., Blumenschein, W., Murphy, E., Sathe, M., Cua, D. J., Kastelein, R. A., and Rennick, D. (2006) IL-23 is essential for T cell-mediated colitis and promotes inflammation via IL-17 and IL-6. *The Journal of clinical investigation* **116**, 1310–1316 10.1172/JCI21404 PMID 16670770
53. Langrish, C. L., Chen, Y., Blumenschein, W. M., Mattson, J., Basham, B., Sedgwick, J. D., McClanahan, T., Kastelein, R. A., and Cua, D. J. (2005) IL-23 drives a pathogenic T cell population that induces autoimmune inflammation. *The Journal of experimental medicine* **201**, 233–240 10.1084/jem.20041257 PMID 15657292
54. Alabbas, S. Y., Begun, J., Florin, T. H., and Oancea, I. (2018) The role of IL-22 in the resolution of sterile and nonsterile inflammation. *Clinical & translational immunology* **7**, e1017 10.1002/cti2.1017 PMID 29713472
55. Qing, C., and Ghorani, E. (2023) Two faces: IL-22 effects prevail over defense against metastasis. *Immunity* **56**, 6–8 10.1016/j.immuni.2022.12.013 PMID 36630918
56. Keir, M., Yi, T., Lu, T., and Ghilardi, N. (2020) The role of IL-22 in intestinal health and disease. *The Journal of experimental medicine* **217**, e20192195 10.1084/jem.20192195 PMID 32997932
57. Dean, L. S., Threatt, A. N., Jones, K., Oyewole, E. O., Pauly, M., Wahl, M., Barahona, M., Reiter, R. W., and Nordgren, T. M. (2024) I don't know about you, but I'm feeling IL-22. *Cytokine & growth factor reviews* **80**, 1–11 10.1016/j.cytogfr.2024.11.001 PMID 39537498
58. Plank, M. W., Kaiko, G. E., Maltby, S., Weaver, J., Tay, H. L., Shen, W., Wilson, M. S., Durum, S. K., and Foster, P. S. (2017) Th22 Cells Form a Distinct Th Lineage from Th17 Cells In Vitro with Unique Transcriptional Properties and Tbet-Dependent Th1 Plasticity. *Journal of immunology (Baltimore, Md. : 1950)* **198**, 2182–2190 10.4049/jimmunol.1601480 PMID 28100680
59. Zheng, Y., Danilenko, D. M., Valdez, P., Kasman, I., Eastham-Anderson, J., Wu, J., and Ouyang, W. (2007) Interleukin-22, a T(H)17 cytokine, mediates IL-23-induced dermal inflammation and acanthosis. *Nature* **445**, 648–651 10.1038/nature05505 PMID 17187052
60. Cineus, R., Luo, Y., Saliutina, M., Manna, S., Cancino, C. A., Velasco Blázquez, L., Wang, L., Bösel, D., Abdelrahman, A., Klementowicz, J. E., Scherl, A., Hainbuch, S., Bréart, B., Kwon, G., Konopka, A., Guerra, G. M., Coburg, E. von, Gerbeth, L., Roels, J., Heinrich, F., Müller, N., Durek, P., Deigendesch, N., Ziai, J., Hung, J., Conrad, T., Kühl, A. A., Wirtz, S., Löhning, M., Keir, M., Diefenbach, A., Mashreghi, M.-F., Siegmund, B., Schumann, M., Romagnani, C., West, N. R., and Hegazy, A. N. (2025) The IL-22-oncostatin M axis promotes intestinal inflammation and tumorigenesis. *Nature immunology* **26**, 837–853 10.1038/s41590-025-02149-z PMID 40447860
61. Briukhovetska, D., Suarez-Gosalvez, J., Voigt, C., Markota, A., Giannou, A. D., Schübel, M., Jobst, J., Zhang, T., Dörr, J., Märkl, F., Majed, L., Müller, P. J., May, P., Gottschlich, A., Tokarew, N., Lücke, J., Oner, A., Schwerdtfeger, M., Andreu-Sanz, D., Grünmeier, R., Seifert, M., Michaelides, S., Hristov, M., König, L. M., Cadilha, B. L., Mikhaylov, O., Anders, H.-J., Rothenfusser, S., Flavell, R. A., Cerezo-Wallis, D., Tejedo, C., Soengas, M. S., Bald, T., Huber, S., Endres, S., and Kobold, S. (2023) T cell-derived interleukin-22 drives the expression of CD155 by cancer cells to suppress NK cell function and promote metastasis. *Immunity* **56**, 143-161.e11 10.1016/j.immuni.2022.12.010 PMID 36630913
62. Chen, W., Jin, W., Hardegen, N., Lei, K.-J., Li, L., Marinos, N., McGrady, G., and Wahl, S. M. (2003) Conversion of peripheral CD4+CD25- naive T cells to CD4+CD25+ regulatory T cells by TGF-beta induction of transcription factor Foxp3. *The Journal of experimental medicine* **198**, 1875–1886 10.1084/jem.20030152 PMID 14676299
63. Yagi, H., Nomura, T., Nakamura, K., Yamazaki, S., Kitawaki, T., Hori, S., Maeda, M., Onodera, M., Uchiyama, T., Fujii, S., and Sakaguchi, S. (2004) Crucial role of FOXP3 in the development and function of human CD25+CD4+ regulatory T cells. *International immunology* **16**, 1643–1656 10.1093/intimm/dxh165 PMID 15466453
64. Yoshimura, A., and Muto, G. (2011) TGF-β function in immune suppression. *Current topics in microbiology and immunology* **350**, 127–147 10.1007/82_2010_87 PMID 20680806

65. Fontenot, J. D., Gavin, M. A., and Rudensky, A. Y. (2003) Foxp3 programs the development and function of CD4+CD25+ regulatory T cells. *Nature immunology* **4**, 330–336 10.1038/ni904 PMID 12612578
66. Hori, S. (2021) FOXP3 as a master regulator of Treg cells. *Nature reviews. Immunology* **21**, 618–619 10.1038/s41577-021-00598-9 PMID 34580451
67. Plitas, G., and Rudensky, A. Y. (2016) Regulatory T Cells: Differentiation and Function. *Cancer immunology research* **4**, 721–725 10.1158/2326-6066.cir-16-0193 PMID 27590281
68. Vignali, D. A. A., Collison, L. W., and Workman, C. J. (2008) How regulatory T cells work. *Nature reviews. Immunology* **8**, 523–532 10.1038/nri2343 PMID 18566595
69. Liao, W., Lin, J.-X., and Leonard, W. J. (2013) Interleukin-2 at the crossroads of effector responses, tolerance, and immunotherapy. *Immunity* **38**, 13–25 10.1016/j.immuni.2013.01.004 PMID 23352221
70. Malek, T. R. (2008) The biology of interleukin-2. *Annual review of immunology* **26**, 453–479 10.1146/annurev.immunol.26.021607.090357 PMID 18062768
71. Malek, T. R., and Castro, I. (2010) Interleukin-2 receptor signaling: at the interface between tolerance and immunity. *Immunity* **33**, 153–165 10.1016/j.immuni.2010.08.004 PMID 20732639
72. Wuest, S. C., Edwan, J. H., Martin, J. F., Han, S., Perry, J. S. A., Cartagena, C. M., Matsuura, E., Maric, D., Waldmann, T. A., and Bielekova, B. (2011) A role for interleukin-2 trans-presentation in dendritic cell-mediated T cell activation in humans, as revealed by daclizumab therapy. *Nature medicine* **17**, 604–609 10.1038/nm.2365 PMID 21532597
73. Liao, W., Lin, J.-X., and Leonard, W. J. (2011) IL-2 family cytokines: new insights into the complex roles of IL-2 as a broad regulator of T helper cell differentiation. *Current opinion in immunology* **23**, 598–604 10.1016/j.coi.2011.08.003 PMID 21889323
74. Lin, J. X., and Leonard, W. J. (2000) The role of Stat5a and Stat5b in signaling by IL-2 family cytokines. *Oncogene* **19**, 2566–2576 10.1038/sj.onc.1203523 PMID 10851055
75. Shah, K., Al-Haidari, A., Sun, J., and Kazi, J. U. (2021) T cell receptor (TCR) signaling in health and disease. *Signal transduction and targeted therapy* **6**, 412 10.1038/s41392-021-00823-w PMID 34897277
76. Wilkinson, B., Wang, H., and Rudd, C. E. (2004) Positive and negative adaptors in T-cell signalling. *Immunology* **111**, 368–374 10.1111/j.0019-2805.2004.01832.x PMID 15056371
77. Alcover, A., and Alarcón, B. (2000) Internalization and intracellular fate of TCR-CD3 complexes. *Critical reviews in immunology* **20**, 325–346 PMID 11100805
78. Chao, Z., Mei, Q., Yang, C., Luo, J., Liu, P., Peng, H., Guo, X., Yin, Z., Le Li, and Wang, Z. (2025) Immunological synapse: structures, molecular mechanisms and therapeutic implications in disease. *Signal transduction and targeted therapy* **10**, 254 10.1038/s41392-025-02332-6 PMID 40784895
79. Freiberg, B. A., Kupfer, H., Maslanik, W., Delli, J., Kappler, J., Zaller, D. M., and Kupfer, A. (2002) Staging and resetting T cell activation in SMACs. *Nature immunology* **3**, 911–917 10.1038/ni836 PMID 12244310
80. Monks, C. R., Freiberg, B. A., Kupfer, H., Sciaky, N., and Kupfer, A. (1998) Three-dimensional segregation of supramolecular activation clusters in T cells. *Nature* **395**, 82–86 10.1038/25764 PMID 9738502
81. Kvalvaag, A., Valvo, S., Céspedes, P. F., Saliba, D. G., Kurz, E., Korobchevskaya, K., and Dustin, M. L. (2023) Clathrin mediates both internalization and vesicular release of triggered T cell receptor at the immunological synapse. *Proceedings of the National Academy of Sciences of the United States of America* **120**, e2211368120 10.1073/pnas.2211368120 PMID 36730202
82. Xie, J., Tato, C. M., and Davis, M. M. (2013) How the immune system talks to itself: the varied role of synapses. *Immunological reviews* **251**, 65–79 10.1111/imr.12017 PMID 23278741
83. Martínez-Martín, N., Fernández-Arenas, E., Cemerski, S., Delgado, P., Turner, M., Heuser, J., Irvine, D. J., Huang, B., Bustelo, X. R., Shaw, A., and Alarcón, B. (2011) T cell receptor internalization from the immunological synapse is mediated by TC21 and RhoG GTPase-dependent phagocytosis. *Immunity* **35**, 208–222 10.1016/j.immuni.2011.06.003 PMID 21820331

84. Cemerski, S., Das, J., Giurisato, E., Markiewicz, M. A., Allen, P. M., Chakraborty, A. K., and Shaw, A. S. (2008) The balance between T cell receptor signaling and degradation at the center of the immunological synapse is determined by antigen quality. *Immunity* **29**, 414–422 10.1016/j.immuni.2008.06.014 PMID 18760640
85. Dietrich, J., Hou, X., Wegener, A. M., and Geisler, C. (1994) CD3 gamma contains a phosphoserine-dependent di-leucine motif involved in down-regulation of the T cell receptor. *The EMBO journal* **13**, 2156–2166 10.1002/j.1460-2075.1994.tb06492.x PMID 8187769
86. Monjas, A., Alcover, A., and Alarcón, B. (2004) Engaged and bystander T cell receptors are down-modulated by different endocytotic pathways. *The Journal of biological chemistry* **279**, 55376–55384 10.1074/jbc.M409342200 PMID 15516342
87. Evnouchidou, I., Caillens, V., Koumantou, D., and Saveanu, L. (2022) The role of endocytic trafficking in antigen T cell receptor activation. *Biomedical journal* **45**, 310–320 10.1016/j.bj.2021.09.004 PMID 34592497
88. Kuhns, M. S., and Davis, M. M. (2008) The safety on the TCR trigger. *Cell* **135**, 594–596 10.1016/j.cell.2008.10.033 PMID 19013269
89. Xu, X., Li, H., and Xu, C. (2020) Structural understanding of T cell receptor triggering. *Cellular & molecular immunology* **17**, 193–202 10.1038/s41423-020-0367-1 PMID 32047259
90. Wang, H., Kadlecek, T. A., Au-Yeung, B. B., Goodfellow, H. E. S., Hsu, L.-Y., Freedman, T. S., and Weiss, A. (2010) ZAP-70: an essential kinase in T-cell signaling. *Cold Spring Harbor perspectives in biology* **2**, a002279 10.1101/cshperspect.a002279 PMID 20452964
91. June, C. H., Fletcher, M. C., Ledbetter, J. A., and Samelson, L. E. (1990) Increases in tyrosine phosphorylation are detectable before phospholipase C activation after T cell receptor stimulation. *Journal of immunology (Baltimore, Md. : 1950)* **144**, 1591–1599 PMID 1689750
92. Williams, B. L., Irvin, B. J., Sutor, S. L., Chini, C. C., Yacyshyn, E., Bubeck Wardenburg, J., Dalton, M., Chan, A. C., and Abraham, R. T. (1999) Phosphorylation of Tyr319 in ZAP-70 is required for T-cell antigen receptor-dependent phospholipase C-gamma1 and Ras activation. *The EMBO journal* **18**, 1832–1844 10.1093/emboj/18.7.1832 PMID 10202147
93. Williams, B. L., Schreiber, K. L., Zhang, W., Wange, R. L., Samelson, L. E., Leibson, P. J., and Abraham, R. T. (1998) Genetic evidence for differential coupling of Syk family kinases to the T-cell receptor: reconstitution studies in a ZAP-70-deficient Jurkat T-cell line. *Molecular and cellular biology* **18**, 1388–1399 10.1128/mcb.18.3.1388 PMID 9488454
94. Zhang, W., Trible, R. P., Zhu, M., Liu, S. K., McGlade, C. J., and Samelson, L. E. (2000) Association of Grb2, Gads, and phospholipase C-gamma 1 with phosphorylated LAT tyrosine residues. Effect of LAT tyrosine mutations on T cell angigen receptor-mediated signaling. *The Journal of biological chemistry* **275**, 23355–23361 10.1074/jbc.m000404200 PMID 10811803
95. Simon, J. A., and Schreiber, S. L. (1995) Grb2 SH3 binding to peptides from Sos: evaluation of a general model for SH3-ligand interactions. *Chemistry & biology* **2**, 53–60 10.1016/1074-5521(95)90080-2 PMID 9383403
96. Kazemein Jasemi, N. S., and Ahmadian, M. R. (2022) Allosteric regulation of GRB2 modulates RAS activation. *Small GTPases* **13**, 282–286 10.1080/21541248.2022.2089001 PMID 35703160
97. Egan, S. E., Giddings, B. W., Brooks, M. W., Buday, L., Sizeland, A. M., and Weinberg, R. A. (1993) Association of Sos Ras exchange protein with Grb2 is implicated in tyrosine kinase signal transduction and transformation. *Nature* **363**, 45–51 10.1038/363045a0 PMID 8479536
98. Naramura, M., Jang, I.-K., Kole, H., Huang, F., Haines, D., and Gu, H. (2002) c-Cbl and Cbl-b regulate T cell responsiveness by promoting ligand-induced TCR down-modulation. *Nature immunology* **3**, 1192–1199 10.1038/ni855 PMID 12415267
99. Liu, S. K., Fang, N., Koretzky, G. A., and McGlade, C. J. (1999) The hematopoietic-specific adaptor protein gads functions in T-cell signaling via interactions with the SLP-76 and LAT adaptors. *Current biology : CB* **9**, 67–75 10.1016/s0960-9822(99)80017-7 PMID 10021361
100. Yoder, J., Pham, C., Iizuka, Y. M., Kanagawa, O., Liu, S. K., McGlade, J., and Cheng, A. M. (2001) Requirement for the SLP-76 adaptor GADS in T cell development. *Science (New York, N.Y.)* **291**, 1987–1991 10.1126/science.1057176 PMID 11239162

101. Higgs, H. N., and Pollard, T. D. (1999) Regulation of actin polymerization by Arp2/3 complex and WASp/Scar proteins. *The Journal of biological chemistry* **274**, 32531–32534 10.1074/jbc.274.46.32531 PMID 10551802
102. Liu, J., Kang, H., Raab, M., Da Silva, A. J., Kraeft, S. K., and Rudd, C. E. (1998) FYB (FYN binding protein) serves as a binding partner for lymphoid protein and FYN kinase substrate SKAP55 and a SKAP55-related protein in T cells. *Proceedings of the National Academy of Sciences of the United States of America* **95**, 8779–8784 10.1073/pnas.95.15.8779 PMID 9671755
103. Mullins, R. D. (2000) How WASP-family proteins and the Arp2/3 complex convert intracellular signals into cytoskeletal structures. *Current opinion in cell biology* **12**, 91–96 10.1016/s0955-0674(99)00061-7 PMID 10679362
104. Rivero-Lezcano, O. M., Marcilla, A., Sameshima, J. H., and Robbins, K. C. (1995) Wiskott-Aldrich syndrome protein physically associates with Nck through Src homology 3 domains. *Molecular and cellular biology* **15**, 5725–5731 10.1128/mcb.15.10.5725 PMID 7565724
105. Wang, H., Moon, E.-Y., Azouz, A., Wu, X., Smith, A., Schneider, H., Hogg, N., and Rudd, C. E. (2003) SKAP-55 regulates integrin adhesion and formation of T cell-APC conjugates. *Nature immunology* **4**, 366–374 10.1038/ni913 PMID 12652296
106. Zeng, R., Cannon, J. L., Abraham, R. T., Way, M., Billadeau, D. D., Bubeck-Wardenberg, J., and Burkhardt, J. K. (2003) SLP-76 coordinates Nck-dependent Wiskott-Aldrich syndrome protein recruitment with Vav-1/Cdc42-dependent Wiskott-Aldrich syndrome protein activation at the T cell-APC contact site. *Journal of immunology (Baltimore, Md. : 1950)* **171**, 1360–1368 10.4049/jimmunol.171.3.1360 PMID 12874226
107. Granum, S., Sundvold-Gjerstad, V., Gopalakrishnan, R. P., Berge, T., Koll, L., Abrahamsen, G., Sørlie, M., and Spurkland, A. (2014) The kinase Itk and the adaptor TSAd change the specificity of the kinase Lck in T cells by promoting the phosphorylation of Tyr192. *Science signaling* **7**, ra118 10.1126/scisignal.2005384 PMID 25492967
108. Sela, M., Bogin, Y., Beach, D., Oellerich, T., Lehne, J., Smith-Garvin, J. E., Okumura, M., Starosvetsky, E., Kosoff, R., Libman, E., Koretzky, G., Kambayashi, T., Urlaub, H., Wienands, J., Chernoff, J., and Yablonski, D. (2011) Sequential phosphorylation of SLP-76 at tyrosine 173 is required for activation of T and mast cells. *The EMBO journal* **30**, 3160–3172 10.1038/emboj.2011.213 PMID 21725281
109. Devkota, S., Joseph, R. E., Min, L., Bruce Fulton, D., and Andreotti, A. H. (2015) Scaffold Protein SLP-76 Primes PLCγ1 for Activation by ITK-Mediated Phosphorylation. *Journal of molecular biology* **427**, 2734–2747 10.1016/j.jmb.2015.04.012 PMID 25916191
110. Nishibe, S., Wahl, M. I., Hernández-Sotomayor, S. M., Tonks, N. K., Rhee, S. G., and Carpenter, G. (1990) Increase of the catalytic activity of phospholipase C-gamma 1 by tyrosine phosphorylation. *Science (New York, N.Y.)* **250**, 1253–1256 10.1126/science.1700866 PMID 1700866
111. Zhong, X.-P., Guo, R., Zhou, H., Liu, C., and Wan, C.-K. (2008) Diacylglycerol kinases in immune cell function and self-tolerance. *Immunological reviews* **224**, 249–264 10.1111/j.1600-065x.2008.00647.x PMID 18759932
112. Imboden, J. B., and Stobo, J. D. (1985) Transmembrane signalling by the T cell antigen receptor. Perturbation of the T3-antigen receptor complex generates inositol phosphates and releases calcium ions from intracellular stores. *The Journal of experimental medicine* **161**, 446–456 10.1084/jem.161.3.446 PMID 3919143
113. Kania, E., Roest, G., Vervliet, T., Parys, J. B., and Bultynck, G. (2017) IP3 Receptor-Mediated Calcium Signaling and Its Role in Autophagy in Cancer. *Frontiers in oncology* **7**, 140 10.3389/fonc.2017.00140 PMID 28725634
114. Park, Y.-J., Yoo, S.-A., Kim, M., and Kim, W.-U. (2020) The Role of Calcium-Calcineurin-NFAT Signaling Pathway in Health and Autoimmune Diseases. *Frontiers in immunology* **11**, 195 10.3389/fimmu.2020.00195 PMID 32210952

115. Sun, Z. (2012) Intervention of PKC-θ as an immunosuppressive regimen. *Frontiers in immunology* **3**, 225 10.3389/fimmu.2012.00225 PMID 22876242
116. Szamel, M., and Resch, K. (1995) T-cell antigen receptor-induced signal-transduction pathways--activation and function of protein kinases C in T lymphocytes. *European journal of biochemistry* **228**, 1–15 10.1111/j.1432-1033.1995.tb20221.x PMID 7882988
117. Krappmann, D., Emmerich, F., Kordes, U., Scharschmidt, E., Dörken, B., and Scheidereit, C. (1999) Molecular mechanisms of constitutive NF-kappaB/Rel activation in Hodgkin/Reed-Sternberg cells. *Oncogene* **18**, 943–953 10.1038/sj.onc.1202351 PMID 10023670
118. Krishna, S., Xie, D., Gorentla, B., Shin, J., Gao, J., and Zhong, X.-P. (2012) Chronic activation of the kinase IKKβ impairs T cell function and survival. *Journal of immunology (Baltimore, Md. : 1950)* **189**, 1209–1219 10.4049/jimmunol.1102429 PMID 22753932
119. Staudt, L. M. (2010) Oncogenic activation of NF-kappaB. *Cold Spring Harbor perspectives in biology* **2**, a000109 10.1101/cshperspect.a000109 PMID 20516126
120. Daniels, M. A., and Teixeiro, E. (2025) The NF-κB signaling network in the life of T cells. *Frontiers in immunology* **16**, 1559494 10.3389/fimmu.2025.1559494 PMID 40370445
121. Ebinu, J. O., Bottorff, D. A., Chan, E. Y., Stang, S. L., Dunn, R. J., and Stone, J. C. (1998) RasGRP, a Ras guanyl nucleotide- releasing protein with calcium- and diacylglycerol-binding motifs. *Science (New York, N.Y.)* **280**, 1082–1086 10.1126/science.280.5366.1082 PMID 9582122
122. Gorentla, B. K., and Zhong, X.-P. (2012) T cell Receptor Signal Transduction in T lymphocytes. *J Clin Cell Immunol* **2012**, 5 10.4172/2155-9899.S12-005 PMID 23946894
123. Smith-Garvin, J. E., Koretzky, G. A., and Jordan, M. S. (2009) T cell activation. *Annual review of immunology* **27**, 591–619 10.1146/annurev.immunol.021908.132706 PMID 19132916
124. Kolch, W. (2005) Coordinating ERK/MAPK signalling through scaffolds and inhibitors. *Nature reviews. Molecular cell biology* **6**, 827–837 10.1038/nrm1743 PMID 16227978
125. Janknecht, R., Ernst, W. H., Pingoud, V., and Nordheim, A. (1993) Activation of ternary complex factor Elk-1 by MAP kinases. *The EMBO journal* **12**, 5097–5104 10.1002/j.1460-2075.1993.tb06204.x PMID 8262053
126. Macián, F., López-Rodríguez, C., and Rao, A. (2001) Partners in transcription: NFAT and AP-1. *Oncogene* **20**, 2476–2489 10.1038/sj.onc.1204386 PMID 11402342
127. Behrens, A., Sabapathy, K., Graef, I., Cleary, M., Crabtree, G. R., and Wagner, E. F. (2001) Jun N-terminal kinase 2 modulates thymocyte apoptosis and T cell activation through c-Jun and nuclear factor of activated T cell (NF-AT). *Proceedings of the National Academy of Sciences of the United States of America* **98**, 1769–1774 10.1073/pnas.98.4.1769 PMID 11172026
128. Kaminuma, O., Deckert, M., Elly, C., Liu, Y. C., and Altman, A. (2001) Vav-Rac1-mediated activation of the c-Jun N-terminal kinase/c-Jun/AP-1 pathway plays a major role in stimulation of the distal NFAT site in the interleukin-2 gene promoter. *Molecular and cellular biology* **21**, 3126–3136 10.1128/mcb.21.9.3126-3136.2001 PMID 11287617
129. Cianferoni, A., Massaad, M., Feske, S., La Fuente, M. A. de, Gallego, L., Ramesh, N., and Geha, R. S. (2005) Defective nuclear translocation of nuclear factor of activated T cells and extracellular signal-regulated kinase underlies deficient IL-2 gene expression in Wiskott-Aldrich syndrome. *The Journal of allergy and clinical immunology* **116**, 1364–1371 10.1016/j.jaci.2005.09.006 PMID 16337472
130. Macian, F. (2005) NFAT proteins: key regulators of T-cell development and function. *Nature reviews. Immunology* **5**, 472–484 10.1038/nri1632 PMID 15928679
131. Bertin, S., Lozano-Ruiz, B., Bachiller, V., García-Martínez, I., Herdman, S., Zapater, P., Francés, R., Such, J., Lee, J., Raz, E., and González-Navajas, J. M. (2015) Dual-specificity phosphatase 6 regulates CD4+ T-cell functions and restrains spontaneous colitis in IL-10-deficient mice. *Mucosal immunology* **8**, 505–515 10.1038/mi.2014.84 PMID 25227984
132. Damasio, M. P., Marchingo, J. M., Spinelli, L., Hukelmann, J. L., Cantrell, D. A., and Howden, A. J. M. (2021) Extracellular signal-regulated kinase (ERK) pathway control of CD8+ T cell differentiation. *The Biochemical journal* **478**, 79–98 10.1042/bcj20200661 PMID 33305809

133. Chung, J., Uchida, E., Grammer, T. C., and Blenis, J. (1997) STAT3 serine phosphorylation by ERK-dependent and -independent pathways negatively modulates its tyrosine phosphorylation. *Molecular and cellular biology* **17**, 6508–6516 10.1128/mcb.17.11.6508 PMID 9343414
134. Rohrs, J. A., Siegler, E. L., Wang, P., and Finley, S. D. (2020) ERK Activation in CAR T Cells Is Amplified by CD28-Mediated Increase in CD3ζ Phosphorylation. *iScience* **23**, 101023 10.1016/j.isci.2020.101023 PMID 32325413
135. Samelson, L. E. (2002) Signal transduction mediated by the T cell antigen receptor: the role of adapter proteins. *Annual review of immunology* **20**, 371–394 10.1146/annurev.immunol.20.092601.111357 PMID 11861607
136. Hawkins, P. T., Anderson, K. E., Davidson, K., and Stephens, L. R. (2006) Signalling through Class I PI3Ks in mammalian cells. *Biochemical Society transactions* **34**, 647–662 10.1042/bst0340647 PMID 17052169
137. Vanhaesebroeck, B., Leevers, S. J., Ahmadi, K., Timms, J., Katso, R., Driscoll, P. C., Woscholski, R., Parker, P. J., and Waterfield, M. D. (2001) Synthesis and function of 3-phosphorylated inositol lipids. *Annual review of biochemistry* **70**, 535–602 10.1146/annurev.biochem.70.1.535 PMID 11395417
138. Park, S.-G., Schulze-Luehrman, J., Hayden, M. S., Hashimoto, N., Ogawa, W., Kasuga, M., and Ghosh, S. (2009) The kinase PDK1 integrates T cell antigen receptor and CD28 coreceptor signaling to induce NF-kappaB and activate T cells. *Nature immunology* **10**, 158–166 10.1038/ni.1687 PMID 19122654
139. Ishimaru, N., Kishimoto, H., Hayashi, Y., and Sprent, J. (2006) Regulation of naive T cell function by the NF-kappaB2 pathway. *Nature immunology* **7**, 763–772 10.1038/ni1351 PMID 16732290
140. Scheid, M. P., Marignani, P. A., and Woodgett, J. R. (2002) Multiple phosphoinositide 3-kinase-dependent steps in activation of protein kinase B. *Molecular and cellular biology* **22**, 6247–6260 10.1128/mcb.22.17.6247-6260.2002 PMID 12167717
141. Shaw, A. L., and Burke, J. E. (2025) Molecular insight on the role of the phosphoinositide PIP3 in regulating the protein kinases Akt, PDK1, and BTK. *Biochemical Society transactions* **53**, 737–749 10.1042/BST20253059 PMID 40613782
142. Chan, T. O., Rittenhouse, S. E., and Tsichlis, P. N. (1999) AKT/PKB and other D3 phosphoinositide-regulated kinases: kinase activation by phosphoinositide-dependent phosphorylation. *Annual review of biochemistry* **68**, 965–1014 10.1146/annurev.biochem.68.1.965 PMID 10872470
143. Bellacosa, A., Chan, T. O., Ahmed, N. N., Datta, K., Malstrom, S., Stokoe, D., McCormick, F., Feng, J., and Tsichlis, P. (1998) Akt activation by growth factors is a multiple-step process: the role of the PH domain. *Oncogene* **17**, 313–325 10.1038/sj.onc.1201947 PMID 9690513
144. Anderson, K. E., Coadwell, J., Stephens, L. R., and Hawkins, P. T. (1998) Translocation of PDK-1 to the plasma membrane is important in allowing PDK-1 to activate protein kinase B. *Current biology : CB* **8**, 684–691 10.1016/s0960-9822(98)70274-x PMID 9637919
145. Alessi, D. R., James, S. R., Downes, C. P., Holmes, A. B., Gaffney, P. R., Reese, C. B., and Cohen, P. (1997) Characterization of a 3-phosphoinositide-dependent protein kinase which phosphorylates and activates protein kinase Balpha. *Current biology : CB* **7**, 261–269 10.1016/s0960-9822(06)00122-9 PMID 9094314
146. Sinclair, L. V., Finlay, D., Feijoo, C., Cornish, G. H., Gray, A., Ager, A., Okkenhaug, K., Hagenbeek, T. J., Spits, H., and Cantrell, D. A. (2008) Phosphatidylinositol-3-OH kinase and nutrient-sensing mTOR pathways control T lymphocyte trafficking. *Nature immunology* **9**, 513–521 10.1038/ni.1603 PMID 18391955
147. Lee, K., Gudapati, P., Dragovic, S., Spencer, C., Joyce, S., Killeen, N., Magnuson, M. A., and Boothby, M. (2010) Mammalian target of rapamycin protein complex 2 regulates differentiation of Th1 and Th2 cell subsets via distinct signaling pathways. *Immunity* **32**, 743–753 10.1016/j.immuni.2010.06.002 PMID 20620941

148. Hermida, M. A., Dinesh Kumar, J., and Leslie, N. R. (2017) GSK3 and its interactions with the PI3K/AKT/mTOR signalling network. *Advances in biological regulation* **65**, 5–15 10.1016/j.jbior.2017.06.003 PMID 28712664
149. Neal, J. W., and Clipstone, N. A. (2001) Glycogen synthase kinase-3 inhibits the DNA binding activity of NFATc. *The Journal of biological chemistry* **276**, 3666–3673 10.1074/jbc.M004888200 PMID 11063740
150. Witte, A. (2013) Emerging Roles of ADAP, SKAP55, and SKAP-HOM for Integrin and NF-κB Signaling in T cells. *J Clin Cell Immunol* **01** 10.4172/2155-9899.S12-007
151. Roux, P. P., Ballif, B. A., Anjum, R., Gygi, S. P., and Blenis, J. (2004) Tumor-promoting phorbol esters and activated Ras inactivate the tuberous sclerosis tumor suppressor complex via p90 ribosomal S6 kinase. *Proceedings of the National Academy of Sciences of the United States of America* **101**, 13489–13494 10.1073/pnas.0405659101 PMID 15342917
152. Ma, L., Chen, Z., Erdjument-Bromage, H., Tempst, P., and Pandolfi, P. P. (2005) Phosphorylation and functional inactivation of TSC2 by Erk implications for tuberous sclerosis and cancer pathogenesis. *Cell* **121**, 179–193 10.1016/j.cell.2005.02.031 PMID 15851026
153. Chi, H. (2012) Regulation and function of mTOR signalling in T cell fate decisions. *Nature reviews. Immunology* **12**, 325–338 10.1038/nri3198 PMID 22517423
154. Waickman, A. T., and Powell, J. D. (2012) mTOR, metabolism, and the regulation of T-cell differentiation and function. *Immunological reviews* **249**, 43–58 10.1111/j.1600-065X.2012.01152.x PMID 22889214
155. Kim, L. C., Cook, R. S., and Chen, J. (2017) mTORC1 and mTORC2 in cancer and the tumor microenvironment. *Oncogene* **36**, 2191–2201 10.1038/onc.2016.363 PMID 27748764
156. Way, E. E., Trevejo-Nunez, G., Kane, L. P., Steiner, B. H., Puri, K. D., Kolls, J. K., and Chen, K. (2016) Dose-Dependent Suppression of Cytokine production from T cells by a Novel Phosphoinositide 3-Kinase Delta Inhibitor. *Scientific reports* **6**, 30384 10.1038/srep30384 PMID 27461849
157. Panwar, V., Singh, A., Bhatt, M., Tonk, R. K., Azizov, S., Raza, A. S., Sengupta, S., Kumar, D., and Garg, M. (2023) Multifaceted role of mTOR (mammalian target of rapamycin) signaling pathway in human health and disease. *Signal transduction and targeted therapy* **8**, 375 10.1038/s41392-023-01608-z PMID 37779156
158. Kusaba, H., Ghosh, P., Derin, R., Buchholz, M., Sasaki, C., Madara, K., and Longo, D. L. (2005) Interleukin-12-induced interferon-gamma production by human peripheral blood T cells is regulated by mammalian target of rapamycin (mTOR). *The Journal of biological chemistry* **280**, 1037–1043 10.1074/jbc.m405204200 PMID 15522880
159. Jurgens, A. P., Zwijnen, J., Bradarić, A., van Alphen, F. P. J., Bresser, K., Rooijers, K., Hoogendijk, A. J., Popović, B., and Wolkers, M. C. (2025) mTOR signaling during T cell activation promotes cytokine production in T cells through 3' UTR-mediated translation control. *Molecular cell* **85**, 4452-4462.e5 10.1016/j.molcel.2025.11.005 PMID 41349520
160. Peng, H.-Y., Lucavs, J., Ballard, D., Das, J. K., Kumar, A., Wang, L., Ren, Y., Xiong, X., and Song, J. (2021) Metabolic Reprogramming and Reactive Oxygen Species in T Cell Immunity. *Frontiers in immunology* **12**, 652687 10.3389/fimmu.2021.652687 PMID 33868291
161. Kornberg, M. D. (2020) The immunologic Warburg effect: Evidence and therapeutic opportunities in autoimmunity. *Wiley interdisciplinary reviews. Systems biology and medicine* **12**, e1486 10.1002/wsbm.1486 PMID 32105390
162. Zhang, W., Chen, Y., Guan, Z., Wang, Y., Tang, M., Du, Z., Zhang, J., Cheng, M., Zuo, J., Liu, Y., Wang, Q., Liu, Y., Zhang, D., Yin, P., Ma, L., and Liu, Z. (2025) Structural insights into the mechanism of phosphate recognition and transport by XPR1. *Nature communications* **16**, 18 10.1038/s41467-024-55471-9 PMID 39747008
163. Yan, R., Chen, H., Liu, C., Zhao, J., Di Wu, Jiang, J., Gong, J., and Jiang, D. (2024) Human XPR1 structures reveal phosphate export mechanism. *Nature* **633**, 960–967 10.1038/s41586-024-07852-9 PMID 39169184

164. Wu, H., Sun, L., Huo, T., Wensel, T. G., Horrigan, F. T., and Wang, Z. (2025) The identification of XPR1 as a voltage- and phosphate-activated phosphate-permeable ion channel. *Nature communications* **16**, 4519 10.1038/s41467-025-59678-2 PMID 40374661
165. Wang, X., Bai, Z., Wallis, C., Wang, H., Han, Y., Jin, R., Lei, M., Yang, T., Gu, C., Jessen, H., Shears, S., Sun, Y., Corry, B., and Zhang, Y. (2025) KIDINS220 and InsP8 safeguard the stepwise regulation of phosphate exporter XPR1. *Molecular cell* **85**, 3209-3224.e8 10.1016/j.molcel.2025.08.003 PMID 40858110
166. Zuo, P., Wang, W., Dai, Z., Zheng, J., Yu, S., Wang, G., Yin, Y., Liang, L., and Yin, Y. (2025) Synergistic activation of the human phosphate exporter XPR1 by KIDINS220 and inositol pyrophosphate. *Nature communications* **16**, 2879 10.1038/s41467-025-58200-y PMID 40128258
167. Anheim, M., López-Sánchez, U., Giovannini, D., Richard, A.-C., Touhami, J., N'Guyen, L., Rudolf, G., Thibault-Stoll, A., Frebourg, T., Hannequin, D., Campion, D., Battini, J.-L., Sitbon, M., and Nicolas, G. (2016) XPR1 mutations are a rare cause of primary familial brain calcification. *Journal of neurology* **263**, 1559–1564 10.1007/s00415-016-8166-4 PMID 27230854
168. Balck, A., Schaake, S., Kuhnke, N. S., Domingo, A., Madoev, H., Margolesky, J., Dobricic, V., Alvarez-Fischer, D., Laabs, B.-H., Kasten, M., Luo, W., Nicolas, G., Marras, C., Lohmann, K., Klein, C., and Westenberger, A. (2021) Genotype-Phenotype Relations in Primary Familial Brain Calcification: Systematic MDSGene Review. *Movement disorders : official journal of the Movement Disorder Society* **36**, 2468–2480 10.1002/mds.28753 PMID 34432325
169. Legati, A., Giovannini, D., Nicolas, G., López-Sánchez, U., Quintáns, B., Oliveira, J. R. M., Sears, R. L., Ramos, E. M., Spiteri, E., Sobrido, M.-J., Carracedo, Á., Castro-Fernández, C., Cubizolle, S., Fogel, B. L., Goizet, C., Jen, J. C., Kirdlarp, S., Lang, A. E., Miedzybrodzka, Z., Mitarnun, W., Paucar, M., Paulson, H., Pariente, J., Richard, A.-C., Salins, N. S., Simpson, S. A., Striano, P., Svenningsson, P., Tison, F., Unni, V. K., Vanakker, O., Wessels, M. W., Wetchaphanphesat, S., Yang, M., Boller, F., Campion, D., Hannequin, D., Sitbon, M., Geschwind, D. H., Battini, J.-L., and Coppola, G. (2015) Mutations in XPR1 cause primary familial brain calcification associated with altered phosphate export. *Nature genetics* **47**, 579–581 10.1038/ng.3289 PMID 25938945
170. Yao, X.-P., Zhao, M., Wang, C., Guo, X.-X., Su, H.-Z., Dong, E.-L., Chen, H.-T., Lai, J.-H., Liu, Y.-B., Wang, N., and Chen, W.-J. (2017) Analysis of gene expression and functional characterization of XPR1: a pathogenic gene for primary familial brain calcification. *Cell and tissue research* **370**, 267–273 10.1007/s00441-017-2663-3 PMID 28766044
171. Ramos, E. M., Carecchio, M., Lemos, R., Ferreira, J., Legati, A., Sears, R. L., Hsu, S. C., Panteghini, C., Magistrelli, L., Salsano, E., Esposito, S., Taroni, F., Richard, A.-C., Tranchant, C., Anheim, M., Ayrignac, X., Goizet, C., Vidailhet, M., Maltete, D., Wallon, D., Frebourg, T., Pimentel, L., Geschwind, D. H., Vanakker, O., Galasko, D., Fogel, B. L., Innes, A. M., Ross, A., Dobyns, W. B., Alcantara, D., O'Driscoll, M., Hannequin, D., Campion, D., Oliveira, J. R., Garavaglia, B., Coppola, G., and Nicolas, G. (2018) Primary brain calcification: an international study reporting novel variants and associated phenotypes. *European journal of human genetics : EJHG* **26**, 1462–1477 10.1038/s41431-018-0185-4 PMID 29955172
172. Nicolas, G., Charbonnier, C., Lemos, R. R. de, Richard, A.-C., Guillin, O., Wallon, D., Legati, A., Geschwind, D., Coppola, G., Frebourg, T., Campion, D., Oliveira, J. R. M. de, and Hannequin, D. (2015) Brain calcification process and phenotypes according to age and sex: Lessons from SLC20A2, PDGFB, and PDGFRB mutation carriers. *American journal of medical genetics. Part B, Neuropsychiatric genetics : the official publication of the International Society of Psychiatric Genetics* **168**, 586–594 10.1002/ajmg.b.32336 PMID 26129893
173. López-Sánchez, U., Tury, S., Nicolas, G., Wilson, M. S., Jurici, S., Ayrignac, X., Courgnaud, V., Saiardi, A., Sitbon, M., and Battini, J.-L. (2020) Interplay between primary familial brain calcification-associated SLC20A2 and XPR1 phosphate transporters requires inositol polyphosphates for control of cellular phosphate homeostasis. *The Journal of biological chemistry* **295**, 9366–9378 10.1074/jbc.RA119.011376 PMID 32393577

174. Chen, L., He, J., Wang, M., and She, J. (2025) Structure and function of human XPR1 in phosphate export. *Nature communications* **16**, 2983 10.1038/s41467-025-58195-6 PMID 40140662
175. Wang, H., Luo, X., Yang, B., Tang, F., Jiang, X., Zhu, H., and Hu, J. (2025) XPR1 promotes ovarian cancer growth and regulates MHC-I through autophagy. *Genes & diseases* **12**, 101507 10.1016/j.gendis.2024.101507 PMID 40641524
176. Bondeson, D. P., Paolella, B. R., Asfaw, A., Rothberg, M. V., Skipper, T. A., Langan, C., Mesa, G., Gonzalez, A., Surface, L. E., Ito, K., Kazachkova, M., Colgan, W. N., Warren, A., Dempster, J. M., Krill-Burger, J. M., Ericsson, M., Tang, A. A., Fung, I., Chambers, E. S., Abdusamad, M., Dumont, N., Doench, J. G., Piccioni, F., Root, D. E., Boehm, J., Hahn, W. C., Mannstadt, M., McFarland, J. M., Vazquez, F., and Golub, T. R. (2022) Phosphate dysregulation via the XPR1-KIDINS220 protein complex is a therapeutic vulnerability in ovarian cancer. *Nature cancer* **3**, 681–695 10.1038/s43018-022-00360-7 PMID 35437317
177. Xu, X., Li, X., Sun, H., Cao, Z., Gao, R., Niu, T., Wang, Y., Ma, T., Chen, R., Wang, C., Yang, Z., and Liu, J. Y. (2020) Murine Placental-Fetal Phosphate Dyshomeostasis Caused by an Xpr1 Deficiency Accelerates Placental Calcification and Restricts Fetal Growth in Late Gestation. *Journal of bone and mineral research : the official journal of the American Society for Bone and Mineral Research* **35**, 116–129 10.1002/jbmr.3866 PMID 31498925
178. Maheshwari, U., Mateos, J. M., Weber-Stadlbauer, U., Ni, R., Tamatey, V., Sridhar, S., Restrepo, A., Jong, P. A. de, Huang, S.-F., Schaffenrath, J., Stifter, S. A., Szeri, F., Greter, M., Koek, H. L., and Keller, A. (2023) Inorganic phosphate exporter heterozygosity in mice leads to brain vascular calcification, microangiopathy, and microgliosis. *Brain pathology (Zurich, Switzerland)* **33**, e13189 10.1111/bpa.13189 PMID 37505935
179. Ansermet, C., Moor, M. B., Centeno, G., Auberson, M., Hu, D. Z., Baron, R., Nikolaeva, S., Haenzi, B., Katanaeva, N., Gautschi, I., Katanaev, V., Rotman, S., Koesters, R., Schild, L., Pradervand, S., Bonny, O., and Firsov, D. (2017) Renal Fanconi Syndrome and Hypophosphatemic Rickets in the Absence of Xenotropic and Polytropic Retroviral Receptor in the Nephron. *Journal of the American Society of Nephrology : JASN* **28**, 1073–1078 10.1681/ASN.2016070726 PMID 27799484
180. Mailer, R. K., Allende, M., Heestermans, M., Schweizer, M., Deppermann, C., Frye, M., Pula, G., Odeberg, J., Gelderblom, M., Rose-John, S., Sickmann, A., Blankenberg, S., Huber, T. B., Kubisch, C., Maas, C., Gambaryan, S., Firsov, D., Stavrou, E. X., Butler, L. M., and Renné, T. (2021) Xenotropic and polytropic retrovirus receptor 1 regulates procoagulant platelet polyphosphate. *Blood* **137**, 1392–1405 10.1182/blood.2019004617 PMID 32932519
181. Smith, S. A., Mutch, N. J., Baskar, D., Rohloff, P., Docampo, R., and Morrissey, J. H. (2006) Polyphosphate modulates blood coagulation and fibrinolysis. *Proceedings of the National Academy of Sciences of the United States of America* **103**, 903–908 10.1073/pnas.0507195103 PMID 16410357
182. Müller, F., Mutch, N. J., Schenk, W. A., Smith, S. A., Esterl, L., Spronk, H. M., Schmidbauer, S., Gahl, W. A., Morrissey, J. H., and Renné, T. (2009) Platelet polyphosphates are proinflammatory and procoagulant mediators in vivo. *Cell* **139**, 1143–1156 10.1016/j.cell.2009.11.001 PMID 20005807
183. Li, X., Gu, C., Hostachy, S., Sahu, S., Wittwer, C., Jessen, H. J., Fiedler, D., Wang, H., and Shears, S. B. (2020) Control of XPR1-dependent cellular phosphate efflux by InsP8 is an exemplar for functionally-exclusive inositol pyrophosphate signaling. *Proceedings of the National Academy of Sciences of the United States of America* **117**, 3568–3574 10.1073/pnas.1908830117 PMID 32019887
184. Li, X., Kirkpatrick, R. B., Wang, X., Tucker, C. J., Shukla, A., Jessen, H. J., Wang, H., Shears, S. B., and Gu, C. (2024) Homeostatic coordination of cellular phosphate uptake and efflux requires an organelle-based receptor for the inositol pyrophosphate IP8. *Cell reports* **43**, 114316 10.1016/j.celrep.2024.114316 PMID 38833370

185. Tello-Lafoz, M., Martínez-Martínez, G., Rodríguez-Rodríguez, C., Albar, J. P., Huse, M., Gharbi, S., and Merida, I. (2017) Sorting nexin 27 interactome in T-lymphocytes identifies zona occludens-2 dynamic redistribution at the immune synapse. *Traffic (Copenhagen, Denmark)* **18**, 491–504 10.1111/tra.12492 PMID 28477369
186. Rodriguez-Rodriguez, C., González-Mancha, N., Ochoa-Echeverría, A., and Mérida, I. (2024) Sorting nexin 27-dependent regulation of Lck and CD4 tunes the initial stages of T-cell activation. *Journal of leukocyte biology* **116**, 793–806 10.1093/jleuko/qiae086 PMID 38648515
187. Bondeson, D. P. (2025) Insights into phosphate homeostasis regulation by XPR1. *Nature structural & molecular biology* **32**, 5–7 10.1038/s41594-024-01460-x PMID 39738853
188. Iglesias, T., Cabrera-Poch, N., Mitchell, M. P., Naven, T. J., Rozengurt, E., and Schiavo, G. (2000) Identification and cloning of Kidins220, a novel neuronal substrate of protein kinase D. *The Journal of biological chemistry* **275**, 40048–40056 10.1074/jbc.M005261200 PMID 10998417
189. Kong, H., Boulter, J., Weber, J. L., Lai, C., and Chao, M. V. (2001) An evolutionarily conserved transmembrane protein that is a novel downstream target of neurotrophin and ephrin receptors. *The Journal of neuroscience : the official journal of the Society for Neuroscience* **21**, 176–185 10.1523/JNEUROSCI.21-01-00176.2001 PMID 11150334
190. Luo, S., Chen, Y., Lai, K.-O., Arévalo, J. C., Froehner, S. C., Adams, M. E., Chao, M. V., and Ip, N. Y. (2005) {alpha}-Syntrophin regulates ARMS localization at the neuromuscular junction and enhances EphA4 signaling in an ARMS-dependent manner. *The Journal of cell biology* **169**, 813–824 10.1083/jcb.200412008 PMID 15939763
191. Arévalo, J. C., Wu, S. H., Takahashi, T., Zhang, H., Yu, T., Yano, H., Milner, T. A., Tessarollo, L., Ninan, I., Arancio, O., and Chao, M. V. (2010) The ARMS/Kidins220 scaffold protein modulates synaptic transmission. *Molecular and cellular neurosciences* **45**, 92–100 10.1016/j.mcn.2010.06.002 PMID 20547223
192. Arévalo, J. C., Yano, H., Teng, K. K., and Chao, M. V. (2004) A unique pathway for sustained neurotrophin signaling through an ankyrin-rich membrane-spanning protein. *The EMBO journal* **23**, 2358–2368 10.1038/sj.emboj.7600253 PMID 15167895
193. López-Menéndez, C., Gascón, S., Sobrado, M., Vidaurre, O. G., Higuero, A. M., Rodríguez-Peña, A., Iglesias, T., and Díaz-Guerra, M. (2009) Kidins220/ARMS downregulation by excitotoxic activation of NMDARs reveals its involvement in neuronal survival and death pathways. *Journal of cell science* **122**, 3554–3565 10.1242/jcs.056473 PMID 19759287
194. Neubrand, V. E., Thomas, C., Schmidt, S., Debant, A., and Schiavo, G. (2010) Kidins220/ARMS regulates Rac1-dependent neurite outgrowth by direct interaction with the RhoGEF Trio. *Journal of cell science* **123**, 2111–2123 10.1242/jcs.064055 PMID 20519585
195. Del Puerto, A., Pose-Utrilla, J., Simón-García, A., López-Menéndez, C., Jiménez, A. J., Porlan, E., Pajuelo, L. S. M., Cano-García, G., Martí-Prado, B., Sebastián-Serrano, Á., Sánchez-Carralero, M. P., Cesca, F., Schiavo, G., Ferrer, I., Fariñas, I., Campanero, M. R., and Iglesias, T. (2021) Kidins220 deficiency causes ventriculomegaly via SNX27-retromer-dependent AQP4 degradation. *Molecular psychiatry* **26**, 6411–6426 10.1038/s41380-021-01127-9 PMID 34002021
196. Bracale, A., Cesca, F., Neubrand, V. E., Newsome, T. P., Way, M., and Schiavo, G. (2007) Kidins220/ARMS is transported by a kinesin-1-based mechanism likely to be involved in neuronal differentiation. *Molecular biology of the cell* **18**, 142–152 10.1091/mbc.e06-05-0453 PMID 17079733
197. Deswal, S., Meyer, A., Fiala, G. J., Eisenhardt, A. E., Schmitt, L. C., Salek, M., Brummer, T., Acuto, O., and Schamel, W. W. A. (2013) Kidins220/ARMS associates with B-Raf and the TCR, promoting sustained Erk signaling in T cells. *Journal of immunology (Baltimore, Md. : 1950)* **190**, 1927–1935 10.4049/jimmunol.1200653 PMID 23359496
198. Fiala, G. J., Janowska, I., Prutek, F., Hobeika, E., Satapathy, A., Sprenger, A., Plum, T., Seidl, M., Dengjel, J., Reth, M., Cesca, F., Brummer, T., Minguet, S., and Schamel, W. W. A. (2015) Kidins220/ARMS binds to the B cell antigen receptor and regulates B cell development and activation. *The Journal of experimental medicine* **212**, 1693–1708 10.1084/jem.20141271 PMID 26324445

199. Schaffer, A.-M., Fiala, G. J., Hils, M., Natali, E., Babrak, L., Herr, L. A., Romero-Mulero, M. C., Cabezas-Wallscheid, N., Rizzi, M., Miho, E., Schamel, W. W. A., and Minguet, S. (2024) Kidins220 regulates the development of B cells bearing the λ light chain. *eLife* **13** 10.7554/eLife.83943 PMID 38271217
200. Herr, L. A., Fiala, G. J., Sagar, Schaffer, A.-M., Hummel, J. F., Zintchenko, M., Raute, K., Velasco Cárdenas, R. M.-H., Heizmann, B., Ebert, K., Fehrenbach, K., Janowska, I., Chan, S., Tanriver, Y., Minguet, S., and Schamel, W. W. (2024) Kidins220 and Aiolos promote thymic iNKT cell development by reducing TCR signals. *Science advances* **10**, eadj2802 10.1126/sciadv.adj2802 PMID 38489359
201. Frommelt, F., Ladurner, R., Goldmann, U., Wolf, G., Ingles-Prieto, A., Lineiro-Retes, E., Gelová, Z., Hopp, A.-K., Christodoulaki, E., Teoh, S. T., Leippe, P., Santini, B. L., Rebsamen, M., Lindinger, S., Serrano, I., Onstein, S., Klimek, C., Barbosa, B., Pantielieieva, A., Dvorak, V., Hannich, T. J., Schoenbett, J., Sansig, G., Mocking, T. A. M., Ooms, J. F., IJzerman, A. P., Heitman, L. H., Sykacek, P., Reinhardt, J., Müller, A. C., Wiedmer, T., and Superti-Furga, G. (2025) The solute carrier superfamily interactome. *Molecular systems biology* **21**, 632–675 10.1038/s44320-025-00109-1 PMID 40355756
202. Almacellas-Barbanoj, A., Albini, M., Satapathy, A., Jaudon, F., Michetti, C., Krawczun-Rygmaczewska, A., Huang, H., Manago, F., Papaleo, F., Benfenati, F., and Cesca, F. (2022) Kidins220/ARMS modulates brain morphology and anxiety-like traits in adult mice. *Cell death discovery* **8**, 58 10.1038/s41420-022-00854-4 PMID 35140204
203. Go, C. D., Knight, J. D. R., Rajasekharan, A., Rathod, B., Hesketh, G. G., Abe, K. T., Youn, J.-Y., Samavarchi-Tehrani, P., Zhang, H., Zhu, L. Y., Popiel, E., Lambert, J.-P., Coyaud, É., Cheung, S. W. T., Rajendran, D., Wong, C. J., Antonicka, H., Pelletier, L., Palazzo, A. F., Shoubridge, E. A., Raught, B., and Gingras, A.-C. (2021) A proximity-dependent biotinylation map of a human cell. *Nature* **595**, 120–124 10.1038/s41586-021-03592-2 PMID 34079125
204. Hein, M. Y., Hubner, N. C., Poser, I., Cox, J., Nagaraj, N., Toyoda, Y., Gak, I. A., Weisswange, I., Mansfeld, J., Buchholz, F., Hyman, A. A., and Mann, M. (2015) A human interactome in three quantitative dimensions organized by stoichiometries and abundances. *Cell* **163**, 712–723 10.1016/j.cell.2015.09.053 PMID 26496610
205. Huttlin, E. L., Bruckner, R. J., Navarrete-Perea, J., Cannon, J. R., Baltier, K., Gebreab, F., Gygi, M. P., Thornock, A., Zarraga, G., Tam, S., Szpyt, J., Gassaway, B. M., Panov, A., Parzen, H., Fu, S., Golbazi, A., Maenpaa, E., Stricker, K., Guha Thakurta, S., Zhang, T., Rad, R., Pan, J., Nusinow, D. P., Paulo, J. A., Schweppe, D. K., Vaites, L. P., Harper, J. W., and Gygi, S. P. (2021) Dual proteome-scale networks reveal cell-specific remodeling of the human interactome. *Cell* **184**, 3022-3040.e28 10.1016/j.cell.2021.04.011 PMID 33961781
206. Huttlin, E. L., Bruckner, R. J., Paulo, J. A., Cannon, J. R., Ting, L., Baltier, K., Colby, G., Gebreab, F., Gygi, M. P., Parzen, H., Szpyt, J., Tam, S., Zarraga, G., Pontano-Vaites, L., Swarup, S., White, A. E., Schweppe, D. K., Rad, R., Erickson, B. K., Obar, R. A., Guruharsha, K. G., Li, K., Artavanis-Tsakonas, S., Gygi, S. P., and Harper, J. W. (2017) Architecture of the human interactome defines protein communities and disease networks. *Nature* **545**, 505–509 10.1038/nature22366 PMID 28514442
207. Xu, M., Ito-Kureha, T., Kang, H.-S., Chernev, A., Raj, T., Hoefig, K. P., Hohn, C., Giesert, F., Wang, Y., Pan, W., Ziętara, N., Straub, T., Feederle, R., Daniel, C., Adler, B., König, J., Feske, S., Tsokos, G. C., Wurst, W., Urlaub, H., Sattler, M., Kisielow, J., Wulczyn, F. G., Łyszkiewicz, M., and Heissmeyer, V. (2024) The thymocyte-specific RNA-binding protein Arpp21 provides TCR repertoire diversity by binding to the 3'-UTR and promoting Rag1 mRNA expression. *Nature communications* **15**, 2194 10.1038/s41467-024-46371-z PMID 38467629
208. Fu, G., Vallée, S., Rybakin, V., McGuire, M. V., Ampudia, J., Brockmeyer, C., Salek, M., Fallen, P. R., Hoerter, J. A. H., Munshi, A., Huang, Y. H., Hu, J., Fox, H. S., Sauer, K., Acuto, O., and Gascoigne, N. R. J. (2009) Themis controls thymocyte selection through regulation of T cell antigen receptor-mediated signaling. *Nature immunology* **10**, 848–856 10.1038/ni.1766 PMID 19597499

209. Kim, S., Park, G.-Y., Park, J. S., Park, J., Hong, H., and Lee, Y. (2021) Regulation of positive and negative selection and TCR signaling during thymic T cell development by capicua. *eLife* **10** 10.7554/eLife.71769 PMID 34895467
210. Voisinne, G., Gonzalez de Peredo, A., and Roncagalli, R. (2018) CD5, an Undercover Regulator of TCR Signaling. *Frontiers in immunology* **9**, 2900 10.3389/fimmu.2018.02900 PMID 30581443
211. Peña-Rossi, C., Zuckerman, L. A., Strong, J., Kwan, J., Ferris, W., Chan, S., Tarakhovsky, A., Beyers, A. D., and Killeen, N. (1999) Negative regulation of CD4 lineage development and responses by CD5. *Journal of immunology (Baltimore, Md. : 1950)* **163**, 6494–6501 PMID 10586041
212. Dong, Y., Li, X., Zhang, L., Zhu, Q., Chen, C., Bao, J., and Chen, Y. (2019) CD4+ T cell exhaustion revealed by high PD-1 and LAG-3 expression and the loss of helper T cell function in chronic hepatitis B. *BMC immunology* **20**, 27 10.1186/s12865-019-0309-9 PMID 31390978
213. Adamczyk, M., Bartosińska, J., Raczkiewicz, D., Kowal, M., Surdacka, A., Krasowska, D., Michalak-Stoma, A., and Krasowska, D. (2023) The Expression of Activation Markers CD25 and CD69 Increases during Biologic Treatment of Psoriasis. *Journal of clinical medicine* **12** 10.3390/jcm12206573 PMID 37892710
214. Dutton, R. W., Bradley, L. M., and Swain, S. L. (1998) T cell memory. *Annual review of immunology* **16**, 201–223 10.1146/annurev.immunol.16.1.201 PMID 9597129
215. Gerberick, G. F., Cruse, L. W., Miller, C. M., Sikorski, E. E., and Ridder, G. M. (1997) Selective modulation of T cell memory markers CD62L and CD44 on murine draining lymph node cells following allergen and irritant treatment. *Toxicology and applied pharmacology* **146**, 1–10 10.1006/taap.1997.8218 PMID 9299591
216. Sckisel, G. D., Mirsoian, A., Minnar, C. M., Crittenden, M., Curti, B., Chen, J. Q., Blazar, B. R., Borowsky, A. D., Monjazeb, A. M., and Murphy, W. J. (2017) Differential phenotypes of memory CD4 and CD8 T cells in the spleen and peripheral tissues following immunostimulatory therapy. *Journal for immunotherapy of cancer* **5**, 33 10.1186/s40425-017-0235-4 PMID 28428882
217. Schumann, J., Stanko, K., Schliesser, U., Appelt, C., and Sawitzki, B. (2015) Differences in CD44 Surface Expression Levels and Function Discriminates IL-17 and IFN-γ Producing Helper T Cells. *PloS one* **10**, e0132479 10.1371/journal.pone.0132479 PMID 26172046
218. Shouse, A. N., LaPorte, K. M., and Malek, T. R. (2024) Interleukin-2 signaling in the regulation of T cell biology in autoimmunity and cancer. *Immunity* **57**, 414–428 10.1016/j.immuni.2024.02.001 PMID 38479359
219. Kim, H. P., Imbert, J., and Leonard, W. J. (2006) Both integrated and differential regulation of components of the IL-2/IL-2 receptor system. *Cytokine & growth factor reviews* **17**, 349–366 10.1016/j.cytogfr.2006.07.003 PMID 16911870
220. Peng, T., Fang, Q., Zhao, Z., Chang, Y., Zhao, X., and Li, C. (2025) Multi-omics integration analysis identifies INPP4B as a T-cell-specific activation suppressor. *Clinical and translational medicine* **15**, e70430 10.1002/ctm2.70430 PMID 40754682
221. Lin, C.-C., Bradstreet, T. R., Schwarzkopf, E. A., Sim, J., Carrero, J. A., Chou, C., Cook, L. E., Egawa, T., Taneja, R., Murphy, T. L., Russell, J. H., and Edelson, B. T. (2014) Bhlhe40 controls cytokine production by T cells and is essential for pathogenicity in autoimmune neuroinflammation. *Nature communications* **5**, 3551 10.1038/ncomms4551 PMID 24699451
222. Martínez-Llordella, M., Esensten, J. H., Bailey-Bucktrout, S. L., Lipsky, R. H., Marini, A., Chen, J., Mughal, M., Mattson, M. P., Taub, D. D., and Bluestone, J. A. (2013) CD28-inducible transcription factor DEC1 is required for efficient autoreactive CD4+ T cell response. *The Journal of experimental medicine* **210**, 1603–1619 10.1084/jem.20122387 PMID 23878307
223. Salmon, A. J., Shavkunov, A. S., Miao, Q., Jarjour, N. N., Keshari, S., Esaulova, E., Williams, C. D., Ward, J. P., Highsmith, A. M., Pineda, J. E., Taneja, R., Chen, K., Edelson, B. T., and Gubin, M. M. (2022) BHLHE40 Regulates the T-Cell Effector Function Required for Tumor Microenvironment Remodeling and Immune Checkpoint Therapy Efficacy. *Cancer immunology research* **10**, 597–611 10.1158/2326-6066.CIR-21-0129 PMID 35181783

224. Lozano, E., Dominguez-Villar, M., Kuchroo, V., and Hafler, D. A. (2012) The TIGIT/CD226 axis regulates human T cell function. *Journal of immunology (Baltimore, Md. : 1950)* **188**, 3869–3875 10.4049/jimmunol.1103627 PMID 22427644
225. Watford, W. T., Hissong, B. D., Durant, L. R., Yamane, H., Muul, L. M., Kanno, Y., Tato, C. M., Ramos, H. L., Berger, A. E., Mielke, L., Pesu, M., Solomon, B., Frucht, D. M., Paul, W. E., Sher, A., Jankovic, D., Tsichlis, P. N., and O'Shea, J. J. (2008) Tpl2 kinase regulates T cell interferon-gamma production and host resistance to Toxoplasma gondii. *The Journal of experimental medicine* **205**, 2803–2812 10.1084/jem.20081461 PMID 19001140
226. López-Peláez, M., Soria-Castro, I., Boscá, L., Fernández, M., and Alemany, S. (2011) Cot/tpl2 activity is required for TLR-induced activation of the Akt p70 S6k pathway in macrophages: Implications for NO synthase 2 expression. *Eur. J. Immunol.* **41**, 1733–1741 10.1002/eji.201041101 PMID 21469113
227. Tsatsanis, C., Vaporidi, K., Zacharioudaki, V., Androulidaki, A., Sykulev, Y., Margioris, A. N., and Tsichlis, P. N. (2008) Tpl2 and ERK transduce antiproliferative T cell receptor signals and inhibit transformation of chronically stimulated T cells. *Proceedings of the National Academy of Sciences of the United States of America* **105**, 2987–2992 10.1073/pnas.0708381104 PMID 18287049
228. Watford, W. T., Wang, C.-C., Tsatsanis, C., Mielke, L. A., Eliopoulos, A. G., Daskalakis, C., Charles, N., Odom, S., Rivera, J., O'Shea, J., and Tsichlis, P. N. (2010) Ablation of tumor progression locus 2 promotes a type 2 Th cell response in Ovalbumin-immunized mice. *Journal of immunology (Baltimore, Md. : 1950)* **184**, 105–113 10.4049/jimmunol.0803730 PMID 19955521
229. Dumitru, C. D., Ceci, J. D., Tsatsanis, C., Kontoyiannis, D., Stamatakis, K., Lin, J. H., Patriotis, C., Jenkins, N. A., Copeland, N. G., Kollias, G., and Tsichlis, P. N. (2000) TNF-alpha induction by LPS is regulated posttranscriptionally via a Tpl2/ERK-dependent pathway. *Cell* **103**, 1071–1083 10.1016/s0092-8674(00)00210-5 PMID 11163183
230. Tsatsanis, C., Patriotis, C., Bear, S. E., and Tsichlis, P. N. (1998) The Tpl-2 protooncoprotein activates the nuclear factor of activated T cells and induces interleukin 2 expression in T cell lines. *Proceedings of the National Academy of Sciences of the United States of America* **95**, 3827–3832 10.1073/pnas.95.7.3827 PMID 9520452
231. Babu, G. J., Lalli, M. J., Sussman, M. A., Sadoshima, J., and Periasamy, M. (2000) Phosphorylation of elk-1 by MEK/ERK pathway is necessary for c-fos gene activation during cardiac myocyte hypertrophy. *Journal of molecular and cellular cardiology* **32**, 1447–1457 10.1006/jmcc.2000.1185 PMID 10900171
232. Wang, Y., and Prywes, R. (2000) Activation of the c-fos enhancer by the erk MAP kinase pathway through two sequence elements: the c-fos AP-1 and p62TCF sites. *Oncogene* **19**, 1379–1385 10.1038/sj.onc.1203443 PMID 10723128
233. Liu, S.-C., Tsang, N.-M., Chiang, W.-C., Chang, K.-P., Hsueh, C., Liang, Y., Juang, J.-L., Chow, K.-P. N., and Chang, Y.-S. (2013) Leukemia inhibitory factor promotes nasopharyngeal carcinoma progression and radioresistance. *The Journal of clinical investigation* **123**, 5269–5283 10.1172/jci63428 PMID 24270418
234. Li, X., Yang, Q., Yu, H., Wu, L., Zhao, Y., Zhang, C., Yue, X., Liu, Z., Wu, H., Haffty, B. G., Feng, Z., and Hu, W. (2014) LIF promotes tumorigenesis and metastasis of breast cancer through the AKT-mTOR pathway. *Oncotarget* **5**, 788–801 10.18632/oncotarget.1772 PMID 24553191
235. Metcalfe, S. M., Watson, T. J., Shurey, S., Adams, E., and Green, C. J. (2005) Leukemia inhibitory factor is linked to regulatory transplantation tolerance. *Transplantation* **79**, 726–730 10.1097/01.tp.0000149324.42994.38 PMID 15785381
236. Metcalfe, S. M. (2011) LIF in the regulation of T-cell fate and as a potential therapeutic. *Genes and immunity* **12**, 157–168 10.1038/gene.2011.9 PMID 21368774
237. Park, J., Gao, W., Whiston, R., Strom, T. B., Metcalfe, S., and Fahmy, T. M. (2011) Modulation of CD4+ T lymphocyte lineage outcomes with targeted, nanoparticle-mediated cytokine delivery. *Molecular pharmaceutics* **8**, 143–152 10.1021/mp100203a PMID 20977190

238. Gao, W., Thompson, L., Zhou, Q., Putheti, P., Fahmy, T. M., Strom, T. B., and Metcalfe, S. M. (2009) Treg versus Th17 lymphocyte lineages are cross-regulated by LIF versus IL-6. *Cell cycle (Georgetown, Tex.)* **8**, 1444–1450 10.4161/cc.8.9.8348 PMID 19342884
239. Luo, W., Sun, Y., and Cao, L. (2025) TSPAN31 Activates Fatty Acid Metabolism and PI3K/AKT Pathway to Promote Tumor Progression in Breast Cancer. *Molecular carcinogenesis* **64**, 1078–1089 10.1002/mc.23912 PMID 40135650
240. Tong, H., Zhang, A., Shi, Y., Zhu, S., and Liu, L. (2025) TSPAN31 Activates EMT Through the PI3 K/AKT Signaling Pathway to Promote Glioma Progression. *Neurochemical research* **50**, 192 10.1007/s11064-025-04439-2 PMID 40488790
241. Jin, X., Wang, D., Lei, M., Guo, Y., Cui, Y., Chen, F., Sun, W., and Chen, X. (2022) TPI1 activates the PI3K/AKT/mTOR signaling pathway to induce breast cancer progression by stabilizing CDCA5. *Journal of translational medicine* **20**, 191 10.1186/s12967-022-03370-2 PMID 35509067
242. Wang, C., Wan, S., Li, K., Chen, S., Shu, Y., Liu, S., and Yang, L. (2025) TPI1 promotes p53 ubiquitination in bladder cancer by recruiting AKT to enhance MDM2 phosphorylation. *Pharmacological research* **215**, 107695 10.1016/j.phrs.2025.107695 PMID 40097123
243. Guo, H., Sun, Q., Huang, X., Wang, X., Zhang, F., Qu, W., Liu, J., Cheng, X., Zhu, Q., Yi, W., Shu, Q., and Li, X. (2024) Fucosyltransferase 8 regulates adult neurogenesis and cognition of mice by modulating the Itga6-PI3K/Akt signaling pathway. *Science China. Life sciences* **67**, 1427–1440 10.1007/s11427-023-2510-0 PMID 38523237
244. Calleja, V., Alcor, D., Laguerre, M., Park, J., Vojnovic, B., Hemmings, B. A., Downward, J., Parker, P. J., and Larijani, B. (2007) Intramolecular and intermolecular interactions of protein kinase B define its activation in vivo. *PLoS biology* **5**, e95 10.1371/journal.pbio.0050095 PMID 17407381
245. Vanhaesebroeck, B., and Alessi, D. R. (2000) The PI3K-PDK1 connection: more than just a road to PKB. *The Biochemical journal* **346 Pt 3**, 561–576 PMID 10698680
246. Cai, W.-W., Gao, Y., Cheng, J.-W., Yu, Y., Zong, S.-Y., Li, Y.-H., Wang, Y., Song, Y.-N., Mao, X.-T., Guan, J., Xu, L., Zhang, D.-Y., Li, K., and Wei, F. (2024) Berberine modulates the immunometabolism and differentiation of CD4+ T cells alleviating experimental arthritis by suppression of M1-exo-miR155. *Phytomedicine : international journal of phytotherapy and phytopharmacology* **124**, 155255 10.1016/j.phymed.2023.155255 PMID 38181528
247. Jung, B., Ferrer, G., Chiu, P. Y., Aslam, R., Ng, A., Palacios, F., Wysota, M., Cardillo, M., Kolitz, J. E., Allen, S. L., Barrientos, J. C., Rai, K. R., Chiorazzi, N., and Sherry, B. (2022) Activated CLL cells regulate IL-17F-producing Th17 cells in miR155-dependent and outcome-specific manners. *JCI insight* **7** 10.1172/jci.insight.158243 PMID 35511436
248. Lee, S., Kim, S. M., and Lee, R. T. (2013) Thioredoxin and thioredoxin target proteins: from molecular mechanisms to functional significance. *Antioxidants & redox signaling* **18**, 1165–1207 10.1089/ars.2011.4322 PMID 22607099
249. Chakraborty, P., Chatterjee, S., Kesarwani, P., Thyagarajan, K., Iamsawat, S., Dalheim, A., Nguyen, H., Selvam, S. P., Nasarre, P., Scurti, G., Hardiman, G., Maulik, N., Ball, L., Gangaraju, V., Rubinstein, M. P., Klauber-DeMore, N., Hill, E. G., Ogretmen, B., Yu, X.-Z., Nishimura, M. I., and Mehrotra, S. (2019) Thioredoxin-1 improves the immunometabolic phenotype of antitumor T cells. *The Journal of biological chemistry* **294**, 9198–9212 10.1074/jbc.RA118.006753 PMID 30971427
250. Muri, J., and Kopf, M. (2021) Redox regulation of immunometabolism. *Nature reviews. Immunology* **21**, 363–381 10.1038/s41577-020-00478-8 PMID 33340021
251. Levring, T. B., Kongsbak, M., Rode, A. K. O., Woetmann, A., Ødum, N., Bonefeld, C. M., and Geisler, C. (2015) Human CD4+ T cells require exogenous cystine for glutathione and DNA synthesis. *Oncotarget* **6**, 21853–21864 10.18632/oncotarget.5213 PMID 26392411
252. Muri, J., Heer, S., Matsushita, M., Pohlmeier, L., Tortola, L., Fuhrer, T., Conrad, M., Zamboni, N., Kisielow, J., and Kopf, M. (2018) The thioredoxin-1 system is essential for fueling DNA

synthesis during T-cell metabolic reprogramming and proliferation. *Nature communications* **9**, 1851 10.1038/s41467-018-04274-w PMID 29749372
253. Hariharan, S., and Dharmaraj, S. (2020) Selenium and selenoproteins: it's role in regulation of inflammation. *Inflammopharmacology* **28**, 667–695 10.1007/s10787-020-00690-x PMID 32144521
254. Kurokawa, S., Eriksson, S., Rose, K. L., Wu, S., Motley, A. K., Hill, S., Winfrey, V. P., McDonald, W. H., Capecchi, M. R., Atkins, J. F., Arnér, E. S. J., Hill, K. E., and Burk, R. F. (2014) Sepp1(UF) forms are N-terminal selenoprotein P truncations that have peroxidase activity when coupled with thioredoxin reductase-1. *Free radical biology & medicine* **69**, 67–76 10.1016/j.freeradbiomed.2014.01.010 PMID 24434121
255. Burk, R. F., and Hill, K. E. (2005) Selenoprotein P: an extracellular protein with unique physical characteristics and a role in selenium homeostasis. *Annual review of nutrition* **25**, 215–235 10.1146/annurev.nutr.24.012003.132120 PMID 16011466
256. Hu, Y., Feng, W., Chen, H., Shi, H., Jiang, L., Zheng, X., Liu, X., Zhang, W., Ge, Y., Liu, Y., and Cui, D. (2021) Effect of selenium on thyroid autoimmunity and regulatory T cells in patients with Hashimoto's thyroiditis: A prospective randomized-controlled trial. *Clinical and translational science* **14**, 1390–1402 10.1111/cts.12993 PMID 33650299
257. Chatila, T., Silverman, L., Miller, R., and Geha, R. (1989) Mechanisms of T cell activation by the calcium ionophore ionomycin. *Journal of immunology (Baltimore, Md. : 1950)* **143**, 1283–1289 PMID 2545785
258. Oh-hora, M. (2009) Calcium signaling in the development and function of T-lineage cells. *Immunological reviews* **231**, 210–224 10.1111/j.1600-065x.2009.00819.x PMID 19754899
259. Matthews, S. A., and Cantrell, D. A. (2009) New insights into the regulation and function of serine/threonine kinases in T lymphocytes. *Immunological reviews* **228**, 241–252 10.1111/j.1600-065x.2008.00759.x PMID 19290932
260. Kunkl, M., Amormino, C., Caristi, S., Tedeschi, V., Fiorillo, M. T., Levy, R., Popugailo, A., Kaempfer, R., and Tuosto, L. (2021) Binding of Staphylococcal Enterotoxin B (SEB) to B7 Receptors Triggers TCR- and CD28-Mediated Inflammatory Signals in the Absence of MHC Class II Molecules. *Frontiers in immunology* **12**, 723689 10.3389/fimmu.2021.723689 PMID 34489975
261. Marrack, P., Blackman, M., Kushnir, E., and Kappler, J. (1990) The toxicity of staphylococcal enterotoxin B in mice is mediated by T cells. *The Journal of experimental medicine* **171**, 455–464 10.1084/jem.171.2.455 PMID 2303780
262. Zhang, H., Monk, I. R., Braverman, J., Jones, C. M., Brooks, A. G., Stinear, T. P., and Wakim, L. M. (2024) Staphylococcal superantigens evoke temporary and reversible T cell anergy, but fail to block the development of a bacterium specific cellular immune response. *Nature communications* **15**, 9872 10.1038/s41467-024-54074-8 PMID 39543088
263. Krakauer, T. (2019) Staphylococcal Superantigens: Pyrogenic Toxins Induce Toxic Shock. *Toxins* **11** 10.3390/toxins11030178 PMID 30909619
264. Szabo, P. A., Goswami, A., Mazzuca, D. M., Kim, K., O'Gorman, D. B., Hess, D. A., Welch, I. D., Young, H. A., Singh, B., McCormick, J. K., and Haeryfar, S. M. M. (2017) Rapid and Rigorous IL-17A Production by a Distinct Subpopulation of Effector Memory T Lymphocytes Constitutes a Novel Mechanism of Toxic Shock Syndrome Immunopathology. *Journal of immunology (Baltimore, Md. : 1950)* **198**, 2805–2818 10.4049/jimmunol.1601366 PMID 28219889
265. Laurence, A., Tato, C. M., Davidson, T. S., Kanno, Y., Chen, Z., Yao, Z., Blank, R. B., Meylan, F., Siegel, R., Hennighausen, L., Shevach, E. M., and O'Shea, J. J. (2007) Interleukin-2 signaling via STAT5 constrains T helper 17 cell generation. *Immunity* **26**, 371–381 10.1016/j.immuni.2007.02.009 PMID 17363300
266. Pagliarani, A., Nesci, S., and Ventrella, V. (2013) Modifiers of the oligomycin sensitivity of the mitochondrial F1F0-ATPase. *Mitochondrion* **13**, 312–319 10.1016/j.mito.2013.04.005 PMID 23597783
267. Xiong, G., Zhang, K., Ma, Y., Song, Y., Zhang, W., Qi, T., Qiu, H., Shi, J., Kan, C., Zhang, J., and Sun, X. (2023) BAM15 as a mitochondrial uncoupler: a promising therapeutic agent for

diverse diseases. *Frontiers in endocrinology* **14**, 1252141 10.3389/fendo.2023.1252141 PMID 37900126

268. Zikaki, K., Kiachaki, E., Gaitanaki, C., and Aggeli, I.-K. (2025) "Villains" Turning Good: Antimycin A and Rotenone, Mitochondrial Respiratory Chain Inhibitors, Protect H9c2 Cardiac Cells Against Insults Triggering the Intrinsic Apoptotic Pathway. *International journal of molecular sciences* **26** 10.3390/ijms26062435 PMID 40141079
269. Żuberek, M., Paciorek, P., Rakowski, M., and Grzelak, A. (2022) How to Use Respiratory Chain Inhibitors in Toxicology Studies-Whole-Cell Measurements. *International journal of molecular sciences* **23** 10.3390/ijms23169076 PMID 36012337
270. Chacko, B. K., Kramer, P. A., Ravi, S., Benavides, G. A., Mitchell, T., Dranka, B. P., Ferrick, D., Singal, A. K., Ballinger, S. W., Bailey, S. M., Hardy, R. W., Zhang, J., Zhi, D., and Darley-Usmar, V. M. (2014) The Bioenergetic Health Index: a new concept in mitochondrial translational research. *Clinical science (London, England : 1979)* **127**, 367–373 10.1042/CS20140101 PMID 24895057
271. Dranka, B. P., Hill, B. G., and Darley-Usmar, V. M. (2010) Mitochondrial reserve capacity in endothelial cells: The impact of nitric oxide and reactive oxygen species. *Free radical biology & medicine* **48**, 905–914 10.1016/j.freeradbiomed.2010.01.015 PMID 20093177
272. Hill, B. G., Benavides, G. A., Lancaster, J. R., Ballinger, S., Dell'Italia, L., Jianhua, Z., and Darley-Usmar, V. M. (2012) Integration of cellular bioenergetics with mitochondrial quality control and autophagy. *Biological chemistry* **393**, 1485–1512 10.1515/hsz-2012-0198 PMID 23092819
273. Sun, W., Zhu, C., Li, Y., Wu, X., Shi, X., and Liu, W. (2024) B cell activation and autoantibody production in autoimmune diseases. *Best practice & research. Clinical rheumatology* **38**, 101936 10.1016/j.berh.2024.101936 PMID 38326197
274. Kulkarni, H. S. (2024) Hexamerization: explaining the original sin of IgG-mediated complement activation in acute lung injury. *The Journal of clinical investigation* **134** 10.1172/JCI181137 PMID 38828725
275. Koike, T., Yamagishi, H., Hatanaka, Y., Fukushima, A., Chang, J., Xia, Y., Fields, M., Chandler, P., and Iwashima, M. (2003) A novel ERK-dependent signaling process that regulates interleukin-2 expression in a late phase of T cell activation. *The Journal of biological chemistry* **278**, 15685–15692 10.1074/jbc.M210829200 PMID 12595531
276. Tsukamoto, H., Irie, A., and Nishimura, Y. (2004) B-Raf contributes to sustained extracellular signal-regulated kinase activation associated with interleukin-2 production stimulated through the T cell receptor. *The Journal of biological chemistry* **279**, 48457–48465 10.1074/jbc.M403087200 PMID 15339934
277. Whitehurst, C. E., and Geppert, T. D. (1996) MEK1 and the extracellular signal-regulated kinases are required for the stimulation of IL-2 gene transcription in T cells. *Journal of immunology (Baltimore, Md. : 1950)* **156**, 1020–1029 PMID 8557975
278. Balagopalan, L., Kortum, R. L., Coussens, N. P., Barr, V. A., and Samelson, L. E. (2015) The linker for activation of T cells (LAT) signaling hub: from signaling complexes to microclusters. *The Journal of biological chemistry* **290**, 26422–26429 10.1074/jbc.R115.665869 PMID 26354432
279. Lo, W.-L., Shah, N. H., Ahsan, N., Horkova, V., Stepanek, O., Salomon, A. R., Kuriyan, J., and Weiss, A. (2018) Lck promotes Zap70-dependent LAT phosphorylation by bridging Zap70 to LAT. *Nature immunology* **19**, 733–741 10.1038/s41590-018-0131-1 PMID 29915297
280. Adachi, K., and Davis, M. M. (2011) T-cell receptor ligation induces distinct signaling pathways in naive vs. antigen-experienced T cells. *Proceedings of the National Academy of Sciences of the United States of America* **108**, 1549–1554 10.1073/pnas.1017340108 PMID 21205892
281. Atherfold, P. A., Norris, M. S., Robinson, P. J., Gelfand, E. W., and Franklin, R. A. (1999) Calcium-induced ERK activation in human T lymphocytes. *Molecular immunology* **36**, 543–549 10.1016/s0161-5890(99)00076-0 PMID 10475609
282. Thastrup, O., Cullen, P. J., Drøbak, B. K., Hanley, M. R., and Dawson, A. P. (1990) Thapsigargin, a tumor promoter, discharges intracellular Ca2+ stores by specific inhibition of the

endoplasmic reticulum Ca2(+)-ATPase. *Proceedings of the National Academy of Sciences of the United States of America* **87**, 2466–2470 10.1073/pnas.87.7.2466 PMID 2138778
283. Crispín, J. C., and Tsokos, G. C. (2009) Transcriptional regulation of IL-2 in health and autoimmunity. *Autoimmunity reviews* **8**, 190–195 10.1016/j.autrev.2008.07.042 PMID 18723131
284. Hogan, P. G. (2017) Calcium-NFAT transcriptional signalling in T cell activation and T cell exhaustion. *Cell calcium* **63**, 66–69 10.1016/j.ceca.2017.01.014 PMID 28153342
285. Pollizzi, K. N., and Powell, J. D. (2015) Regulation of T cells by mTOR: the known knowns and the known unknowns. *Trends in immunology* **36**, 13–20 10.1016/j.it.2014.11.005 PMID 25522665
286. Kane, L. P., Andres, P. G., Howland, K. C., Abbas, A. K., and Weiss, A. (2001) Akt provides the CD28 costimulatory signal for up-regulation of IL-2 and IFN-gamma but not TH2 cytokines. *Nature immunology* **2**, 37–44 10.1038/83144 PMID 11135576
287. Marcais, A., Blevins, R., Graumann, J., Feytout, A., Dharmalingam, G., Carroll, T., Amado, I. F., Bruno, L., Lee, K., Walzer, T., Mann, M., Freitas, A. A., Boothby, M., Fisher, A. G., and Merkenschlager, M. (2014) microRNA-mediated regulation of mTOR complex components facilitates discrimination between activation and anergy in CD4 T cells. *The Journal of experimental medicine* **211**, 2281–2295 10.1084/jem.20132059 PMID 25311506
288. Battini, J. L., Rasko, J. E., and Miller, A. D. (1999) A human cell-surface receptor for xenotropic and polytropic murine leukemia viruses: possible role in G protein-coupled signal transduction. *Proceedings of the National Academy of Sciences of the United States of America* **96**, 1385–1390 10.1073/pnas.96.4.1385 PMID 9990033
289. Giovannini, D., Touhami, J., Charnet, P., Sitbon, M., and Battini, J.-L. (2013) Inorganic phosphate export by the retrovirus receptor XPR1 in metazoans. *Cell reports* **3**, 1866–1873 10.1016/j.celrep.2013.05.035 PMID 23791524
290. Zhou, Y., Mukherjee, S., Huang, D., Chakraborty, M., Gu, C., Zong, G., Stashko, M. A., Pearce, K. H., Shears, S. B., Chakraborty, A., Wang, H., and Wang, X. (2022) Development of Novel IP6K Inhibitors for the Treatment of Obesity and Obesity-Induced Metabolic Dysfunctions. *Journal of medicinal chemistry* **65**, 6869–6887 10.1021/acs.jmedchem.2c00220 PMID 35467861
291. Chakkour, M., and Greenberg, M. L. (2024) Insights into the roles of inositol hexakisphosphate kinase 1 (IP6K1) in mammalian cellular processes. *The Journal of biological chemistry* **300**, 107116 10.1016/j.jbc.2024.107116 PMID 38403246
292. Riley, J. L., and June, C. H. (2005) The CD28 family: a T-cell rheostat for therapeutic control of T-cell activation. *Blood* **105**, 13–21 10.1182/blood-2004-04-1596 PMID 15353480
293. Gamir-Morralla, A., López-Menéndez, C., Ayuso-Dolado, S., Tejeda, G. S., Montaner, J., Rosell, A., Iglesias, T., and Díaz-Guerra, M. (2015) Development of a neuroprotective peptide that preserves survival pathways by preventing Kidins220/ARMS calpain processing induced by excitotoxicity. *Cell death & disease* **6**, e1939 10.1038/cddis.2015.307 PMID 26492372
294. Dixon, J. F., Law, J. L., and Favero, J. J. (1989) Activation of human T lymphocytes by crosslinking of anti-CD3 monoclonal antibodies. *Journal of leukocyte biology* **46**, 214–220 10.1002/jlb.46.3.214 PMID 2788205
295. Walker, C., Bettens, F., and Pichler, W. J. (1987) T cell activation by cross-linking anti-CD3 antibodies with second anti-T cell antibodies: dual antibody cross-linking mimics physical monocyte interaction. *Eur. J. Immunol.* **17**, 1611–1618 10.1002/eji.1830171114 PMID 2960544
296. Beyersdorf, N., Kerkau, T., and Hünig, T. (2015) CD28 co-stimulation in T-cell homeostasis: a recent perspective. *ImmunoTargets and therapy* **4**, 111–122 10.2147/ITT.S61647 PMID 27471717
297. Lantz, O., Grandjean, I., Matzinger, P., and Di Santo, J. P. (2000) Gamma chain required for naïve CD4+ T cell survival but not for antigen proliferation. *Nature immunology* **1**, 54–58 10.1038/76917 PMID 10881175
298. Valujskikh, A., Lantz, O., Celli, S., Matzinger, P., and Heeger, P. S. (2002) Cross-primed CD8(+) T cells mediate graft rejection via a distinct effector pathway. *Nature immunology* **3**, 844–851 10.1038/ni831 PMID 12172545

299. Grandjean, I., Duban, L., Bonney, E. A., Corcuff, E., Di Santo, J. P., Matzinger, P., and Lantz, O. (2003) Are major histocompatibility complex molecules involved in the survival of naive CD4+ T cells? *The Journal of experimental medicine* **198**, 1089–1102 10.1084/jem.20030963 PMID 14517277
300. Perez-Diez, A., Joncker, N. T., Choi, K., Chan, W. F. N., Anderson, C. C., Lantz, O., and Matzinger, P. (2007) CD4 cells can be more efficient at tumor rejection than CD8 cells. *Blood* **109**, 5346–5354 10.1182/blood-2006-10-051318 PMID 17327412
301. Jelley-Gibbs, D. M., Dibble, J. P., Filipson, S., Haynes, L., Kemp, R. A., and Swain, S. L. (2005) Repeated stimulation of CD4 effector T cells can limit their protective function. *The Journal of experimental medicine* **201**, 1101–1112 10.1084/jem.20041852 PMID 15795235
302. Mailer, R. K., Konrath, S., Zhan, L., Thode, H., Beerens, M., Frye, M., Ketelhuth, D. F. J., Renné, T., and Hansson, G. K. (2023) Repetitive Antigen Responses of LDL-Reactive CD4+ T Cells Induce Tr1 Cell-Mediated Immune Tolerance. *Arteriosclerosis, thrombosis, and vascular biology* **43**, 1510–1523 10.1161/ATVBAHA.123.319135 PMID 37259863
303. Prlic, M., Blazar, B. R., Khoruts, A., Zell, T., and Jameson, S. C. (2001) Homeostatic expansion occurs independently of costimulatory signals. *Journal of immunology (Baltimore, Md. : 1950)* **167**, 5664–5668 10.4049/jimmunol.167.10.5664 PMID 11698438
304. Chen, Y., Liang, W., Yang, S., Wu, N., Gao, H., Sheng, J., Yao, H., Wo, J., Fang, Q., Cui, D., Li, Y., Yao, X., Zhang, Y., Wu, H., Zheng, S., Diao, H., Xia, S., Zhang, Y., Chan, K.-H., Tsoi, H.-W., Teng, J. L.-L., Song, W., Wang, P., Lau, S.-Y., Zheng, M., Chan, J. F.-W., To, K. K.-W., Chen, H., Li, L., and Yuen, K.-Y. (2013) Human infections with the emerging avian influenza A H7N9 virus from wet market poultry: clinical analysis and characterisation of viral genome. *Lancet (London, England)* **381**, 1916–1925 10.1016/S0140-6736(13)60903-4 PMID 23623390
305. Min, B., McHugh, R., Sempowski, G. D., Mackall, C., Foucras, G., and Paul, W. E. (2003) Neonates support lymphopenia-induced proliferation. *Immunity* **18**, 131–140 10.1016/s1074-7613(02)00508-3 PMID 12530982
306. Surh, C. D., and Sprent, J. (2000) Homeostatic T cell proliferation: how far can T cells be activated to self-ligands? *The Journal of experimental medicine* **192**, F9-F14 10.1084/jem.192.4.f9 PMID 10952731
307. Min, B. (2018) Spontaneous T Cell Proliferation: A Physiologic Process to Create and Maintain Homeostatic Balance and Diversity of the Immune System. *Frontiers in immunology* **9**, 547 10.3389/fimmu.2018.00547 PMID 29616038
308. Wege, S., and Poirier, Y. (2014) Expression of the mammalian Xenotropic Polytropic Virus Receptor 1 (XPR1) in tobacco leaves leads to phosphate export. *FEBS letters* **588**, 482–489 10.1016/j.febslet.2013.12.013 PMID 24374333
309. Jennings, M. L. (2023) Role of transporters in regulating mammalian intracellular inorganic phosphate. *Frontiers in pharmacology* **14**, 1163442 10.3389/fphar.2023.1163442 PMID 37063296
310. Lu, Y., Yue, C.-X., Zhang, L., Yao, D., Xia, Y., Zhang, Q., Zhang, X., Li, S., Shen, Y., Cao, M., Guo, C.-R., an Qin, Zhao, J., Zhou, L., Yu, Y., and Cao, Y. (2024) Structural basis for inositol pyrophosphate gating of the phosphate channel XPR1. *Science (New York, N.Y.)* **386**, eadp3252 10.1126/science.adp3252 PMID 39325866
311. Bass, J. J., Wilkinson, D. J., Rankin, D., Phillips, B. E., Szewczyk, N. J., Smith, K., and Atherton, P. J. (2017) An overview of technical considerations for Western blotting applications to physiological research. *Scandinavian journal of medicine & science in sports* **27**, 4–25 10.1111/sms.12702 PMID 27263489
312. Holden, P., and Horton, W. A. (2009) Crude subcellular fractionation of cultured mammalian cell lines. *BMC research notes* **2**, 243 10.1186/1756-0500-2-243 PMID 20003239
313. Tsuji, Y. (2020) Transmembrane protein western blotting: Impact of sample preparation on detection of SLC11A2 (DMT1) and SLC40A1 (ferroportin). *PloS one* **15**, e0235563 10.1371/journal.pone.0235563 PMID 32645092

314. Xiao, Y.-X., Wei, J., Philip, R., Sharma, A., Pelletier, L., and Moffat, J. (2024) Protocol for CRISPR-based endogenous protein tagging in mammalian cells. *STAR Protocols* **5**, 103404 10.1016/j.xpro.2024.103404
315. Zhao, C., Cao, Y., Ibrahim, N., Wang, Y., and Martemyanov, K. A. (2025) Efficient in vivo labeling of endogenous proteins with SMART delineates retina cellular and synaptic organization. *Nature communications* **16**, 3768 10.1038/s41467-025-58945-6 PMID 40263339
316. Koch, B., Nijmeijer, B., Kueblbeck, M., Cai, Y., Walther, N., and Ellenberg, J. (2018) Generation and validation of homozygous fluorescent knock-in cells using CRISPR-Cas9 genome editing. *Nature protocols* **13**, 1465–1487 10.1038/nprot.2018.042 PMID 29844520
317. McDonald, D. T., Wang, P. S., Moitoza Johnson, J., and Tsai, M.-S. (2023) Using Affinity Pulldown Assays to Study Protein-Protein Interactions of Human NEIL1 Glycosylase and the Checkpoint Protein RAD9-RAD1-HUS1 (9-1-1) Complex. *Methods in molecular biology (Clifton, N.J.)* **2701**, 199–207 10.1007/978-1-0716-3373-1_13 PMID 37574484
318. Wolfer, A., Wilson, A., Nemir, M., MacDonald, H. R., and Radtke, F. (2002) Inactivation of Notch1 impairs VDJbeta rearrangement and allows pre-TCR-independent survival of early alpha beta Lineage Thymocytes. *Immunity* **16**, 869–879 10.1016/s1074-7613(02)00330-8 PMID 12121668
319. Shen, S., Zhu, M., Lau, J., Chuck, M., and Zhang, W. (2009) The essential role of LAT in thymocyte development during transition from the double-positive to single-positive stage. *Journal of immunology (Baltimore, Md. : 1950)* **182**, 5596–5604 10.4049/jimmunol.0803170 PMID 19380807
320. Smid, A. I., Garforth, S. J., Obaid, M. S., Bollons, H. R., and James, J. R. (2023) Pre-T cell receptor localization and trafficking are independent of its signaling. *The Journal of cell biology* **222** 10.1083/jcb.202212106 PMID 37516909
321. Yamashita, I., Nagata, T., Tada, T., and Nakayama, T. (1993) CD69 cell surface expression identifies developing thymocytes which audition for T cell antigen receptor-mediated positive selection. *International immunology* **5**, 1139–1150 10.1093/intimm/5.9.1139 PMID 7902130
322. Hsieh, C.-S., Zheng, Y., Liang, Y., Fontenot, J. D., and Rudensky, A. Y. (2006) An intersection between the self-reactive regulatory and nonregulatory T cell receptor repertoires. *Nature immunology* **7**, 401–410 10.1038/ni1318 PMID 16532000
323. Hsieh, C.-S., Liang, Y., Tyznik, A. J., Self, S. G., Liggitt, D., and Rudensky, A. Y. (2004) Recognition of the peripheral self by naturally arising CD25+ CD4+ T cell receptors. *Immunity* **21**, 267–277 10.1016/j.immuni.2004.07.009 PMID 15308106
324. Rogers, D., Sood, A., Wang, H., van Beek, J. J. P., Rademaker, T. J., Artusa, P., Schneider, C., Shen, C., Wong, D. C., Bhagrath, A., Lebel, M.-È., Condotta, S. A., Richer, M. J., Martins, A. J., Tsang, J. S., Barreiro, L. B., François, P., Langlais, D., Melichar, H. J., Textor, J., and Mandl, J. N. (2021) Pre-existing chromatin accessibility and gene expression differences among naive CD4+ T cells influence effector potential. *Cell reports* **37**, 110064 10.1016/j.celrep.2021.110064 PMID 34852223
325. Fulton, R. B., Hamilton, S. E., Xing, Y., Best, J. A., Goldrath, A. W., Hogquist, K. A., and Jameson, S. C. (2015) The TCR's sensitivity to self peptide-MHC dictates the ability of naive CD8(+) T cells to respond to foreign antigens. *Nature immunology* **16**, 107–117 10.1038/ni.3043 PMID 25419629
326. Henderson, J. G., Opejin, A., Jones, A., Gross, C., and Hawiger, D. (2015) CD5 instructs extrathymic regulatory T cell development in response to self and tolerizing antigens. *Immunity* **42**, 471–483 10.1016/j.immuni.2015.02.010 PMID 25786177
327. Mandl, J. N., Monteiro, J. P., Vrisekoop, N., and Germain, R. N. (2013) T cell-positive selection uses self-ligand binding strength to optimize repertoire recognition of foreign antigens. *Immunity* **38**, 263–274 10.1016/j.immuni.2012.09.011 PMID 23290521
328. Martin, B., Auffray, C., Delpoux, A., Pommier, A., Durand, A., Charvet, C., Yakonowsky, P., Boysson, H. de, Bonilla, N., Audemard, A., Sparwasser, T., Salomon, B. L., Malissen, B., and

Lucas, B. (2013) Highly self-reactive naive CD4 T cells are prone to differentiate into regulatory T cells. *Nature communications* **4**, 2209 10.1038/ncomms3209 PMID 23900386
329. Matson, C. A., Choi, S., Livak, F., Zhao, B., Mitra, A., Love, P. E., and Singh, N. J. (2020) CD5 dynamically calibrates basal NF-κB signaling in T cells during thymic development and peripheral activation. *Proceedings of the National Academy of Sciences of the United States of America* **117**, 14342–14353 10.1073/pnas.1922525117 PMID 32513716
330. Persaud, S. P., Parker, C. R., Lo, W.-L., Weber, K. S., and Allen, P. M. (2014) Intrinsic CD4+ T cell sensitivity and response to a pathogen are set and sustained by avidity for thymic and peripheral complexes of self peptide and MHC. *Nature immunology* **15**, 266–274 10.1038/ni.2822 PMID 24487322
331. Sood, A., Lebel, M.-È., Fournier, M., Rogers, D., Mandl, J. N., and Melichar, H. J. (2019) Differential interferon-gamma production potential among naïve CD4+ T cells exists prior to antigen encounter. *Immunology and cell biology* **97**, 931–940 10.1111/imcb.12287 PMID 31420892
332. Kreisel, D., Sankaran, D., Wells, A. D., and Turka, L. A. (2002) Interleukin-2-mediated survival and proliferative signals are uncoupled in T lymphocytes that fail to divide after activation. *American journal of transplantation : official journal of the American Society of Transplantation and the American Society of Transplant Surgeons* **2**, 120–128 10.1034/j.1600-6143.2002.020202.x PMID 12099513
333. Ross, S. H., and Cantrell, D. A. (2018) Signaling and Function of Interleukin-2 in T Lymphocytes. *Annual review of immunology* **36**, 411–433 10.1146/annurev-immunol-042617-053352 PMID 29677473
334. Baaten, B. J., Li, C.-R., and Bradley, L. M. (2010) Multifaceted regulation of T cells by CD44. *Communicative & integrative biology* **3**, 508–512 10.4161/cib.3.6.13495 PMID 21331226
335. DeGrendele, H. C., Estess, P., and Siegelman, M. H. (1997) Requirement for CD44 in Activated T Cell Extravasation into an Inflammatory Site. *Science (New York, N.Y.)* **278**, 672–675 10.1126/science.278.5338.672
336. Goodison, S., Urquidi, V., and Tarin, D. (1999) CD44 cell adhesion molecules. *Molecular pathology : MP* **52**, 189–196 10.1136/mp.52.4.189 PMID 10694938
337. Hegde, V. L., Singh, N. P., Nagarkatti, P. S., and Nagarkatti, M. (2008) CD44 mobilization in allogeneic dendritic cell-T cell immunological synapse plays a key role in T cell activation. *Journal of leukocyte biology* **84**, 134–142 10.1189/jlb.1107752 PMID 18388297
338. Poloni, C., Schonhofer, C., Ivison, S., Levings, M. K., Steiner, T. S., and Cook, L. (2023) T-cell activation-induced marker assays in health and disease. *Immunology and cell biology* **101**, 491–503 10.1111/imcb.12636 PMID 36825901
339. Shatrova, A. N., Mityushova, E. V., Vassilieva, I. O., Aksenov, N. D., Zenin, V. V., Nikolsky, N. N., and Marakhova, I. I. (2016) Time-Dependent Regulation of IL-2R α-Chain (CD25) Expression by TCR Signal Strength and IL-2-Induced STAT5 Signaling in Activated Human Blood T Lymphocytes. *PloS one* **11**, e0167215 10.1371/journal.pone.0167215 PMID 27936140
340. Peng, Y., Tao, Y., Zhang, Y., Wang, J., Yang, J., and Wang, Y. (2023) CD25: A potential tumor therapeutic target. *International journal of cancer* **152**, 1290–1303 10.1002/ijc.34281 PMID 36082452
341. Malek, T. R., Robb, R. J., and Shevach, E. M. (1983) Identification and initial characterization of a rat monoclonal antibody reactive with the murine interleukin 2 receptor-ligand complex. *Proceedings of the National Academy of Sciences of the United States of America* **80**, 5694–5698 10.1073/pnas.80.18.5694 PMID 6412230
342. McHugh, R. S., Shevach, E. M., and Thornton, A. M. (2001) Control of organ-specific autoimmunity by immunoregulatory CD4(+)CD25(+) T cells. *Microbes and infection* **3**, 919–927 10.1016/S1286-4579(01)01453-8 PMID 11564440
343. Gorabi, A. M., Hajighasemi, S., Kiaie, N., Gheibi Hayat, S. M., Jamialahmadi, T., Johnston, T. P., and Sahebkar, A. (2020) The pivotal role of CD69 in autoimmunity. *Journal of autoimmunity* **111**, 102453 10.1016/j.jaut.2020.102453 PMID 32291138

344. Radulovic, K., and Niess, J. H. (2015) CD69 is the crucial regulator of intestinal inflammation: a new target molecule for IBD treatment? *Journal of immunology research* **2015**, 497056 10.1155/2015/497056 PMID 25759842
345. Galkina, E., Tanousis, K., Preece, G., Tolaini, M., Kioussis, D., Florey, O., Haskard, D. O., Tedder, T. F., and Ager, A. (2003) L-selectin shedding does not regulate constitutive T cell trafficking but controls the migration pathways of antigen-activated T lymphocytes. *The Journal of experimental medicine* **198**, 1323–1335 10.1084/jem.20030485 PMID 14597735
346. Hengel, R. L., Thaker, V., Pavlick, M. V., Metcalf, J. A., Dennis, G., Yang, J., Lempicki, R. A., Sereti, I., and Lane, H. C. (2003) Cutting edge: L-selectin (CD62L) expression distinguishes small resting memory CD4+ T cells that preferentially respond to recall antigen. *Journal of immunology (Baltimore, Md. : 1950)* **170**, 28–32 10.4049/jimmunol.170.1.28 PMID 12496379
347. Kahn, J., Ingraham, R. H., Shirley, F., Migaki, G. I., and Kishimoto, T. K. (1994) Membrane proximal cleavage of L-selectin: identification of the cleavage site and a 6-kD transmembrane peptide fragment of L-selectin. *The Journal of cell biology* **125**, 461–470 10.1083/jcb.125.2.461 PMID 7512970
348. Peschon, J. J., Slack, J. L., Reddy, P., Stocking, K. L., Sunnarborg, S. W., Lee, D. C., Russell, W. E., Castner, B. J., Johnson, R. S., Fitzner, J. N., Boyce, R. W., Nelson, N., Kozlosky, C. J., Wolfson, M. F., Rauch, C. T., Cerretti, D. P., Paxton, R. J., March, C. J., and Black, R. A. (1998) An essential role for ectodomain shedding in mammalian development. *Science (New York, N.Y.)* **282**, 1281–1284 10.1126/science.282.5392.1281 PMID 9812885
349. Tedder, T. F., Steeber, D. A., and Pizcueta, P. (1995) L-selectin-deficient mice have impaired leukocyte recruitment into inflammatory sites. *The Journal of experimental medicine* **181**, 2259–2264 10.1084/jem.181.6.2259
350. Arbonés, M. L., Ord, D. C., Ley, K., Ratech, H., Maynard-Curry, C., Otten, G., Capon, D. J., and Tedder, T. F. (1994) Lymphocyte homing and leukocyte rolling and migration are impaired in L-selectin-deficient mice. *Immunity* **1**, 247–260 10.1016/1074-7613(94)90076-0 PMID 7534203
351. Bradley, L. M., Watson, S. R., and Swain, S. L. (1994) Entry of naive CD4 T cells into peripheral lymph nodes requires L-selectin. *The Journal of experimental medicine* **180**, 2401–2406 10.1084/jem.180.6.2401 PMID 7525854
352. Chen, A., Engel, P., and Tedder, T. F. (1995) Structural requirements regulate endoproteolytic release of the L-selectin (CD62L) adhesion receptor from the cell surface of leukocytes. *The Journal of experimental medicine* **182**, 519–530 10.1084/jem.182.2.519 PMID 7543141
353. Campbell, J. J., Bowman, E. P., Murphy, K., Youngman, K. R., Siani, M. A., Thompson, D. A., Wu, L., Zlotnik, A., and Butcher, E. C. (1998) 6-C-kine (SLC), a lymphocyte adhesion-triggering chemokine expressed by high endothelium, is an agonist for the MIP-3beta receptor CCR7. *The Journal of cell biology* **141**, 1053–1059 10.1083/jcb.141.4.1053 PMID 9585422
354. Förster, R., Schubel, A., Breitfeld, D., Kremmer, E., Renner-Müller, I., Wolf, E., and Lipp, M. (1999) CCR7 coordinates the primary immune response by establishing functional microenvironments in secondary lymphoid organs. *Cell* **99**, 23–33 10.1016/s0092-8674(00)80059-8 PMID 10520991
355. Sallusto, F., Lenig, D., Förster, R., Lipp, M., and Lanzavecchia, A. (1999) Two subsets of memory T lymphocytes with distinct homing potentials and effector functions. *Nature* **401**, 708–712 10.1038/44385 PMID 10537110
356. Sallusto, F., Geginat, J., and Lanzavecchia, A. (2004) Central memory and effector memory T cell subsets: function, generation, and maintenance. *Annual review of immunology* **22**, 745–763 10.1146/annurev.immunol.22.012703.104702 PMID 15032595
357. Yang, S., Liu, F., Wang, Q. J., Rosenberg, S. A., and Morgan, R. A. (2011) The shedding of CD62L (L-selectin) regulates the acquisition of lytic activity in human tumor reactive T lymphocytes. *PloS one* **6**, e22560 10.1371/journal.pone.0022560 PMID 21829468

358. Baumeister, S. H., Freeman, G. J., Dranoff, G., and Sharpe, A. H. (2016) Coinhibitory Pathways in Immunotherapy for Cancer. *Annual review of immunology* **34**, 539–573 10.1146/annurev-immunol-032414-112049 PMID 26927206
359. Nettersheim, F. S., Brunel, S., Sinkovits, R. S., Armstrong, S. S., Roy, P., Billitti, M., Kobiyama, K., Alimadadi, A., Bombin, S., Lu, L., Zoccheddu, M., Oliaeimotlagh, M., Benedict, C. A., Sette, A., and Ley, K. (2025) PD-1 and CD73 on naive CD4+ T cells synergistically limit responses to self. *Nature immunology* **26**, 105–115 10.1038/s41590-024-02021-6 PMID 39572641
360. Kaempfer, R. (2018) Bacterial Superantigen Toxins, CD28, and Drug Development. *Toxins* **10** 10.3390/toxins10110459 PMID 30404186
361. Ramachandran, G. (2014) Gram-positive and gram-negative bacterial toxins in sepsis: a brief review. *Virulence* **5**, 213–218 10.4161/viru.27024 PMID 24193365
362. Kunkl, M., Amormino, C., Spallotta, F., Caristi, S., Fiorillo, M. T., Paiardini, A., Kaempfer, R., and Tuosto, L. (2023) Bivalent binding of staphylococcal superantigens to the TCR and CD28 triggers inflammatory signals independently of antigen presenting cells. *Frontiers in immunology* **14**, 1170821 10.3389/fimmu.2023.1170821 PMID 37207220
363. Ivashkiv, L. B. (2018) IFNγ: signalling, epigenetics and roles in immunity, metabolism, disease and cancer immunotherapy. *Nature reviews. Immunology* **18**, 545–558 10.1038/s41577-018-0029-z PMID 29921905
364. Djuretic, I. M., Levanon, D., Negreanu, V., Groner, Y., Rao, A., and Ansel, K. M. (2007) Transcription factors T-bet and Runx3 cooperate to activate Ifng and silence Il4 in T helper type 1 cells. *Nature immunology* **8**, 145–153 10.1038/ni1424 PMID 17195845
365. Zhong, L., Wang, Y.-H., Kahlfuss, S., Jishage, M., McDermott, M., Yang, J., Tao, A. Y., Hu, K., Noyer, L., Raphael, D., Patel, D., Knight, T. E., Chitlur, M., Machaca, K., and Feske, S. (2025) STIM1-mediated NFAT signaling synergizes with STAT1 to control T-bet expression and TH1 differentiation. *Nature immunology* **26**, 484–496 10.1038/s41590-025-02089-8 PMID 39984734
366. Huangfu, L., Li, R., Huang, Y., and Wang, S. (2023) The IL-17 family in diseases: from bench to bedside. *Signal transduction and targeted therapy* **8**, 402 10.1038/s41392-023-01620-3 PMID 37816755
367. Eken, A., Singh, A. K., Treuting, P. M., and Oukka, M. (2014) IL-23R+ innate lymphoid cells induce colitis via interleukin-22-dependent mechanism. *Mucosal immunology* **7**, 143–154 10.1038/mi.2013.33 PMID 23715173
368. Dudakov, J. A., Hanash, A. M., and van den Brink, M. R. M. (2015) Interleukin-22: immunobiology and pathology. *Annual review of immunology* **33**, 747–785 10.1146/annurev-immunol-032414-112123 PMID 25706098
369. Giannou, A. D., Kempski, J., Shiri, A. M., Lücke, J., Zhang, T., Zhao, L., Zazara, D. E., Cortesi, F., Riecken, K., Amezcua Vesely, M. C., Low, J. S., Xu, H., Kaffe, E., Garcia-Perez, L., Agalioti, T., Yamada, Y., Jungraithmayr, W., Zigmond, E., Karstens, K.-F., Steglich, B., Wagner, J., Konczalla, L., Carambia, A., Schulze, K., Felden, J. von, May, P., Briukhovetska, D., Bedke, T., Brockmann, L., Starzonek, S., Lange, T., Koch, C., Riethdorf, S., Pelczar, P., Böttcher, M., Sabihi, M., Huber, F. J., Reeh, M., Grass, J. K., Wahib, R., Seese, H., Stüben, B.-O., Fard-Aghaie, M., Duprée, A., Scognamiglio, P., Plitzko, G., Meiners, J., Soukou, S., Wittek, A., Manthey, C., Maroulis, I. C., Arck, P. C., Perez, D., Gao, B., Zarogiannis, S. G., Strowig, T., Pasqualini, R., Arap, W., Gosálvez, J. S., Kobold, S., Prinz, I., Guse, A. H., Tachezy, M., Ghadban, T., Heumann, A., Li, J., Melling, N., Mann, O., Izbicki, J. R., Pantel, K., Schumacher, U., Lohse, A. W., Flavell, R. A., Gagliani, N., and Huber, S. (2023) Tissue resident iNKT17 cells facilitate cancer cell extravasation in liver metastasis via interleukin-22. *Immunity* **56**, 125-142.e12 10.1016/j.immuni.2022.12.014 PMID 36630911
370. Lazarevic, V., Chen, X., Shim, J.-H., Hwang, E.-S., Jang, E., Bolm, A. N., Oukka, M., Kuchroo, V. K., and Glimcher, L. H. (2011) T-bet represses T(H)17 differentiation by preventing Runx1-mediated activation of the gene encoding RORγt. *Nature immunology* **12**, 96–104 10.1038/ni.1969 PMID 21151104

371. Hirota, K., Duarte, J. H., Veldhoen, M., Hornsby, E., Li, Y., Cua, D. J., Ahlfors, H., Wilhelm, C., Tolaini, M., Menzel, U., Garefalaki, A., Potocnik, A. J., and Stockinger, B. (2011) Fate mapping of IL-17-producing T cells in inflammatory responses. *Nature immunology* **12**, 255–263 10.1038/ni.1993 PMID 21278737
372. Bouguermouh, S., Fortin, G., Baba, N., Rubio, M., and Sarfati, M. (2009) CD28 co-stimulation down regulates Th17 development. *PloS one* **4**, e5087 10.1371/journal.pone.0005087 PMID 19333372
373. Hori, S., Nomura, T., and Sakaguchi, S. (2003) Control of regulatory T cell development by the transcription factor Foxp3. *Science (New York, N.Y.)* **299**, 1057–1061 10.1126/science.1079490 PMID 12522256
374. Dardalhon, V., Korn, T., Kuchroo, V. K., and Anderson, A. C. (2008) Role of Th1 and Th17 cells in organ-specific autoimmunity. *Journal of autoimmunity* **31**, 252–256 10.1016/j.jaut.2008.04.017 PMID 18502610
375. Kamali, A. N., Noorbakhsh, S. M., Hamedifar, H., Jadidi-Niaragh, F., Yazdani, R., Bautista, J. M., and Azizi, G. (2019) A role for Th1-like Th17 cells in the pathogenesis of inflammatory and autoimmune disorders. *Molecular immunology* **105**, 107–115 10.1016/j.molimm.2018.11.015 PMID 30502718
376. Luger, D., Silver, P. B., Tang, J., Cua, D., Chen, Z., Iwakura, Y., Bowman, E. P., Sgambellone, N. M., Chan, C.-C., and Caspi, R. R. (2008) Either a Th17 or a Th1 effector response can drive autoimmunity: conditions of disease induction affect dominant effector category. *The Journal of experimental medicine* **205**, 799–810 10.1084/jem.20071258 PMID 18391061
377. Park, E., and Ciofani, M. (2025) Th17 cell pathogenicity in autoimmune disease. *Experimental & molecular medicine* **57**, 1913–1927 10.1038/s12276-025-01535-9 PMID 40887501
378. Schmidt, A., Éliás, S., Joshi, R. N., and Tegnér, J. (2016) In Vitro Differentiation of Human CD4+FOXP3+ Induced Regulatory T Cells (iTregs) from Naïve CD4+ T Cells Using a TGF-β-containing Protocol. *Journal of visualized experiments : JoVE* 10.3791/55015 PMID 28060341
379. Liu, M., Zhang, J., Pinder, B. D., Liu, Q., Wang, D., Yao, H., Gao, Y., Toker, A., Gao, J., Peterson, A., Qu, J., and Siminovitch, K. A. (2021) WAVE2 suppresses mTOR activation to maintain T cell homeostasis and prevent autoimmunity. *Science (New York, N.Y.)* **371** 10.1126/science.aaz4544 PMID 33766857
380. Hajighasemi, F., Mirshafiey, and Abbas (2017) Expression Pattern of Interferon-γ in Human Leukemic T Cell Lines Following Treatment with Phytoheamagglutinin, phorbol myristate acetate and Lipopolysaccharide. *IJBC* **9**, 12 EP - 17
381. Rudloff, I., Bachmann, M., Pfeilschifter, J., and Mühl, H. (2012) Mechanisms of rapid induction of interleukin-22 in activated T cells and its modulation by cyclosporin a. *The Journal of biological chemistry* **287**, 4531–4543 10.1074/jbc.M111.286492 PMID 22170067
382. Sharma, V., and Kaur, J. (2023) Acidic environment could modulate the interferon-γ expression: Implication on modulation of cancer and immune cells' interactions. *Asian biomedicine : research, reviews and news* **17**, 72–83 10.2478/abm-2023-0047 PMID 37719323
383. Sung, S. S., Bjorndahl, J. M., Wang, C. Y., Kao, H. T., and Fu, S. M. (1988) Production of tumor necrosis factor/cachectin by human T cell lines and peripheral blood T lymphocytes stimulated by phorbol myristate acetate and anti-CD3 antibody. *The Journal of experimental medicine* **167**, 937–953 10.1084/jem.167.3.937 PMID 2965212
384. Takei, S., Redford, A., Katayama, S., and Toyoda, H. (2000) Destabilization of tumor necrosis factor-alpha mRNA by 5-alpha dihydrotestosterone in Jurkat cells. *Life sciences* **66**, PL277-82 10.1016/S0024-3205(00)00526-9 PMID 10821125
385. Hayashi, K., Ishizuka, S., Yokoyama, C., and Hatae, T. (2008) Attenuation of interferon-gamma mRNA expression in activated Jurkat T cells by exogenous zinc via down-regulation of the calcium-independent PKC-AP-1 signaling pathway. *Life sciences* **83**, 6–11 10.1016/j.lfs.2008.04.022 PMID 18541274

386. Gerdes, J., Lemke, H., Baisch, H., Wacker, H. H., Schwab, U., and Stein, H. (1984) Cell cycle analysis of a cell proliferation-associated human nuclear antigen defined by the monoclonal antibody Ki-67. *Journal of immunology (Baltimore, Md. : 1950)* **133**, 1710–1715 PMID 6206131
387. Miller, I., Min, M., Yang, C., Tian, C., Gookin, S., Carter, D., and Spencer, S. L. (2018) Ki67 is a Graded Rather than a Binary Marker of Proliferation versus Quiescence. *Cell reports* **24**, 1105-1112.e5 10.1016/j.celrep.2018.06.110 PMID 30067968
388. Kuwabara, T., Ishikawa, F., Kondo, M., and Kakiuchi, T. (2017) The Role of IL-17 and Related Cytokines in Inflammatory Autoimmune Diseases. *Mediators of inflammation* **2017**, 3908061 10.1155/2017/3908061 PMID 28316374
389. Antigny, F., Jousset, H., König, S., and Frieden, M. (2011) Thapsigargin activates Ca²+ entry both by store-dependent, STIM1/Orai1-mediated, and store-independent, TRPC3/PLC/PKC-mediated pathways in human endothelial cells. *Cell calcium* **49**, 115–127 10.1016/j.ceca.2010.12.001 PMID 21193229
390. Eisner, D., Neher, E., Taschenberger, H., and Smith, G. (2023) Physiology of intracellular calcium buffering. *Physiological reviews* **103**, 2767–2845 10.1152/physrev.00042.2022 PMID 37326298
391. Raffaello, A., Mammucari, C., Gherardi, G., and Rizzuto, R. (2016) Calcium at the Center of Cell Signaling: Interplay between Endoplasmic Reticulum, Mitochondria, and Lysosomes. *Trends in biochemical sciences* **41**, 1035–1049 10.1016/j.tibs.2016.09.001 PMID 27692849
392. Marshall, C. J. (1995) Specificity of receptor tyrosine kinase signaling: transient versus sustained extracellular signal-regulated kinase activation. *Cell* **80**, 179–185 10.1016/0092-8674(95)90401-8 PMID 7834738
393. Schamel, W. W., and Dick, T. P. (1996) Signal transduction: specificity of growth factors explained by parallel distributed processing. *Medical hypotheses* **47**, 249–255 10.1016/s0306-9877(96)90088-2 PMID 8898327
394. Tsukamoto, H., Irie, A., Senju, S., Hatzopoulos, A. K., Wojnowski, L., and Nishimura, Y. (2008) B-Raf-mediated signaling pathway regulates T cell development. *Eur. J. Immunol.* **38**, 518–527 10.1002/eji.200737430 PMID 18228248
395. Pende, M., Um, S. H., Mieulet, V., Sticker, M., Goss, V. L., Mestan, J., Mueller, M., Fumagalli, S., Kozma, S. C., and Thomas, G. (2004) S6K1(-/-)/S6K2(-/-) mice exhibit perinatal lethality and rapamycin-sensitive 5'-terminal oligopyrimidine mRNA translation and reveal a mitogen-activated protein kinase-dependent S6 kinase pathway. *Molecular and cellular biology* **24**, 3112–3124 10.1128/MCB.24.8.3112-3124.2004 PMID 15060135
396. Burnett, P. E., Barrow, R. K., Cohen, N. A., Snyder, S. H., and Sabatini, D. M. (1998) RAFT1 phosphorylation of the translational regulators p70 S6 kinase and 4E-BP1. *Proceedings of the National Academy of Sciences of the United States of America* **95**, 1432–1437 10.1073/pnas.95.4.1432 PMID 9465032
397. Guertin, D. A., Stevens, D. M., Thoreen, C. C., Burds, A. A., Kalaany, N. Y., Moffat, J., Brown, M., Fitzgerald, K. J., and Sabatini, D. M. (2006) Ablation in mice of the mTORC components raptor, rictor, or mLST8 reveals that mTORC2 is required for signaling to Akt-FOXO and PKCalpha, but not S6K1. *Developmental cell* **11**, 859–871 10.1016/j.devcel.2006.10.007 PMID 17141160
398. Jacinto, E., Facchinetti, V., Liu, D., Soto, N., Wei, S., Jung, S. Y., Huang, Q., Qin, J., and Su, B. (2006) SIN1/MIP1 maintains rictor-mTOR complex integrity and regulates Akt phosphorylation and substrate specificity. *Cell* **127**, 125–137 10.1016/j.cell.2006.08.033 PMID 16962653
399. Delgoffe, G. M., Pollizzi, K. N., Waickman, A. T., Heikamp, E., Meyers, D. J., Horton, M. R., Xiao, B., Worley, P. F., and Powell, J. D. (2011) The kinase mTOR regulates the differentiation of helper T cells through the selective activation of signaling by mTORC1 and mTORC2. *Nature immunology* **12**, 295–303 10.1038/ni.2005 PMID 21358638
400. Yang, L., Qiao, G., Ying, H., Zhang, J., and Yin, F. (2010) TCR-induced Akt serine 473 phosphorylation is regulated by protein kinase C-alpha. *Biochemical and biophysical research communications* **400**, 16–20 10.1016/j.bbrc.2010.07.126 PMID 20691662

401. Arcangelis, A. de, Hamade, H., Alpy, F., Normand, S., Bruyère, E., Lefebvre, O., Méchine-Neuville, A., Siebert, S., Pfister, V., Lepage, P., Laquerriere, P., Dembele, D., Delanoye-Crespin, A., Rodius, S., Robine, S., Kedinger, M., van Seuningen, I., Simon-Assmann, P., Chamaillard, M., Labouesse, M., and Georges-Labouesse, E. (2017) Hemidesmosome integrity protects the colon against colitis and colorectal cancer. *Gut* **66**, 1748–1760 10.1136/gutjnl-2015-310847 PMID 27371534
402. Shi, L. Z., Wang, R., Huang, G., Vogel, P., Neale, G., Green, D. R., and Chi, H. (2011) HIF1alpha-dependent glycolytic pathway orchestrates a metabolic checkpoint for the differentiation of TH17 and Treg cells. *The Journal of experimental medicine* **208**, 1367–1376 10.1084/jem.20110278 PMID 21708926
403. Schieke, S. M., Phillips, D., McCoy, J. P., Aponte, A. M., Shen, R.-F., Balaban, R. S., and Finkel, T. (2006) The mammalian target of rapamycin (mTOR) pathway regulates mitochondrial oxygen consumption and oxidative capacity. *The Journal of biological chemistry* **281**, 27643–27652 10.1074/jbc.M603536200 PMID 16847060
404. Düvel, K., Yecies, J. L., Menon, S., Raman, P., Lipovsky, A. I., Souza, A. L., Triantafellow, E., Ma, Q., Gorski, R., Cleaver, S., Vander Heiden, M. G., MacKeigan, J. P., Finan, P. M., Clish, C. B., Murphy, L. O., and Manning, B. D. (2010) Activation of a metabolic gene regulatory network downstream of mTOR complex 1. *Molecular cell* **39**, 171–183 10.1016/j.molcel.2010.06.022 PMID 20670887
405. Shevyrev, D., Tereshchenko, V., Manova, O., and kozlov, V. (2021) Homeostatic proliferation as a physiological process and a risk factor for autoimmune pathology. *AIMS Allergy and Immunology* **5**, 18–32 10.3934/Allergy.2021002
406. Li, O., Zheng, P., and Liu, Y. (2004) CD24 expression on T cells is required for optimal T cell proliferation in lymphopenic host. *The Journal of experimental medicine* **200**, 1083–1089 10.1084/jem.20040779 PMID 15477346
407. Yamaki, S., Ine, S., Kawabe, T., Okuyama, Y., Suzuki, N., Soroosh, P., Mousavi, S. F., Nagashima, H., Sun, S., So, T., Sasaki, T., Harigae, H., Sugamura, K., Kudo, H., Wada, M., Nio, M., and Ishii, N. (2014) OX40 and IL-7 play synergistic roles in the homeostatic proliferation of effector memory $CD4^+$ T cells. *Eur. J. Immunol.* **44**, 3015–3025 10.1002/eji.201444701 PMID 25103720
408. Bolotin, E., Annett, G., Parkman, R., and Weinberg, K. (1999) Serum levels of IL-7 in bone marrow transplant recipients: relationship to clinical characteristics and lymphocyte count. *Bone marrow transplantation* **23**, 783–788 10.1038/sj.bmt.1701655 PMID 10231140
409. Guimond, M., Veenstra, R. G., Grindler, D. J., Zhang, H., Cui, Y., Murphy, R. D., Kim, S. Y., Na, R., Hennighausen, L., Kurtulus, S., Erman, B., Matzinger, P., Merchant, M. S., and Mackall, C. L. (2009) Interleukin 7 signaling in dendritic cells regulates the homeostatic proliferation and niche size of CD4+ T cells. *Nature immunology* **10**, 149–157 10.1038/ni.1695 PMID 19136960
410. Yang, K., Neale, G., Green, D. R., He, W., and Chi, H. (2011) The tumor suppressor Tsc1 enforces quiescence of naive T cells to promote immune homeostasis and function. *Nature immunology* **12**, 888–897 10.1038/ni.2068 PMID 21765414
411. Camperio, C., Muscolini, M., Volpe, E., Di Mitri, D., Mechelli, R., Buscarinu, M. C., Ruggieri, S., Piccolella, E., Salvetti, M., Gasperini, C., Battistini, L., and Tuosto, L. (2014) CD28 ligation in the absence of TCR stimulation up-regulates IL-17A and pro-inflammatory cytokines in relapsing-remitting multiple sclerosis T lymphocytes. *Immunology letters* **158**, 134–142 10.1016/j.imlet.2013.12.020 PMID 24412596
412. Batoulis, H., Addicks, K., and Kuerten, S. (2010) Emerging concepts in autoimmune encephalomyelitis beyond the CD4/T(H)1 paradigm. *Annals of anatomy = Anatomischer Anzeiger : official organ of the Anatomische Gesellschaft* **192**, 179–193 10.1016/j.aanat.2010.06.006 PMID 20692821
413. Frohman, E. M., Racke, M. K., and Raine, C. S. (2006) Multiple sclerosis--the plaque and its pathogenesis. *The New England journal of medicine* **354**, 942–955 10.1056/NEJMra052130 PMID 16510748

414. Sospedra, M., and Martin, R. (2005) Immunology of multiple sclerosis. *Annual review of immunology* **23**, 683–747 10.1146/annurev.immunol.23.021704.115707 PMID 15771584
415. Kunkl, M., Amormino, C., Frascolla, S., Sambucci, M., Bardi, M. de, Caristi, S., Arcieri, S., Battistini, L., and Tuosto, L. (2020) CD28 Autonomous Signaling Orchestrates IL-22 Expression and IL-22-Regulated Epithelial Barrier Functions in Human T Lymphocytes. *Frontiers in immunology* **11**, 590964 10.3389/fimmu.2020.590964 PMID 33178223
416. Abou-Alfa, G. K., Lau, G., Kudo, M., Chan, S. L., Kelley, R. K., Furuse, J., Sukeepaisarnjaroen, W., Kang, Y.-K., van Dao, T., Toni, E. N. de, Rimassa, L., Breder, V., Vasilyev, A., Heurgué, A., Tam, V. C., Mody, K., Thungappa, S. C., Ostapenko, Y., Yau, T., Azevedo, S., Varela, M., Cheng, A.-L., Qin, S., Galle, P. R., Ali, S., Marcovitz, M., Makowsky, M., He, P., Kurland, J. F., Negro, A., and Sangro, B. (2022) Tremelimumab plus Durvalumab in Unresectable Hepatocellular Carcinoma. *NEJM evidence* **1**, EVIDoa2100070 10.1056/evidoa2100070 PMID 38319892
417. Cho, B. C., Abreu, D. R., Hussein, M., Cobo, M., Patel, A. J., Secen, N., Lee, K. H., Massuti, B., Hiret, S., Yang, J. C. H., Barlesi, F., Lee, D. H., Ares, L. P., Hsieh, R. W., Patil, N. S., Twomey, P., Yang, X., Meng, R., and Johnson, M. L. (2022) Tiragolumab plus atezolizumab versus placebo plus atezolizumab as a first-line treatment for PD-L1-selected non-small-cell lung cancer (CITYSCAPE): primary and follow-up analyses of a randomised, double-blind, phase 2 study. *The Lancet. Oncology* **23**, 781–792 10.1016/s1470-2045(22)00226-1 PMID 35576957
418. Hodi, F. S., O'Day, S. J., McDermott, D. F., Weber, R. W., Sosman, J. A., Haanen, J. B., Gonzalez, R., Robert, C., Schadendorf, D., Hassel, J. C., Akerley, W., van den Eertwegh, A. J. M., Lutzky, J., Lorigan, P., Vaubel, J. M., Linette, G. P., Hogg, D., Ottensmeier, C. H., Lebbé, C., Peschel, C., Quirt, I., Clark, J. I., Wolchok, J. D., Weber, J. S., Tian, J., Yellin, M. J., Nichol, G. M., Hoos, A., and Urba, W. J. (2010) Improved survival with ipilimumab in patients with metastatic melanoma. *The New England journal of medicine* **363**, 711–723 10.1056/nejmoa1003466 PMID 20525992
419. Le, D. T., Durham, J. N., Smith, K. N., Wang, H., Bartlett, B. R., Aulakh, L. K., Lu, S., Kemberling, H., Wilt, C., Luber, B. S., Wong, F., Azad, N. S., Rucki, A. A., Laheru, D., Donehower, R., Zaheer, A., Fisher, G. A., Crocenzi, T. S., Lee, J. J., Greten, T. F., Duffy, A. G., Ciombor, K. K., Eyring, A. D., Lam, B. H., Joe, A., Kang, S. P., Holdhoff, M., Danilova, L., Cope, L., Meyer, C., Zhou, S., Goldberg, R. M., Armstrong, D. K., Bever, K. M., Fader, A. N., Taube, J., Housseau, F., Spetzler, D., Xiao, N., Pardoll, D. M., Papadopoulos, N., Kinzler, K. W., Eshleman, J. R., Vogelstein, B., Anders, R. A., and Diaz, L. A. (2017) Mismatch repair deficiency predicts response of solid tumors to PD-1 blockade. *Science (New York, N.Y.)* **357**, 409–413 10.1126/science.aan6733 PMID 28596308
420. Tawbi, H. A., Schadendorf, D., Lipson, E. J., Ascierto, P. A., Matamala, L., Castillo Gutiérrez, E., Rutkowski, P., Gogas, H. J., Lao, C. D., Menezes, J. J. de, Dalle, S., Arance, A., Grob, J.-J., Srivastava, S., Abaskharoun, M., Hamilton, M., Keidel, S., Simonsen, K. L., Sobiesk, A. M., Li, B., Hodi, F. S., and Long, G. V. (2022) Relatlimab and Nivolumab versus Nivolumab in Untreated Advanced Melanoma. *The New England journal of medicine* **386**, 24–34 10.1056/nejmoa2109970 PMID 34986285
421. Lee, H., Park, S. J., Hong, S., Lim, S.-W., and Kim, S. (2022) Deletion of IP6K1 in mice accelerates tumor growth by dysregulating the tumor-immune microenvironment. *Animal cells and systems* **26**, 19–27 10.1080/19768354.2022.2029560 PMID 35308129
422. Machado, A., Pouzolles, M., Gailhac, S., Fritz, V., Craveiro, M., López-Sánchez, U., Kondo, T., Pala, F., Bosticardo, M., Notarangelo, L. D., Petit, V., Taylor, N., and Zimmermann, V. S. (2020) Phosphate Transporter Profiles in Murine and Human Thymi Identify Thymocytes at Distinct Stages of Differentiation. *Frontiers in immunology* **11**, 1562 10.3389/fimmu.2020.01562 PMID 32793218
423. Rosário, M., Paterson, H. F., and Marshall, C. J. (2001) Activation of the Ral and phosphatidylinositol 3' kinase signaling pathways by the ras-related protein TC21. *Molecular and cellular biology* **21**, 3750–3762 10.1128/MCB.21.11.3750-3762.2001 PMID 11340168

424. Delgado, P., Cubelos, B., Calleja, E., Martínez-Martín, N., Ciprés, A., Mérida, I., Bellas, C., Bustelo, X. R., and Alarcón, B. (2009) Essential function for the GTPase TC21 in homeostatic antigen receptor signaling. *Nature immunology* **10**, 880–888 10.1038/ni.1749 PMID 19561613
425. Murphy, G. A., Graham, S. M., Morita, S., Reks, S. E., Rogers-Graham, K., Vojtek, A., Kelley, G. G., and Der, C. J. (2002) Involvement of phosphatidylinositol 3-kinase, but not RalGDS, in TC21/R-Ras2-mediated transformation. *The Journal of biological chemistry* **277**, 9966–9975 10.1074/jbc.M109059200 PMID 11788587
426. Rodriguez-Viciana, P., Sabatier, C., and McCormick, F. (2004) Signaling specificity by Ras family GTPases is determined by the full spectrum of effectors they regulate. *Molecular and cellular biology* **24**, 4943–4954 10.1128/MCB.24.11.4943-4954.2004 PMID 15143186
427. Rong, R., He, Q., Liu, Y., Sheikh, M. S., and Huang, Y. (2002) TC21 mediates transformation and cell survival via activation of phosphatidylinositol 3-kinase/Akt and NF-kappaB signaling pathway. *Oncogene* **21**, 1062–1070 10.1038/sj.onc.1205154 PMID 11850823
428. Barral, D. C., Staiano, L., Guimas Almeida, C., Cutler, D. F., Eden, E. R., Futter, C. E., Galione, A., Marques, A. R. A., Medina, D. L., Napolitano, G., Settembre, C., Vieira, O. V., Aerts, J. M. F. G., Atakpa-Adaji, P., Bruno, G., Capuozzo, A., Leonibus, E. de, Di Malta, C., Escrevente, C., Esposito, A., Grumati, P., Hall, M. J., Teodoro, R. O., Lopes, S. S., Luzio, J. P., Monfregola, J., Montefusco, S., Platt, F. M., Polishchuck, R., Risi, M. de, Sambri, I., Soldati, C., and Seabra, M. C. (2022) Current methods to analyze lysosome morphology, positioning, motility and function. *Traffic (Copenhagen, Denmark)* **23**, 238–269 10.1111/tra.12839 PMID 35343629
429. Luzio, J. P., Brake, B., Banting, G., Howell, K. E., Braghetta, P., and Stanley, K. K. (1990) Identification, sequencing and expression of an integral membrane protein of the trans-Golgi network (TGN38). *The Biochemical journal* **270**, 97–102 10.1042/bj2700097 PMID 2204342
430. Ahn, J., Febbraio, M., and Silverstein, R. L. (2005) A novel isoform of human Golgi complex-localized glycoprotein-1 (also known as E-selectin ligand-1, MG-160 and cysteine-rich fibroblast growth factor receptor) targets differential subcellular localization. *Journal of cell science* **118**, 1725–1731 10.1242/jcs.02310 PMID 15797922
431. Hu, L., Li, L., Xie, H., Gu, Y., and Peng, T. (2011) The Golgi localization of GOLPH2 (GP73/GOLM1) is determined by the transmembrane and cytoplamic sequences. *PloS one* **6**, e28207 10.1371/journal.pone.0028207 PMID 22140547
432. Bai, Y., Cui, X., Gao, D., Wang, Y., Wang, B., and Wang, W. (2018) Golgi integral membrane protein 4 manipulates cellular proliferation, apoptosis, and cell cycle in human head and neck cancer. *Bioscience reports* **38** 10.1042/bsr20180454 PMID 30068697
433. Liu, T., Liu, B., Liu, Y., Feng, X., Jiang, X., Long, J., Gao, Q., and Yang, Z. (2021) Vesicle transporter GOLT1B mediates the cell membrane localization of DVL2 and PD-L2 and promotes colorectal cancer metastasis. *Cancer cell international* **21**, 287 10.1186/s12935-021-01991-z PMID 34059062
434. Rofe, A. P., Davis, L. J., Whittingham, J. L., Latimer-Bowman, E. C., Wilkinson, A. J., and Pryor, P. R. (2017) The Rhodococcus equi virulence protein VapA disrupts endolysosome function and stimulates lysosome biogenesis. *MicrobiologyOpen* **6** 10.1002/mbo3.416 PMID 27762083
435. Shafaq-Zadah, M., Dransart, E., and Johannes, L. (2020) Clathrin-independent endocytosis, retrograde trafficking, and cell polarity. *Current opinion in cell biology* **65**, 112–121 10.1016/j.ceb.2020.05.009 PMID 32688213
436. Trejo, H. E., Lecuona, E., Grillo, D., Szleifer, I., Nekrasova, O. E., Gelfand, V. I., and Sznajder, J. I. (2010) Role of kinesin light chain-2 of kinesin-1 in the traffic of Na,K-ATPase-containing vesicles in alveolar epithelial cells. *FASEB journal : official publication of the Federation of American Societies for Experimental Biology* **24**, 374–382 10.1096/fj.09-137802 PMID 19773350
437. Schnapp, B. J. (2003) Trafficking of signaling modules by kinesin motors. *Journal of cell science* **116**, 2125–2135 10.1242/jcs.00488 PMID 12730289

438. Zadeh, A. D., Cheng, Y., Xu, H., Wong, N., Wang, Z., Goonasekara, C., Steele, D. F., and Fedida, D. (2009) Kif5b is an essential forward trafficking motor for the Kv1.5 cardiac potassium channel. *The Journal of physiology* **587**, 4565–4574 10.1113/jphysiol.2009.178442 PMID 19675065
439. Astanina, K., and Jacob, R. (2010) KIF5C, a kinesin motor involved in apical trafficking of MDCK cells. *Cellular and molecular life sciences : CMLS* **67**, 1331–1342 10.1007/s00018-009-0253-6 PMID 20094756
440. Hosokawa, T., Kimura, T., Nada, S., Okuno, T., Ito, D., Kang, S., Nojima, S., Yamashita, K., Nakatani, T., Hayama, Y., Kato, Y., Kinehara, Y., Nishide, M., Mikami, N., Koyama, S., Takamatsu, H., Okuzaki, D., Ohkura, N., Sakaguchi, S., Okada, M., and Kumanogoh, A. (2017) Lamtor1 Is Critically Required for CD4+ T Cell Proliferation and Regulatory T Cell Suppressive Function. *Journal of immunology (Baltimore, Md. : 1950)* **199**, 2008–2019 10.4049/jimmunol.1700157 PMID 28768723
441. L'Estrange-Stranieri, E., Gottschalk, T. A., Wright, M. D., and Hibbs, M. L. (2024) The dualistic role of Lyn tyrosine kinase in immune cell signaling: implications for systemic lupus erythematosus. *Frontiers in immunology* **15**, 1395427 10.3389/fimmu.2024.1395427 PMID 39007135
442. Gaud, G., Roncagalli, R., Chaoui, K., Bernard, I., Familiades, J., Colacios, C., Kassem, S., Monsarrat, B., Burlet-Schiltz, O., Peredo, A. G. de, Malissen, B., and Saoudi, A. (2018) The costimulatory molecule CD226 signals through VAV1 to amplify TCR signals and promote IL-17 production by CD4+ T cells. *Science signaling* **11** 10.1126/scisignal.aar3083 PMID 29991650
443. Han, J., Das, B., Wei, W., van Aelst, L., Mosteller, R. D., Khosravi-Far, R., Westwick, J. K., Der, C. J., and Broek, D. (1997) Lck regulates Vav activation of members of the Rho family of GTPases. *Molecular and cellular biology* **17**, 1346–1353 10.1128/mcb.17.3.1346 PMID 9032261
444. Costello, P. S., Walters, A. E., Mee, P. J., Turner, M., Reynolds, L. F., Prisco, A., Sarner, N., Zamoyska, R., and Tybulewicz, V. L. (1999) The Rho-family GTP exchange factor Vav is a critical transducer of T cell receptor signals to the calcium, ERK, and NF-kappaB pathways. *Proceedings of the National Academy of Sciences of the United States of America* **96**, 3035–3040 10.1073/pnas.96.6.3035 PMID 10077632
445. Fischer, K. D., Kong, Y. Y., Nishina, H., Tedford, K., Marengère, L. E., Kozieradzki, I., Sasaki, T., Starr, M., Chan, G., Gardener, S., Nghiem, M. P., Bouchard, D., Barbacid, M., Bernstein, A., and Penninger, J. M. (1998) Vav is a regulator of cytoskeletal reorganization mediated by the T-cell receptor. *Current biology : CB* **8**, 554–562 10.1016/s0960-9822(98)70224-6 PMID 9601639
446. Reynolds, L. F., Smyth, L. A., Norton, T., Freshney, N., Downward, J., Kioussis, D., and Tybulewicz, V. L. J. (2002) Vav1 transduces T cell receptor signals to the activation of phospholipase C-gamma1 via phosphoinositide 3-kinase-dependent and -independent pathways. *The Journal of experimental medicine* **195**, 1103–1114 10.1084/jem.20011663 PMID 11994416
447. Tybulewicz, V. L. J. (2005) Vav-family proteins in T-cell signalling. *Current opinion in immunology* **17**, 267–274 10.1016/j.coi.2005.04.003 PMID 15886116
448. Wong, H. K., Wilson, A. J., Gibson, H. M., Hafner, M. S., Hedgcock, C. J., Berger, C. L., Edelson, R. L., and Lim, H. W. (2006) Increased expression of CTLA-4 in malignant T-cells from patients with mycosis fungoides -- cutaneous T cell lymphoma. *The Journal of investigative dermatology* **126**, 212–219 10.1038/sj.jid.5700029 PMID 16417239
449. Neubrand, V. E., Cesca, F., Benfenati, F., and Schiavo, G. (2012) Kidins220/ARMS as a functional mediator of multiple receptor signalling pathways. *Journal of cell science* **125**, 1845–1854 10.1242/jcs.102764 PMID 22562556
450. Kim, E., Dede, M., Lenoir, W. F., Wang, G., Srinivasan, S., Colic, M., and Hart, T. (2019) A network of human functional gene interactions from knockout fitness screens in cancer cells. *Life science alliance* **2** 10.26508/lsa.201800278 PMID 30979825
451. Wege, S., Khan, G. A., Jung, J.-Y., Vogiatzaki, E., Pradervand, S., Aller, I., Meyer, A. J., and Poirier, Y. (2015) The EXS Domain of PHO1 Participates in the Response of Shoots to Phosphate

Deficiency via a Root-to-Shoot Signal. *Plant physiology* **170**, 385–400 10.1104/pp.15.00975 PMID 26546667

452. Barnden, M. J., Allison, J., Heath, W. R., and Carbone, F. R. (1998) Defective TCR expression in transgenic mice constructed using cDNA-based alpha- and beta-chain genes under the control of heterologous regulatory elements. *Immunology and cell biology* **76**, 34–40 10.1046/j.1440-1711.1998.00709.x PMID 9553774
453. Leyton-Pereira, A., Fernández-Delgado, I., Rodríguez-Lagunas, M. J., Català, C., Casadó-Llombart, S., Martin-Cofreces, N. B., Bustos-Morán, E., Díaz-Garrido, N., Consuegra-Fernández, M., Calpena, A. C., Aranda, F., Andrés, M. V., Baldomà, L., Sánchez-Madrid, F., and Lozano, F. (2025) The OT-II model reveals dual in vitro and in vivo immunomodulatory properties of CD6 in T cell activation. *Frontiers in immunology* **16**, 1571590 10.3389/fimmu.2025.1571590 PMID 40642095
454. Overwijk, W. W., and Restifo, N. P. (2001) B16 as a mouse model for human melanoma. *Current protocols in immunology* **Chapter 20**, Unit 20.1 10.1002/0471142735.im2001s39 PMID 18432774
455. Park, H.-B., Lim, S.-M., Hwang, J., Zhang, W., You, S., and Jin, J.-O. (2020) Cancer immunotherapy using a polysaccharide from Codium fragile in a murine model. *Oncoimmunology* **9**, 1772663 10.1080/2162402X.2020.1772663 PMID 32923129
456. Arens, R., Wang, P., Sidney, J., Loewendorf, A., Sette, A., Schoenberger, S. P., Peters, B., and Benedict, C. A. (2008) Cutting edge: murine cytomegalovirus induces a polyfunctional CD4 T cell response. *Journal of immunology (Baltimore, Md. : 1950)* **180**, 6472–6476 10.4049/jimmunol.180.10.6472 PMID 18453564
457. Imai, N., Ikeda, H., Tawara, I., and Shiku, H. (2009) Tumor progression inhibits the induction of multifunctionality in adoptively transferred tumor-specific CD8+ T cells. *Eur. J. Immunol.* **39**, 241–253 10.1002/eji.200838824 PMID 19089817
458. Liu, Q., Wang, L., Lin, H., Wang, Z., Wu, J., Guo, J., Wen, S., Ran, L., Yue, Z., Su, X., Wu, Q., Tang, J., Li, Z., Hu, L., Xu, L., Ye, L., and Huang, Q. (2022) Tumor-Specific CD4+ T Cells Restrain Established Metastatic Melanoma by Developing Into Cytotoxic CD4- T Cells. *Frontiers in immunology* **13**, 875718 10.3389/fimmu.2022.875718 PMID 35784297
459. Markota, A., Endres, S., and Kobold, S. (2018) Targeting interleukin-22 for cancer therapy. *Human vaccines & immunotherapeutics* **14**, 2012–2015 10.1080/21645515.2018.1461300 PMID 29617184
460. Yan, Y., Liu, Q., Wollenberg, K., Martin, C., Buckler-White, A., and Kozak, C. A. (2010) Evolution of functional and sequence variants of the mammalian XPR1 receptor for mouse xenotropic gammaretroviruses and the human-derived retrovirus XMRV. *Journal of virology* **84**, 11970–11980 10.1128/JVI.01549-10 PMID 20844050
461. Christ, J. J., and Blank, L. M. (2018) Analytical polyphosphate extraction from Saccharomyces cerevisiae. *Analytical biochemistry* **563**, 71–78 10.1016/j.ab.2018.09.021 PMID 30287204
462. Smith, S. A., and Morrissey, J. H. (2007) Sensitive fluorescence detection of polyphosphate in polyacrylamide gels using 4',6-diamidino-2-phenylindol. *Electrophoresis* **28**, 3461–3465 10.1002/elps.200700041 PMID 17847128

8. Appendix

8.1. Abbreviations

Table 22: List of used abbreviations.

Abbreviation	Description
ADAP	Adhesion and degranulation promoting adaptor protein
AhR	Aryl hydrocarbon receptor
AKT	Protein kinase B
AMP	Antimicrobial peptide
AP-1	Activator protein-1
APC	Antigen-presenting cell
ARMS	Ankyrin repeat-rich membrane spanning
AUC	area under the curve
BCR	B-cell receptor
CBM	CARMA1-BCL10-MALT1
CD	Cluster of differentiation
Cdc42	Cell division cycle 42
cHET	*Cd4-Cre*$^{+}$ *Xpr1*$^{+/fl}$
cKO	*Cd4-Cre*$^{+}$ *Xpr1*$^{fl/fl}$
cTEC	Cortical thymic epithelial cells
CTL	*Cd4-Cre*$^{-}$ *Xpr1*$^{fl/fl}$
CTL*	*Cd4-Cre*$^{+}$ *Xpr1*$^{+/+}$
CTLA-4	Cytotoxic T-lymphocyte associated protein 4
DAG	Diacylglycerol
DAMP	Danger-associated molecular pattern
DN	Double negative
DP	Double positive
ECAR	Extracellular acidification rate
ECM	Extracellular matrix
ELISA	Enzyme-linked immunosorbent assay
EM	Electron microscopy
ERK1/2	Extracellular signal-regulated kinase
ETP	Early T-cell progenitors
EXS	ERD1/XPR1/SYG1
GADS	GRB2-related adaptor downstream of Shc

(continued)

GEF	Guanine nucleotide exchange factor
GM-CSF	Granulocyte-macrophage colony-stimulating factor
GRB2	Growth factor receptor-bound protein 2
IBD	Inflammatory bowel disease
ICAM-1	Intercellular adhesion molecule-1
ICOS	Inducible T-cell co-stimulator
ICT	Immune checkpoint therapy
IFN	Interferon
IKK	IκB kinases
IL	Interleukin
INPP4B	Inositol polyphosphate-4-phosphatase, type II, 105kDa
IP3	Inositol-3-phosphate
IP3R	IP3 receptor
IP6K1	Inositol hexakisphosphate kinase 1
IP7	Diphosphoinositol pentakisphosphate
IP8	Inositol pyrophosphate
IS	Immunological synapse
ITAM	Immunoreceptor tyrosine-based activation motif
ITK	IL-2 inducible T-cell kinase
Kidins220	Kinase D interacting substrate 220
LAG3	Lymphocyte-Activation Gene 3
LAMP	lysosomal-associated membrane protein
LAT	Linker for activation of T cells
LCK	Lymphocyte-specific cytoplasmic kinase
LN	lymph node
LPS	lipopolysaccharide
MAPK	RAS-mitogen-activated protein kinase
MEK1/2	Mitogen-activated protein kinase kinase
MHC	Major histocompability complex
miR	micro-RNA
mLN	mesenteric lymph node
MLV	Murine leukaemia virus
MS	Multiple sclerosis
mTEC	Medullary thymic epithelial cells

(continued)

mTOR	Mechanistic target of rapamycin
mTORC	mTOR complex
NFAT	Nuclear factor of activated T cells
NF-κB	Nuclear factor κ-light chain enhancer of activated B cells
NLR	NOD-like receptor
OCR	Oxygen consumption rate
OX40	Tumour necrosis factor receptor superfamily member 4
OXPHOS	Oxidative phosphorylation
p-	Phospho-
PAGE	Polyacrylamid gel electrophoresis
PAMP	Pathogen-associated molecular pattern
PD-1	Programmed cell death protein 1
PDK1	Phosphoinositide-dependent kinase-1
PFBC	Primary familiar brain calcification
PI3K	Phosphatidylinositol 3-kinase
PIP2	Phosphatidylinositol 4,5-bisphosphate
PIP3	Phosphatidylinositol (3,4,5)-triphosphate
PiT1	Phosphate transporter 1
PKC	Protein kinase C
PKCθ	Protein kinase Cθ
PLA	Proximity ligation assay
PLCγ1	Phospholipase C-γ1
PMA	Phorbol 12-myristate 13-acetate
pMHC	peptide-MHC
P-MLV	Polytropic MLV
PolyP	Polyphosphate
PPI5K1	Diphosphoinositol pentakisphosphate kinase type 1
PRM	Pattern-recognition molecule
pTreg	Peripheral regulatory T cell
PVDL	Polytropic virus-derived ligand
qPCR	Quantitative polymerase chain reaction
RA	Rheumatoid arthritis
RAG	Recombination activating gene
RasGRP1	RAS guanyl releasing protein 1

(continued)

RBD	Receptor binding domains
RhoGEF	Rho guanine nucleotide exchange factor
Ror-γt	RAR-related orphan receptor γ-T
RRMS	Relapsing-remitting multiple sclerosis
SEB	Staphylococcal enterotoxin B
SEPP1	Selenoprotein P
SERCA	Sarcoplasmic/Endoplasmic Reticulum Calcium ATPase
siCtrl	Scrambled control siRNA
siXPR1	siRNA targeting *XPR1* transcripts
SKAP-55	SRC kinase-associated phosphoprotein of 55 kDa
SLE	Systemic lupus erythematosus
SLP-76	SH2 domain-containing leukocyte protein of 76 kDa
SMAC	Supramolecular activation cluster
SNX27	Sorting nexin 27
SOS	Son of sevenless
SP	Single positive
SPX	SYG/PHO/XPR1
STAT	Signal transducer and activator of transcription
TCR	T-cell receptor
TGF-β	Transforming growth factor β
Th	T-helper
TIGIT	T-cell immunoreceptor with Ig and ITIM domains
TLR	Toll-like receptor
TNF-α	tumour necrosis factor α
Treg	regulatory T cell
TRX	Thioredoxin-1
tTreg	thymic-derived regulatory T cell
TXN1	Thioredoxin-1
VAV1	Vav guanine nucleotide exchange factor 1
WASP	Wiskott-Aldrich syndrome protein
X-MLV	Xenotropic MLV
XPR1	Xenotropic and polytropic retrovirus receptor 1
XVDL	Xenotropic virus-derived ligand
ZAP-70	Zeta-chain-associated protein kinase 70

8.2. Gene expression array hits

Table 23: Significant (*P* < 0.05), filtered hits from gene expression array with fold change >|2| (Figure 10).

Gene symbol	Fold Change (log2)	P-Value
Il2	23.21	0.021
Bhlhe40	10.99	0.0006
Cdkn1a	5.35	0.0282
Clic4	5.17	0.0417
Lif	4.84	0.0000418
Ccl22	4.47	0.0362
Map3k8	3.97	0.0139
Gadd45b	3.87	0.0081
Cd44	3.65	0.035
Ly96	3.21	0.036
Mir155	3.13	0.0027
Tspan31	2.96	0.0041
Atf6	2.74	0.0092
Tigit	2.73	0.0279
Txn1	2.72	0.0474
Tpi1	2.55	0.0173
Mir1938	2.51	0.0362
Myo1g	2.43	0.0127
Jun	2.38	0.0492
Mir7683	2.36	0.006
Fos	2.32	0.0073
Nfkbie	2.28	0.0062
Bcl2l1	2.27	0.0265
Ifih1	2.26	0.0394
Syngr2	2.2	0.0464
Crip1	2.12	0.0121
Mir219c	2.07	0.0272
Tnfaip8	2.06	0.0005
Il3	2.06	0.0429
Havcr1	2.04	0.0274
Ifit3b	2.03	0.0361
Snord49a	-2.12	0.0217
Rapgef4	-2.12	0.0144
H2-Ob	-2.26	0.0247
Aaed1	-2.29	0.0286
Snord110	-2.35	0.0057
Inpp4b	-2.36	0.0007
Snord66	-2.39	0.0007
Ldlrap1	-2.44	0.0412
Sepp1	-2.57	0.0353

(continued)

Slc12a7	-2.59	0.0261
Pydc4	-2.6	0.0198
Pdk1	-2.86	0.0407
Snord8	-3.03	0.0485
Mex3b	-3.23	0.0089
Acpp	-3.24	0.0035
Snord61	-3.54	0.0062
Fam78a	-3.69	0.0289
Itga6	-4.17	0.0273
Pydc3	-4.41	0.0308
Slc28a2	-5.19	0.0192
TCR genes		
Trdj1; Trdj2; Trdc	4.26	0.0132
Traj57	4.11	0.0064
Traj46	2.97	0.0051
Tcrg-C4; Trgj4	2.77	0.046
Tcrg-C3	2.38	0.0413
Trdv1	2.28	0.0073
Traj59	2.1	0.0011
Trav19	2.09	0.0237
Trav2	-2.23	0.0194

8.3. List of potentially hazardous substances

Table 24: List of potentially hazardous substances.

Substance	GHS symbol	Hazard statement	Precautionary statement
2-Mercaptoethanol		H301+H331, H310, H315, H317, H318, H361f, H373, H400, H410	P273, P280, P301+P310, P302+P352+P310, P304+P430+P311, P305+P351+P338
Acetic acid (glacial)		H226, H314, H318	P210, P280, P301+P330+P331, P303+P361+P353, P305+P351+P338, P310

(continued)

Acrylamid		H301, H312, H322, H315, H317, H319, H340, H350, H361f, H372	P201, P280, P301+P310, P302+P352+P312, P304+P340+P312, P305+P351+P338
Ammonium chloride		H302, H319	P264, P270, P280, P301+P312, P305+P351+P338, P337+P313
Ammonium persulfate		H272, H302, H315, H317, H319, H334, H335	P210, P280, P301+P312, P304+P340+P312, P305+P351+P338
Ampicillin sodium salt		H317, H334	P261, P272, P280, P284, P302+P352, P333+P313
Bisacrylamid		H301, H312, H340, H350, H361fd, H372	P202, P260, P264, P280, P301+P310, P302+P352+P312
Boric acid		H360FD	P201, P304+P340, P308+P313
Chloroform		H302, H331, H315, H319, H351, H361d, H336, H372	P202, P301+P312, P302+P352, P304+P340+P311, P305+P351+P338, P308+P313
Comassie Brilliant Blue R-250 Solution		H301, H311, H314, H332, H370, H290, H226	P210, P303+P361+P353, P370+P378, P403+P235, P301+P330+P331, P305+P351+P338, P501

(continued)

cOmplete ULTRA Tablets, EDTA-free Protease Inhibitor cocktail		H314, H412	P260, P273, P280, P303+P361+P353, P304+P340+P310, P305+P351+P338
Copper(II) sulphate pentahydrate		H302, H315, H319, H400, H410	P273, P280, P305+P351+P338, P391, P310, P501
DNase I		H317, H334	P261, P280, P304+P340, P342+P311
Duolink In Situ Detection Reagents Red		H334, H411, EUH430	P201, P202, P273, P391, P405, P501
Duolink In Situ Mounting Medium with DAPI		H290, H412	P234, P273, P390, P501
Duolink In Situ PLA Probe Anti-Mouse MINUS		H317, H411	P261, P272, P273, P280, P302+P352, P333+P313
Duolink In Situ PLA Probe Anti-Rabbit PLUS		H317, H411	P261, P272, P273, P280, P302+P352, P333+P313
Ethanol		H225, H319	P210, P233, P240, P241, P242, P305+P351+P338
Ethylenediamine-tetraacetic acid (EDTA)		H319, H332, H373	P280, P304+P340, P312, P305+P351+P338, P337+P313
Formaldehyde		H301+H311+H331, H314, H317, H335, H341, H350, H370	P201, P280, P301+P330+P331, P303+P361+P353, P304+P340, P305+P351+P338, P308+P310

(continued)

Halt Protease and Phosphatase Inhibitor Cocktail, EDTA-free, 100X		H315, H319	P280, P264, P302+P352, P305+P351+P338, P332+P313, P337+P313, P362+P364
Hydrochloric acid, 4 M		H290, H314, H335	P234, P261, P271, P280, P303+P361+P353, P305+P351+P338
Imidazole		H302, H314, H360D	P260, P280, P301+P312, P303+P361+P353, P304+P340+P310, P305+P351+P338
Ionomycin		H302	P264, P270, P301+P312, P501
Isoflurane (Sedaconda)		H336	P261, P271, P304+P340+P312, P403+P233, P501
Isopropyl alcohol		H225, H319, H336	P210, P233, P240, P241, P242, P305+P351+P338
Isopropyl β-D-1-thiogalactopyranoside (IPTG)		H319, H350, H351, EUH019	P202, P264, P280, P281, P305+P351+P338, P308+P313, P337+P313
KAPA2G Fast HotStart Readymix 2x		H371	P260, P264, P270, P308+P311, P405, P501
Laemmli Sample Buffer, 4X		H318	P305+P351+P338, P310, P280

(continued)

Malachite green oxalate		H301, H318, H361d, H410	P202, P264, P273, P280, P301+P310, P305+P351+P338
Methanol		H225, H301+H311+H331, H370	P210, P233, P280, P301+P310, P303+P361+P353, P304+P340+P311
Minimal essential medium, non essential amino acid solution (MEM NEAA), 100x		H315, H319	P280, P264, P302+P352, P305+P351+P338, P332+P313, P337+P313, P362+P364
Oxygen, medical grade		H270, H280	P220, P244, P370+P376, P410+P403
Paraformaldehyde (PFA)		H228, H302+H332, H315, H317, H318, H335, H341, H350	P210, P280, P301+P312, P304+P340+P312, P305+P351+P338, P308+P313
Penicillin-Streptomycin 10.000 U/mL		H317, H361fd	P201, P202, P261, P272, P280, P302+P352, P308+P313, P333+P313, P362+P364

(continued)

Phenol, TE-saturated		H301+H311+H331, H314, H341, H373, H411	P202, P273, P280, P303+P361+P353, P304+P340+P310, P305+P351+P338
Phorbol myristate acetate (PMA)		H315	P280, P264, P332+P313, P362+P364
Protein Transport Inhibitor Cocktail, 500x		H225, H319	P210, P280, P233, P242, P243, P370+P378, P303+P361+P353, P305+P351+P338, P337+P313, P403+P235, P501
QIAprep Spin Miniprep kit (250) Buffer N3		H315, H319	P280
QIAprep Spin Miniprep kit (250) Buffer P2		H290, H314	P280, P303+P361+P353, P305+P351+P338+ P310
QIAprep Spin Miniprep kit (250) Buffer PB		H225, H315, H319, H336	P210, P280
Recombinant human IL-2		H225, H319	P280, P210, P305+P351+P338, P337+P313, P501
Recombinant mouse IL-6		H226	P210, P501
RIPA lysis buffer		H319	P280, P264, P305+P351+P338
RNase A		H334	P261, P280, P304+P340, P342+P311

(continued)

RNeasy Micro/Mini Kit Buffer RLT		H302, H318, H412, EUH032	P273, P280, P305+P351+P228+ P310
RNeasy Micro/Mini Kit Buffer RW1		H226, H318, EUH032	P210, P280, P305+P351+P338+ P310
ROTI Phenol Chloroform/Isoamylalcohol		H301+H331, H312, H314, H341, H351, H361d, H372, H411	P201, P270, P280, P304+P340, P305+P351+P338, P308+P313
Seahorse XF Pyruvate Solution, 100 mM		H317	P280, P261, P302+P353, P333+P313, P363, P501
Seahorse XFp T Cell Metabolic Profiling Kit: rotenone/antimycin A		H400, H410	P273, P391, P501
Sodium azide (in MACS buffer)		H300+H310+H330, H373, H410, EUH032	P262, P264, P273, P280, P302+P352+P310, P304+P340+P310
Sodium carbonate		H319	P264, P280, P305+P351+P338, P337+P313
Sodium dodecyl sulfate, 20 % solution		H228, H302+H332, H315, H318, H335, H412	P210, P261, P280, P301+P312+P330, P305+P351+P338+ P310, P370+P378
Sodium hydroxide, 4 M		H290, H314	P234, P260, P280, P303+P361+P353, P304+P340+P310, P305+P351+P338

(continued)

Staphylococcal enterotoxin B (SEB) from *Staphylococcus aureus*		H300+H310+H330, H315, H319, H335	P262, P264, P280, P302+P352+P310, P304+P340+P310, P305+P351+P338
Sulfric acid, 1 M		H290, H315, H319	P280, P305+P351+P338, P337+P313
TBE urea sample buffer		H360FD	P210, P280, P308+P313
Tetramethylethylene-diamine (TEMED)		H225, H331, H302, H314	P210, P280, P301+P312, P303+P361+P353, P304+P340+P310, P305+P351+P338
Thapsigargin		H315, H319, H334, H335	P261, P264, P271, P280, P302+P352, P305+P351+P338
Trypan Blue solution (0.4 %)		H350, H361	P201, P280, P202, P308+P313, P501

8.4. Acknowledgements

I would like to thank my supervisors, Prof. Dr. Hartmut Schlüter, and Dr. Reiner Mailer, for giving me the opportunity to do my PhD studies at the Institute for Clinical Chemistry and Laboratory Medicine at the University Medical Centre Hamburg-Eppendorf (UKE). A special thanks goes to Dr. Reiner Mailer for providing me with the opportunity to conduct research on this fascinating topic. I valued the trust in my skills and opinions, the freedom and independence in pursuing a wide range of methods, and the input on my research topic.

Moreover, I would like to extend the thanks to Prof. Dr. Eva Tolosa, Prof. Dr. Sebastian Wicha, and Prof. Dr. Louisa Temme, for the willingness to be part of my defence committee.

I would like to gratefully acknowledge the UKE Microscopy Imaging Facility (UMIF) for providing the instruments and technical support to conduct confocal imaging. Further, a heartfelt thanks goes to the kind and helpful staff of the Cytometry und Cell Sorting Core Facility of the UKE for the amazing working atmosphere.

My gratitude is extended to Dr. Timur Yorgan, and Dr. Björn Diercks and Anette Rosche for cooperating with the transcriptome analysis and the Ca^{2+} live cell imaging, respectively.

I would further like to thank all the members of the Institute for Clinical Chemistry, for providing me with helpful support, and fuelling my motivation to always strive for a positive working environment. I will always cherish the fun we had. My gratitude is especially extended towards the members of the group for Molecular T-Cell Immunology for the input on methods.

I would like to acknowledge Renata Aguilar who did her Bachelor thesis in association with my project, and Nele Wichern who did an internship in association with my project. Supervising both of you was incredibly fun and motivating, and it taught me a lot about teaching.

A heartfelt thanks goes to Benita, Hanna, and Claudia for reading and correcting my thesis.

A huge and loving thank you goes to Benita, who was there with me from the beginning. Without you I would not have persisted, and your input and kind words were crucial in keeping me going. Thank you for all the soap bubbles, the memes, the canteen plan sessions, the soothing sounds of a rattle next to me, the epic narrating of the tales of Tungdil, and just being the perfect colleague for the last three years. I hope you have the best life and achieve everything you want to achieve!

Thank you, Hanna, for always being positive and ready to help, for being the strongest, most powerful role model one could ever imagine, and my best friend here. I cannot believe the luck I had in meeting you, becoming friends with you, and now living in the same house. Love you!

Last, I would like to thank my friends and family. Thank you, Mama, Papa, Armin, for always supporting me and believing in me. Thank you, Rasmus, for carrying me through yet another stressful time and never faltering in sharing your heart with me. Thank you to all my friends who for one, supported me in having the strength to pursue the things I want to, and for the other, love me for being the authentic me, even – especially – when I'm struggling. Feel loved so much at all times!

9. Statement of contribution by others

The Transcriptome analysis was performed by Dr. Timur Yorgan at the Institute for Osteology and Biomechanics, UKE. Ca^{2+} live cell imaging was performed by Dr. Björn Diercks and Anette Rosche at the Institute of Biochemistry and Molecular Cell Biology, UKE. Overexpression and purification of the viral ligands PVDL and XVDL, as well as establishment of suited conditions for treatment of cells for proliferation assays was done by Renata Aguilar. For some experiments, in particular ELISAs, genotyping of transgenic mice, T-cell isolations, Malachite Green Assays, and urea PAGE, technical assistance was provided through cooperation work practice within the Molecular T-cell Immunology group, namely Mandy Malle, Benita Kröger, Nele Wichern, Renata Aguilar, Amrei Mack, Maren Sandkuhl, and Dr. Reiner Mailer.

10. Eidesstattliche Versicherung

Hiermit versichere ich an Eides statt, die vorliegende Dissertationsschrift selbst verfasst und keine anderen als die angegebenen Quellen und Hilfsmittel benutzt zu haben. Sofern im Zuge der Erstellung der vorliegenden Dissertationsschrift generative Künstliche Intelligenz (gKI) basierte elektronische Hilfsmittel verwendet wurden, versichere ich, dass meine eigene Leistung im Vordergrund stand und dass eine vollständige Dokumentation aller verwendeten Hilfsmittel gemäß der Guten wissenschaftlichen Praxis vorliegt. Ich trage die Verantwortung für eventuell durch die gKI generierte fehlerhafte oder verzerrte Inhalte, fehlerhafte Referenzen, Verstöße gegen das Datenschutz- und Urheberrecht oder Plagiate.

Hamburg, 15.04.2026 

Marion Mengel